Cranfield University
Silsoe College
Department of Agricultural and Environmental Engineering

A Thesis Submitted for the Degree of
Doctor of Philosophy
Academic year 1994-95

by

ATHANASSIOS ALEXANDROU
Sponsored by the Greek State Scholarships Foundation

The development of techniques for assessing compactibility of field soils.

Supervisor: Dr. R. Earl

July 1995

To

SELENE BARCELO MONROY

To

my parents and brother

ABSTRACT

During the last five decades, effects of soil compaction on crop growth and yield have been of increasing concern due to the introduction of heavier agricultural machinery. Most researchers agree that, although a certain degree of compaction can be beneficial to crops, loading beyond this can be very detrimental and, therefore, soil compaction should be considered as an important factor which should be managed in crop production systems. The majority of work to date has been conducted using disturbed soil samples and hence not representative of field situations.

The aim of this project was to investigate further the compactibility behaviour of field soils. Work was conducted in a soil bin as well as on field soils (sandy loam and clay) in a range of climatic conditions. Techniques for assessing soil compactibility are proposed, based on the stress-strain (load-sinkage) characteristics of soil, soil strength prior to loading, and the mode and extent of soil deformation for a given loading situation. The determination of these soil characteristics proved somewhat cumbersome and time consuming and, therefore, the prediction of these variables from more easily determined soil properties (volumetric water content, initial dry bulk density, void ratio and degree of saturation) was investigated with promising results. In addition, a model is proposed which predicts the extent of deformation within the soil profile for a given loading situation.

ACKNOWLEDGEMENTS

The author is grateful to Dr R. Earl, Prof. G. Spoor, Dr. M. Hann, S. Grant and Prof. M. O' Dogherty for their encouragement and constructive criticism.

Grateful thanks are also due to the Greek State Scholarships Foundation which funded this project and also to its scientific consultant Prof. T. Gemtos for his continuous support.

The author would also like to acknowledge help received from the technicians responsible for laboratories used during this project namely, Tony Reynolds, Roy Newland, Peter Prudden, Andrew Weaving, Mick Cox, Jim Holmes, Bob Walker, Simon Stranks, Tony Kalupa, Roger Swatland, Stuart Poole, Mrs G. Lovelace, Mrs M. Boon and Mrs M. Biskupska who played a very important role during the experimental work.

The moral support of Lic. Selene Barcelo Monroy as well as of the families A. Alexandrou and V. M. Barcelo Rodringez during the project is also very much appreciated.

During my long stay in Silsoe there were moments when the support of friends became of paramount importance. I would like to thank these friends and especially my fellow countrymen Dr Yannis Chronacis and Maria Papageorgiou with whom I shared much of the four year period, Dr Francisco 'Pancho' Coycoolea for his friendly advice, Dr Limb and David Pullen for their moral support.

The following research note has been published from this work:-

"In situ Determination of the Pre-compaction Stress of a Soil"
by A. Alexandrou and R. Earl

Journal of Agricultural Engineering Research (**61**, 67-72).

In addition the following paper was presented in the Second International Conference on Soil Dynamics, 23-27 August 1994, Silsoe, UK:-

"The Development of a Technique for Assessing Soil Compactibility (Part II)"
by A. Alexandrou and R. Earl

This paper has been submitted to the Journal of Agricultural Engineering Research.

TABLE OF CONTENTS

TABLE OF CONTENTS

LIST OF FIGURES

Page

Page

Page

LIST OF TABLES

Page

LIST OF SYMBOLS

A	Area (m^2)
b	Confining stress of a soil (kPa)
c	Cohesion (kPa)
D_B	Initial dry bulk density (Mg/m^3)
D	Diameter of the plate (m)
e	Void ratio
F_f	Total passive force due to applied load (kN)
g_i	Initial gradient (mm^{-1})
h	Height of soil cone (m)
K_o	Coefficient of earth pressure at rest
l	Distance (m)
m	Lateral displacement from plate (m)
m_n	Initial compressive soil strength (kPa/mm)
P	Total shear stress (kPa)
R	Sinkage (m)
S_r	Degree of saturation
V	Volume (m^3)
W	Weight (kN)
WC	Volumetric water content (%)
γ	Bulk unit weight (kg/m^3)
σ	Stress (kPa)
τ	Shear stress (kPa)
φ	Angle of shearing resistance (internal friction ^{o})

Suffixes

A	Axial
c	cone
cp	compaction point
max	Maximum
N	Normal
P	Passive
pr	Pre-compaction
R	Radial
v	Volumetric
ult	Ultimate
I, II, III	phases

Addendum:-

It should be noted that initial compressive soil strength, m_p (kPa/mm), represents soil 'stiffness' rather than soil strength. m_p can be expressed in terms of 'strength' if it is divided by the diameter of the sinkage plate.

CHAPTER 1

INTRODUCTION AND LITERATURE REVIEW

1.1 Overall objective

The development of techniques for assessing the compactibility of field soils.

1.2 Background and literature review

The compaction of soil by agricultural equipment has become a matter of increasing concern. This is due to developments in the mechanisation of agricultural operations resulting in a steady increase in the average size of tractors and equipment since the second world war. Soil compaction can be defined as the volume change produced by load application. It involves an expulsion of air without significant change in the amount of water in the soil mass (Bradford and Gupta, 1986).

For farmers, the effect of soil compaction is of major interest, however, the relationship between soil compaction and crop yield is complex and has been the subject of much research effort.

It should be noted that results of experiments in this area are often contradictory. Taylor (1971) and Carter and Colwick (1971), for example, conducted experiments on the same soil type but achieved different results. The former found a downward trend in cotton yield as soil compaction was artificially increased, however in contrast, the latter did not find any significant difference in cotton yield for a similar set of circumstances. Green et al (1988) studied the effects of soil compaction on potato yields. They concluded that the yield of potatoes was significantly greater from non-compacted plots for similar irrigation rates. Das (1972) conducted experiments on corn plots. He concluded that there was no significant difference in crop yield and plant growth when his compacted plots had been irrigated weekly. For less frequently irrigated plots, however, early root development was severely retarded in compacted soils to such an extent that plants could not extract water which was available from the soil at greater depths. As a result of this, these plants

suffered greater moisture stress during early growth stages and as a consequence, they were shorter and the development of reproductive parts was hampered. Tu and Tan (1991) investigated the effects of compaction on plant growth, yield and root rot severity of white beans in sandy loam and clay loam soils. There were significant reductions in yield and an increase in root rot severity as soil compaction increased. At the same degree of compaction, plants grew better and yielded more in clay loam than in sandy loam. Boone et al (1987) studied the effect of soil compaction on the yield of maize for silage. They conducted experiments on 3 soil types on a) loose soil, b) lightly compacted, c) moderately compacted and d) heavily compacted soil. There were small yield reductions in loose soil and large reductions in heavily compacted soil resulting from insufficient soil aeration.

Soane (1985) states that for each crop, soil and season there is an optimum level of compaction for maximum crop yield. The bulletin of University of California (1975), concludes that the relationship between soil compaction and yield is not straightforward. It involves the interaction of water, air and soil and this affects plants differently depending on the stage of development. Lipiec and Simota (1994) conclude that the variable crop responses to compaction depends on interactions, between crop type, soil type, weather conditions and the degree of compactness. In these interactions, soil water status plays a very important role. Most researchers agree that, although a certain degree of compaction can be beneficial to crops, loading beyond this can be very detrimental and, therefore, soil compaction should be considered as an important factor which should be managed in crop production systems (Schafer et al, 1990).

The development of techniques which will identify and quantify compactibility of field soils, is a first step towards compaction management. Soil compactibility can be defined as the ease with which a soil compacts and, as such, is related to how a soil will behave under load. Research workers have employed various tests in order to assess soil compactibility. Triaxial apparatus has been used extensively for soil compactibility assessment. It provides opportunities for testing a wide variety of stress-strain conditions. Bailey et al (1984) and Bailey and Johnson (1989) for example, developed a three-parameter model for soil compaction and conducted triaxial compaction tests to study soil compaction on two agricultural soils. The proposed model satisfies boundary conditions at low and high stress levels and adequately represents compaction of triaxial soil samples subjected to hydrostatic stress. Vanden Berg (1966), using a modified triaxial apparatus, concluded that

bulk density is a function of mean normal stress and shearing strain, whilst Bailey and Vanden Berg (1968), using triaxial apparatus, studied the hypothesis that soil compaction is a function of mean normal stress and maximum shearing stress. Dunlap and Weber (1971) developed a soil test (similar to the triaxial test) to investigate soil compaction. An equation was derived which would accurately predict the bulk weight volume of soil at any given level of mean normal stress. The use of triaxial or similar laboratory apparatus undermines the validity of the above mentioned work for field soils.

Another technique which has been widely used for soil compactibility assessment is the confined, or uniaxial, compression test. Nichols (1929) was the first to describe such apparatus. It consists of a cylinder which contains a soil sample on which a normal force is applied (*Figure 1.1*). Although constraint of the diameter of the sample does not allow the expansion of the sample which is likely to occur under field conditions when a force is applied, the technique has been used extensively for soil compactibility assessment. Soehne (1958), for example, used a kneading test on loamy and loess soils and suggested a logarithmic equation to describe his results. According to his model porosity decreases with the logarithm of the applied pressure. Koolen (1974) used the same test and showed it to be a relevant method for soil compactibility determination. It provides a hyperbolic relationship between void ratio and applied normal stress. For tests on two soil types at a series of moisture contents he concluded that parameters of the equation appear to have a physical meaning. Larson et al (1980) used a confined compression test to determine the compression curves (bulk density vs. log applied stress) of 36 agricultural soils. Compression curves determined for soils at different water contents were approximately parallel to each other over the range of initial pore water potentials from -0.05 to -1.0 bar. A procedure is suggested to predict compression curves for other water contents. Gupta et al (1985) also used the confined compression test to study the compressibility of world agricultural soils adding more results to those previously reported by Larson et al (1980). They suggested that it is more appropriate to categorise world soils in terms of the level of compaction reached in a specified test. The use of a laboratory test and an inability to accurately simulate field soil behaviour questions the accuracy of this test for field situations.

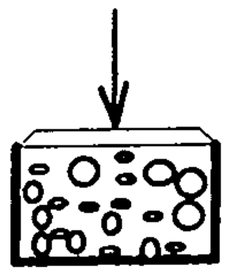

Figure 1.1. Confined compression test.

Hakansson (1988), used degree of compactness to assess soil compactibility of an annually tilled soil. He compared the dry bulk density of the soil with bulk density of the same soil in a compact reference state, determined with an oedometer. He tested his method over a 15-year period concluding that the optimum degree of compactness, in terms of grain yield, is almost independent of soil type, exclusive of organic soils. This method, however, uses bulk density which as Soane (1985) noted, does not adequately describe the detrimental effects of compaction. Chancellor et al (1962) measured bulk density changes under a piston in a soil bin, in order to measure soil compaction. They used a layer method as well as an X-ray method for this purpose and identified compaction using lines of equal volume reduction under the piston. The use of layer and X-ray methods make these techniques inappropriate for field use. Guerif (1984) employed a pressure-plate test in connection with a twin probe gamma-ray transmission equipment. The gamma-ray equipment monitored changes in the distribution of bulk density, however, he recognised a number of problems using this apparatus.

Proctor (1933) introduced a test in order to determine a satisfactory state for the compaction of soils being used in the construction of large dams and to provide means for controlling the degree of compaction during construction. The test makes use of a hand rammer and a cylindrical mould, but the impact loading of the Proctor test may bear little resemblance to the stress regime encountered during field operations.

The Cambridge critical state model (Roscoe et al 1958) prescribes the way the pore space of a given soil (quantified by its void ratio) alters with applied stresses (Hettiarachi 1987) and it can be used for soil compactibility assessment. The applied stress in this theory is identified using mean normal stress and deviatoric stress. There is considerable problem of determining what mean normal stress and deviatoric stress are for a given field situation and, for this reason, this approach was not investigated further during this project.

The validity of the majority of techniques for compactibility assessment of field soils is questionable. There is, therefore, a need for the development of techniques for assessing the compactive state of a field soil which will increase the understanding of how field soils behave under load. To assess compactibility requires the determination of relevant soil properties.

1.2.1 Relevant soil properties for compactibility assessment

In the past, densification of soil (Hakansson 1988, Vanden Berg et al 1958), changes in porosity (Soehne 1958), void ratio (Koolen 1974) and pore size distribution (Eriksson 1982) have been used for soil compactibility assessment. However, Soane (1985) noted that packing state properties do not adequately describe the detrimental effects of compaction. Detrimental effects of compaction include the effect of compaction on penetration resistance which limits root elongation and permeability to water and gases. He suggests that soil strength and permeability to water and gases are appropriate soil properties to be used for this purpose. Guerif (1984) proposed that both intra-aggregate and inter-aggregate pore space, could be used for soil compactibility assessment, both terms being expressed as components of void ratio.

To adequately describe soil compactibility, a measure of the following components is required:-

(1) the stress-strain (load-sinkage) characteristics of a soil,

(2) soil strength prior to loading, and

(3) the mode and extent of soil deformation within the soil profile for a given loading situation.

1.2.1.1 Stress-strain (load-sinkage) characteristics of a soil

The stress-strain characteristic of a soil can be obtained from a plate sinkage test. The test consists of a plate on which a normal force is applied. Sinkage and force are monitored and the stress-sinkage relationship determined. From the relationship

obtained a point can be identified beyond which, the resulting sinkage, due to load, is excessive. The precise location of this point is very dependent on past loading history of the soil (or preloading).

Preloading is a very common event in nature. In the case of a soil it can be due to its geological history or to a mechanically applied load. Soil which has been subjected to a compaction process is called pre-compacted soil. Pre-compacted soil resists any further compaction until the applied load exceeds the pre-loading level for that soil -termed pre-compacted soil. Loading a soil to below pre-compaction stress (*Figure 1.2*) will lead to very restricted compaction (Koolen, 1982).

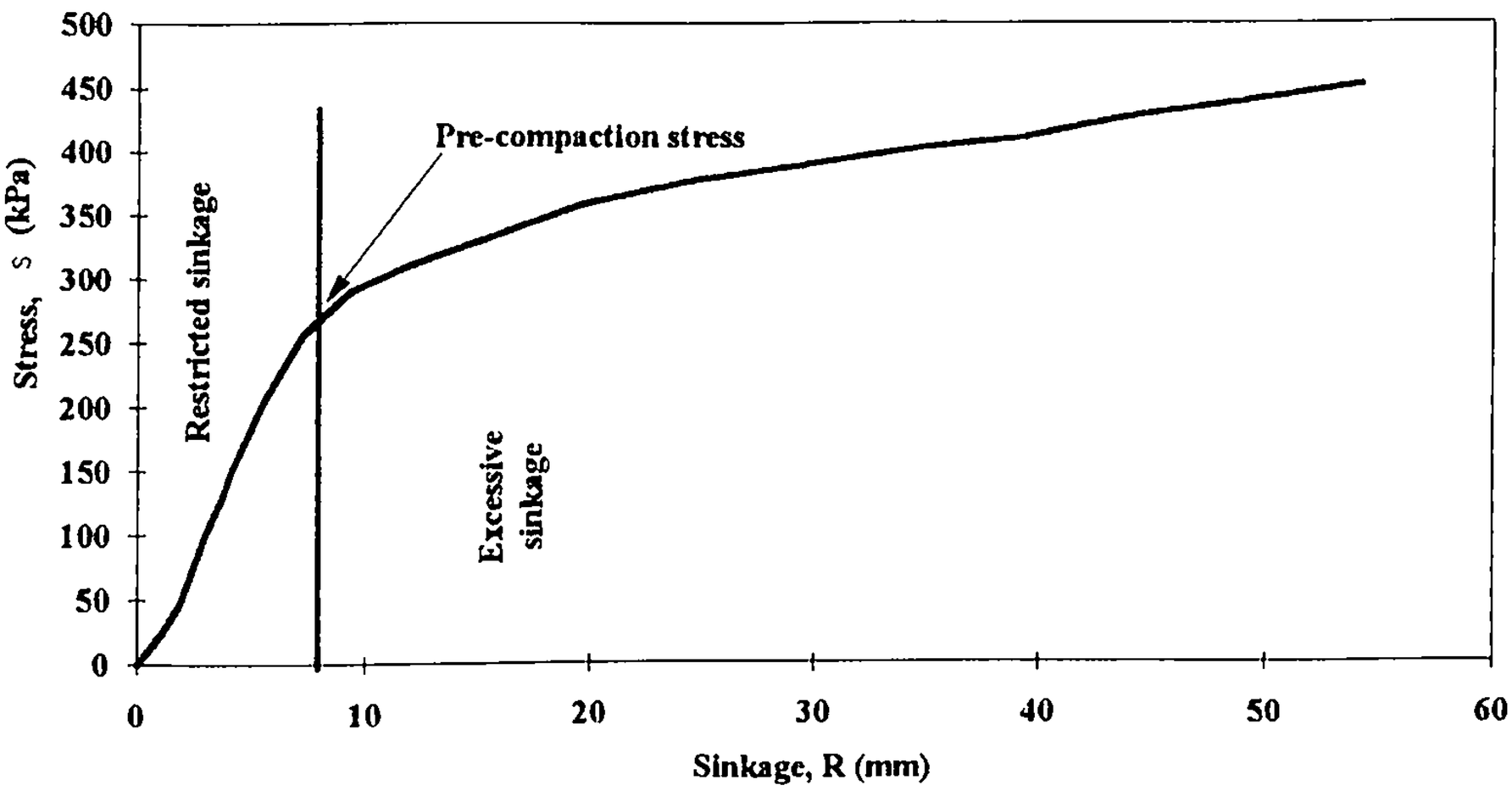

Figure 1.2. Typical plate sinkage test results for a clay soil.

If the pre-compaction stress of a soil is known, then soil compaction can be limited if the magnitude of the applied load is restricted to values below the pre-compaction stress and as such, pre-compaction stress is an important factor in compactibility assessment.

Casagrande (1936), Horn (1981), Burmister (1951), and Schmertmann (1953), used the results of consolidation tests to develop techniques for calculating pre-consolidation load whereas Koolen (1982) used a uni-axial compression test in order to determine the pre-compaction stress of a soil. In all cases, soil samples where removed from the field and loaded in the laboratory. This practice, unavoidably, increases margins of error through deformation during sampling and unknown amounts of swelling of the sample prior to loading. There is, therefore, a need for an in situ field test to determine the pre-compaction stress of soil.

A plate sinkage test was employed during this work in order to determine the pre-compaction stress of field soils.

1.2.1.2 Soil strength

Soil strength can be defined as the ability of a soil to resist or endure an applied force (Gill and Vanden Berg 1968) and, as such, is related to soil compactibility since compaction is the result of an applied load.

Strength is imparted to soil by cohesive forces between particles and by the frictional resistance met by particles that are forced to slide over one another to move out of interlocked positions (Marshall and Holmes 1988). Cohesive forces are greatly influenced by moisture content, whereas frictional resistance is influenced by the packing state of the soil.

Scientists have encountered difficulties when evaluating soil strength in such a way that a number can be assigned to it. Many different tests were employed to evaluate the strength of soil. Shear strength for example, can be reliably measured by the triaxial compression method. Terzaghi and Peck (1967) measured soil strength indirectly using the unconfined compressive strength of a soil. It was defined as the load per unit area at which unconfined prismatic or cylindrical samples fail in a simple compression test (triaxial test). Increased margins of error through deformation during sampling and unknown amounts of swelling of the sample prior to loading make this technique unattractive for field use.

Another indirect measurement of soil strength can be made in the field by forcing a probe into the soil by means of a numbered blows from a hammer, or more commonly by pressing it in at a steady rate whilst recording load (penetrometer). Resistance in this case is due to the combined effect of shear strength, compression and soil-metal friction. Gill (1968) studied penetration resistance of compactible soils. He found that the soil instrument induced compaction of soil ahead of the penetrometer tip. This increase in compactness increased the penetration resistance of the soil so that the original strength of the soil was difficult to evaluate.

The bevameter technique, developed by Bekker, can identify soil cohesion, angle of shearing resistance and the pressure-sinkage relationship of a soil in relation to vehicle mobility. It consists of two separate tests, a plate sinkage test for determining stress-sinkage relationship and a shear test to determine the shear strength of the soil. The pressure-sinkage relationship is approximated with the equation:-

$$p = (\frac{k_c}{b} + k\phi)z^n \qquad (1.1)$$

Where:-

p = the ground pressure (kPa)
b = the width of a rectangular plate or radius of a circular plate (m)
z = sinkage (m)
n = the exponent of deformation (constant)
k_c = empirically determined terrain constant (kPa/m^{n-1})
k_ϕ = empirically determined terrain constant (kPa/m^n)

Karafiath and Nowatzki (1978), noted that Bekker model is conceptually inadequate because the sinkage curve is generated from several physical processes. Initially, the sinkage process is governed by elastic deformation but very quickly changes to an elastic-plastic phase before passing to one of plastic failure. For this reason soil values k_c and k_ϕ possess peculiar dimensions which can not be related to any soil deformation characteristic (Youssef and Ali 1982).

Kondner and Krizek (1962) approximated the stress-strain relationship obtained from a plate sinkage test using a hyperbolic equation. They suggested that the relationship includes the soil strength factor within it. Earl (1993) used the same relationship to approximate the soil stress relationship obtained from a plate sinkage test. He suggested that the initial modulus of the curve (i.e. gradient) is related to the initial soil strength (*Figure 1.3*).

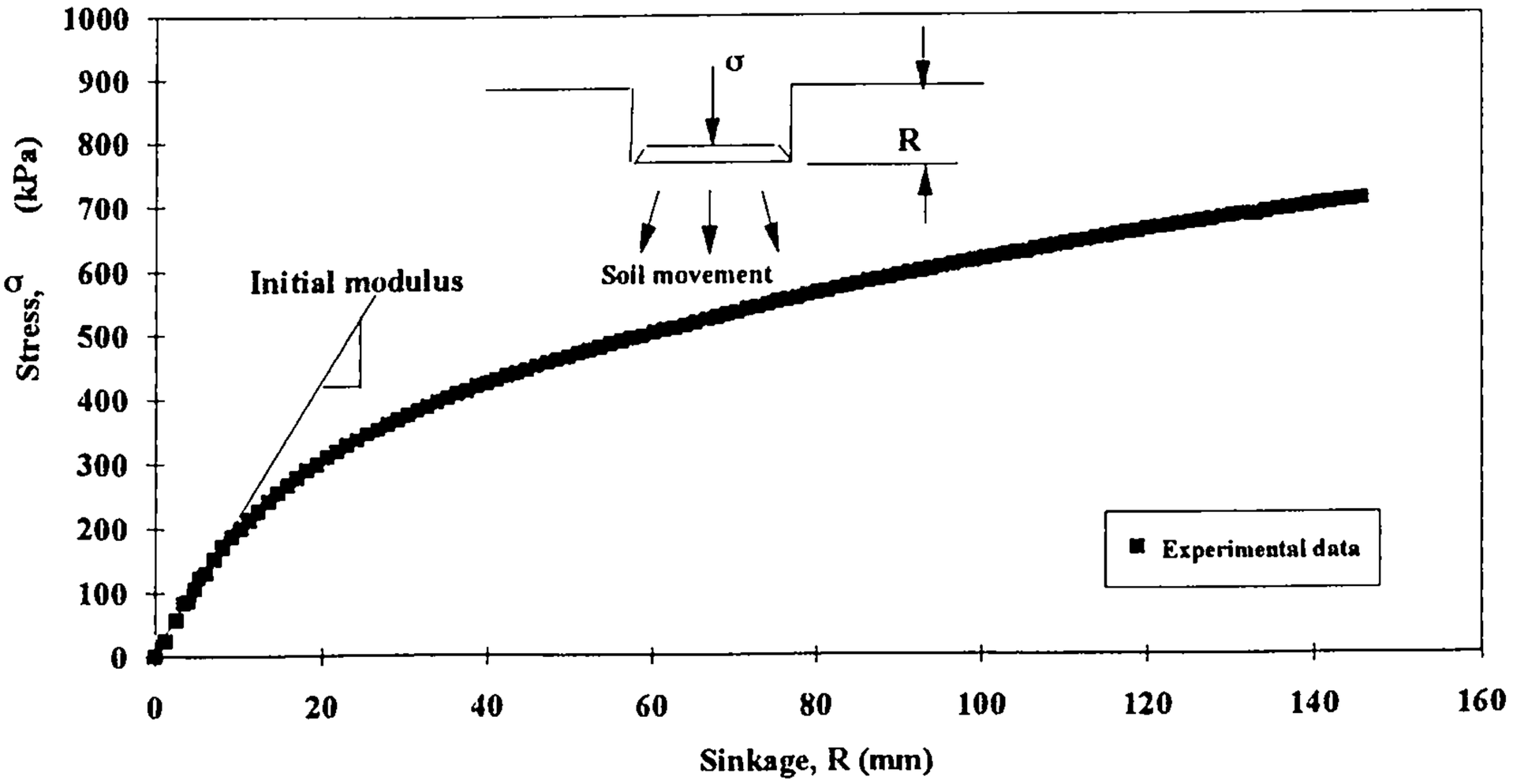

Figure 1.3. Typical stress-sinkage curve obtained from a plate sinkage test.

A plate sinkage test offers the advantage that it can be readily adapted to a tractor and used for in situ measurements. In this work soil strength of field soils has been assessed using results obtained from plate sinkage tests.

1.2.1.3 Mode and extent of soil deformation

In order to adequately describe soil compactibility, the mode and extent of deformation should be identified. The mode of deformation below a sinkage plate can be identified, in terms of stress and sinkage, using a technique proposed by Earl (1993). Earl's work is developed further using soil bin experiments to observe the soil deformation processes occuring below a sinkage test.

Earl (1993) introduced a procedure for defining the point at which the mode of deformation of soil under load changes from pure compaction (one dimensional) to a combination of lateral and vertical compaction (three dimensional). The point of change of the process was named the compaction point (CP). This information was used to assess soil compactibility. The basis of the procedure was plate sinkage, and confined compression, tests conducted in the field. The deformation process during a confined compression test can be considered to be pure compaction, providing air is allowed to escape during compression and the test is terminated prior to soil water expulsion. The compaction point for a soil, therefore, can be determined by

superimposing results from a plate sinkage test onto those from a confined compression test. The point at which the two curves diverge can be considered to be the compaction point (*Figure 1.4*).

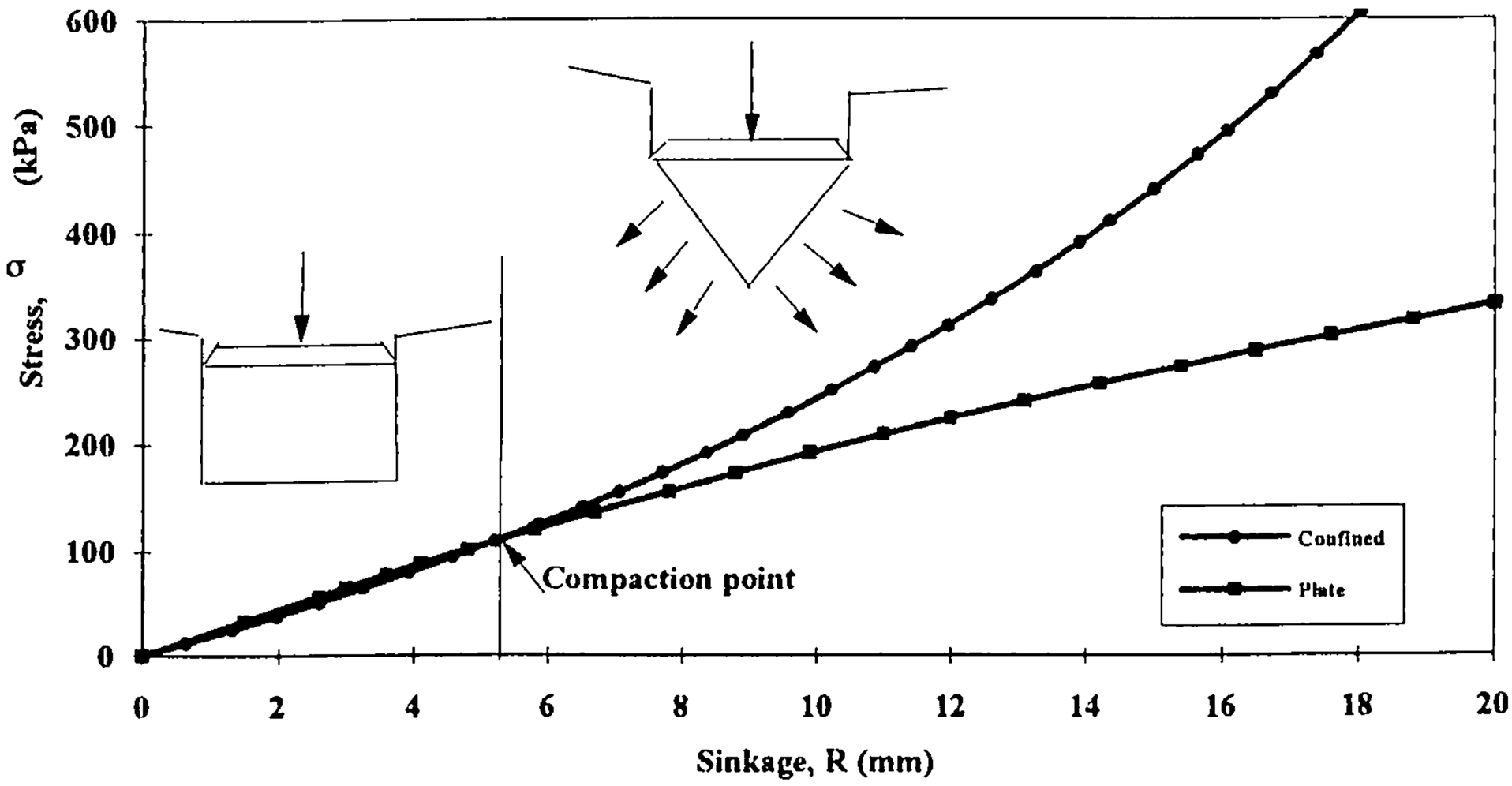

Figure 1.4. Typical results from plate sinkage and confined compression tests and the compaction point theory.

This technique has the following advantages:-

(1) is easy to carry out in situ

(2) uses the plate sinkage test which can provide information on strength and pre-compaction stress of the tested soil.

There is, however, a need to carry out soil bin studies behind glass to:-

(1) validate the compaction point theory, and

(2) model the extent of soil disturbance below a plate.

1.3 Aim of project

To develop practical techniques for assessing the compactibility of field soils in situ.

1.4 Detailed objectives

(1) To develop a technique for in situ determination of soil strength and in situ determination of pre-compaction stress.

(2) To investigate and model the mode and extent of soil disturbance under a sinkage plate.

(3) To develop a coherent procedure, based on (1) and (2), for assessing compactibility of field soils.

1.5 Thesis structure

The nature of this Thesis is such that the main body of it is divided into 8 chapters entitled:-

Chapter 2: Experimental equipment and procedures

Chapter 3: Assessing the pre-compaction stress of soil

Chapter 4: Soil strength assessment

Chapter 5: Mechanisms of failure below a sinkage plate

Chapter 6: Stress at the compaction point

Chapter 7: The relationships between pre-compaction stress, initial compressive soil strength and stress at the compaction point

Chapter 8: General discussion, conclusions and recommendations for future work

Chapters 3, 4 and 5 and 6 include separate introductory sections, analysis and conclusions.

CHAPTER 2

EXPERIMENTAL EQUIPMENT AND PROCEDURES

In chapter 1, assessment of soil compactibility has been proposed using stress-strain characteristics, strength prior to loading and mode and extent of deformation for a given loading situation. Chapter 2 is concerned with the development of soil testing equipment and experimental procedures used during this work. The equipment was based on that used by Earl (1993) but modified to fulfil updated safety requirements.

2.1 Methodology

In order to assess soil compactibility, plate sinkage and confined compression tests were carried out, initially in controlled conditions (soil bin) and later on field soils under a range of water contents and packing states.

2.1.1 Soil bin trials

2.1.1.1 Description of soil bin

The soil bin is a tank of soil (12 m long by 1.7 m wide by 1m deep) housed within a laboratory. A tool carrier (*Figure 2.1*) moves along the bin on rails to facilitate the preparation of soil to required specifications. Soil was prepared uniformly throughout its depth to given bulk density and water content specifications using tools and a roller mounted on the carrier. A mast (*Figure 2.1*), on the front of the carrier, can be moved laterally or vertically using hydraulics. This mast was modified to carry out plate sinkage tests. The modification included a support frame on which a steel rod was secured. This rod imparted a vertical load onto the sinkage plate via a ball bearing to allow some degree of freedom (*Figure 2.2*). The vertical velocity of the sinkage plate was governed by a hydraulic control valve, however the load was limited only by the capacity of the hydraulic system powering the rams.

Figure 2.1. The tool carrier.

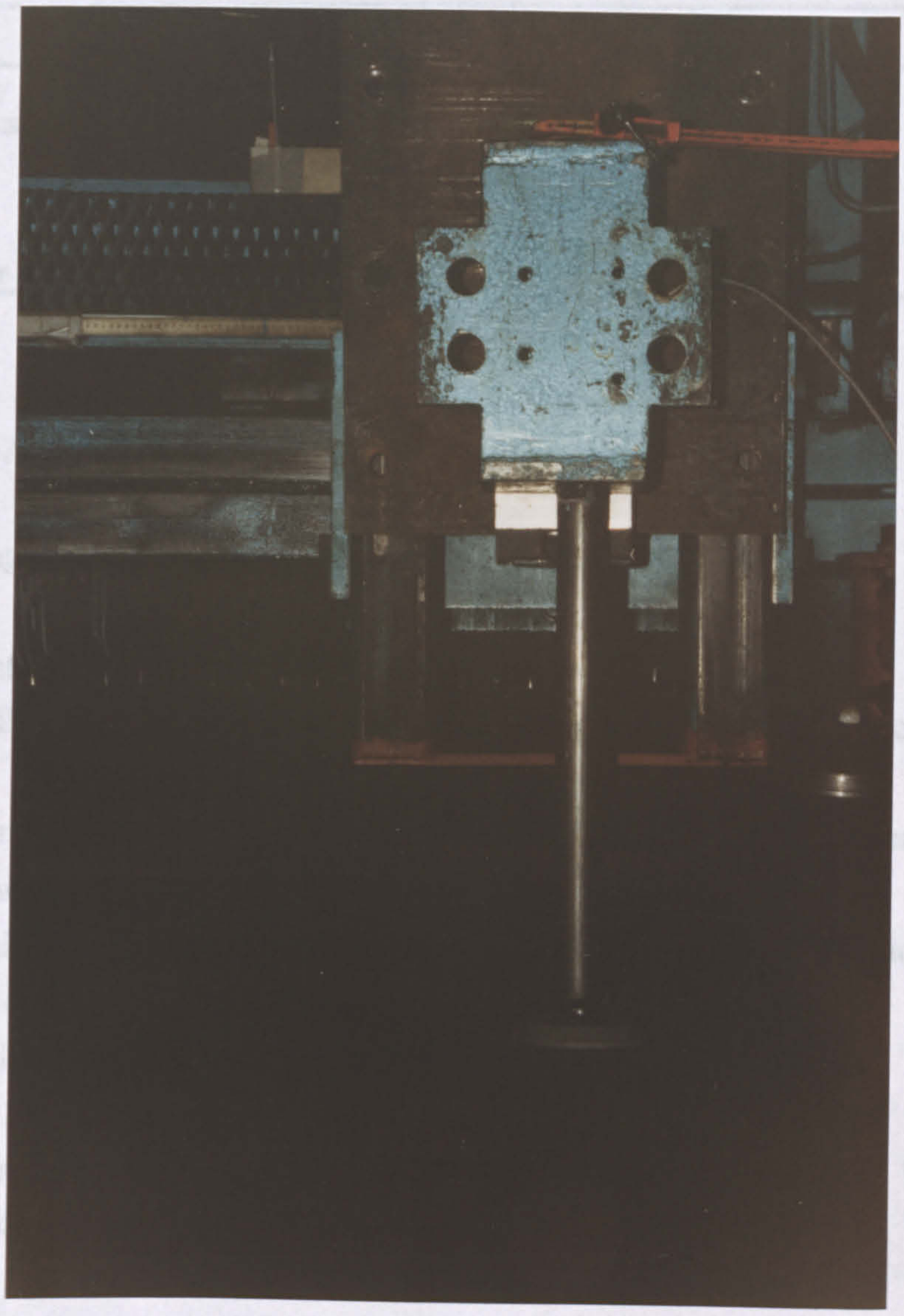

Figure 2.2. A plate sinkage test carried out in the soil bin.

The bin contained sandy loam soil (mechanical analysis results are presented in *Table 2.1*). A total of 36 trials were conducted with initial dry bulk density ranging from 1.13 to 1.55 Mg/m^3, and volumetric water content from 9.8 to 21.9 %.

Table 2.1

Mechanical soil analysis of soil bin soil

Properties	**Method used**	**Results**
Particle density	Pycnometer method	2.593 Mg/m^3
Particle size analysis	Pipette method	
	sand	67 %
	silt	20 %
	clay	13 %
Organic matter	Dichromate oxidation method	3.3 %

2.1.1.1.1 Experimental procedure for soil bin experiments

The following procedure was carried out for each soil treatment:-

1. A plate sinkage test was performed in the soil bin.
2. A soil core was sampled from the soil bin for use in a confined compression test.
3. A confined compression test was performed using an Avery universal testing machine.
4. Initial water content and bulk density were determined from the soil core after compression.
5. Results were analysed.

Special effort was taken to ensure that penetration velocities during both plate sinkage and confined compression tests were approximately similar.

2.1.2 Field soil trials

A Deutz Intrac 2004 tractor was adapted by Earl (1993) to accommodate the field testing equipment. The same tractor was used during these trials (*Figure 2.3).* A hydraulic ram was modified to carry out plate sinkage tests, to sample the soil for confined compression tests, and also to carry out confined compression tests. The vertical velocity of the ram could be controlled by a hydraulic valve.

Figure 2.3. Deutz Intrac 2004 tractor.

In order to assess soil compactibility in field conditions, trials were conducted on sandy loam and clay soil at a range of water contents and packing states. Work was carried out in November 1993, March 1994 and June 1994 to ensure that a wide range of conditions were encountered. Furthermore, tests were conducted at two different depths (topsoil and subsoil), to increase the range of packing states to be tested. Three replicates were carried out at each depth and water content giving a total of 18 trials for the sandy loam soil and 20 for the clay soil (two extra replicates were carried out due to technical problems).

Both experimental sites were located on the Silsoe College Farm and were in 'set aside' for the year concerned (1993-1994) (see *Figure 2.4*).

a)

b)

Figure 2.4. Initial conditions (November 1993) of: a) the sandy site and b) the clay site.

A mechanical analysis was carried out on soil from both sites and results are presented in *Tables 2.2* and *2.3*.

Table 2.2

Mechanical soil analysis of sandy loam soil

Properties	Topsoil	Subsoil
Particle density *(Pycnometer method)*	2.667 Mg/m^3	2.667 Mg/m^3
Sand content	76 %	76 %
Silt content	12 %	13 %
Clay content *(Pipette method)*	12 %	11 %
Organic matter *(Dichromate oxidation method)*	1.8 %	1.3 %

Table 2.3

Mechanical soil analysis of clay soil

Properties	Topsoil	Subsoil
Particle density *(Pycnometer method)*	2.618 Mg/m^3	2.686 Mg/m^3
Sand content	8 %	4 %
Silt content	15 %	18 %
Clay content *(Pipette method)*	77 %	78 %
Organic matter *(Dichromate oxidation method)*	3 %	1.7 %

2.1.2.1 Experimental procedure for field trials

Both sites were divided into three sections for use during each of the three experimental periods. Three plateaus were excavated in both the topsoil and subsoil (approximately 50 cm below the surface *Figure 2.5*). Both plate sinkage, and a confined compression, tests were carried out at each plateau in close proximity to each other (*Figure 2.6*).

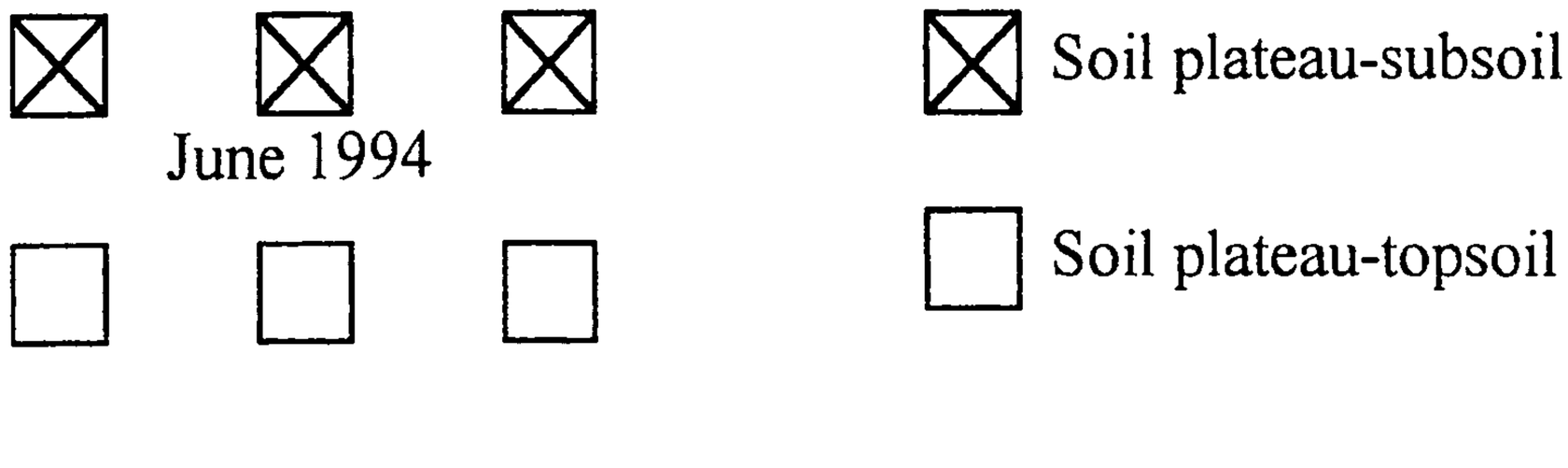

Figure 2.5. Plan view of a field site.

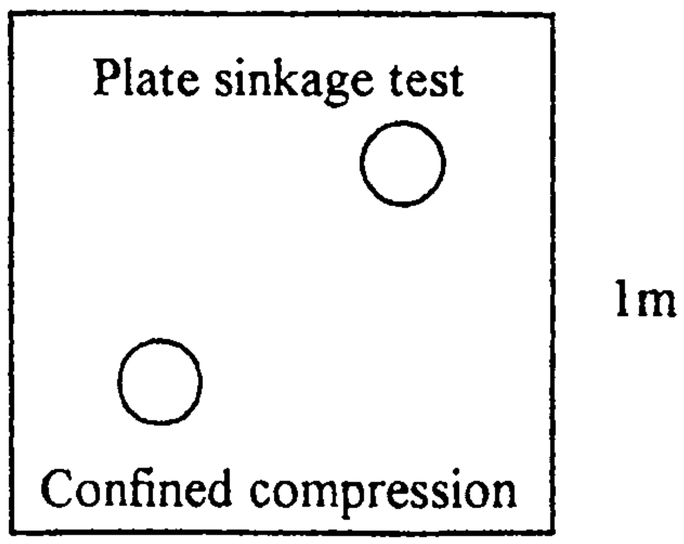

Figure 2.6. Plan view of a plateau.

As in the case of soil bin experiments, special effort was taken to ensure that the penetration velocity during both plate sinkage and confined compression tests was approximately the same. The range of soil conditions encountered in the field are presented in *Table 2.4*.

Table 2.4

Soil conditions encountered during field tests

Soil type	Initial dry bulk density (Mg/m^3)	Volumetric water content (%)
Sandy loam	1.21 to 1.49	10.1 to 21.1
Clay	0.99 to 1.36	25.1 to 51.5

The following procedure was carried out at each soil plateau:-

1. A plate sinkage test was performed.
2. A soil core was sampled for use in a confined compression test.
3. A confined compression test was performed using the compression equipment.
4. Initial water content and dry bulk density were determined from the soil core after compression.
5. The soil water suction was obtained from the tensiometers.
6. Results were analysed.

During both soil bin and field trials the time elapsing between plate sinkage test and the corresponding confined compression test was minimal (not more than 10-15 minutes).

2.2 Equipment and instrumentation used during soil bin experiments

As stated above (paragraph 2.1), tests were initially conducted in soil bin to investigate the validity of the proposed approach to soil compactibility assessment.

2.2.1 Instrumentation used during soil bin experiments

The instrumentation used for the soil bin work was built around a 21x Campbell data logger (*Figure 2.7*) which can monitor instruments and sensors and store the collected data in a digital form.

Figure 2.7. The 21x data logger.

During the plate sinkage tests, vertical force and sinkage were monitored by the data logger. Vertical load was sensed by an extended octagonal ring transducer (Godwin 1975), and sinkage was measured using a linear variable differential transformer (l.v.d.t.).

2.2.1.1 Extended octagonal ring transducer

An extended octagonal ring transducer uses electrical resistance strain gauges for sensing two forces and a torque. The strain gauges were wired in three complete Wheatstone bridge circuits, one for the vertical force, one for the horizontal force and the third for torque. Only the bridge for the vertical force was used during this

work. *Figure 2.8* indicates the position of the strain gauges on the dynamometer and the Wheatstone bridge for our measurements.

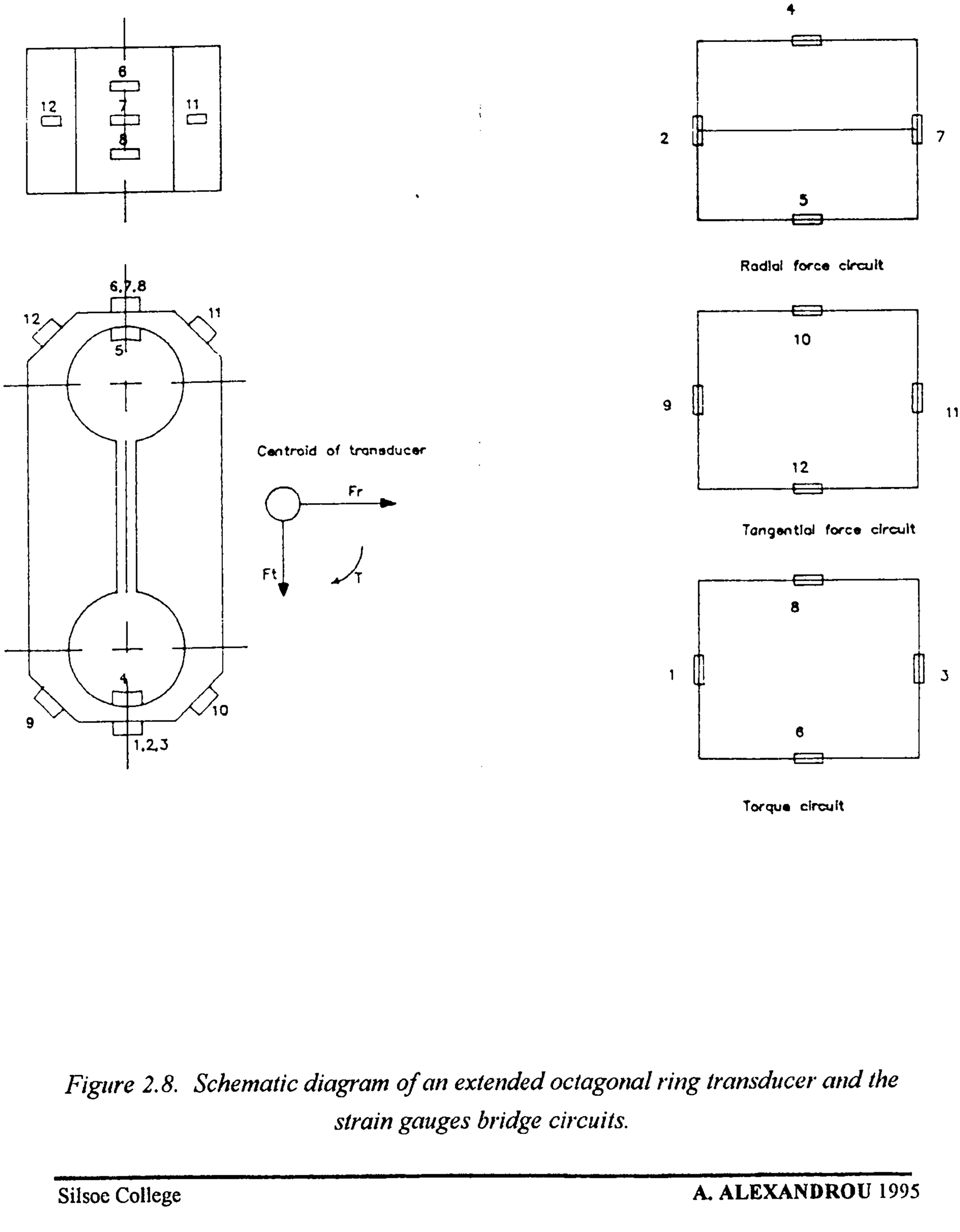

Figure 2.8. Schematic diagram of an extended octagonal ring transducer and the strain gauges bridge circuits.

2.2.1.2 Calibration of the extended octagonal ring transducer

The transducer was connected to the data logger as shown in *Figure 2.9*.

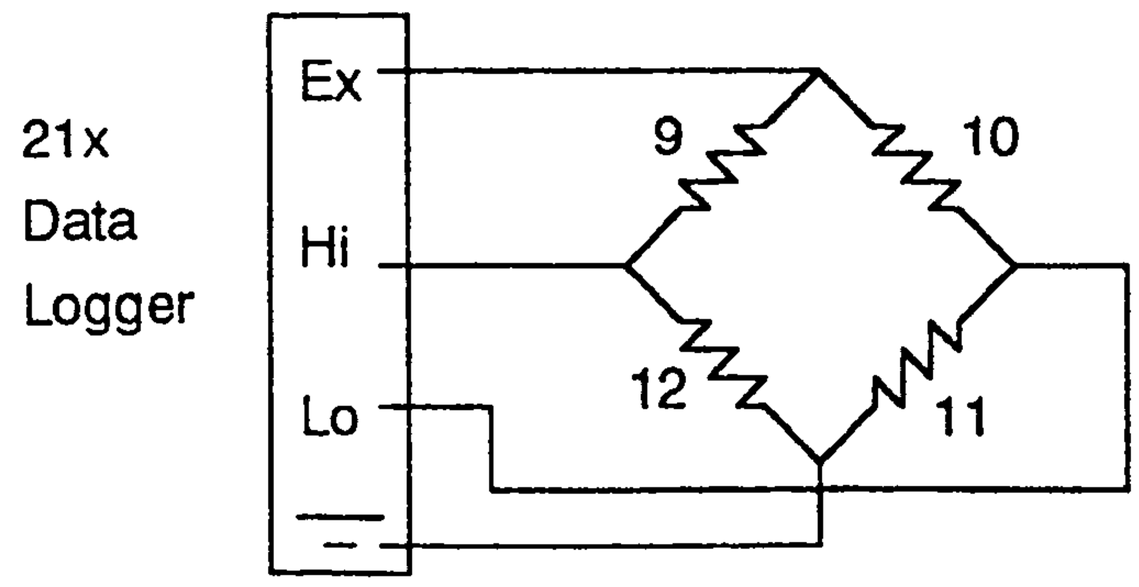

Figure 2.9. Wheatstone bridge circuit connecting the extended octagonal ring transducer to the 21x data logger.

The transducer was calibrated using a special frame from which the weights were hung (*Figure 2.10).*

Figure 2.10 Frame for calibration of the extended octagonal ring transducer.

Weights were applied incrementally to the transducer and the output from the Wheatstone bridge recorded. The procedure was repeated 3 times. The maximum applied load was 190 kg due to practical limitations. The results are presented in

Figure 2.11. It is assumed that the derived line can be extended beyond the calibration range.

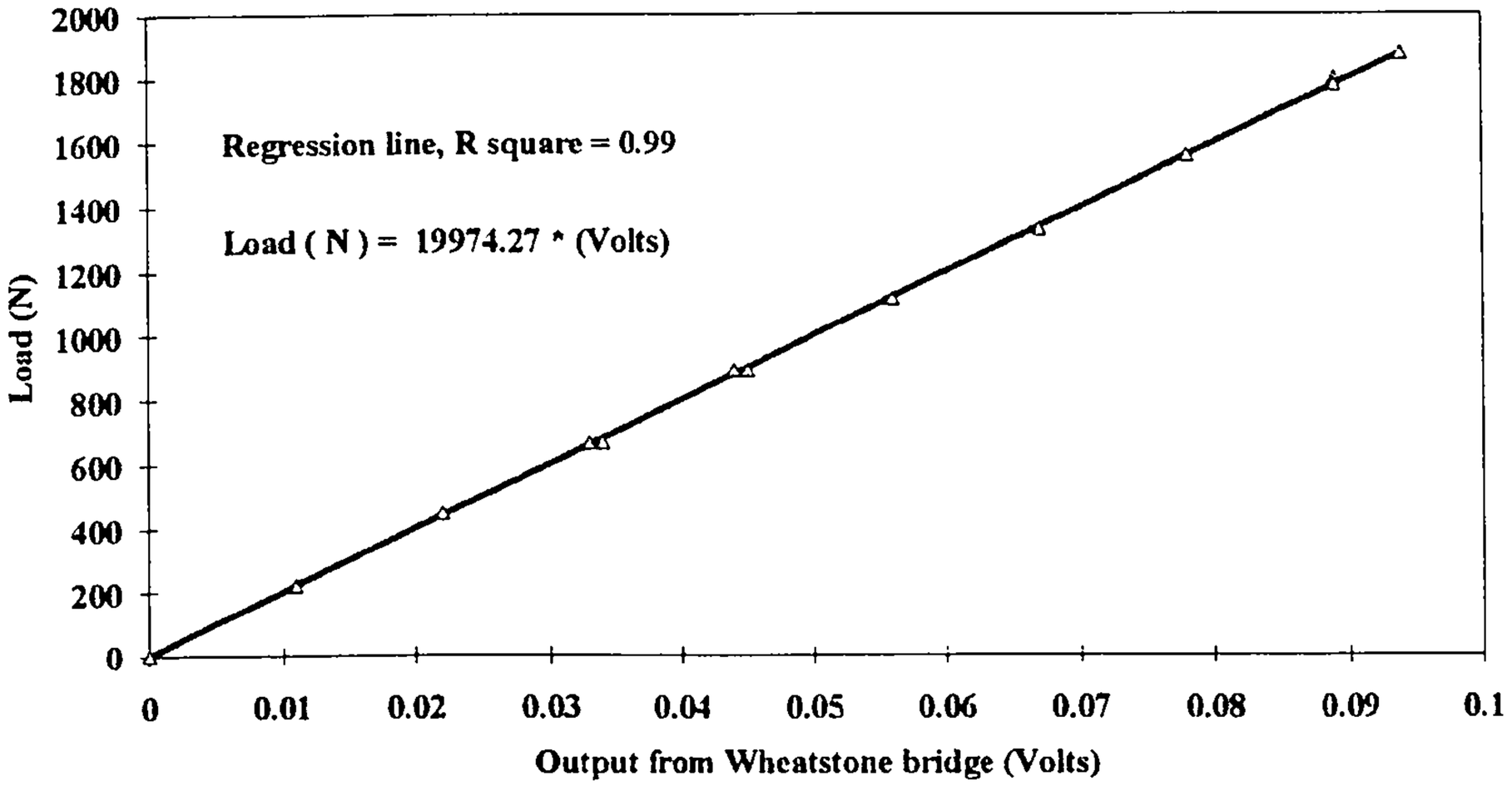

Figure 2.11. Calibration line for the extended octagonal ring transducer (vertical force).

2.2.1.3 Calibration of linear variable differential transformer (l.v.d.t.)

The linear variable differential transformer is a translational transformer which measures displacement. It is based on the mutual inductance (coupling) which is created from the movement of an iron core between two identical coils. It was connected to the 21x data logger as a differential instrument and calibrated using a metre rule.

2.2.1.4 Programming of the data logger

The following programme was used during soil bin experiments:-

Main programme table *1:

```
*1,0.1,P3,1,1,2,1,1,0,      P89,1,2,0,1,      P91,21,0,      P6,1,1,1,1,5000,2,1,0,
P6,1,1,2,2,5000,3,1,0, P2,1,5,3,4,1,0, P18,0,0,6, P86,10, P70,6,1.
```

Subroutine table *3:

P85,1, P91,11,30, P86,21, P94, P86,11, P95, P95.

This sequence of numbers represents instructions used to programme the 21x data logger. They were downloaded to the 21x, from a computer via an interface (RS 232) prior to data collection. Following experimentation, collected data were off loaded to the computer, via the interface, and stored on a floppy disk. Initially, a spreadsheet (Lotus 123) was used to analyse the data.

2.2.2 Equipment used for observing soil failure mechanisms below a sinkage plate

The basis of the technique was to cut a transverse section out of previously prepared soil in the soil bin and place a sheet of laminated glass, within a steel frame, against the soil face (*Figure 2.12*). A semi-circular sinkage plate was used to compress the soil directly behind the sheet of glass allowing soil failure to be observed.

Figure 2.12. The glass sheet prior to installation.

Visual recording of the experiments was carried out using camcorders and still cameras set on long exposure. Two basic operational modes were employed to visualise the experiments (Hettiaratchi and Reece, 1975). For mode 'A', a camcorder and still camera were fixed to a specially manufactured camera carrier which moved with the sinkage plate. For mode 'B' a camcorder together with a still camera were placed on tripods on the bottom of the tank. As Hettiaratchi and Reece explain mode 'A' is particularly suitable for picking out, in sharp focus, the boundary zones in an overall blurred field. On the other hand, mode 'B' brings out the line of velocity discontinuity between the rupture zone in the blurred field against the parent soil, which is in sharp focus. More details for this technique can be found in chapter 5.

2.2.3 The plate sinkage test

The plate sinkage test is a simple technique which provides data on the pressure-sinkage relationship of soils. It consists of a plate on which a known force is applied, and a mechanism for monitoring the resulting sinkage (*Figure 2.2*). Although sinkage tests have been used for a long time, plate dimensions and sinkage velocity have not been standardised and researchers have used plates of many different dimensions and shapes at a range of velocities.

2.2.3.1 Shape and size of the plate

During work by Earl (1993) a circular steel plate of 150 mm diameter was selected as a compromise because a smaller size might not include many peds during field trials, and a larger size would require considerable force to impart sufficient stress to the soil. A plate of similar shape and dimensions was used during this work.

2.2.3.2 Penetration rate

Research workers have carried out tests at many different penetration velocities. Grahn (1987) used velocities ranging from 2.1 cm/s up to 81 cm/s. The variability of the results for the different penetration speeds was so small that it was comparable with much of the expected range under quasi-static conditions. Emori

and Schuring (1966) also report that velocities up to 30 in/s (76.2 cm/s) have very little effect on force-penetration relationship. Since the size and shape of the plates used by the researchers do not coincide with the plate selected for this work, tests were conducted in soil bin to examine the influence of penetration velocity on the stress-sinkage relationships using a 150 mm diameter plate.

Trials were carried out at penetration velocities of approximately 6 mm/s and 33 mm/s. Due to practical limitations (variable temperature of the hydraulic oil) the velocities achieved fluctuated slightly from the nominal target.

The soil bin was divided into two halves and prepared in different ways resulting in initial dry bulk densities of approximately 1.36 Mg/m^3 and 1.26 Mg/m^3. In both cases the gravimetric water content by weight (dry basis) was approximately 8.5 %. Three replicates were carried out at each velocity on both soil preparations.

Stress-sinkage relationships for the denser soil preparation at the two sinkage velocities are presented in *Figure 2.13*. All three replicates of each velocity follow a similar pattern near the origin but then diverge. This can be attributed to the non-homogeneity of the soil. Despite the divergence of the replicates, there is little evidence to suggest, that the slope at the beginning of the curve is influenced greatly by the penetration velocity. At high speed data points are spaced out further and so it is difficult to predict the exact shape of the initial part of the curve. Stress, for a given sinkage, at high speed tends to be greater than that at low speed.

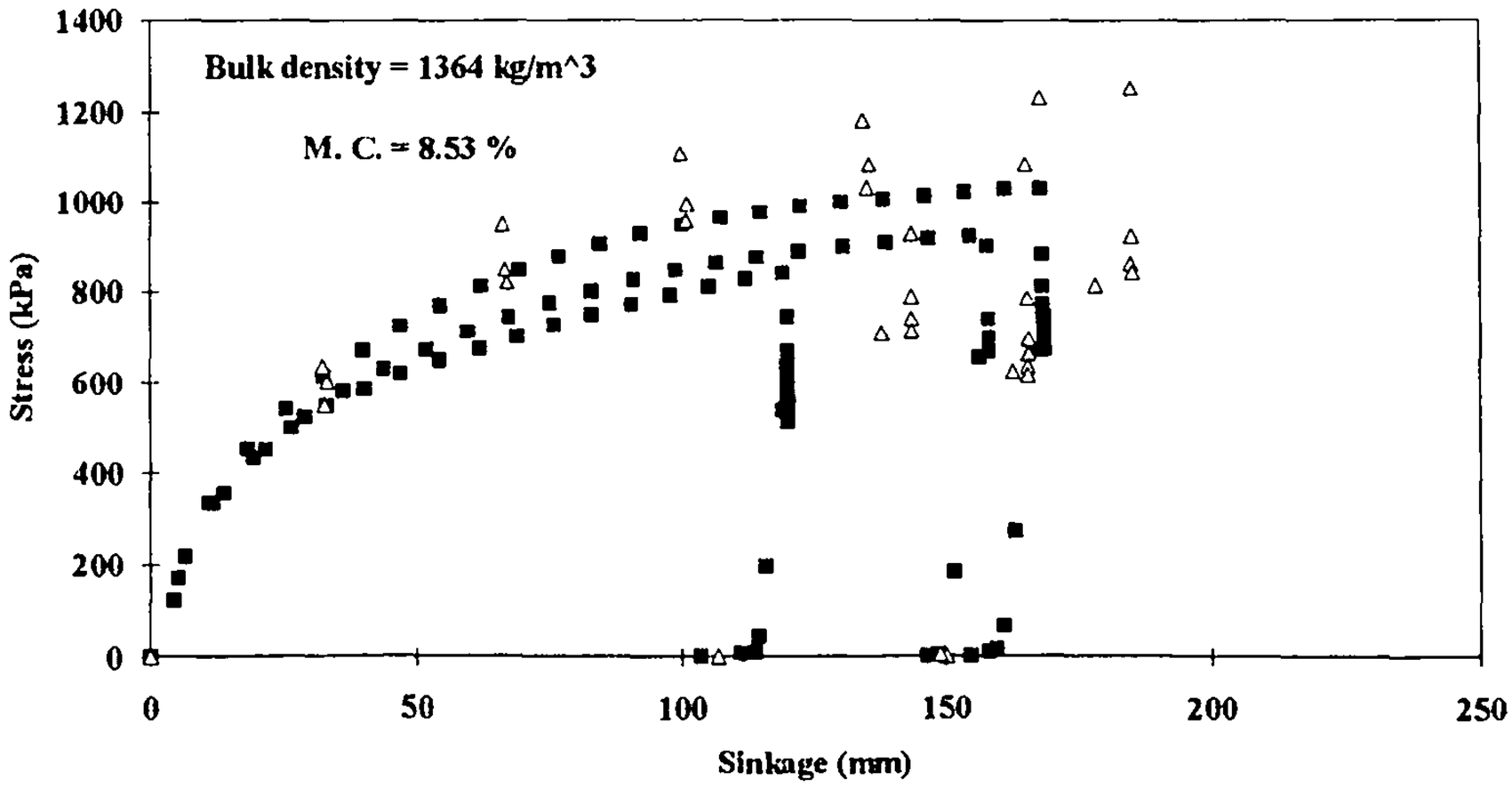

Figure 2.13. Plate sinkage tests in dense soil at two penetration velocities. △ 33 mm/s; ■ 7 mm/s.

Data from plate sinkage tests in loose soil shows a different trend to that in dense soil. The divergence of the curves occurs over the whole range of data at both velocities (*Figure 2.14*). Comparing data for both velocities, stress for a given sinkage, at high speed tends to be less than that at low speed.

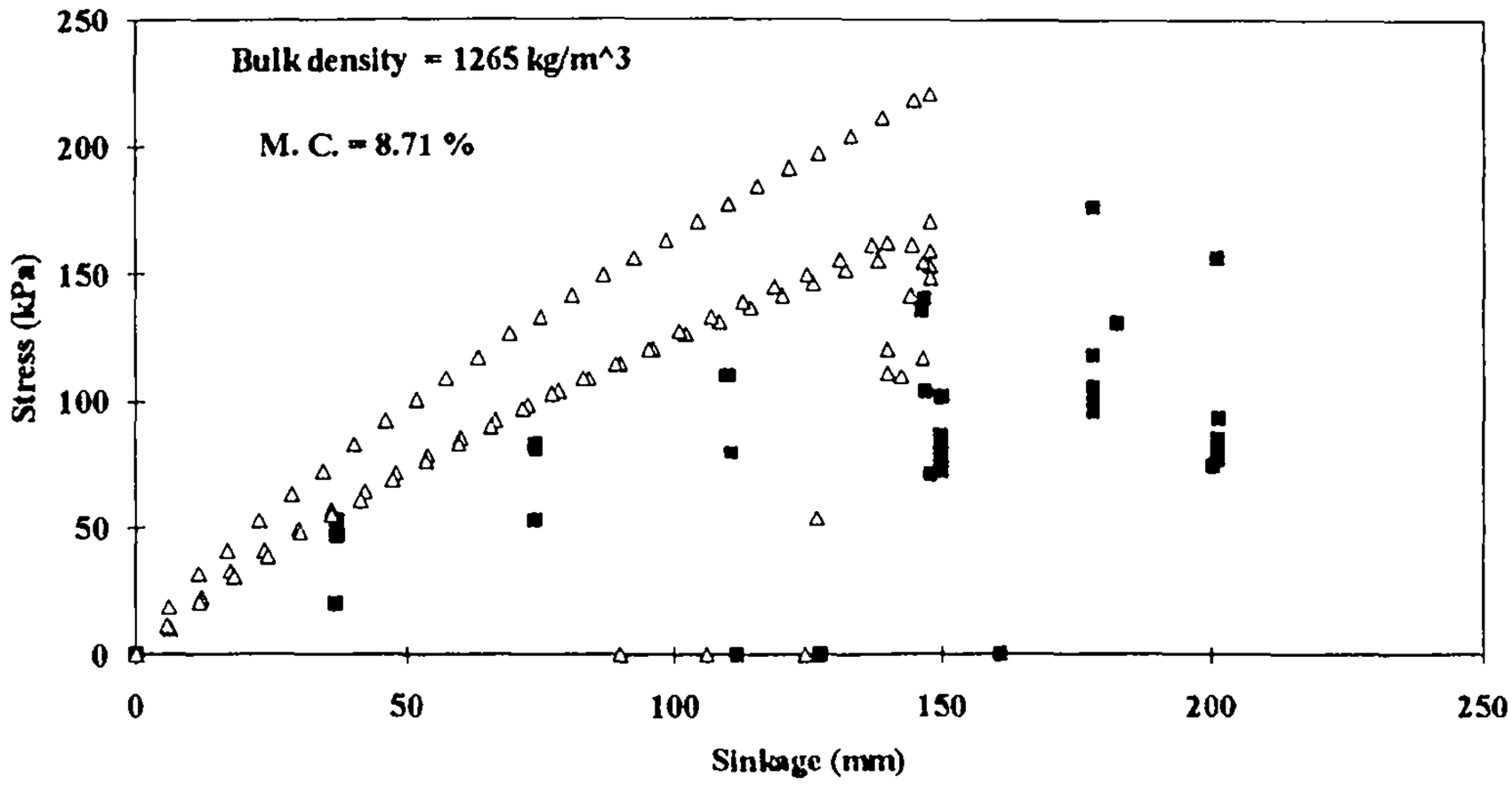

Figure 2.14. Plate sinkage tests in loose soil at two penetration velocities. △ 36.5 mm/s; ■ 5.8 mm/s.

It seems that for dense sandy loam soil and for penetration velocities ranging from approximately 6 mm/s to approximately 33.5 mm/s, there is evidence to suggest that the penetration velocity influences the stress-sinkage relationship of the soil. In the

case of loose soil, there is a clear tendency for the soil to sustain less load at higher speeds.

Schwanghart (1991) found that a tyre 16.9/14-34 with diameter 158.5 cm and width 42.9 cm at an inflation pressure of 80 kPa has a contact area of approximately 2200 cm^2 when loaded with 18 kN and travels on a soft sandy loam soil. The length of the tyre in contact with soil is 51.3 cm and at a speed of 5 km/h, assuming that the soil will remain under stress 0.5 m before the tyre is above it and 0.5 m after it passes, the soil will remain under stress for approximately 1.1 s. If the resulting sinkage is assumed to be 10-15 mm, then the vertical velocity would be approximately 13 mm/s.

One problem encountered during these series of trials was that at high penetration speeds, the density of the obtained data was low (spread out). The 21x executes the instructions from its programme, at a pre-determined interval which is time dependent (for example it can execute its programme every 1 s or 0.4 s etc.). However, there is a minimum execution interval which is needed by the data logger in order to 'read' and 'execute' the instructions of its programme. For the programme used during these trials, the minimum execution interval was 1 second resulting in a low density of data for high speed trials (at a penetration velocity of 30 mm/s only 1 data point was obtained every second). This was not considered satisfactory for the purposes of this work and in combination with the assumption that a penetration velocity of approximately 10 mm/s is commonly the case, a penetration velocity of 10 mm/s was chosen for further work. Efforts were made to reduce the execution interval of the data logger through improvements to the program and finally an execution interval of 0.1 s was achieved.

2.2.4 The confined compression test

During a confined compression test, soil is compressed axially in a rigid cylinder. A typical stress-sinkage relationship is shown in *Figure 2.15*.

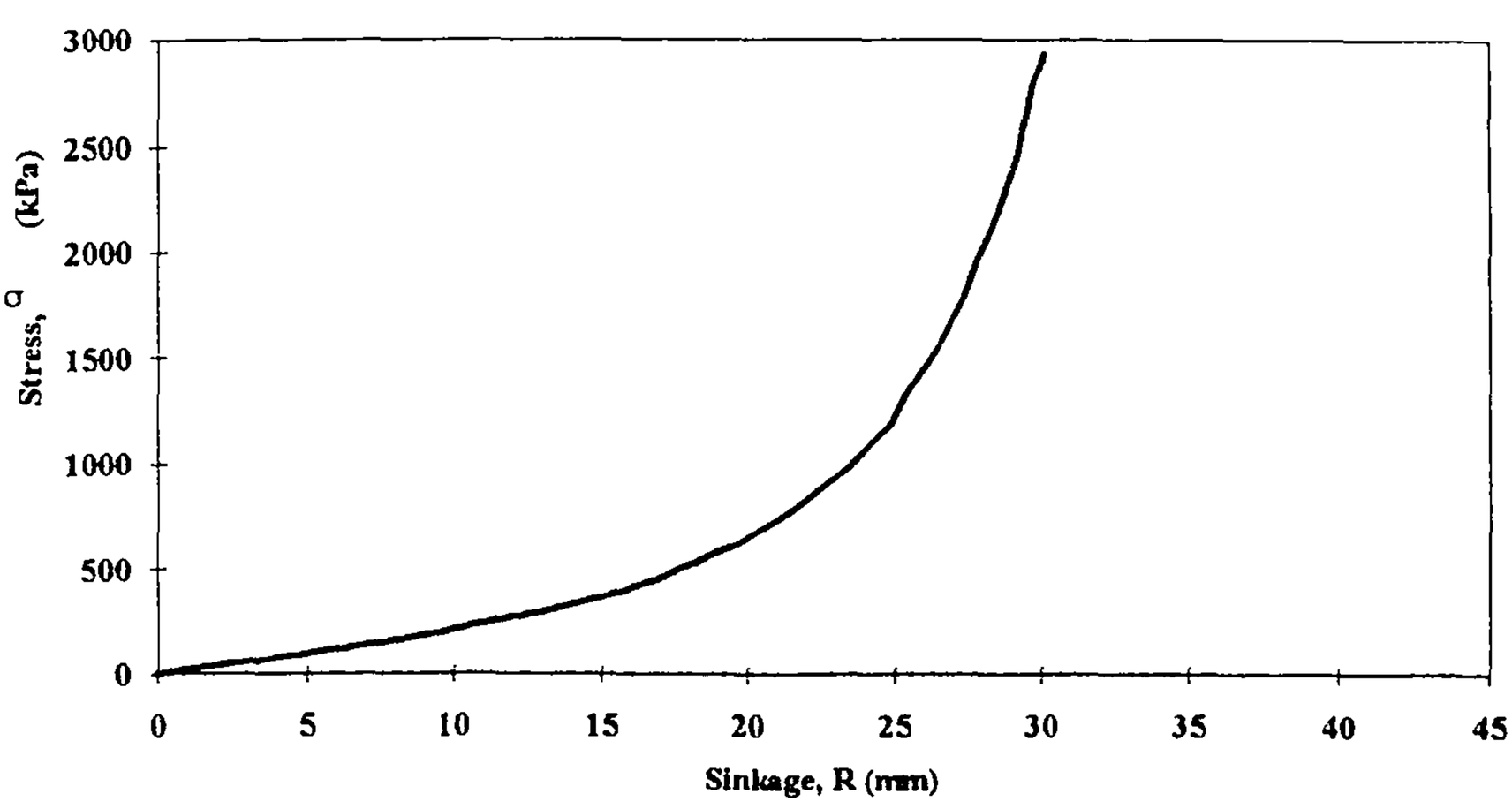

Figure 2.15. Typical stress-sinkage relationship obtained from a confined compression test.

Koolen (1974) developed the test initially using a single piston. Earl (1993) further developed the test using two pistons to reduce the resistance effect at the soil-metal interface (*Figure 2.16*).

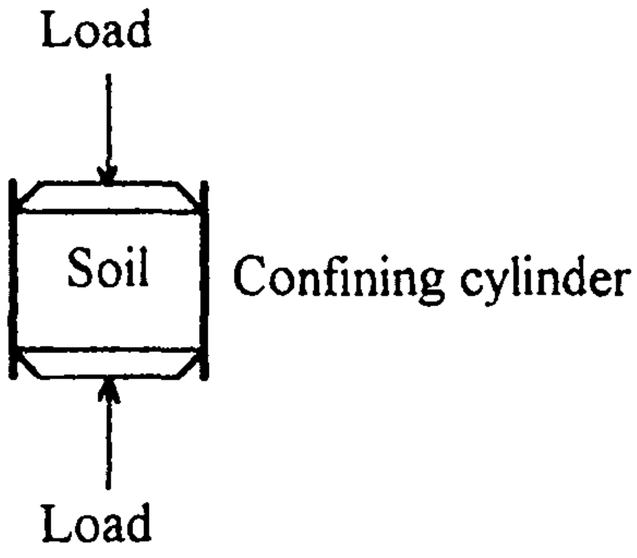

Figure 2.16. Confined compression test (Earl 1993).

2.2.4.1 Confining cylinder

Earl (1993) carried out tests using a brass cylinder with an internal diameter of 150 mm, a height of 150 mm and a wall thickness of 2 mm (*Figure 2.17*). These dimensions were a compromise between testing a representative sample and the logistics of imposing sufficient stress to the sample. The same dimensions were used for the purposes of this research.

Figure 2.17. Confined compression cylinder.

2.2.4.2 Load

The applied load used to produce the compressive stress during this study was limited only by the capability of the equipment used. An Avery universal testing machine was used to axially compress the soil to a maximum load of 30 kPa.

2.2.4.3 Penetration speed

The penetration speed of the pistons was the same as that used during plate sinkage tests (10 mm/s), however, for practical reasons (limitations of the hydraulic system used) the velocities achieved fluctuated slightly from the nominal target.

2.2.4.4 Soil-metal interaction

Earl (1993) carried out a series of tests to determine the most suitable material to be used as a lubricant between the soil and the metal. Polyox resin was found to be appropriate and was used in this study.

2.2.4.5 Instrumentation used during confined compression tests

Two pairs of strain gauges were mounted, one axially and the other circumferentially, on the outside of the confining cylinder (*Figure 2.18*).

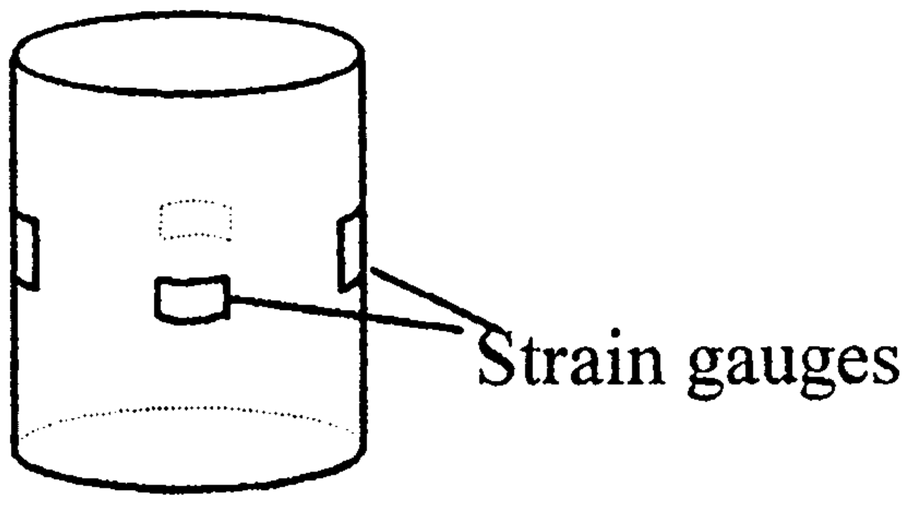

Figure 2.18. The confining cylinder.

The axial and circumferential pairs measure axial load and radial stress respectively. Both were connected into a Wheatstone bridge with two dummy strain gauges, via the 21x, for temperature compensation. Sinkage was measured using a linear variable displacement transformer, and normal stress by the Avery recorder.

2.2.4.5.1 Calibration of confining cylinder for radial stress

The confining cylinder was calibrated in terms of radial stress by pressurising the cylinder with compressed air. A special frame built by Earl (1993), was used during this study to house the cylinder (*Figure 2.19*).

Figure 2.19. Calibration of the confining cylinder for radial stress.

The following calibration procedure was used:-

1. The calibration procedure was repeated six times. The circumferentially mounted pair of strain gauges and two dummy strain gauges were connected, via the data logger, into a Wheatstone bridge circuit as shown in *Figure 2.20*.
2. Pressure was allowed to built up in an air compressor.
3. The cylinder was then pressurised incrementally via a regulator. Due to the internal pressure, the radial pair of strain gauges deformed, unbalancing the

Wheatstone bridge. A switch, connected to the data logger, activated and deactivated the data logger.

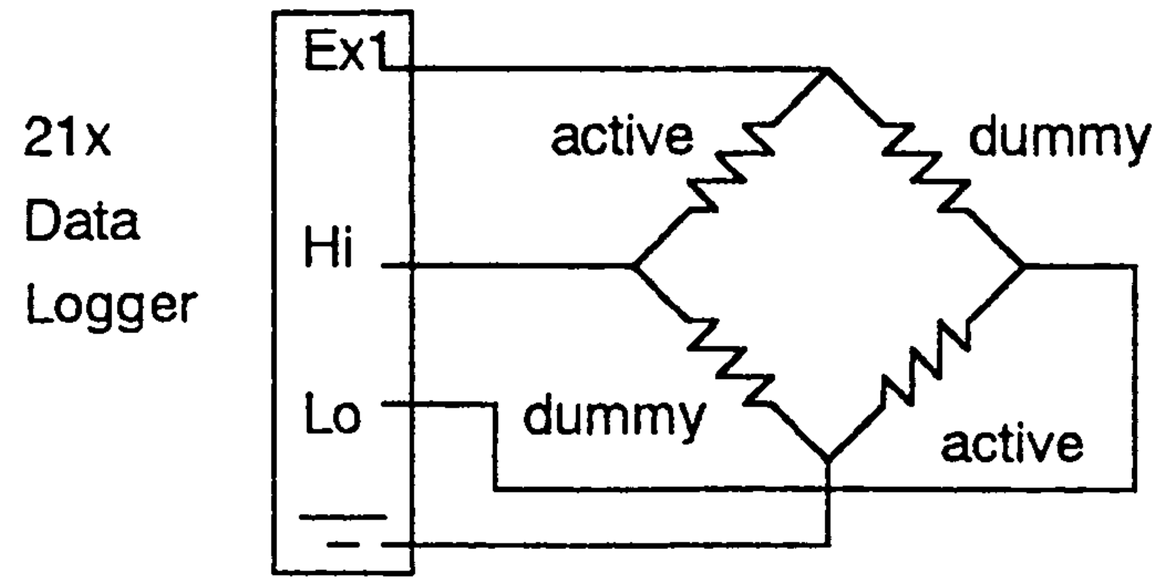

Figure 2.20. Wheatstone bridge for radial stress.

During calibration, sealing of the cylinder to the top and bottom plates of the frame proved problematical. Sealant for brakes and engines was tried unsuccessfully as was the use of a gasket (Neoprene cork composite) due to the required pressure on the plate via the nuts being unacceptably high. Success was finally achieved using silicon rubber which was applied to both plates in large quantities and left to dry overnight. It was possible then to maintain pressures of up to 6.5 bars. A calibration graph for increasing and decreasing radial stress is presented in *Figure 2.21.*

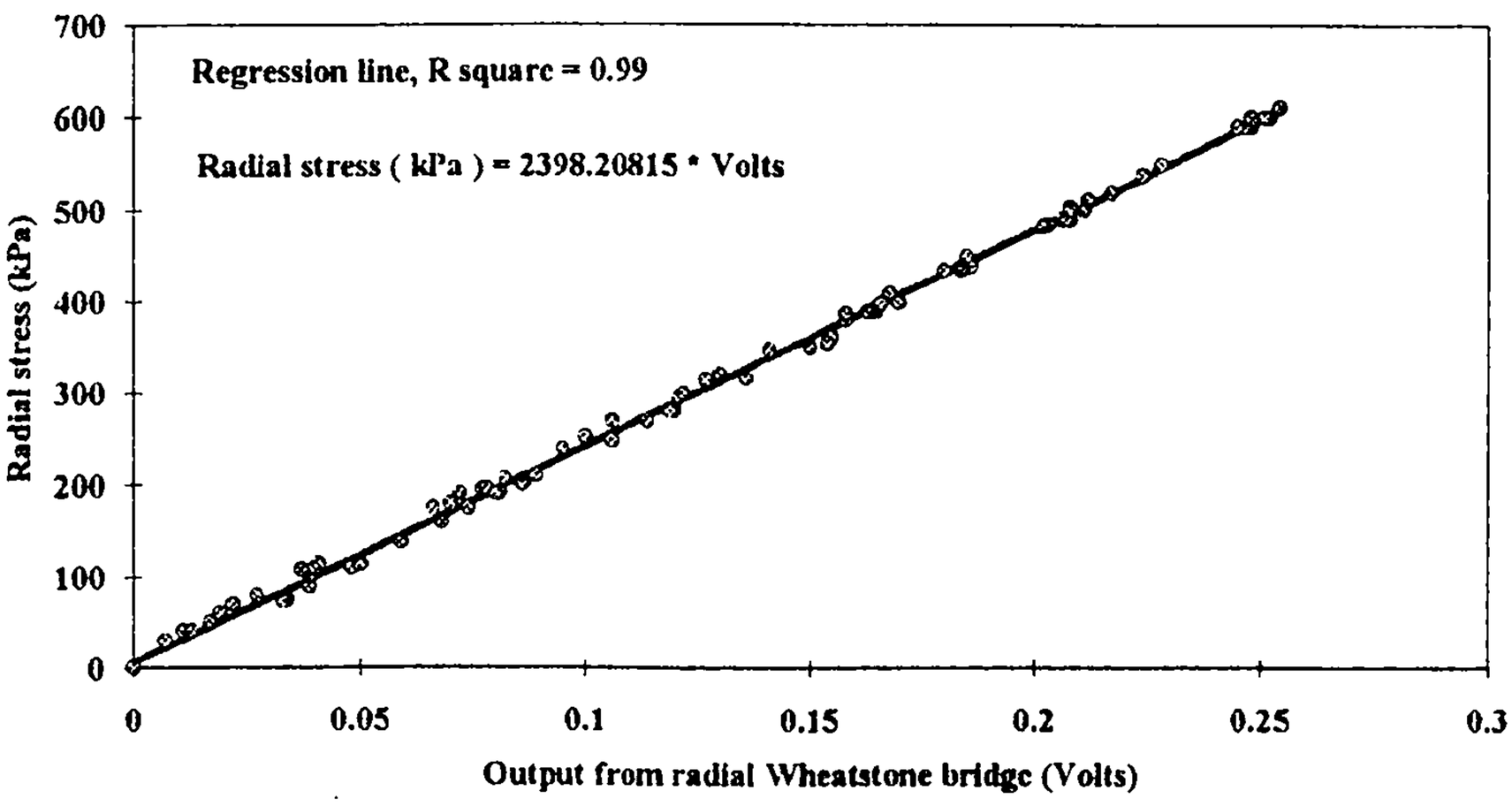

Figure 2.21. Confining cylinder calibration curve.

2.2.4.5.2 Calibration of confining cylinder for axial load

Calibration of the axial load was carried out using an Instron 1122 Universal tester. Special rings built by Earl (1993) were put on the top and the bottom of the cylinder, to distribute the load uniformly. The applied force was increased from 0 to 5 kN and was recorded by a plotter. The axially mounted pair of strain gauges and two dummy strain gauges were connected via the data logger in the Wheatstone bridge circuit shown in *Figure 2.20*.

The force was applied in increments. Every time the load was increased, the bridge output was logged. The results are presented in *Figure 2.22*.

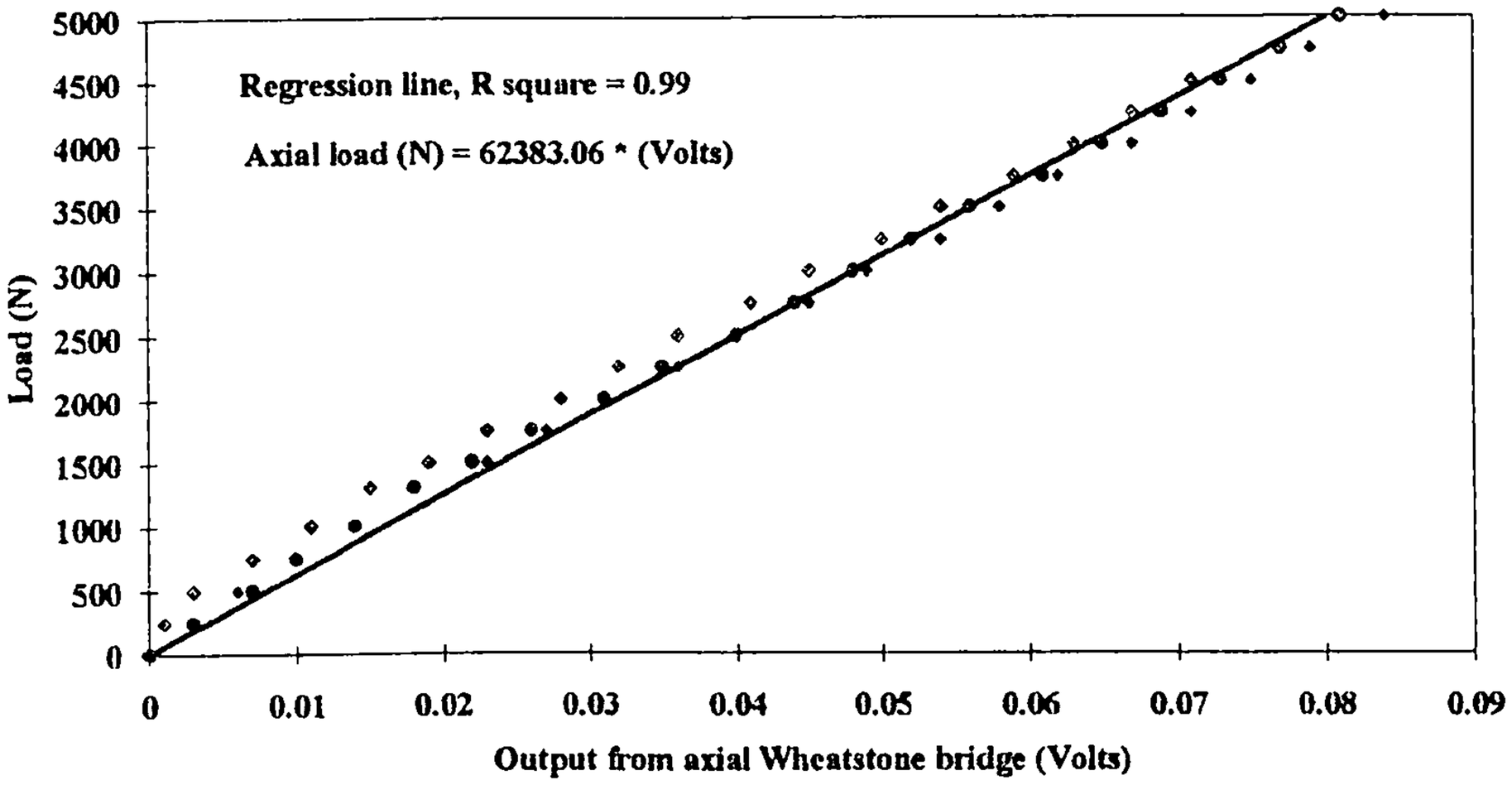

Figure 2.22. Confining cylinder axial load calibration curve.

2.2.4.6 Experimental instrumentation and procedure used during confined compression tests in the soil bin

During sampling, the brass cylinder was placed inside a plastic cylinder which protected its external surface from contact with the soil (*Figure 2.23*). The internal surface of the brass cylinder was smeared with the Polyox resin and the whole assembly mounted onto the carrier and pushed into the soil until the cylinder was full of soil. Care was taken to ensure that the soil inside the cylinder was not compacted by the covering plate (*Figure 2.24*). The cylinder was retrieved with a

help of a spike. Following trimming, pistons were placed at both ends of the cylinder and set up in the Avery universal testing machine for testing to commence (*Figure 2.25*).

Figure 2.23. Confined compression cylinder inside the plastic cylinder.

Figure 2.24. Confined compression cylinder during sampling operation.

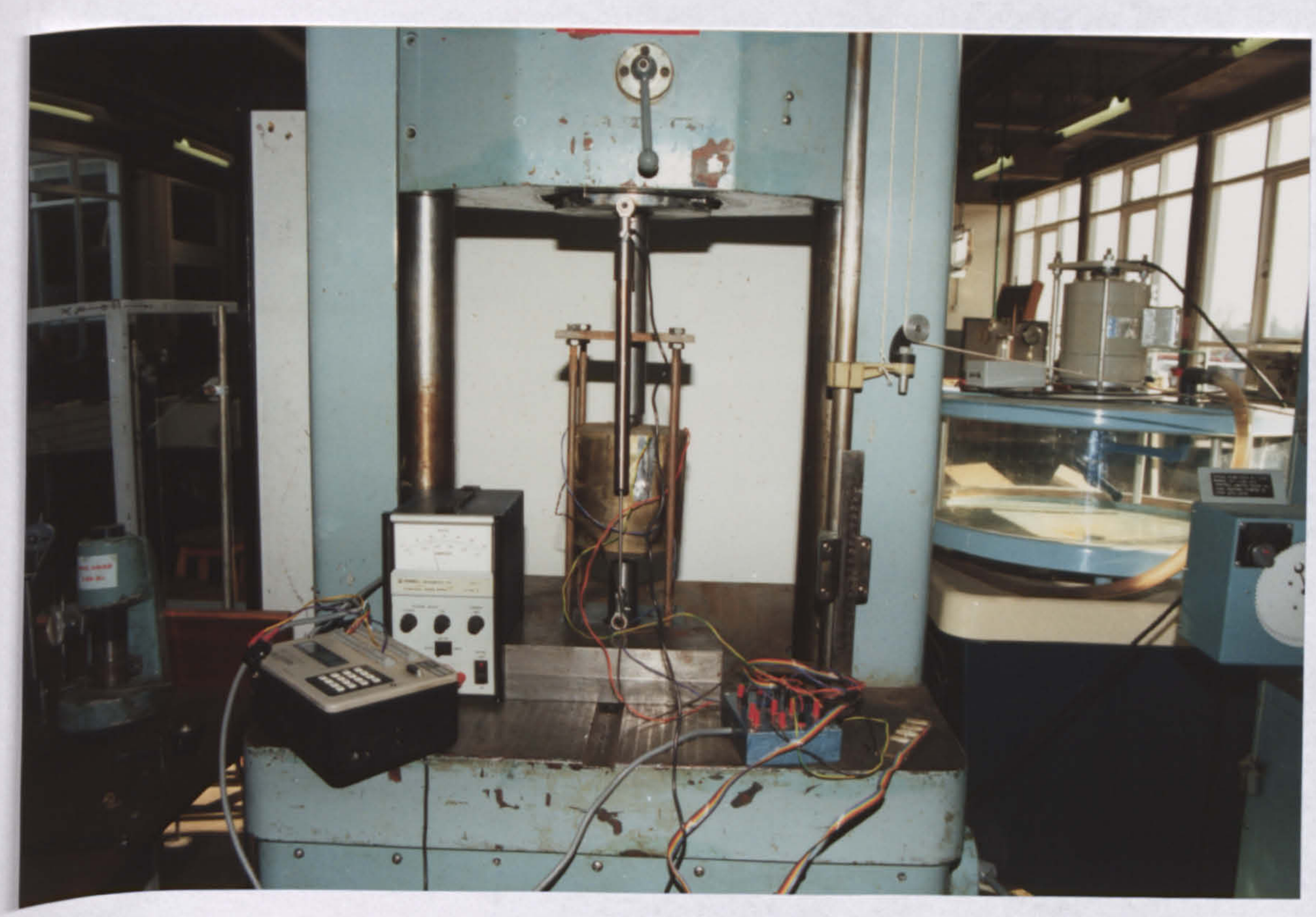

Figure 2.25. Experimental set-up for the confined compression test in the Avery universal testing machine.

During the test the following variables were monitored:-

1. Sinkage
2. Normal stress
3. Radial stress
3. Load on the cylinder wall due to normal stress

Following the test, the soil was retained for determination of volumetric water content and initial dry bulk density.

2.3 Equipment and instrumentation used during field experimentation

During field work, plate sinkage, and confined compression tests were carried out in a similar fashion to those in the soil bin. A tractor was adapted to take the test equipment.

2.3.1 Tractor mounted equipment

As stated in paragraph 2.1.2, a Deutz Intrac 2004 tractor was adapted by Earl (1993) to accommodate the field testing equipment and used during these trials (*Figure 2.3).* For logistical reasons, the sampling/compression equipment, which was initially bolted onto the rear of the tractor (Earl 1993), was mounted on the three point linkage on the rear of the tractor (*Figure 2.26*). Chains were used to allow the transfer of weight from the tractor to the hydraulic ram during testing. The tractor was stabilised during testing by extending two legs at the front of the tractor until the front wheels were clear of the ground.

Figure 2.26. Tractor-mounted testing equipment.

The tractor, when fully equipped, was taken to a local weight bridge to establish the maximum downward force available. The results of the test are shown in *Table 2.5*.

Table 2.5

Weigh-bridge test results

	Weight (tonnes)
Total weight	4.75
Weight of the hydraulic ram	0.40
Load on the rear axle	1.96
Load on the front axle	2.82
Force on the vertical ram (legs of the bucket off the ground)	1.14
Force on the vertical ram (front axle off the ground-legs of the bucket on)	2.14

For safety reasons, the maximum vertical force was restricted to 1.8 t resulting in a maximum plate stress:-

$$\sigma_m = \frac{\text{Vertical force}}{\text{Area of the plate}} = 1000kPa \qquad (2.1)$$

A pressure relief valve was installed and set at 42.19 bar, so that the vertically applied force would not exceed 1.8 t. The equipment used for field compression tests was based on that used by Earl (1993), but modified to fulfil updated safety requirements (*Figure 2.27*).

Figure 2.27. The compression equipment used during field experiments.

2.3.2 Instrumentation used during field experiments

During plate sinkage tests, normal force and sinkage were monitored at 0.4 s intervals. Normal force was monitored using a load cell, while sinkage was measured using a linear variable displacement transformer (l.v.d.t.). The force was converted into normal stress using a spreadsheet. During confined compression tests, radial stress and axial load were monitored, as in soil bin work, at 0.4 s intervals.

2.3.2.1 Calibration of the load cell

A strain-gauge load cell was used for measuring normal force. The strain gauges were connected into a Wheatstone bridge via the 21x data logger.

Calibration was carried out using the Avery universal testing machine. Load was applied incrementally and the output of the Wheatstone bridge was recorded. The procedure was repeated 3 times. The maximum applied load was 20 kN. The results are shown in *Figure 2.28*.

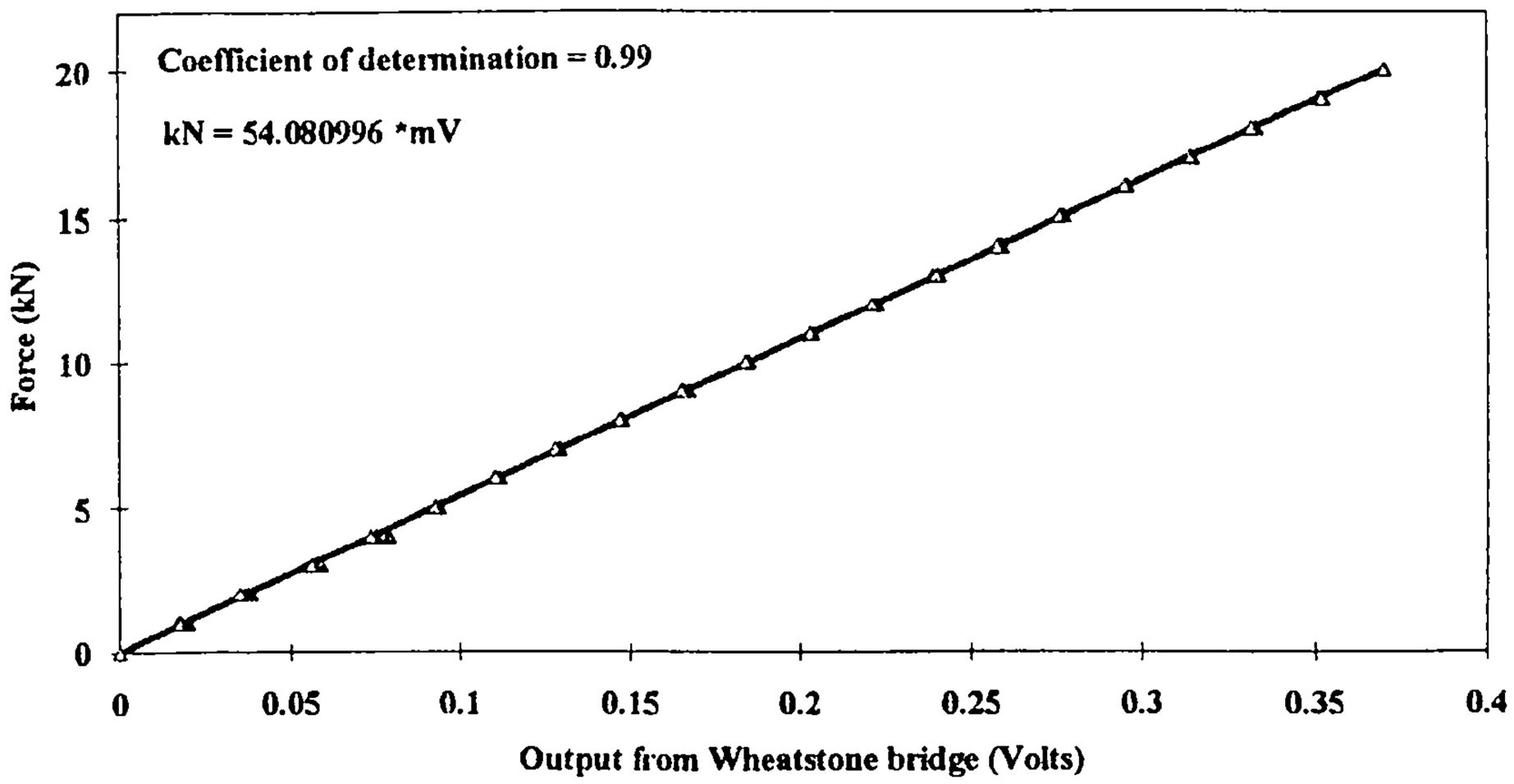

Figure 2.28. Calibration line of load cell.

2.3.2.2 Data collection procedure during field experiments

The data logger was programmed to monitor radial stress, axial load, normal force and sinkage. During plate sinkage, as well as confined compression, tests, the following sequence was used:

Programme sequence for the 21x data logger

Main programme table *1:

*1,0.4,P3,1,1,2,1,1,0, P89,1,2,0,1, P91,21,0, P6,1,1,1,1,5000,2,1,0, P6,1,1,2,2,5000,3,1,0, P6,1,13,3,3,5000,4,1,0, P1,1,5,7,5,1,0, P18,0,0,6, P86,10, P70,6,1.

Subroutine table *3:

P85,1, P91,11,30, P86,21, P94, P86,11, P95, P95.

This sequence of numbers represents instructions used to programme the 21x data logger.

Results obtained from equipment and procedures detailed in this chapter are analysed in the following chapters.

CHAPTER 3

ASSESSING THE PRE-COMPACTION STRESS OF SOIL

In the introductory chapter, pre-compaction stress has been considered a parameter which can be used to describe soil compactibility. This chapter is concerned with identifying the pre-compaction stress of a soil using an in situ method. A technique is proposed for determining the pre-compaction stress of soil based on a plate sinkage test. Trials were carried out to validate the technique in a soil bin as well as on field soils . The technique proved somewhat cumbersome and for this reason prediction of pre-compaction stress from easily determined soil properties is also investigated.

3.1 Introduction

The importance of pre-compaction stress has been discussed in the introductory part of this work. A pre-compacted soil will largely resist further mechanical loading until that loading exceeds the initial pre-compaction stress. In order to minimise further compaction of soil during agricultural operations, it is desirable to limit soil loading to below the pre-compaction stress of the soil (Koolen 1982).

In the past, pre-compaction stress has been determined using consolidation (Casagrande 1936, Horn 1981, Burmister 1951 and Schmertmann 1953) and confined compression (Koolen 1982) tests. Other researchers, such as Cordier (1983), Schmid (1980), Lebert et al (1987) and Konijn (1978) examined the influence of soil properties on pre-compaction stress. In all cases, soil samples were removed from the field and loaded in the laboratory. However, as pointed out in section 1.2, this practice increases margins of error through deformation during sampling and unknown amounts of swelling of the sample prior to testing. In order to avoid such problems, a plate sinkage test was used for in situ determination of pre-compaction stress.

3.2 Stress-strain relationship of a soil obtained from a plate sinkage test

Typical plate sinkage test results from field soils and the soil bin are presented in *Figures 3.1* and *3.2*.

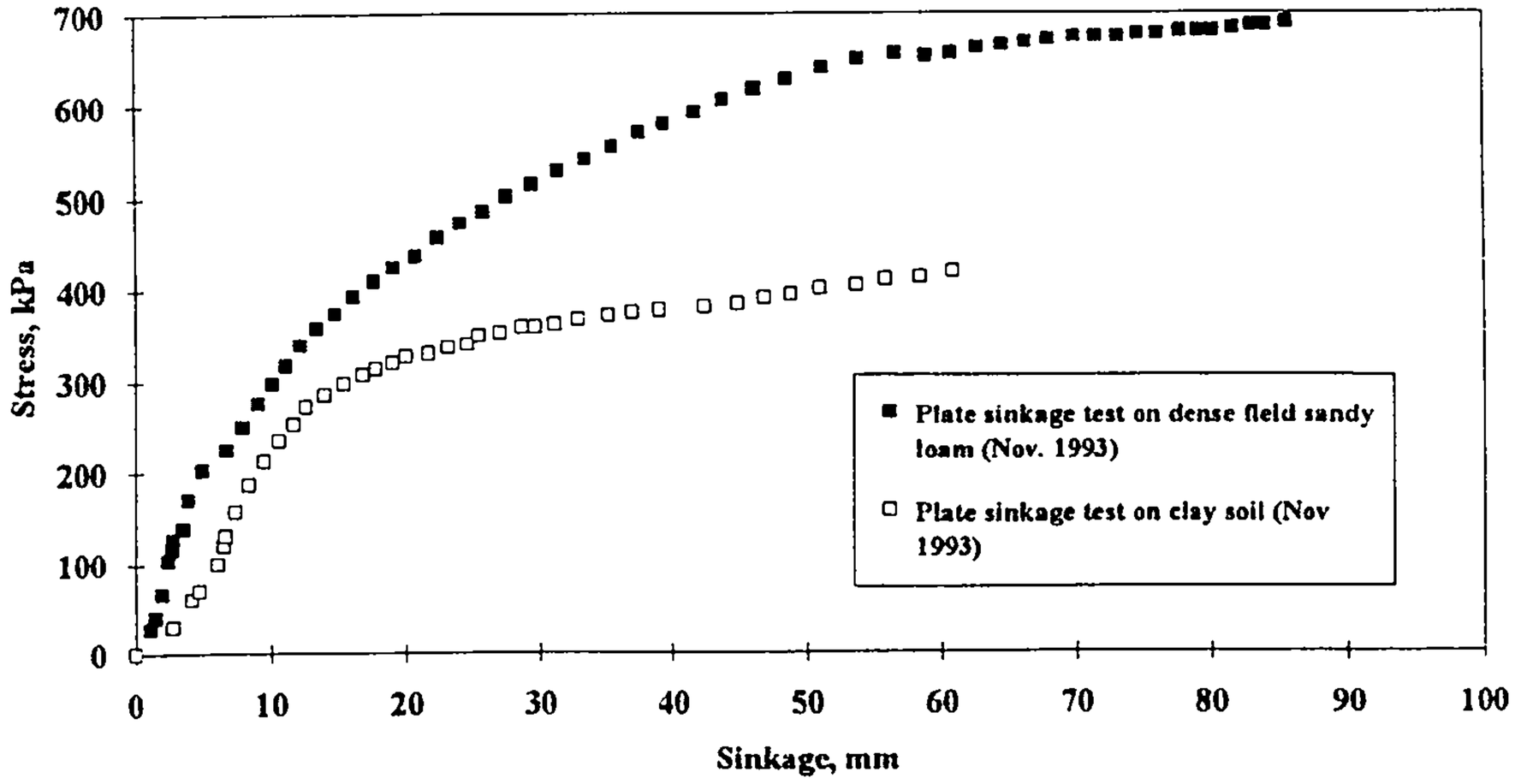

Figure 3.1. Typical stress-sinkage curve obtained from plate sinkage tests on field soils.

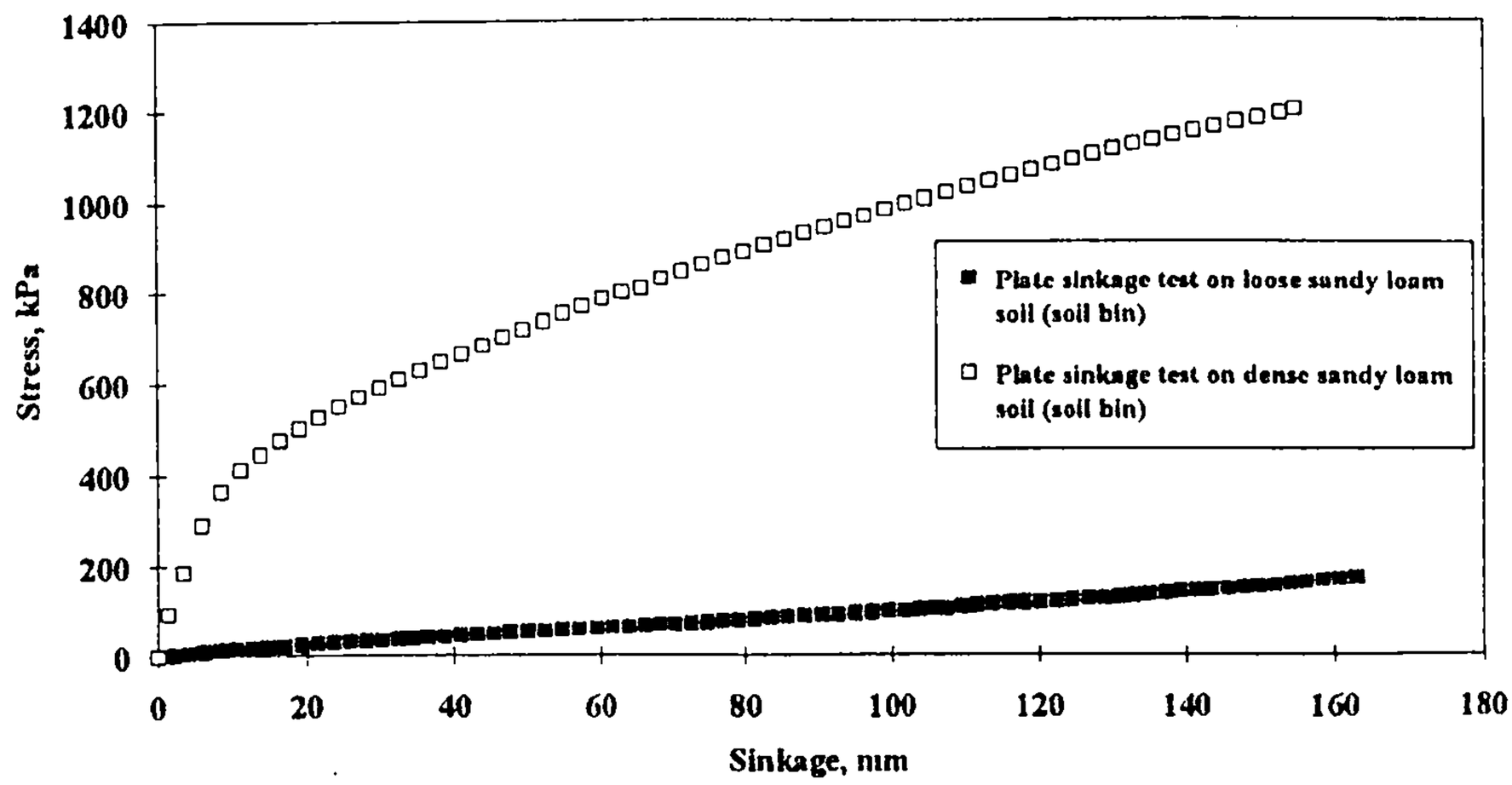

Figure 3.2. Typical stress-sinkage curve obtained from plate sinkage tests on sandy loam (bin soil).

The stress-sinkage relationship obtained from plate sinkage tests on loose sandy soil can be approximated by a straight line, however, this is not the case with denser soil. The difference in stress-sinkage characteristics can be attributed to the packing state of the soils. Grains of a sand in a loose state tend to slide with respect to each other and to assume a more closely packed position under the application of a load (Terzaghi and Peck 1967), whilst in the case of denser sandy soil this cannot be the case because they are already interlocked and continue to resist deformation until the applied load exceeds a certain limit when the grains are forced out of position, resulting in different stress-sinkage relationships.

Typical stress-sinkage relationships obtained from plate sinkage tests on clay soil (dense and loose) follows similar patterns to that of dense sandy loam soil (*Figure 3.1*).

3.3 In situ determination of pre-compaction stress

3.3.1 Experimental procedure

Initial tests were conducted on a sandy loam soil, under controlled conditions, in the soil bin. The results of the mechanical analysis of the soil are presented in *Table 2.1*. The soil was prepared uniformly throughout its depth to given bulk density and water content specifications using the carrier's tools. Initial dry bulk densities ranged from 1.28 to 1.55 Mg/m^3 with volumetric water content from 9.8 to 21.9 %. In total, 24 different preparations of dry bulk density and water content were prepared.

The soil was loaded, unloaded and then reloaded, using plate sinkage tests described in section 2.2.3. The maximum load applied during the first loading operation (pre-compaction load) was chosen arbitrarily.

A Deutz Intrac 2004 tractor (*Figure 2.3*) was adapted to carry out the procedure in the field. Field experiments were conducted at the Silsoe College Farm on two sites which had been fallow for a year. A summary of the mechanical properties of the two field soils used is presented in *Tables 2.2* and *2.3*. Both the topsoil and the subsoil were tested to increase the range of conditions encountered. For the clay and sandy loam soils the initial dry bulk density ranged from 1.00 to 1.36 Mg/m^3

and 1.30 to 1.50 Mg/m^3 respectively. A total of 16 tests were carried out at each site.

Tests were conducted at a penetration velocity of approximately 10 mm/s with vertical force and sinkage logged every 0.1 s.

All field trials were subjected to the same procedure developed in the soil bin.

3.3.2 Method development

A typical stress-strain relationship, obtained from a plate sinkage test in the soil bin and field soils, is presented in *Figure 3.3*. The soil was loaded to represent pre-compacted conditions, unloaded and then reloaded. During the reloading operation, the lower portion of the curve (RL) can be considered to be a recompression curve. The upper portion of this curve can be assumed to be a continuation of the previous compression line (PCL). Schmertmann (1953) defined initial slope as the slope of a straight line drawn through the points which fall on the linear portion of the curve. A similar procedure was adopted for this study. By extending the recompression (RL) and the previous compression (PCL) lines, the point of intersection C can be determined. The stress at this point can be considered to be the pre-compaction stress prior to the second loading, and the sinkage is the maximum allowable for a particular soil if restricted compaction is to be achieved.

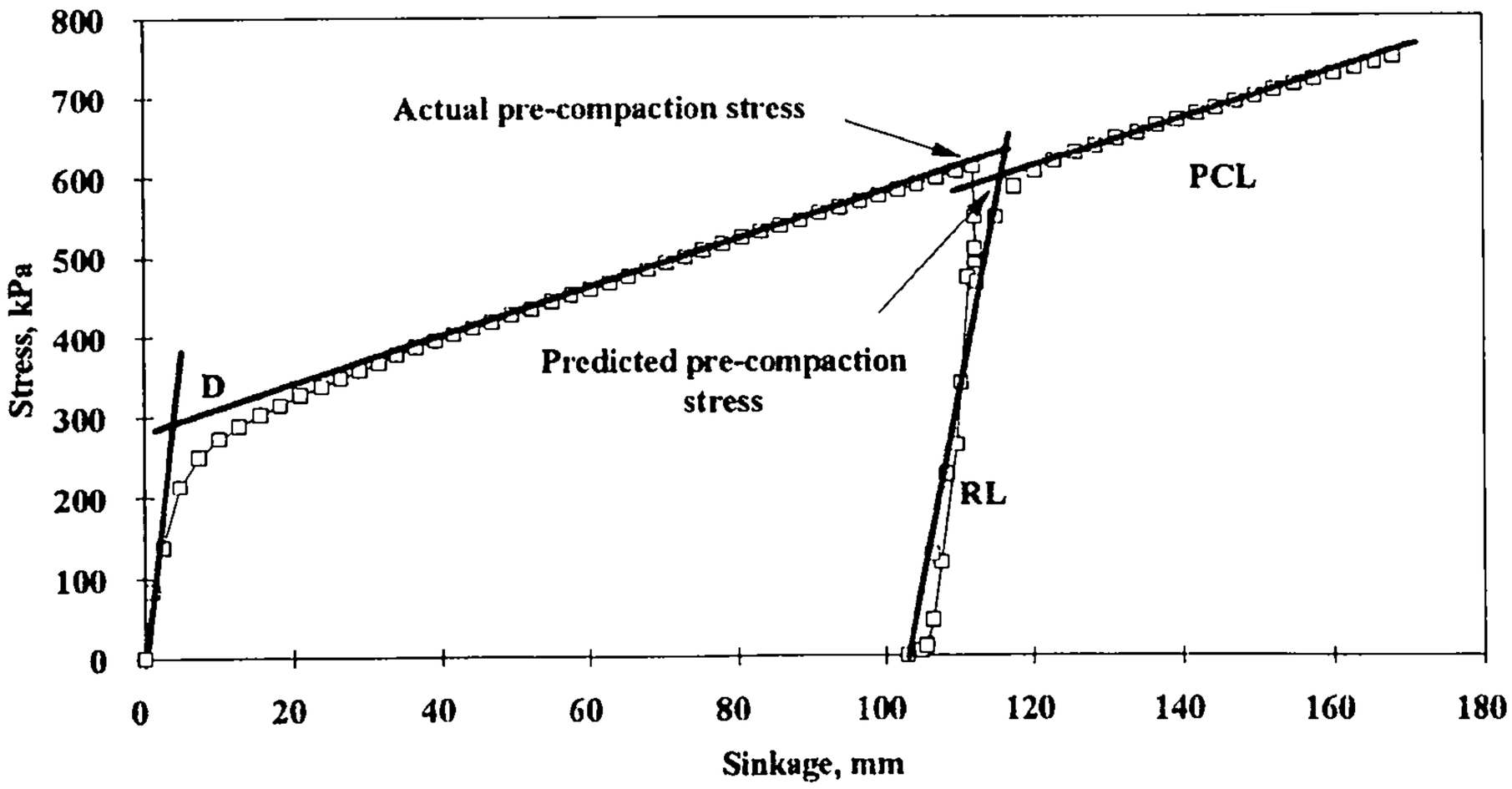

Figure 3.3. Typical results from a plate sinkage test carried out on the soil bin.

A slight difference in the predicted, with respect to the actual, pre-compaction stress is evident. Casagrande (1936) also encountered a similar phenomenon and suggested that it was due to a partial breakdown of the internal structure of the soil.

This technique can be applied to the initial portion of the virgin compression line, as illustrated in *Figure 3.3*, to determine the pre-compaction stress prior to loading in the laboratory i.e. point D. When determining the pre-compaction stress of a soil using this technique, it is essential that the load applied to the soil is well in excess of that at the 'elbow' in the curve, so that the linear portion can be drawn. The accuracy of this technique for a particular soil is somewhat dependent on the shape of the stress-strain curve. Pre-compaction stress will be better predicted from curves where the slope of the upper portion is near horizontal. There might be cases where this slope is steep and therefore results may not be as accurate as those encountered during this study.

A similar procedure was followed for the determination of pre-compaction stress in field conditions (*Figures 3.4 and 3.5*).

In the case of loose sandy loam soil, where the stress-strain relationship of the soil can be approximated by a straight line, the soil has not been compacted and consequently its pre-compaction stress is expected to be very low (identified as zero when using this technique (*Figure 3.5*)).

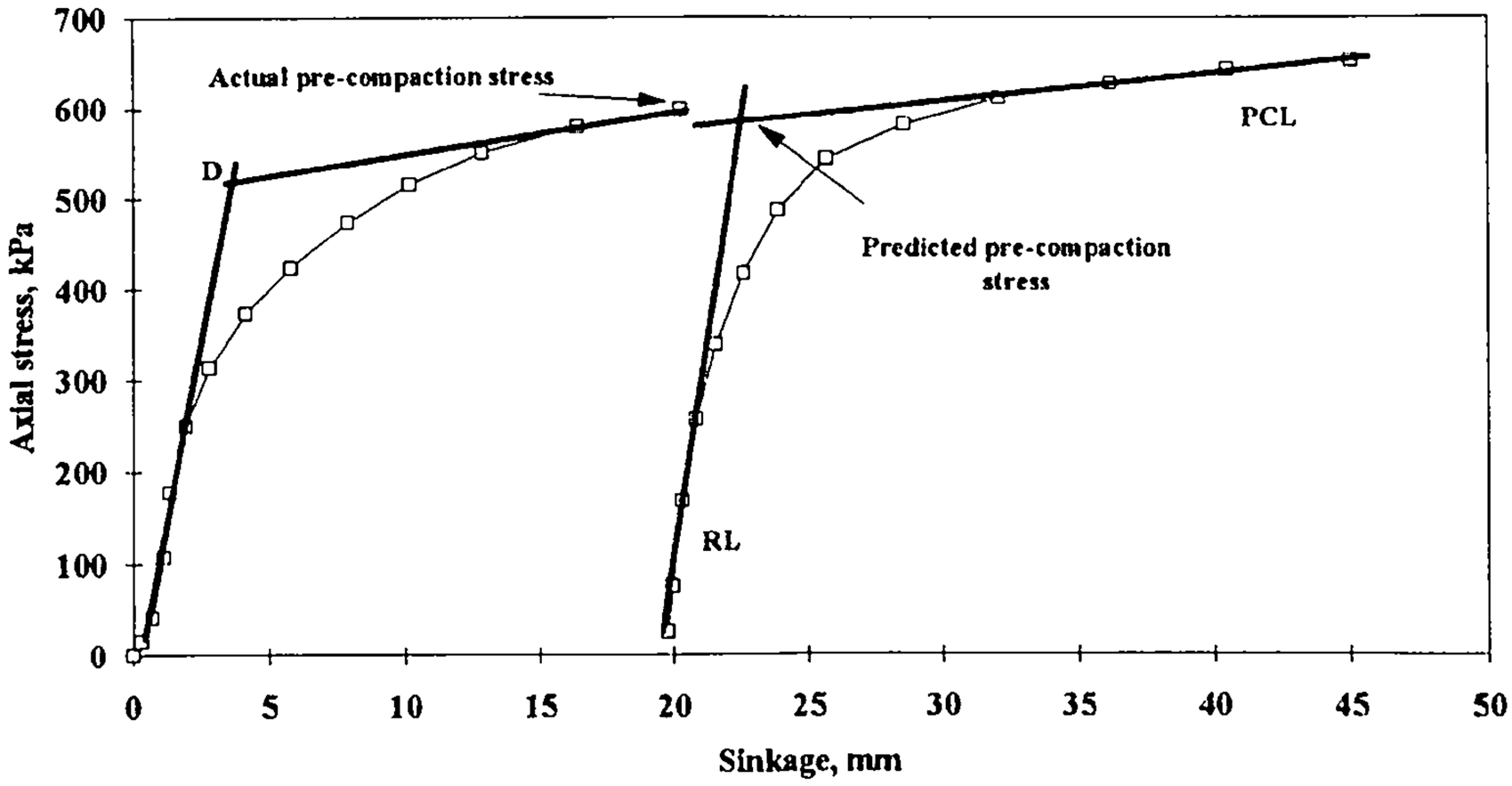

Figure 3.4. Typical results from a plate sinkage test carried out on field clay soil.

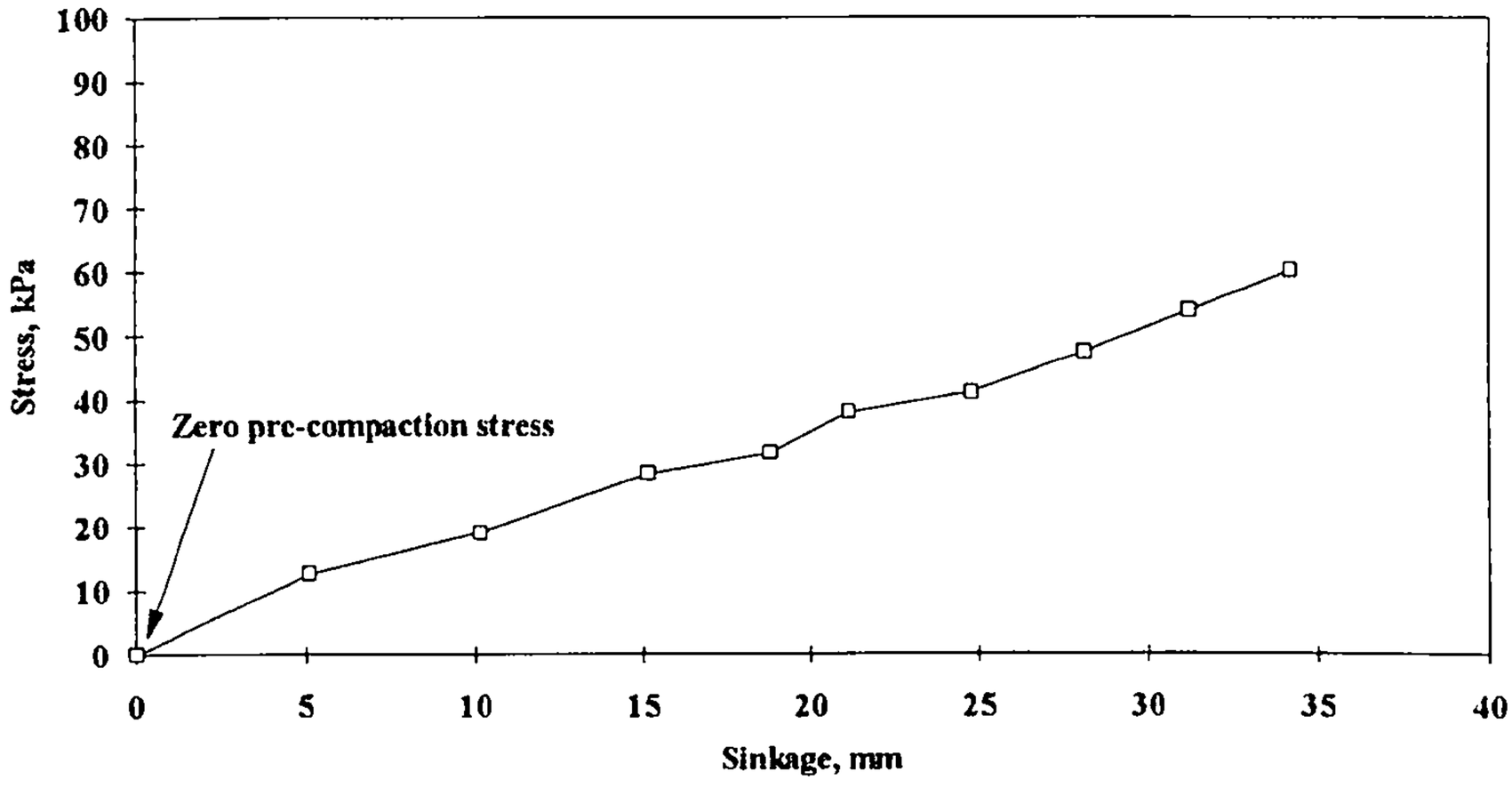

Figure 3.5. Typical results from a plate sinkage test carried out on loose field sandy loam soil.

3.3.3 Results and discussion

3.3.3.1 Soil bin trials

The results of all tests conducted in the soil bin are presented in *Table 3.1* and *Figure 3.6*. Statistical analysis of the data shows that this method can predict pre-

compaction stress with a high degree of accuracy. The relationship can be approximated by the equation:-

$$Predicted = -2.60 + 0.99\ actual \qquad (3.1)$$

which is slightly biased (when x=0 y=-2.596) but highly significant with a coefficient of determination (R^2) of 0.99.

Table 3.1

Values obtained from plate sinkage tests on sandy loam soil (soil bin)

Actual pre-compaction stress (kPa)	Predicted pre-compaction stress (kPa)
611.14	582.55
1200.00	1184.26
1197.69	1194.21
909.75	870.33
853.00	852.02
995.55	984.83
571.75	562.42
521.08	520.10
708.00	691.31
605.30	603.70
618.15	603.94
421.85	408.02
437.04	432.10
453.40	430.20
621.77	617.90
617.00	581.44
368.50	360.18
446.00	438.77
330.66	329.94
348.41	347.20
331.84	328.37
285.70	283.59
296.34	296.26
279.77	276.27

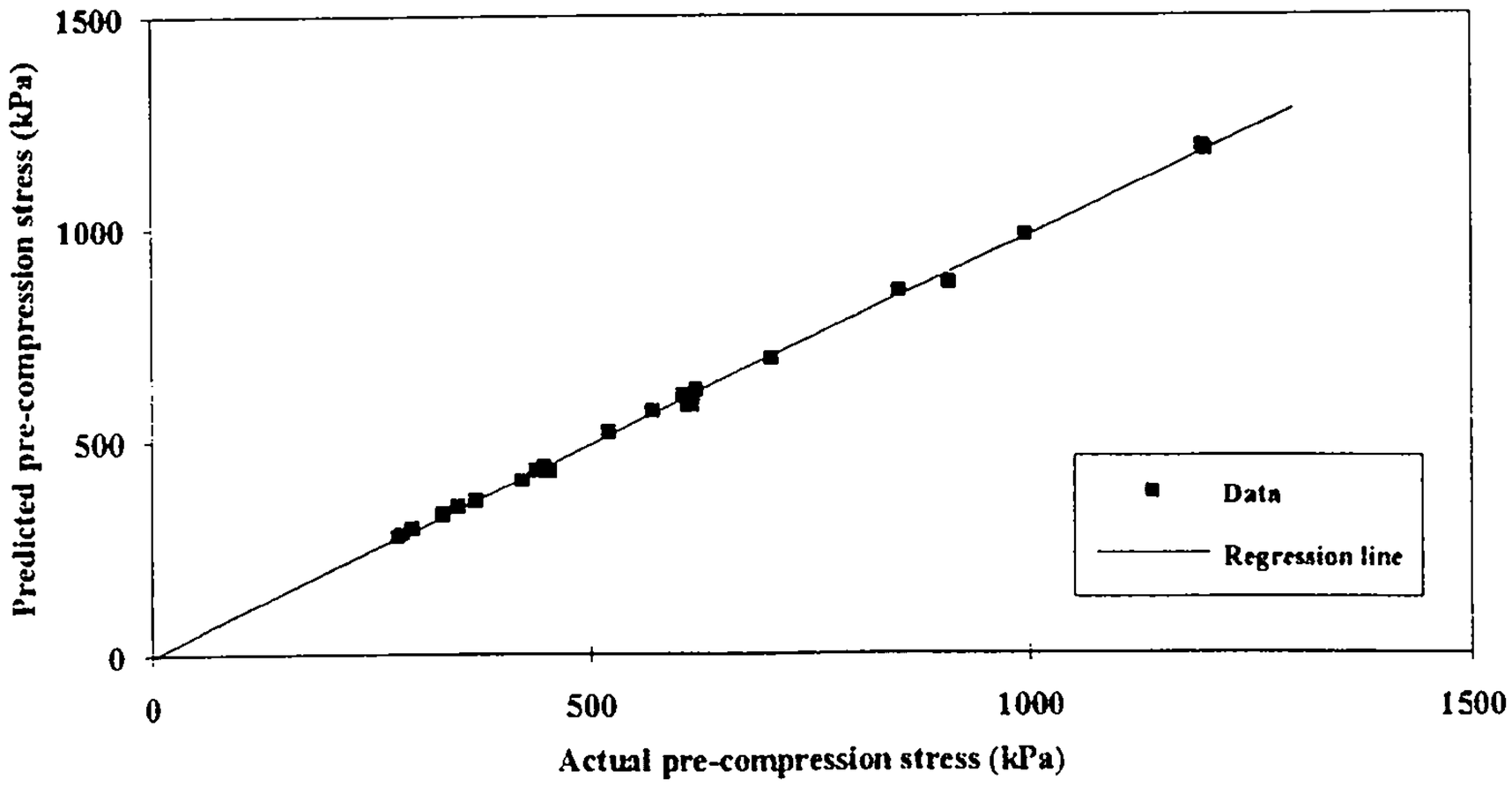

Figure 3.6. Predicted versus actual values of pre-compaction stress determined during soil bin experiments.

3.3.3.2 Field trials

A summary of data from the sandy loam and clay sites are presented in *Tables 3.2* and *3.3*, and in *Figures 3.7* and *3.8*. In both cases, the relationships are highly significant but slightly biased with coefficients of determination (R^2) 0.99 for sandy loam soil and 0.98 in the case of clay soil.

In the case of sandy loam soil the relationship can be approximated by the following equation:-

$$Predicted = -10.77 + 0.99\ actual \qquad (3.2)$$

whilst for clay soil with:-

$$Predicted = 6.12 + 0.94\ actual \qquad (3.3)$$

Table 3.2

Values obtained from plate sinkage tests on field sandy loam soil

Actual pre-compaction stress (kPa)	Predicted pre-compaction stress (kPa)
525.40	520.47
484.24	479.61
683.60	657.37
72.80	62.38
91.91	82.31
91.80	79.72
132.93	118.50
60.13	41.32
65.13	62.32
370.25	363.50
450.00	440.72
573.87	558.38
395.62	383.91
398.00	377.65
408.30	366.10
509.00	506.31

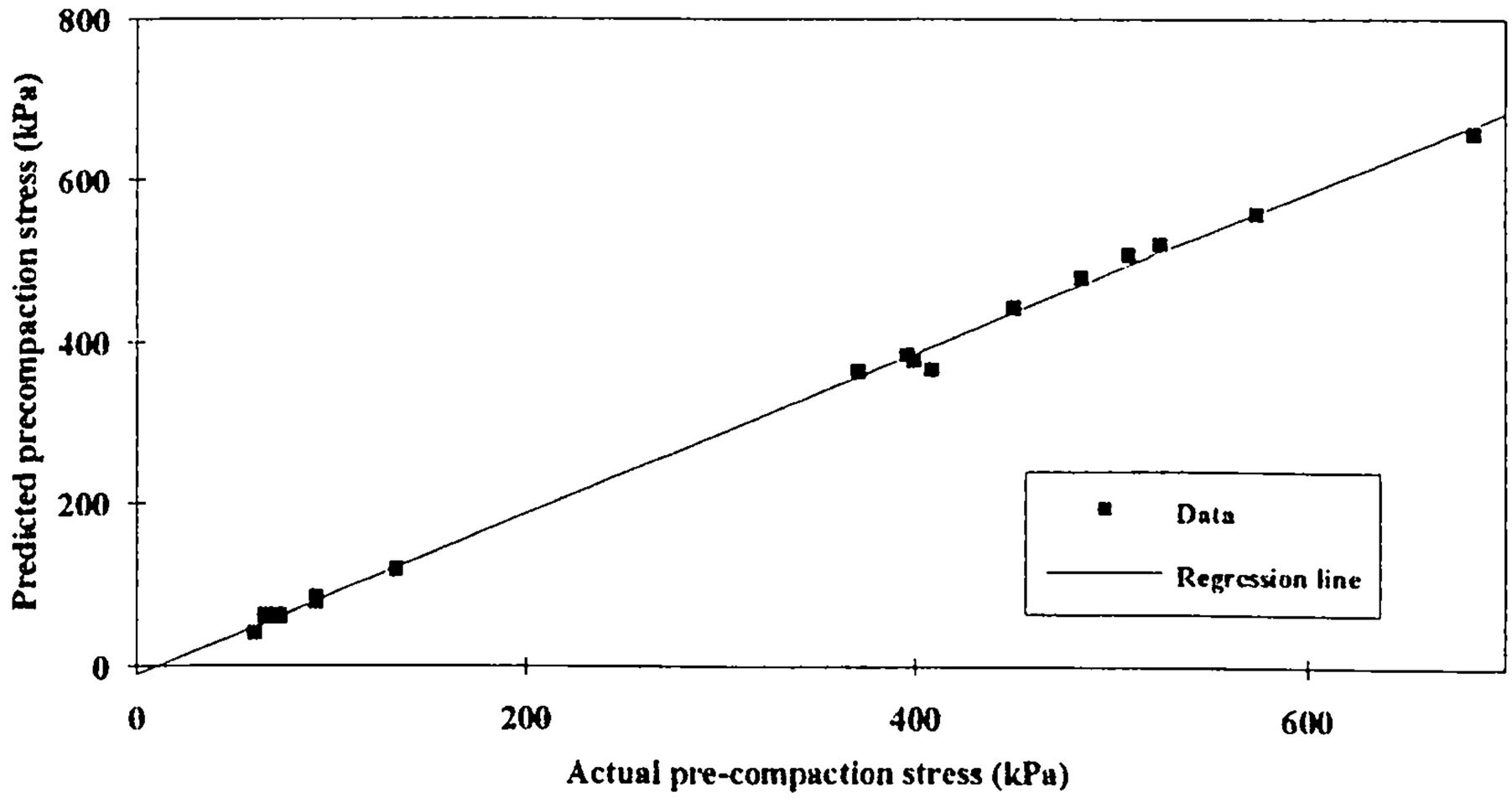

Figure 3.7. Predicted versus actual values of pre-compaction stress determined during field experiments at the sandy site.

Table 3.3

Values obtained from plate sinkage tests on field clay soil

Actual pre-compaction stress (kPa)	Predicted pre-compaction stress (kPa)
583.76	572.86
422.70	411.00
661.48	624.80
630.00	609.23
589.00	562.76
246.90	235.47
266.00	242.40
420.09	403.47
642.50	611.32
658.30	581.70
338.65	337.75
598.18	586.14
465.25	444.33
354.00	331.50
443.10	429.16
500.00	446.11

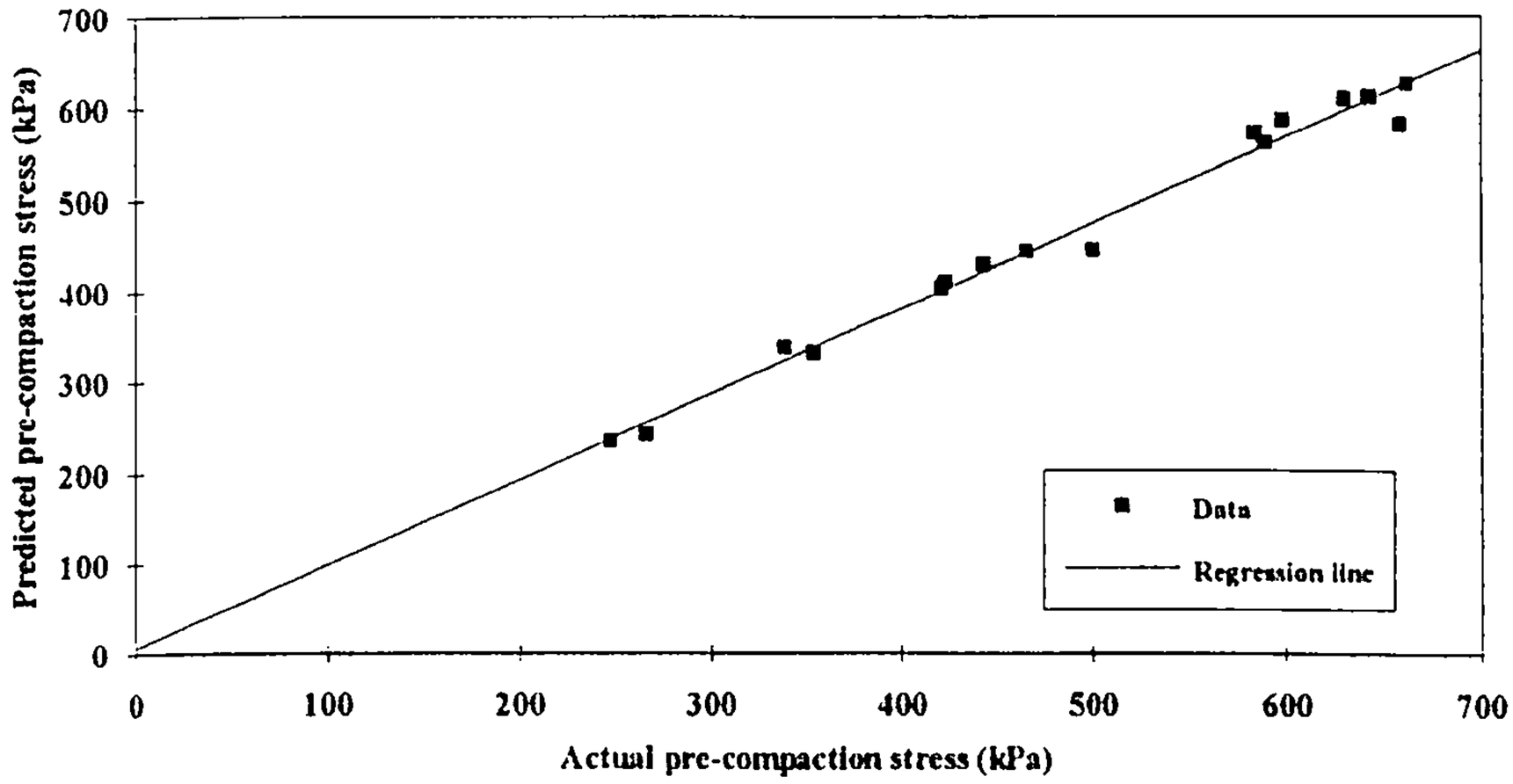

Figure 3.8. Predicted versus actual values of pre-compaction stress determined during field experiments at the clay site.

The above mentioned technique proved capable of predicting the pre-compaction stress of field as well as soil bin soils. Since the determination of pre-compaction stress is a somewhat cumbersome and time consuming procedure, its prediction from easily determined soil properties is desirable. For this reason, further experimentation took place to investigate the relationship between various soil properties and pre-compaction stress.

3.4 Relationship between pre-compaction stress and other soil properties

Pre-compaction stress of a soil is expected to be dependent on cohesive forces and frictional resistance and hence packing state and water content. For this reason soil properties related to the water content and packing state of soil were considered. Volumetric water content provides an insight into the soil mass in terms of volume of water whilst dry bulk density refers to the packing state of the soil. Void ratio and degree of saturation were also considered as they provide a measure of the pore space within the soil mass and can be readily determined (*Table 3.4*). The relationship between these properties and pre-compaction stress will be examined in the following paragraphs.

Table 3.4

Determination of soil properties

	Volumetric water content %	Void ratio (e)	Degree of saturation (Sr)
Formulae	WC_v = Dry bulk density · Gravimetric water content	$\frac{\text{Particle density}}{\text{Dry bulk density}} - 1$	$\frac{\text{Particle density}}{\text{Density of water}} \cdot \frac{\text{Gravimetric water content \%}}{\text{Void ratio}}$

3.4.1 Experimental results

Results from pre-compaction tests carried out in the soil bin and on the field soils are presented in *Tables 3.5, 3.6* and *3.7*.

Table 3.5

Pre-compaction stress experimental results for the soil bin sandy loam soil

Volumetric water content %	Dry bulk density (Mg/m^3)	Void ratio	Degree of saturation	Pre-compaction stress (kPa)
12.78	1.40	0.85	0.27	289.80
12.42	1.41	0.84	0.28	453.85
12.79	1.40	0.85	0.28	391.38
12.91	1.41	0.89	0.27	221.42
13.00	1.41	0.87	0.27	190.00
15.17	1.43	0.84	0.32	362.64
13.48	1.42	0.83	0.29	407.00
20.38	1.42	0.67	0.46	161.06
20.45	1.43	0.68	0.47	160.18
21.89	1.43	0.71	0.50	188.50
14.21	1.45	0.80	0.32	400.27
15.38	1.45	0.75	0.37	330.90
14.55	1.50	0.74	0.34	448.10
14.75	1.49	0.73	0.35	397.02
13.95	1.51	0.72	0.33	437.20
19.22	1.55	0.68	0.47	338.42
20.65	1.50	0.71	0.50	275.08
19.14	1.55	0.65	0.46	351.68
15.98	1.47	0.76	0.37	340.78
14.89	1.47	0.77	0.34	449.80
13.43	1.37	0.90	0.28	163.98
13.39	1.38	0.89	0.28	240.18
12.11	1.35	0.93	0.25	303.00
11.14	1.29	1.02	0.22	109.45
11.18	1.30	1.00	0.22	116.15
10.61	1.31	0.97	0.21	114.56
11.73	1.33	0.95	0.24	159.77
9.79	1.13	1.29	0.17	0
10.08	1.20	1.15	0.19	0
10.11	1.15	1.26	0.18	0
12.79	1.17	1.21	0.23	0
15.23	1.18	1.19	0.28	0
14.00	1.17	1.22	0.25	0
18.04	1.23	1.11	0.34	0
18.31	1.26	1.06	0.35	0
17.86	1.23	1.10	0.34	0

Table 3.6

Pre-compaction stress experimental results for the field sandy loam soil

Volumetric water content %	Dry bulk density (Mg/m^3)	Void ratio	Degree of saturation	Pre-compaction stress (kPa)
16.96	1.49	0.79	0.38	558.90
14.42	1.40	0.91	0.30	580.36
16.49	1.46	0.83	0.36	532.30
16.92	1.41	0.88	0.36	336.36
16.43	1.47	0.86	0.37	387.23
10.22	1.41	0.86	0.22	596.81
10.42	1.42	0.86	0.22	620.00
10.15	1.41	0.87	0.22	643.00
18.63	1.21	1.19	0.34	0
13.80	1.22	1.18	0.26	0
15.08	1.30	1.03	0.30	0
13.47	1.22	1.17	0.25	0
17.62	1.25	1.12	0.34	0
17.92	1.28	1.06	0.35	0
19.84	1.28	1.08	0.38	0
17.98	1.24	1.15	0.33	0
14.96	1.38	0.91	0.31	372.34
21.15	1.33	0.99	0.42	30.02

Table 3.7

Pre-compaction stress experimental results for the field clay soil

Volumetric water content %	Dry bulk density (Mg/m^3)	Void ratio	Degree of saturation	Pre-compaction stress (kPa)
51.55	1.02	1.60	0.84	171.00
46.53	0.99	1.65	0.75	168.62
50.66	1.05	1.51	0.85	242.30
41.56	0.99	1.68	0.65	330.52
38.43	1.05	1.53	0.62	549.80
39.96	1.08	1.45	0.67	354.83
32.95	1.07	1.47	0.55	614.34
31.97	1.06	1.49	0.53	611.40
25.06	1.00	1.67	0.39	653.82
31.66	1.12	1.37	0.54	596.71
46.16	1.23	1.15	0.86	332.62
46.50	1.25	1.13	0.84	295.63
44.70	1.24	1.14	0.85	241.18
40.64	1.28	1.07	0.79	275.06
40.87	1.33	0.99	0.82	392.96
42.16	1.36	0.94	0.88	282.35
43.78	1.32	1.00	0.89	545.18
43.16	1.30	1.04	0.86	572.83
40.63	1.35	0.96	0.83	341.51
42.08	1.34	0.98	0.86	345.40

In the case of loose sandy loam soil, for both cases (soil bin and field), the pre-compaction stress is zero i.e. the soil had not undergone compaction before the tests

were carried out. For these soils, pre-compaction stress is zero when the initial dry bulk density is at around 1.30 Mg/m^3 or less.

3.4.2 Pre-compaction stress, volumetric water content and initial dry bulk density

3.4.2.1 Sandy loam soil

The relationship between pre-compaction stress and initial dry bulk density for the soil bin sandy loam at a given volumetric water content is presented in *Figure 3.9*. It is generally expected that pre-compaction stress for a sandy soil at a constant volumetric water content will increase with initial dry bulk density. This is due to the increased frictional resistance for denser soil. On the other hand, at constant initial dry bulk density, pre-compaction stress should decrease with volumetric water content since bonds which connect the soil crystals are weakened as a result of a reduction of the cohesive forces when more water is absorbed. An area of zero pre-compacted soil appears in *Figure 3.9*. This area has not been taken into account during the derivation of the relationships as soil within this area can be considered as to have undergone no pre-compaction or will have passed through a loosening process.

The data have been divided into categories according to their volumetric water content. This categorisation of data unavoidably increases the margin of error particularly close to boundaries. These categories were set at volumetric water contents of 9-12 %, 13-15 % and 19-22 %. As expected, for the soil bin sandy loam, pre-compaction stress increases with initial dry bulk density at similar volumetric water content, and decreases as volumetric water content increases at a constant dry bulk density. For the soil bin soil the derived equations are presented in *Table 3.8* and confidence intervals in *Figure 3.10*.

Table 3.8

Derived relationships for soil bin soil

Volumetric water content %	Derived equation	R^2	Significance
9-12	$\sigma_{pr} = -2632.44 + 2118.96 * D_B$	0.69	**
13-16	$\sigma_{pr} = -2269.11 + 1809.64 * D_B$	0.68	***
19-22	$\sigma_{pr} = -1856.96 + 1420.80 * D_B$	0.98	***

Where:-

ns = no significant relationship

* = significant at 5% level

** = significant at 1% level

*** = significant at 0.1% level

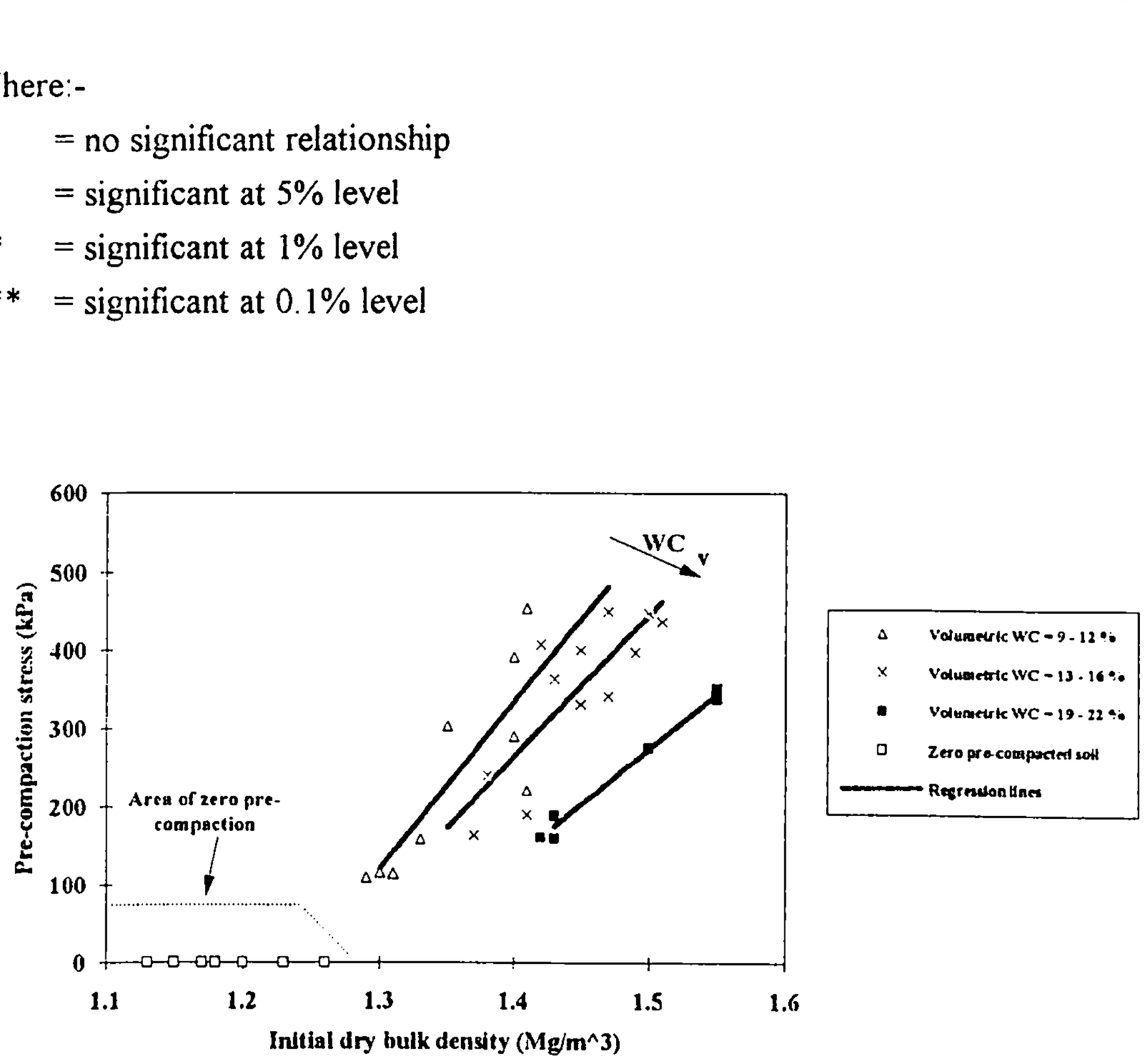

Figure 3.9. The relationship between pre-compaction stress, volumetric water content and initial dry bulk density for soil bin sandy loam.

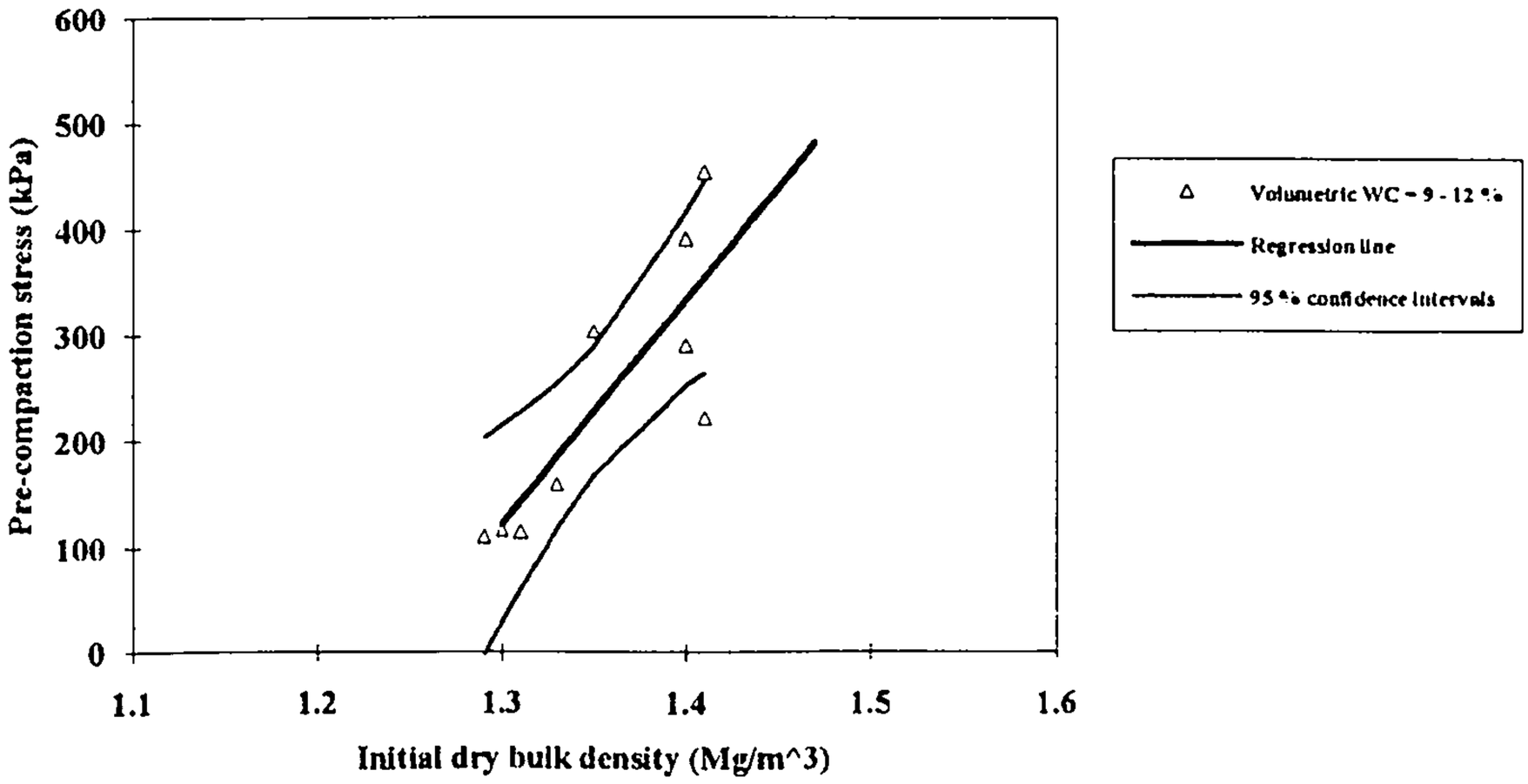
600
500
400
300
200
100
0
Pre-compaction stress (kPa)
1.1
1.2
1.3
1.4
1.5
1.6
Initial dry bulk density (Mg/m^3)
Volumetric WC = 9 - 12 %
Regression line
95 % confidence intervals

a)

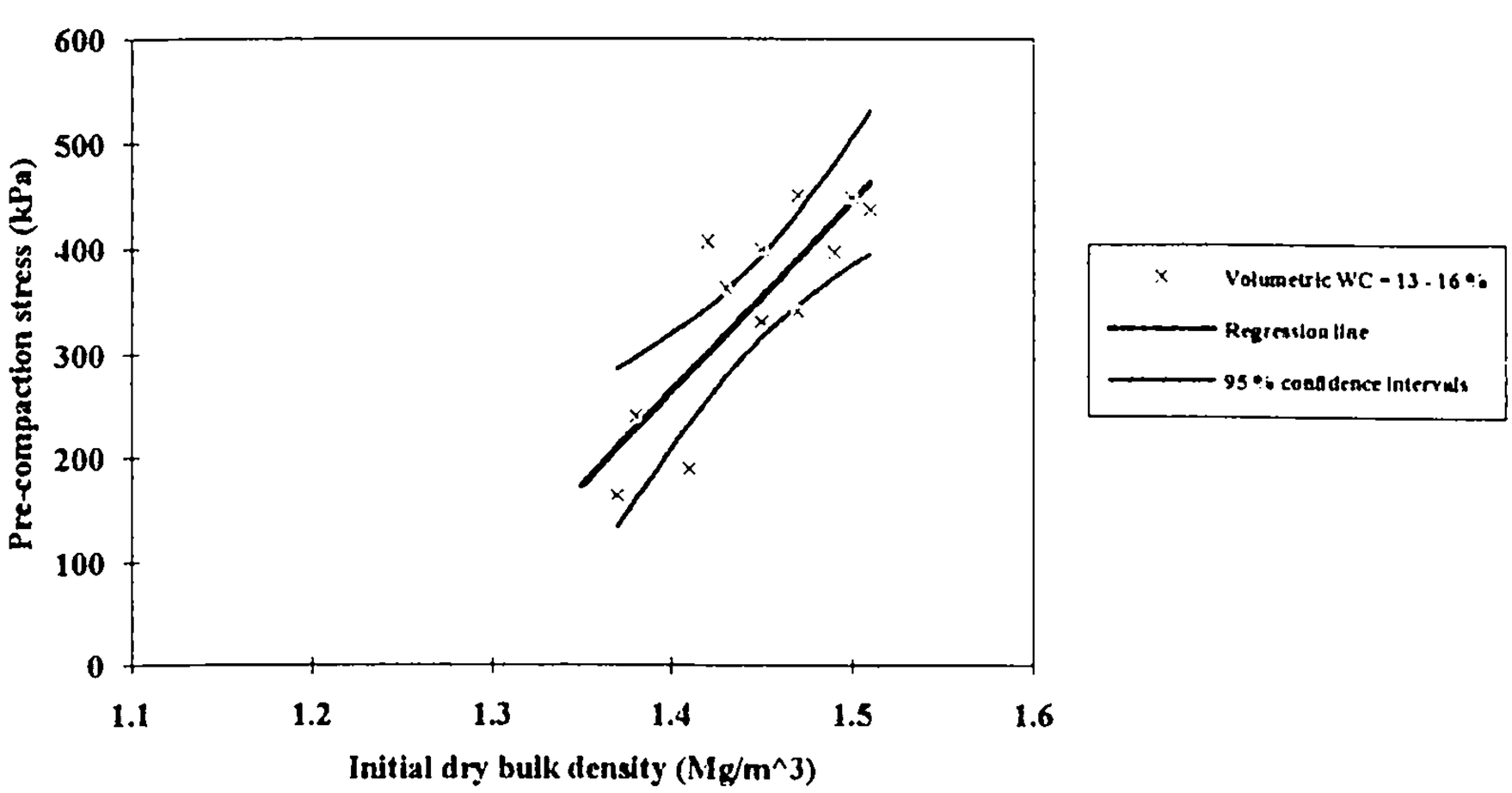
600
500
400
300
200
100
0
Pre-compaction stress (kPa)
1.1
1.2
1.3
1.4
1.5
1.6
Initial dry bulk density (Mg/m^3)
Volumetric WC = 13 - 16 %
Regression line
95 % confidence intervals

b)

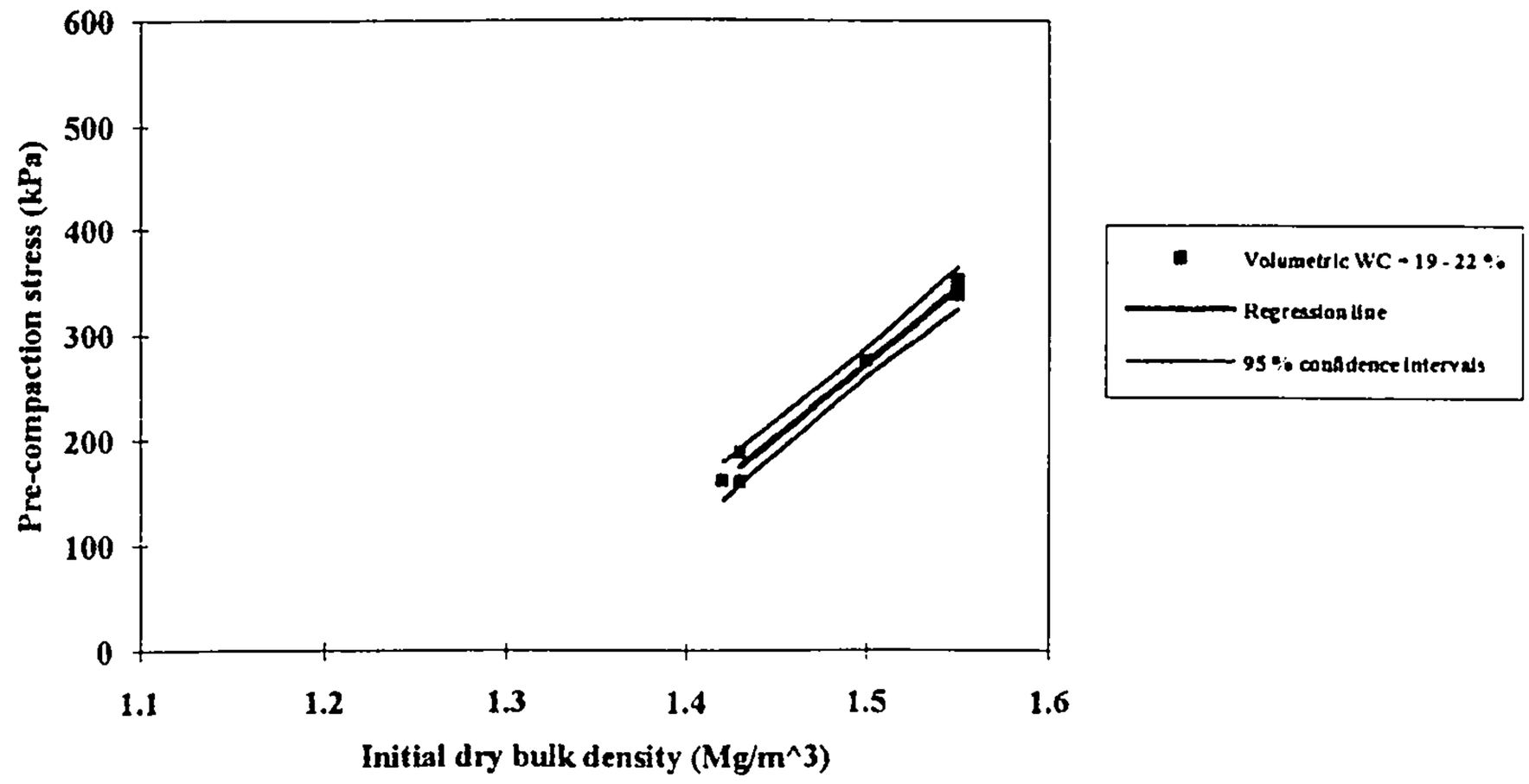

c)

Figure 3.10. The relationship between pre-compaction stress, volumetric water content and initial dry bulk density, with confidence intervals for soil bin sandy loam at volumetric water contents of: a) 9-12 %; b) 13-16 % and c) 19-22%.

The family of curves presented in *Figures 3.9* and *3.10* can be used for prediction purposes. The accuracy is greatly influenced by the selection of the water content categories.

The relationship between pre-compaction stress, volumetric water content and initial dry bulk density for the field sandy loam soil is presented in *Figure 3.11*. The relationships can be approximated by straight lines for data points outside the zero pre-compacted soil area but they are not statistically significant.

The selection of a wide range of volumetric water content (10-15%) was prompted by a lack of data. This, in conjunction with a lack of data to draw a relationship through, may be the reason why these relationships are not statistically significant. All the data within the zero pre-compaction area correspond to the topsoil with the exception of one data point.

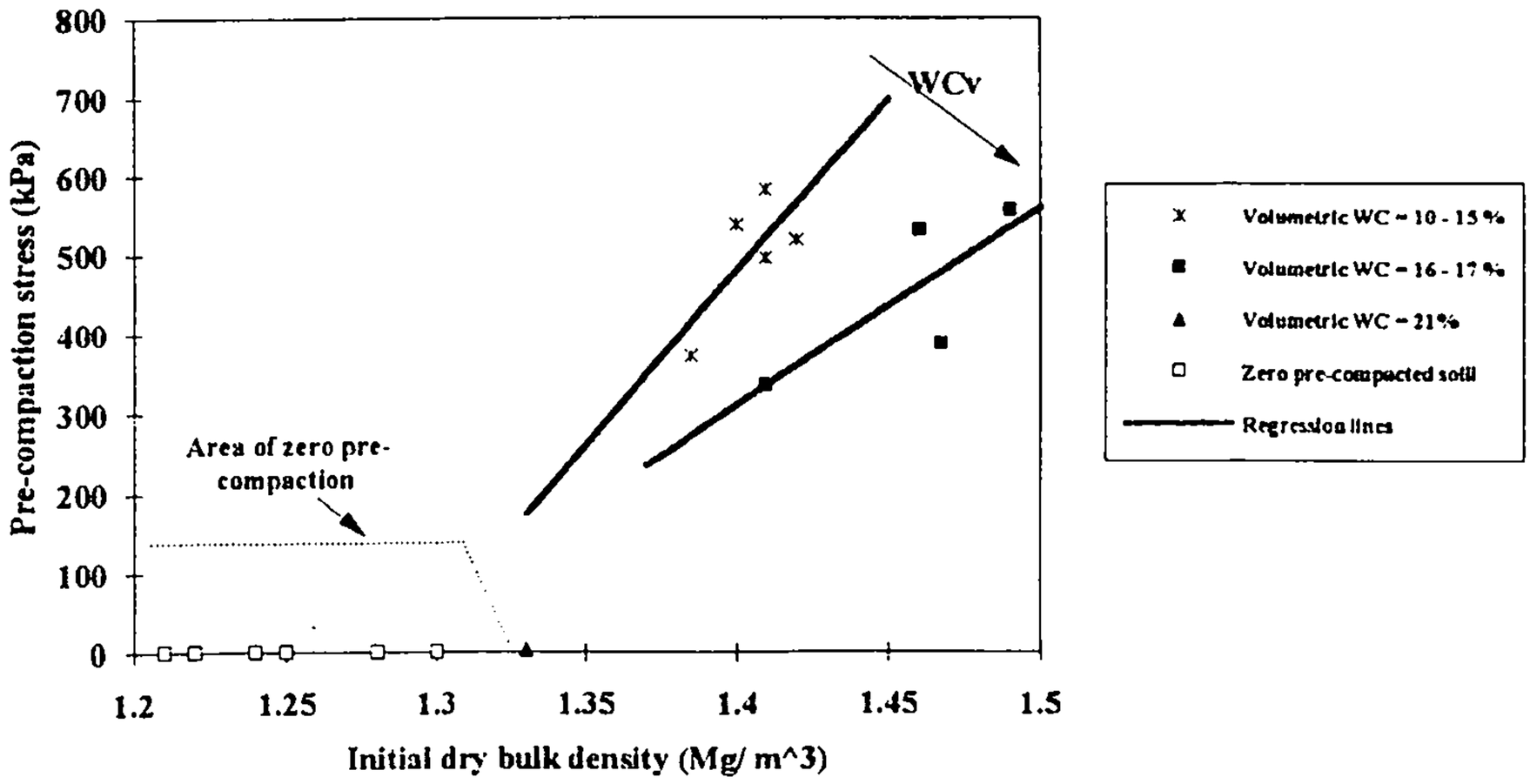

Figure 3.11. The relationship between pre-compaction stress, volumetric water content and initial dry bulk density for field sandy loam soil.

For data outside the loose soil area, there is no statistically significant relationship obtained for field sandy loam soil, although there is a tendency for pre-compaction stress to increase as initial dry bulk density increases.

3.4.2.2 Clay soil

In the case of clay soil, the data have been divided into six categories. Such a division was prompted by the wide range of data encountered during this work. The results are presented in *Figure 3.12*. The relationships are not statistically significant possibly due to a reduced range of data available and also due to the dominance of cohesive forces in clay soil.

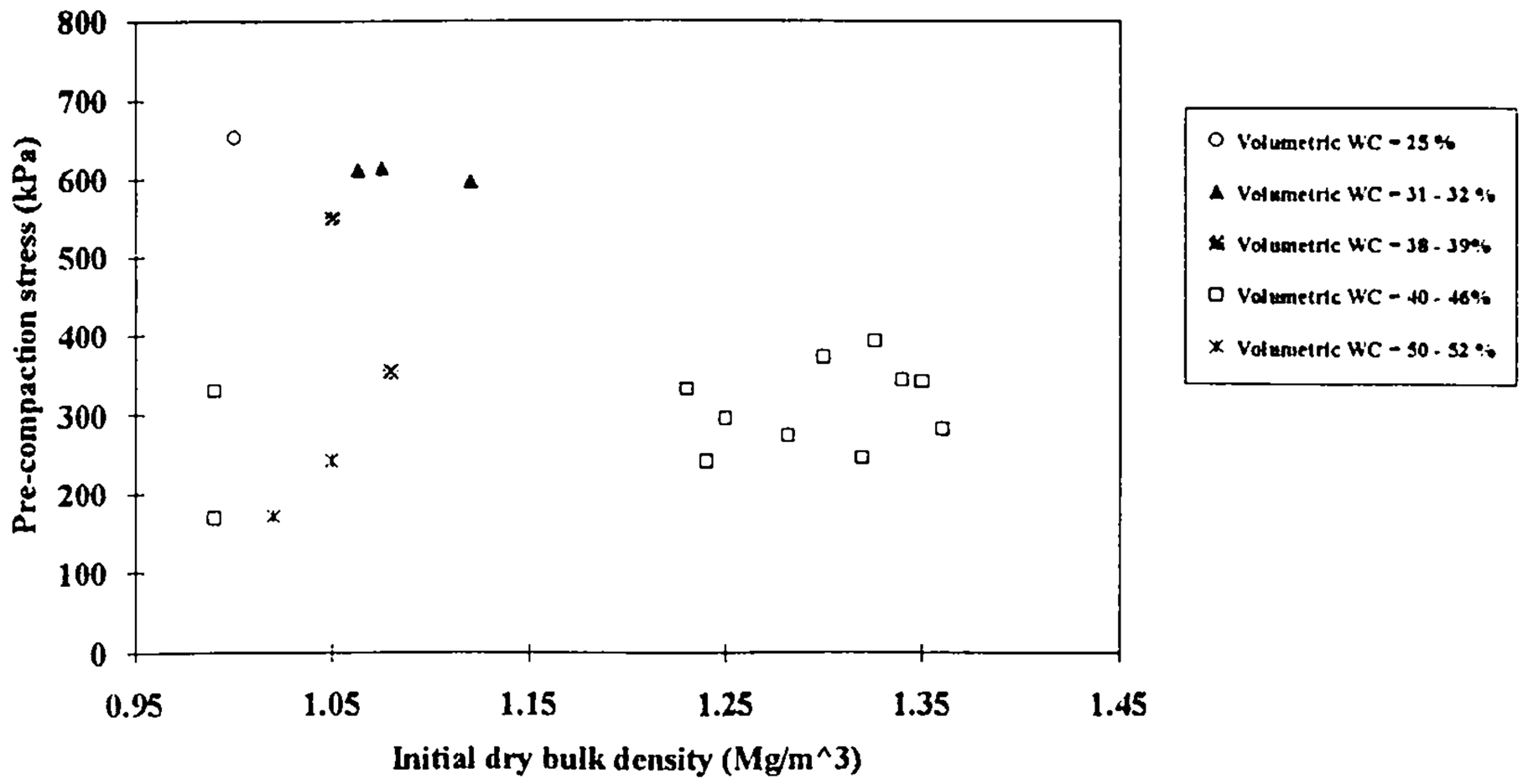

Figure 3.12. The relationship between pre-compaction stress, volumetric water content and initial dry bulk density for field clay soil.

The data were re-analysed to investigate the relationship between pre-compaction stress and volumetric water content for given dry bulk density and results are presented in *Figure 3.13*. The relationship for all data can be approximated by the equation:-

$$\sigma_{pr} = 1236.12 - 21.08 \cdot WC_v \qquad (3.1)$$

with coefficient of determination $R^2 = 0.83$ ***.

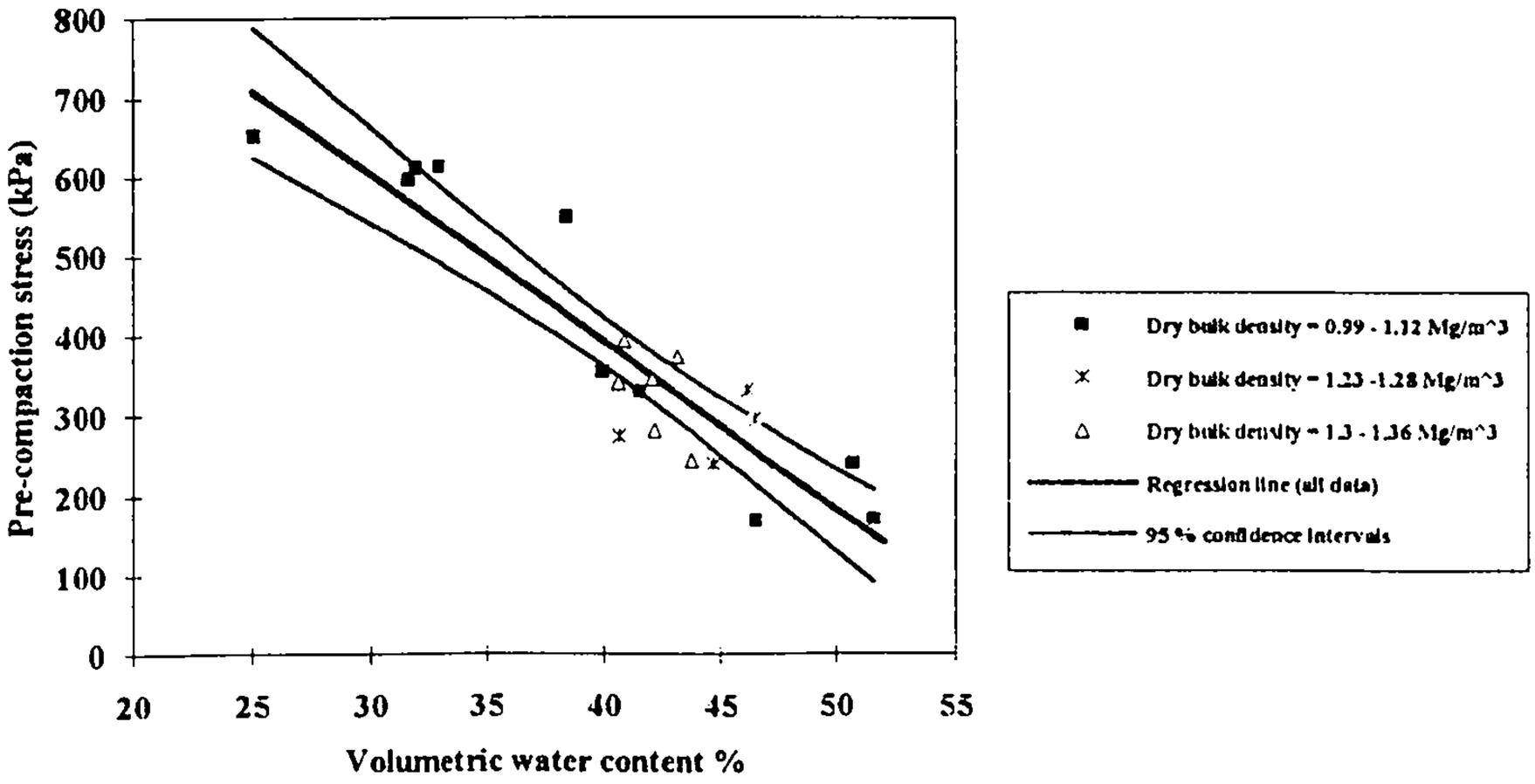

Figure 3.13. The relationship between pre-compaction stress, initial dry bulk density and volumetric water content for field clay soil.

The value of pre-compaction stress in the case of clay soil decreases as volumetric water content increases. This leads to the conclusion that for clay soil pre-compaction stress greatly depends on the cohesive forces. For the clay soil *Figure 3.13* and equation 3.2 can be used for prediction purposes with good accuracy.

3.4.3 Pre-compaction stress, void ratio and degree of saturation

3.4.3.1 Sandy loam soil

The relationship between void ratio and pre-compaction stress for the soil bin sandy loam soil is presented in *Figure 3.14*. The data have been divided into the same categories used in the previous section. It is generally expected for the sandy soil that pre-compaction stress will increase as void ratio decreases, since soil becomes denser and this is the case with soil bin sandy loam. For data outside the zero pre-compacted soil region, the derived relationships are presented in *Table 3.9*.

Table 3.9

Derived relationships for soil bin soil

Volumetric water content %	Derived equation	R^2	Significance
9-12	$\sigma_{pr} = 1799.43 - 1691.84 * e$	0.79	**
13-16	$\sigma_{pr} = 1319.07 - 1214.43 * e$	0.64	**
19-22	No statistically significant relationship		

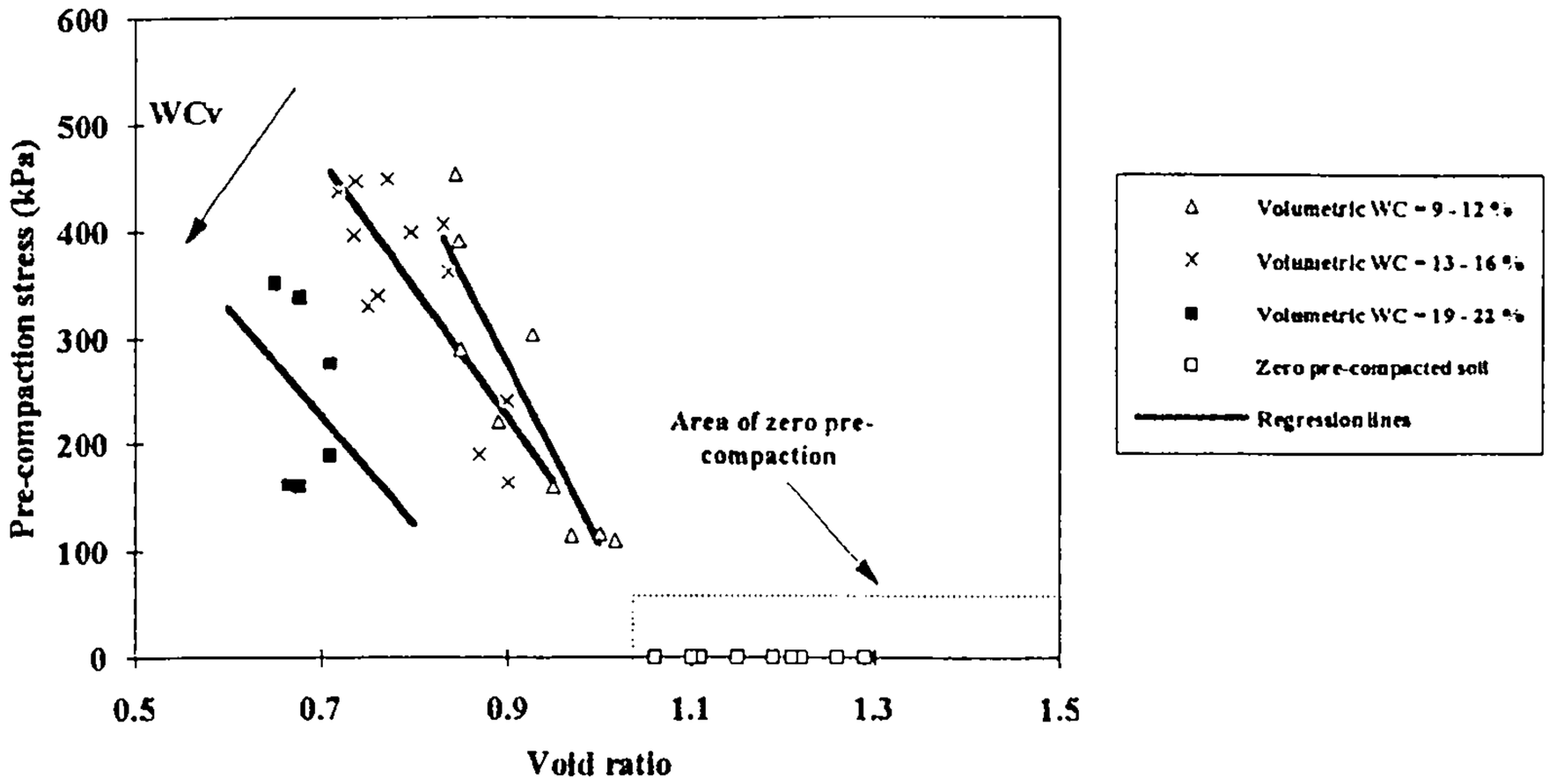

a)

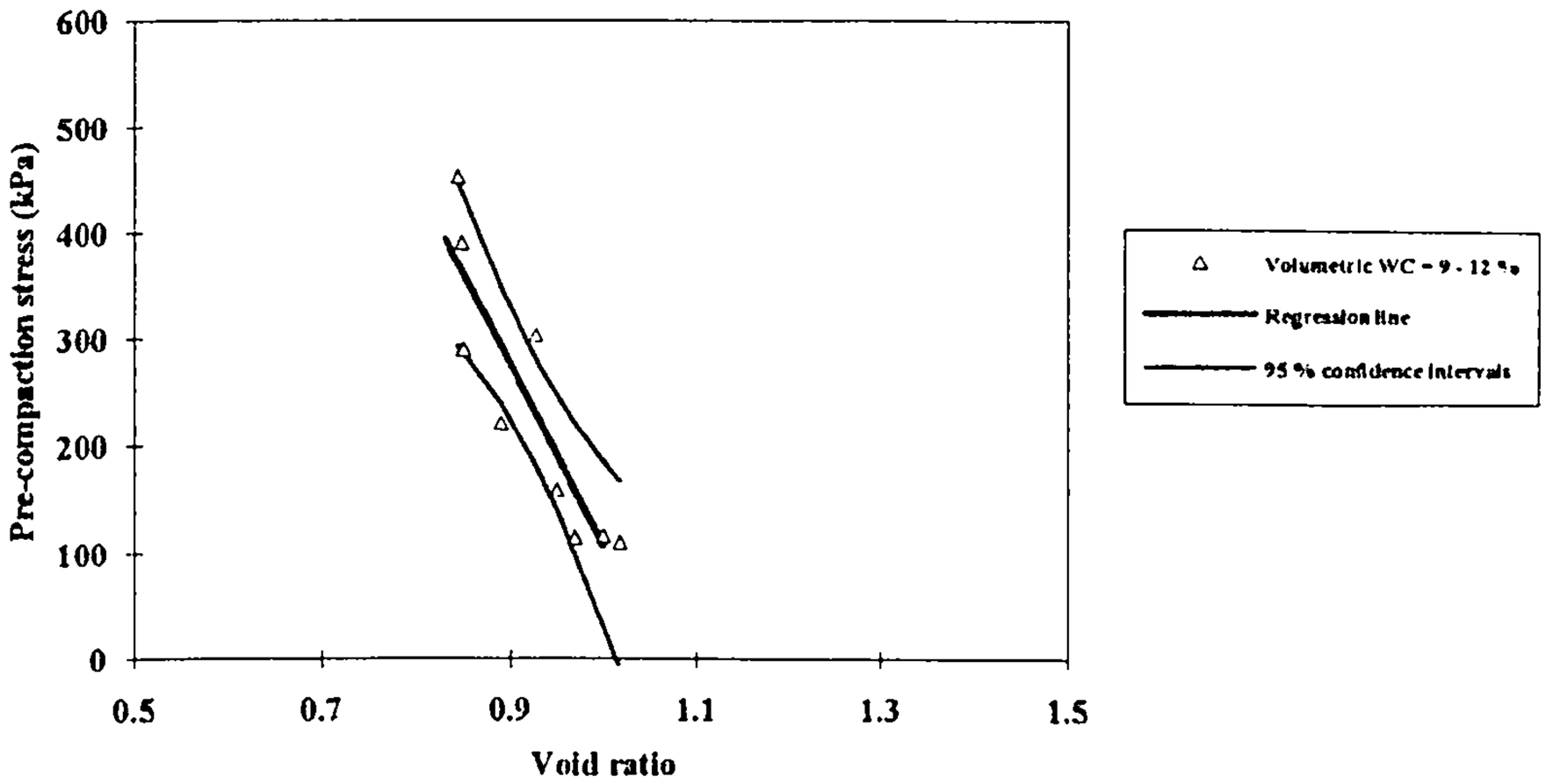

b)

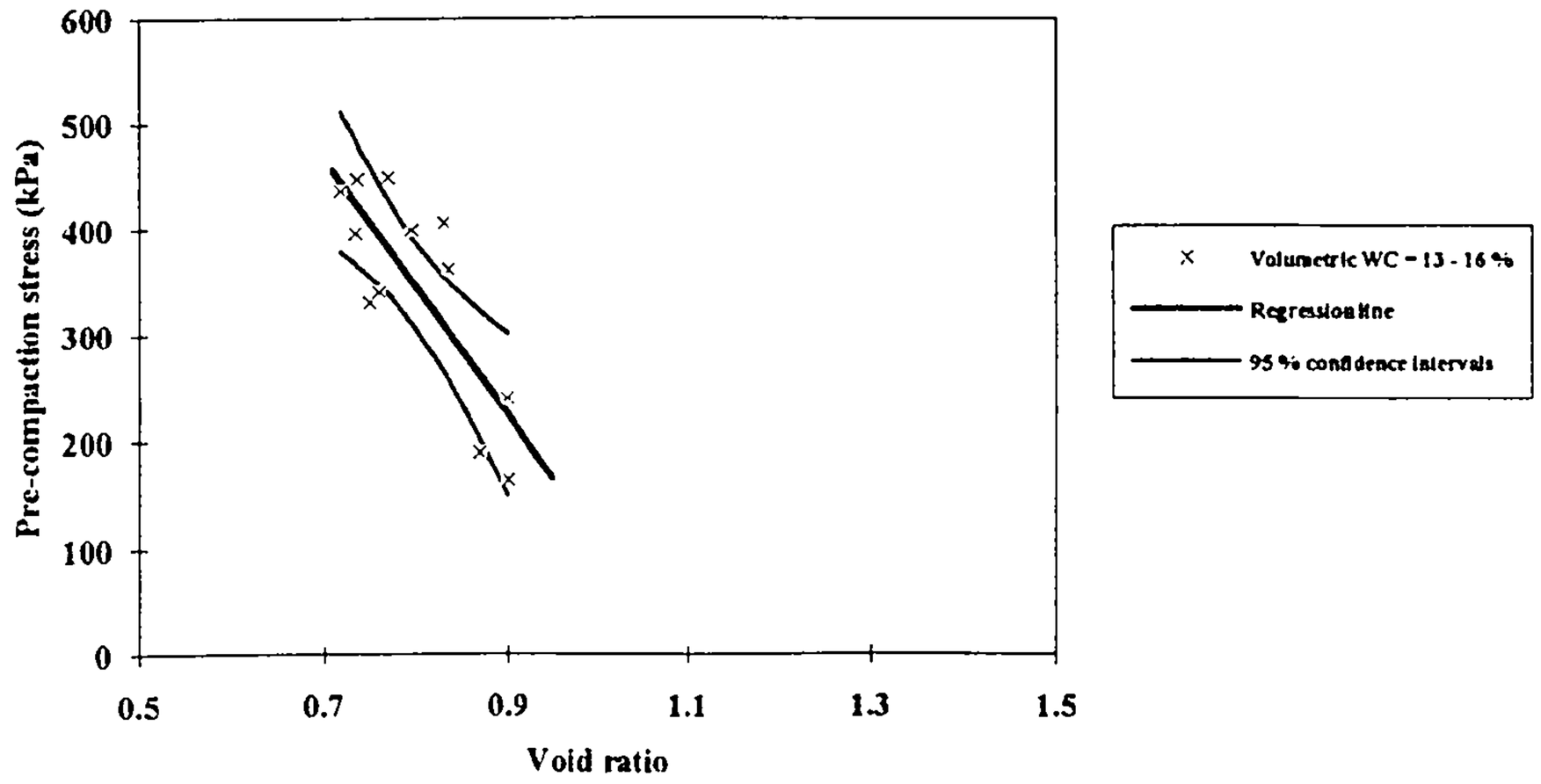

c)

Figure 3.14. The relationship between pre-compaction stress, volumetric water content and void ratio for soil bin sandy loam soil. a) all water contents; b) 9-12 % water content range and c) 13-16 % water content range.

The relationship for the field sandy loam soil is presented in *Figure 3.15*. The trends appear to be similar to that found for the soil bin soil. Results from a regression analysis are presented in *Table 3.10*.

Table 3.10

Derived relationships for field sandy loam soil

Volumetric water content %	Derived equation	R^2	Significance
10-15	No statistically significant relationship		
16-17	$\sigma_{pr} = 2740.46 - 2721.52 * e$	0.92	*

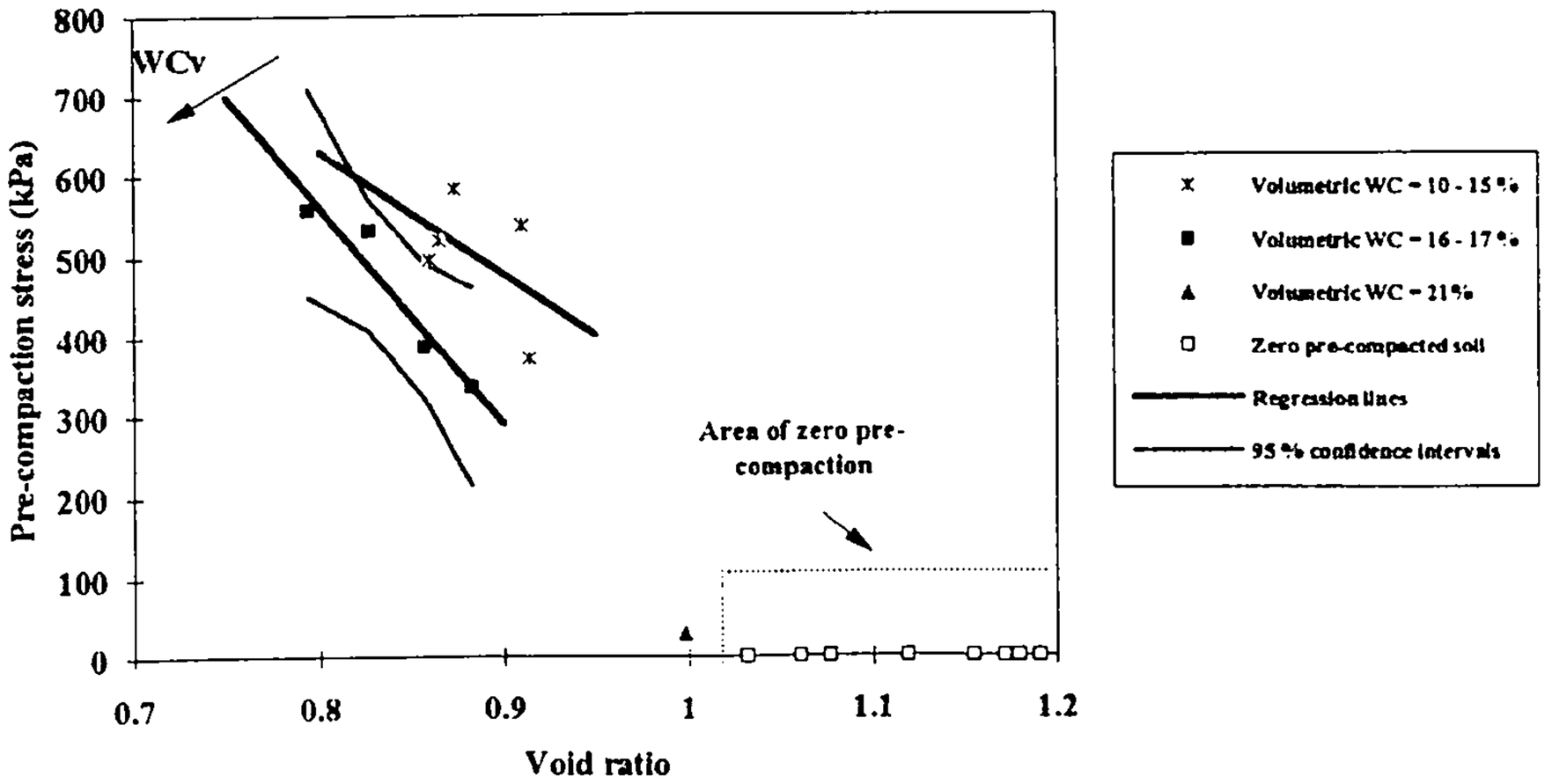

Figure 3.15. The relationship between pre-compaction stress, volumetric water content and void ratio for field sandy loam soil.

For the soil bin sandy loam the relationship between pre-compaction stress, volumetric water content and void ratio could be predicted from the family of curves presented in *Figures 3.13*. However, more data are required to increase the reliability of the relationship. For soil categories where insufficient data exists, the relationships are not statistically significant, however in all cases, pre-compaction stress tends to increase as void ratio decreases. For loose sandy loam soil (void ratio less than 1.02) pre-compaction stress is equal to zero. In the case of field soil pre-compaction stress can be predicted with good accuracy only for the loose soil, due to insufficient data for the rest of the categories.

3.4.3.2 Clay soil

Pre-compaction stress is related to cohesion which, in turn, is related to degree of saturation. For this reason, the relationship between pre-compaction stress and degree of saturation was investigated (*Figure 3.16*). The relationship can be approximated by the following relationship:-

$$\sigma_{pr} = 1017.71 - 868.97 \cdot S_r \qquad (3.2)$$

with coefficient of determination $R^2 = 0.71$ ***.

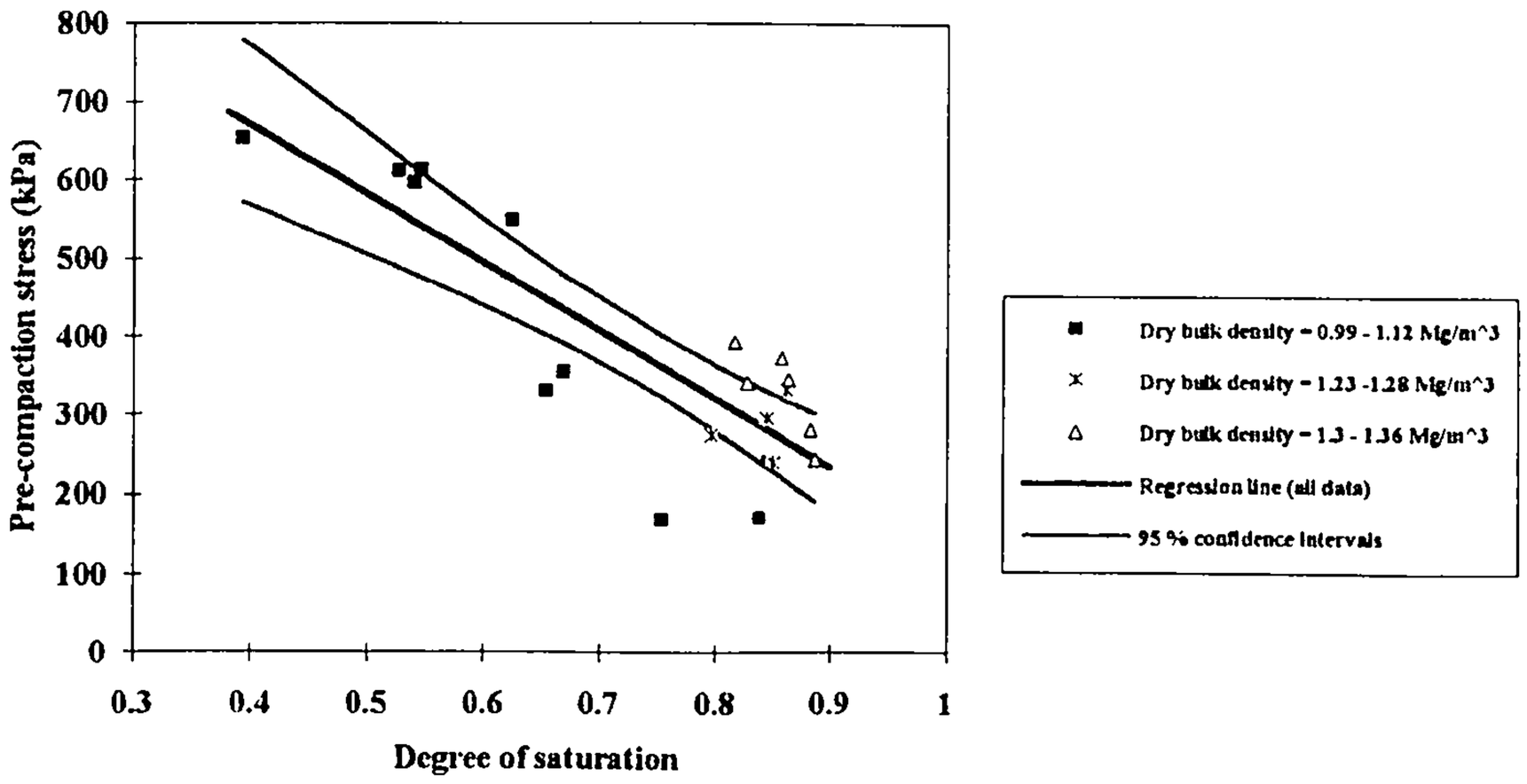

Figure 3.16. The relationship between pre-compaction stress, initial dry bulk density and degree of saturation for field clay soil.

Pre-compaction stress can be predicted for the clay soil with some accuracy if degree of saturation is known.

3.5 Conclusions

A simple technique has been developed for determining pre-compaction stress of soil using results from plate sinkage tests. The method was developed in a soil bin but was tested on field soils. In all cases the difference between observed and predicted pre-compaction stress is not significant.

Pre-compaction stress for the sandy loam soil appears to increase as dry bulk density increases or void ratio decreases at a volumetric water content. A family of curves from which pre-compaction stress of the soil bin sandy loam soil can be predicted has been proposed, allowing the prediction of pre-compaction stress from readily available data.

For the field sandy loam subsoil tested, a tendency exists for pre-compaction stress to increase as initial dry bulk density increases or void ratio decreases for a given volumetric water content, however, more data are required to increase the reliability of the relationships. For topsoil tested, the pre-compaction stress was identified as zero for all but one case and this situation was found to occur where initial dry bulk

density is less than 1.30 Mg/m^3 or void ratio is less than 1.02. A similar situation was found to occur for the soil bin soil.

For the clay soil, pre-compaction stress is more closely related to the volumetric water content than dry bulk density. This can be attributed to the significance of the cohesive forces on soil strength for a clay soil. As a result of this, pre-compaction stress for the clay soil can be predicted with reasonable accuracy if either volumetric water content or degree of saturation is known.

CHAPTER 4

SOIL STRENGTH ASSESSMENT

In chapter 1, soil strength prior to loading was introduced as a parameter which can be used to describe soil compactibility. In this chapter, a technique is proposed for soil strength assessment based on plate sinkage test results. Initial compressive soil strength is introduced as a variable which directly evaluates soil strength. As in the case of pre-compaction stress, the technique proved somewhat cumbersome, and so the feasibility of predicting initial compressive soil strength from various easily determined soil properties is also investigated.

4.1 Introduction

Soil strength can be defined as the ability of a soil to resist or endure an applied force (Gill and Vanden Berg 1967). Strength is imparted to soil by cohesive forces between particles and by the frictional resistance met by particles that are forced to slide over one another to move out of interlocked positions (Marshall and Holmes 1988). A review of techniques used for soil strength assessment was presented in chapter 1. Based on this, plate sinkage tests were used for soil strength assessment during this work.

Evaluating soil strength will enable soils to be ranked according to their compactibility since both strength and compaction are either the result of an applied load (compaction) or express the resistance to it (strength). Soil compactibility assessment using strength may be of great relevance to the suitability of the soil as a rooting medium and consequently related to the detrimental effects of compaction (Soane 1985). In the following paragraphs the use of a plate sinkage test for soil strength assessment is investigated.

4.2 Plate sinkage test used for soil strength assessment

In the past, researchers analysed results obtained from plate sinkage tests in different ways. Ostenberg (1948) for example, found that a logarithmic plot of load-sinkage produced a linear relationship for loading tests on clay. Perloff and Rahim (1966)

found that their experimental results were best described by a hyperbola, however Kasigin and Gustov (1968) proposed an exponential relationship. The pressure sinkage formula (4.1) developed by Bernstein (1913) has been generally used in off-road engineering.

$$p = kz^n \qquad (4.1)$$

Where:-

p = stress
n, k = soil constants
z = sinkage

According to Karafiath and Nowatzki (1978) the Berstein and Bekker (equation 1.1) models are conceptually inadequate because the sinkage curve is generated from several physical processes (see section 1.2.1.2).

Kondner and Krizek (1962) approximated the stress-strain relationship obtained from a plate sinkage test using a hyperbolic equation and suggested that the relationship includes the strength factor in it. Earl (1993) modified it to the following:-

$$\sigma = \frac{R}{\frac{1}{m_p} + \frac{R}{\sigma_{ult}}} \qquad (4.2)$$

Where:-

σ = axial stress (kPa)
σ_{ult} = asymptotic value of σ (kPa)
R = sinkage (mm)
m_p = initial modulus (kPa/mm)

This expression can be represented by the stress-sinkage curve in *Figure 4.1*.

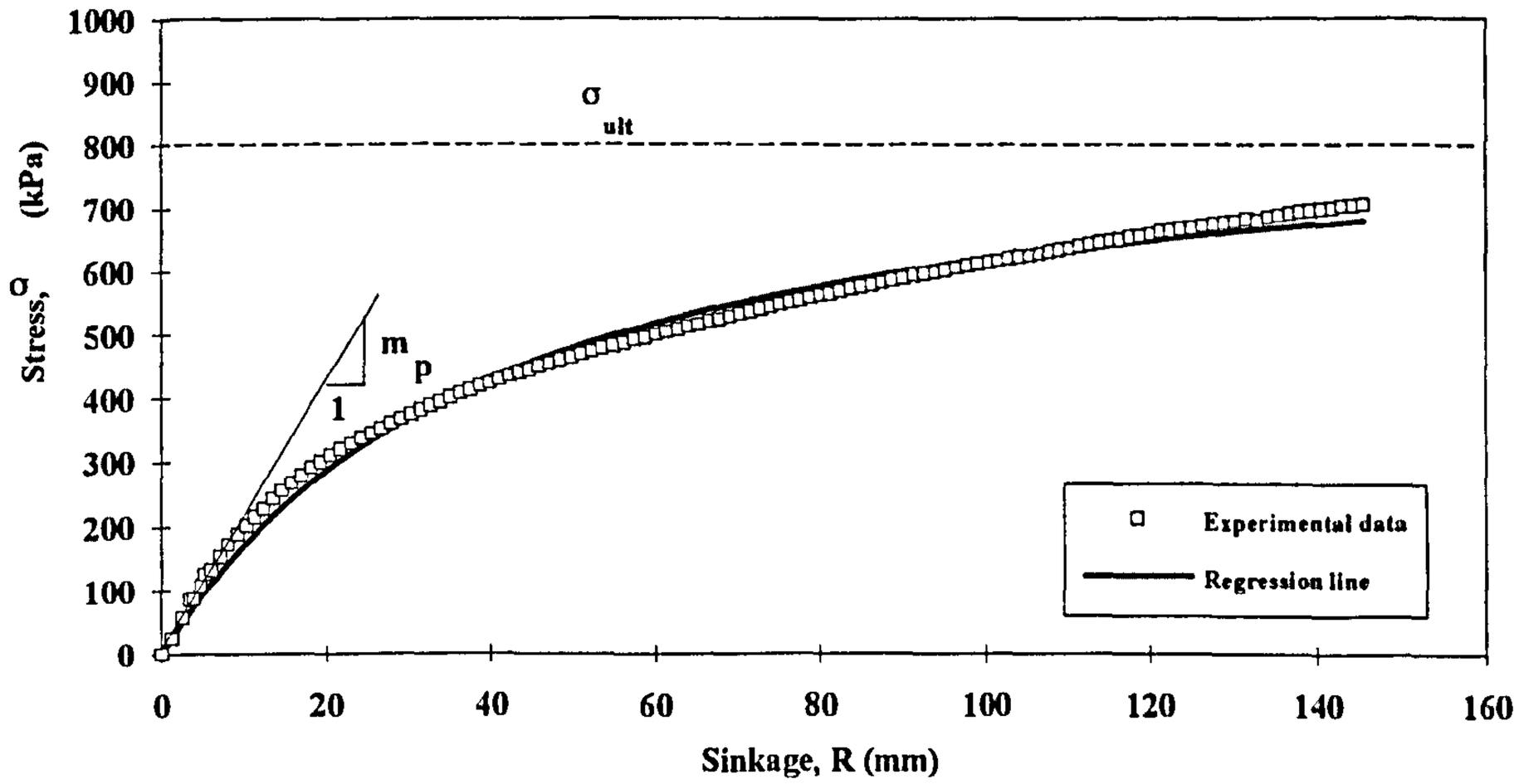

Figure 4.1. Typical stress-sinkage curve obtained from a plate sinkage test on a sandy loam soil (soil bin).

Earl (1993) suggested that the initial modulus, m_p, gives an indication of initial soil strength, since it depends on the soil resistance to the applied mechanical load. It is expected that stronger soil will have a higher value of initial modulus and looser soils a lower one. Because the initial modulus is a direct measure of soil strength, it was renamed 'initial compressive soil strength' for the purposes of this work. It can be defined as the normal stress required to cause 1 mm of sinkage. Experiments were conducted to investigate further the initial compressive soil strength and its properties.

4.2.1 Experimental procedure and results

Plate sinkage tests were carried out in the soil bin as well as in field soils as described in section 2.1. *Figures 3.1 and 3.2* illustrate typical plate sinkage test results from dense and loose sandy loam soil respectively. Generally, the form of the stress-sinkage relationship for most soils can be approximated by a hyperbola, however, loose sandy loam soil appears to be a special case as it is virtually linear and, therefore, a numerical value of the asymptote (equation 4.2) is expected to be meaningless. The desire for a consistent technique for soil strength required this inconvenience to be overlooked.

Results from plate sinkage tests were fitted to equation (4.2) using the software 'Table Curve (version 3.01)'. This uses a Levenburg-Marquardt algorithm which in turn, uses the Gauss-Jordan procedure to calculate the matrix inverse required during each iteration (Bevington, P. R 1969 and Press, W. H. et al 1988). The procedure is considered a standard for non-linear regression analysis.

The results were highly significant for all the cases. A summary of the statistical analyses for all the soils tested is presented in *Tables 4.1*, *4.2* and *4.3*.

Table 4.1
Statistical values obtained from plate sinkage tests on sandy loam soil (soil bin)

Volumetric water content %	Dry bulk density (Mg/m^3)	m_p	σ_{nlt}	R^2
12.78	1.40	30.67	667	0.91
12.42	1.41	31.75	1470	0.96
12.80	1.40	26.04	1613	0.99
12.92	1.41	15.30	819	0.98
13.00	1.41	13.14	876	0.99
12.11	1.35	15.40	893	0.98
11.14	1.29	6.47	549	0.98
11.18	1.30	6.62	550	0.98
10.61	1.31	9.00	565	0.99
14.55	1.50	30.70	1416	0.97
14.75	1.49	28.20	1285	0.98
14.21	1.45	21.20	1042	0.99
13.95	1.51	32.90	1242	0.98
11.73	1.33	9.82	612	0.98
13.48	1.42	18.70	1084	0.99
13.43	1.37	11.83	697	0.99
13.39	1.38	10.66	833	0.99
20.38	1.42	7.80	649	0.99
20.45	1.43	8.85	658	0.99
21.89	1.43	8.50	714	0.99
19.22	1.55	21.10	877	0.99
20.65	1.50	16.70	746	0.99
19.14	1.55	20.20	769	0.99
15.17	1.43	24.00	1295	0.99
15.98	1.47	20.80	1282	0.99
15.38	1.45	22.00	1295	0.98
14.89	1.47	34.50	1295	0.99
9.79	1.13	1.40	418	0.99
10.08	1.20	1.10	793	0.99
10.11	1.15	1.00	-7143	0.99
12.79	1.17	1.00	500	0.99
15.23	1.18	0.90	6370	0.99
14.00	1.17	0.80	454	0.99
18.04	1.23	1.30	-3226	0.99
18.31	1.26	1.15	-17857	0.99
17.86	1.23	1.20	526	0.99

Table 4.2
Statistical values obtained from plate sinkage tests on sandy loam soil (field soil)

Volumetric water content %	Dry bulk density Mg/m^3	m_n	σ_{ult}	R^2
16.96	1.49	46.10	846.4	0.99
14.42	1.40	58.90	779.8	0.99
16.49	1.46	56.50	750.0	0.99
14.96	1.38	35.30	743.1	0.99
16.92	1.41	26.90	682.3	0.99
16.43	1.47	22.30	871.7	0.98
13.86	1.22	1.40	-724.6	0.98
15.08	1.30	1.20	-690.7	0.98
13.47	1.22	2.10	705.4	0.99
21.15	1.33	6.50	-6523.2	0.99
19.84	1.28	5.30	-4854.4	0.99
17.98	1.24	4.30	-4430.7	0.98
18.63	1.21	2.60	140.9	0.96
17.62	1.25	2.00	335.2	0.99
17.92	1.28	1.90	638.1	0.98
10.22	1.41	435.00	678.4	0.97
10.42	1.42	425.00	671.3	0.99
10.15	1.41	277.80	952.0	0.94

Table 4.3
Statistical values obtained from plate sinkage tests on clay soil (field soil)

Volumetric water content %	Dry bulk density Mg/m^3	m_n	σ_{ult}	R^2
46.16	1.23	54.85	527.06	0.98
46.50	1.25	35.15	531.91	0.95
51.55	1.02	21.02	264.55	0.96
46.53	0.99	12.53	308.34	0.99
50.66	1.05	28.73	340.95	0.95
40.64	1.28	47.62	869.60	0.99
41.56	0.99	96.42	467.00	0.99
38.43	1.05	168.57	738.49	0.98
39.96	1.08	107.05	600.20	0.99
43.78	1.32	52.50	395.10	0.99
43.16	1.30	67.80	472.37	0.91
42.16	1.36	83.92	458.50	0.99
42.08	1.34	27.36	5128.00	0.96
32.95	1.07	1492.54	699.30	0.94
31.97	1.06	1229.10	743.27	0.94
25.06	1.00	2801.12	909.10	0.93
31.66	1.12	1957.00	797.00	0.98
40.63	1.35	40.02	771.72	0.99
40.87	1.33	44.84	1005.00	0.99
44.70	1.24	40.30	530.20	0.94

The negative values of the of σ_{ult} obtained for loose sandy loam soil can be attributed to the different stress-strain behaviour explained to earlier (section 3.2). A typical example of this is presented in *Figures 4.2* and *4.3*. For the range

concerned during this work, the hyperbola and data follows similar trends (*Figure 4.2*), however, regression equation tends towards a negative asymptote as sinkage increases well beyond that experienced during normal agronomic practices (*Figure 4.3)*.

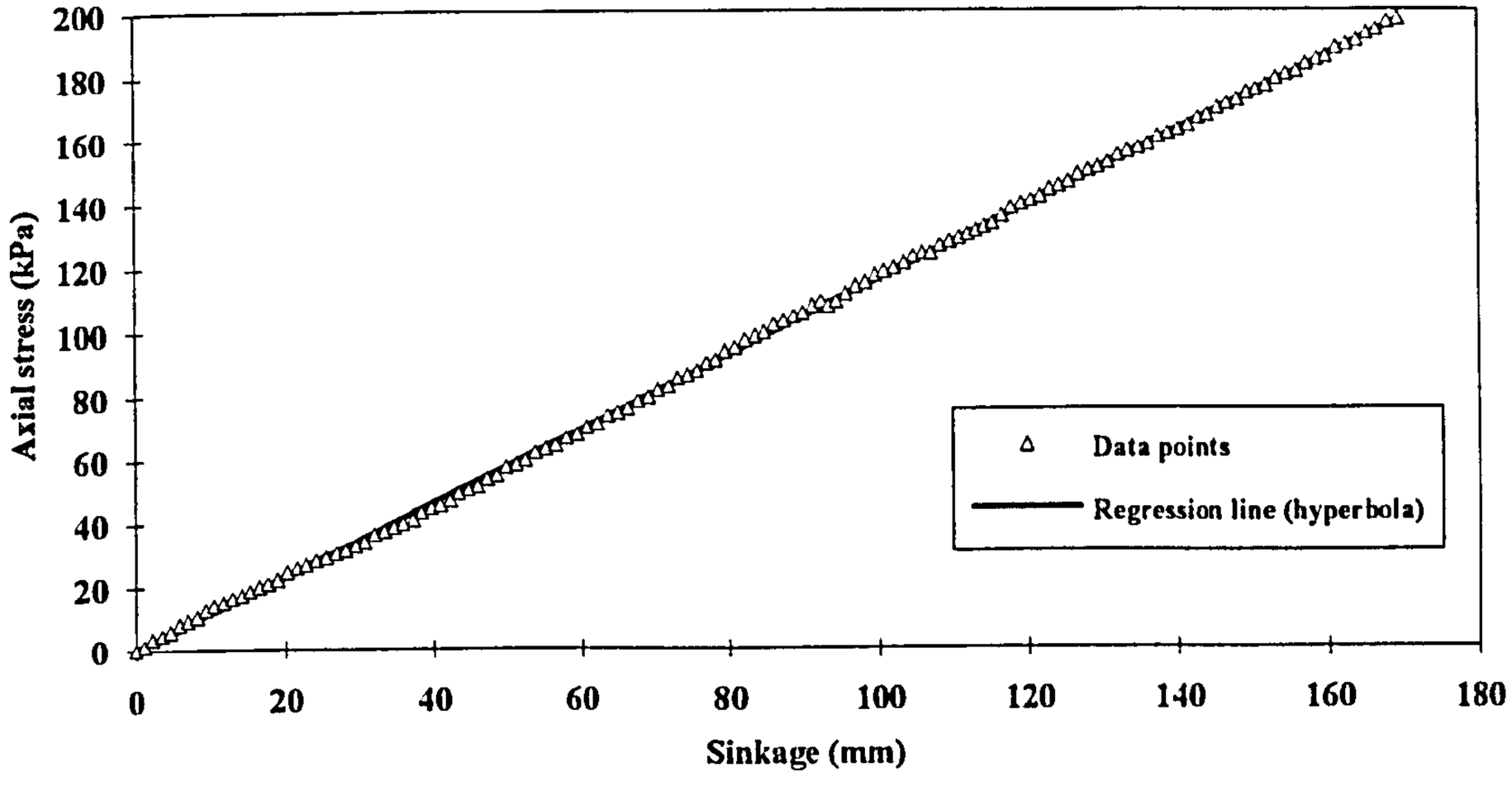

Figure 4.2. The data and the regression hyperbola for loose sandy loam soil, when σ_{ult} is negative.

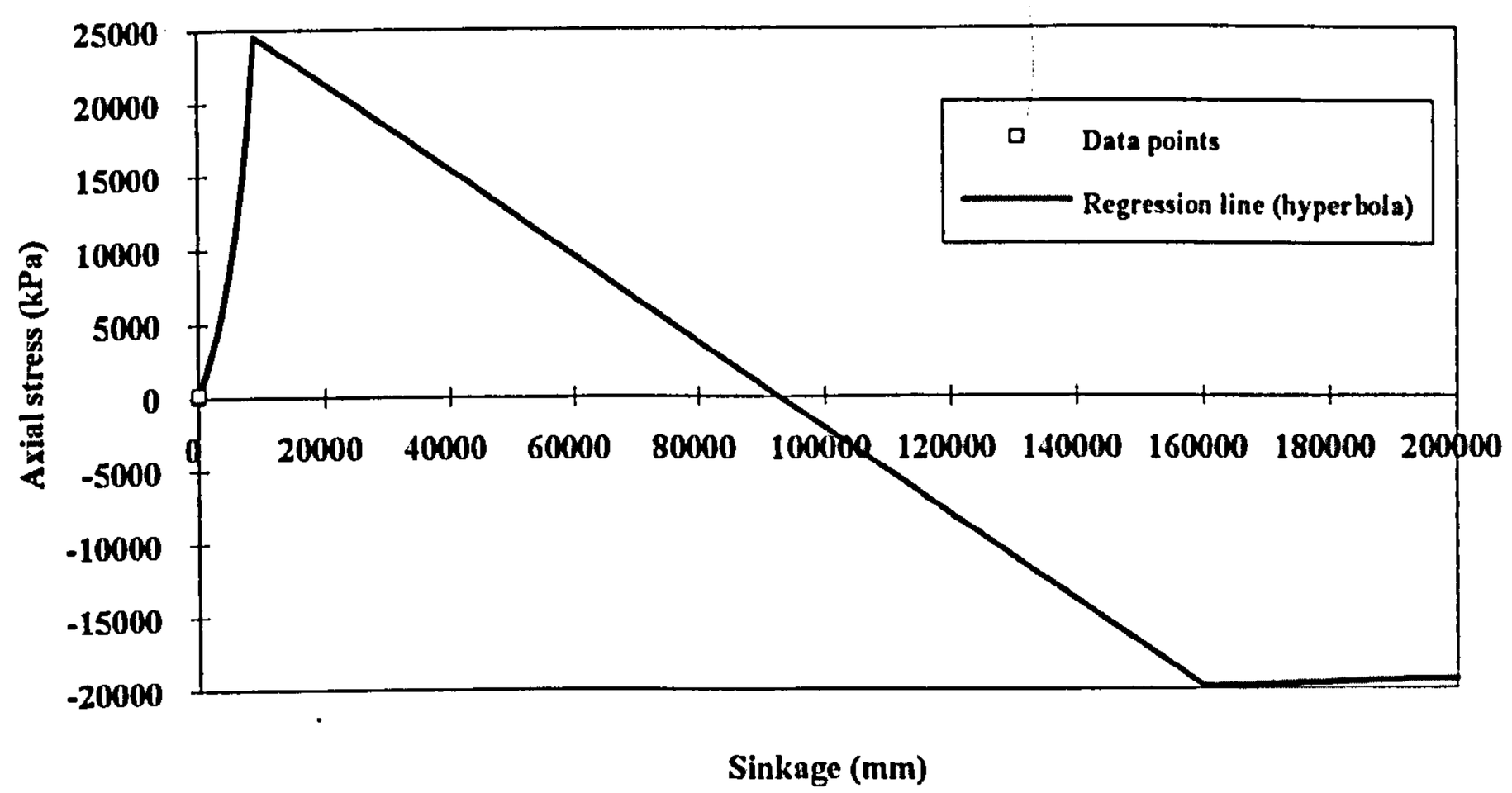

Figure 4.3. The general form of the equation (4.2) when σ_{ult} is negative.

The relationship of initial compressive soil strength to various soil properties is investigated in the following paragraphs.

4.3 The relationship between initial compressive soil strength and a range of soil properties

The determination of initial compressive soil strength is a somewhat cumbersome and time consuming procedure. As in the case of pre-compaction stress, its prediction from easily determined soil properties could be desirable. For this reason the relationships between initial compressive soil strength and various soil properties (the same used for pre-compaction stress) are investigated here.

4.3.1 Initial compressive soil strength, volumetric water content and initial dry bulk density

4.3.1.1 Sandy loam soil

Generally, soil strength is expected to increase with density for constant volumetric water content due to an increase in the frictional resistance of the soil. This was found to be the case for all soil bin trials (*Figure 4.4)*. Conversely, for constant initial dry bulk density, as water content increases, soil strength is expected to decrease, due to weakening of the bonds that hold the particles together in structured units as more water is absorbed (see *Figure 4.4*). For the loose soil with no pre-compaction the value of initial compressive soil strength is so low (m_p<5) as to be considered negligible and therefore these soils were not taken into account for the derivation of the relationships.

During the analysis of soil bin results, data were divided into the same categories as used in the analysis of pre-compaction stress. The relationship between initial compressive soil strength and initial dry bulk density at constant volumetric water content can be approximated by straight lines. For the soil bin soil the derived equations are presented in *Table 4.4* and the data with confidence intervals in *Figure 4.5*.

Table 4.4

Derived relationships for soil bin soil

Volumetric water content %	Derived equation	R^2	Significance
9-12	$m_p = -228.13 + 176.98 * D_B$	0.79	**
13-16	$m_p = -209.23 + 160.20 * D_B$	0.81	***
19-22	$m_p = -134.89 + 100.50 * D_B$	0.99	***

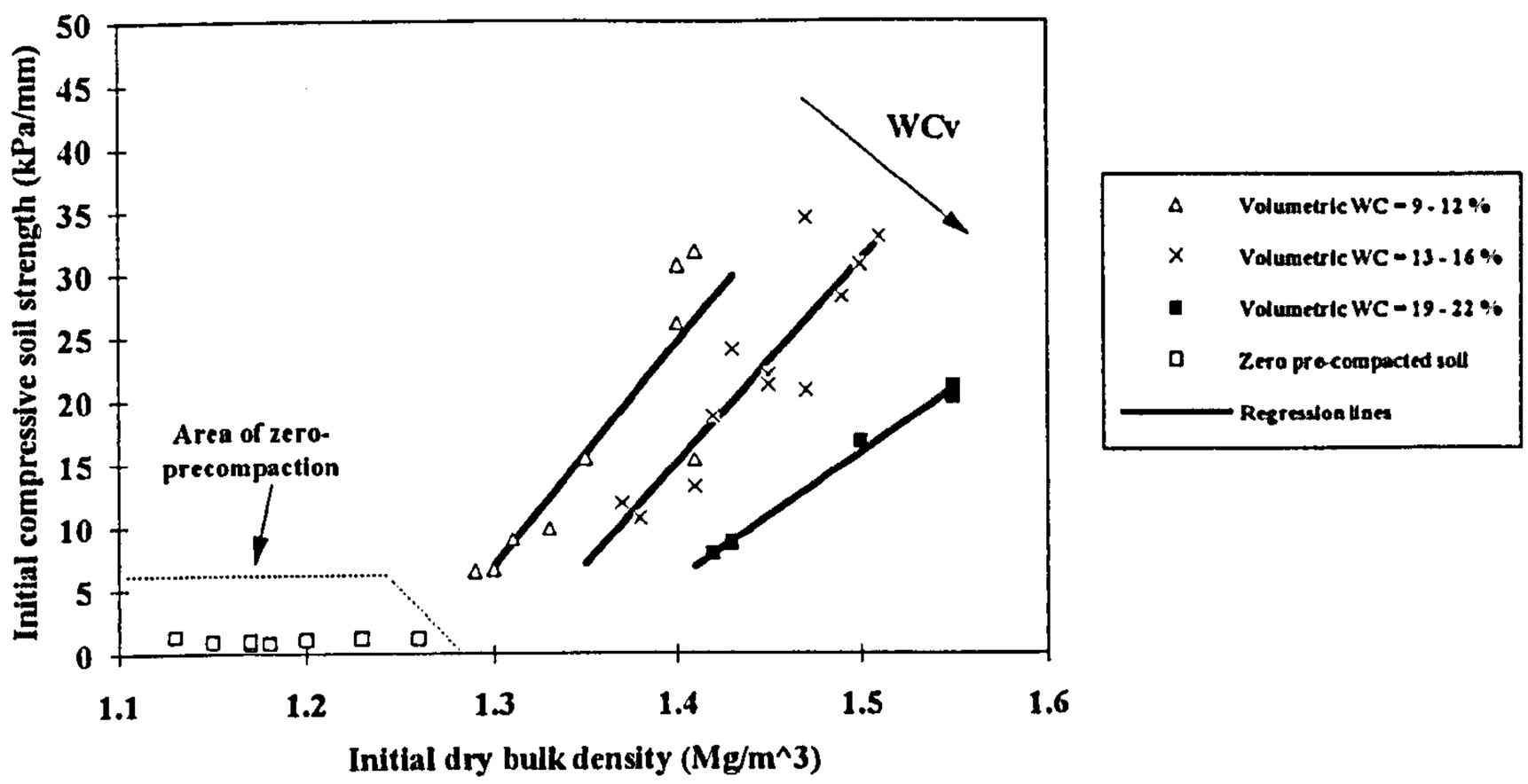

Figure 4.4. The relationship between initial compressive soil strength, volumetric water content and initial dry bulk density (bin sandy loam soil).

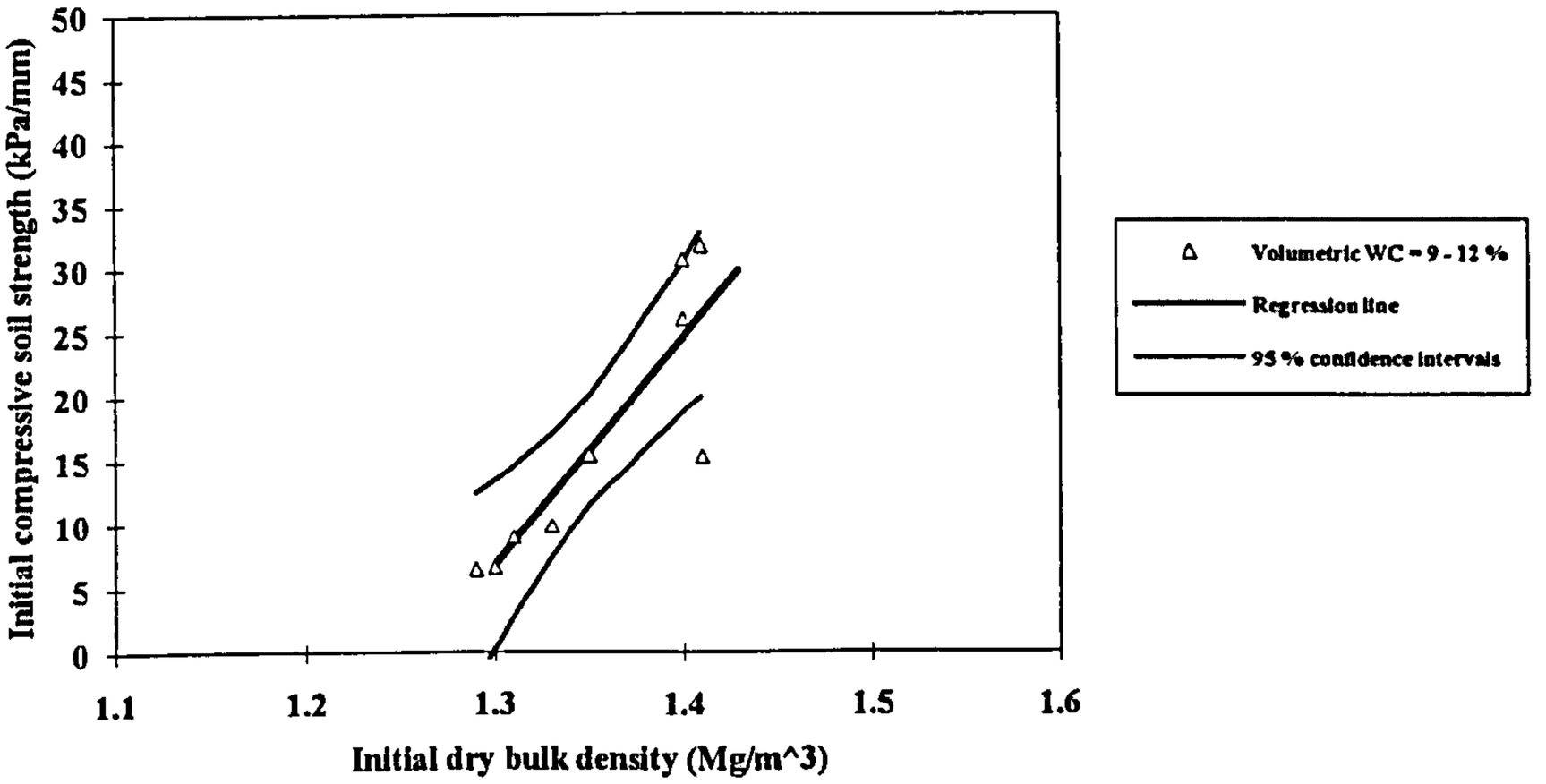
Initial compressive soil strength (kPa/mm)
50
45
40
35
30
25
20
15
10
5
0
1.1
1.2
1.3
1.4
1.5
1.6
Initial dry bulk density (Mg/m^3)
Volumetric WC = 9 - 12 %
Regression line
95 % confidence intervals

a)

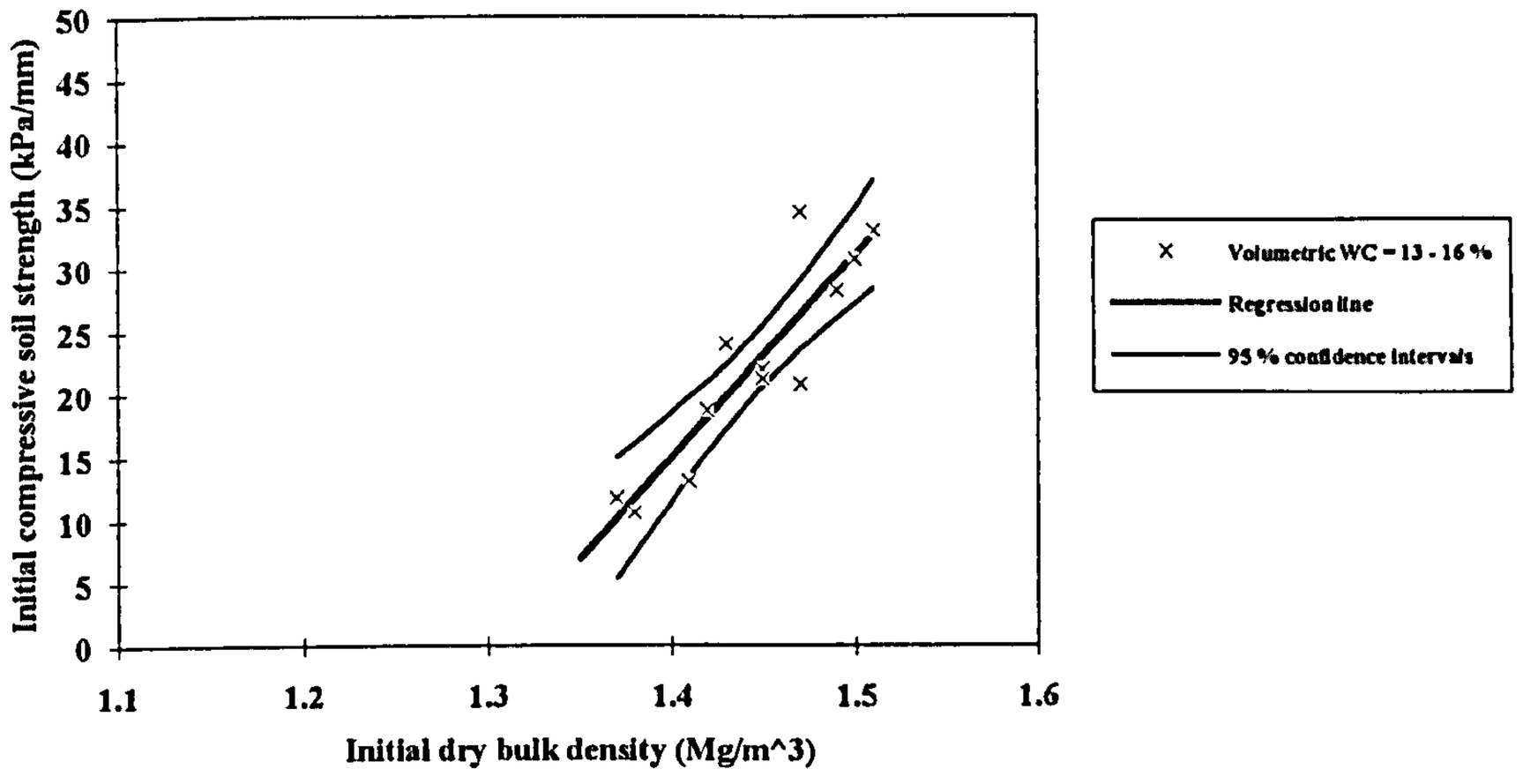
Initial compressive soil strength (kPa/mm)
50
45
40
35
30
25
20
15
10
5
0
1.1
1.2
1.3
1.4
1.5
1.6
Initial dry bulk density (Mg/m^3)
Volumetric WC = 13 - 16 %
Regression line
95 % confidence intervals

b)

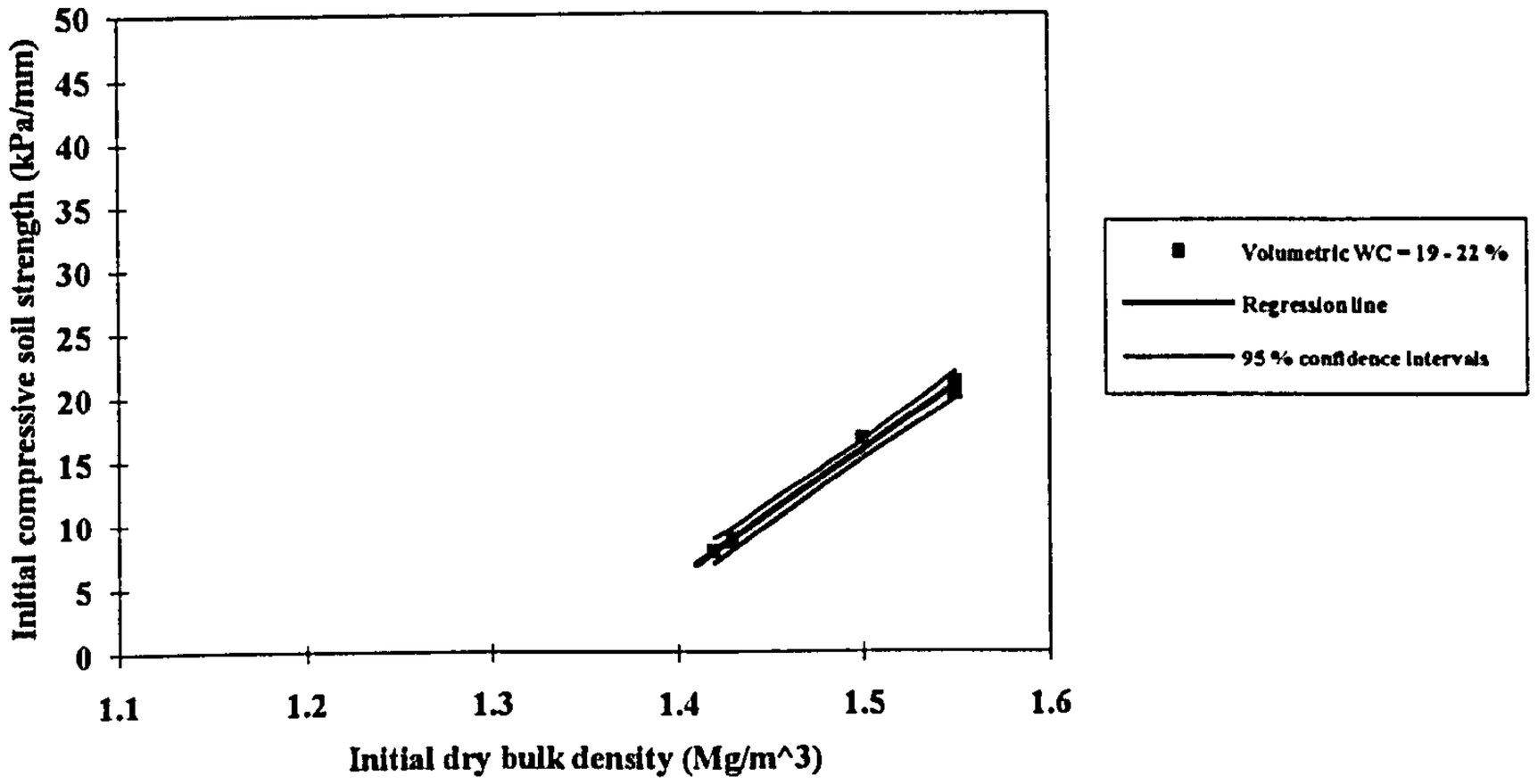

c)

Figure 4.5. The confidence intervals of the relationships between initial compressive soil strength, volumetric water content and initial dry bulk density for water content: a) 9-12 %; b) 13-16 % and c) 19-22%.

The family of curves presented in *Figure 4.4* could enable the accurate prediction of initial compressive soil strength if volumetric water content and initial dry bulk density for the soil in question are known.

Similar relationships are expected for field soil. Data obtained from the field sandy loam soil are presented in *Figure 4.6*. The relationships are not statistically significant due to lack of data (*Table 4.5*).

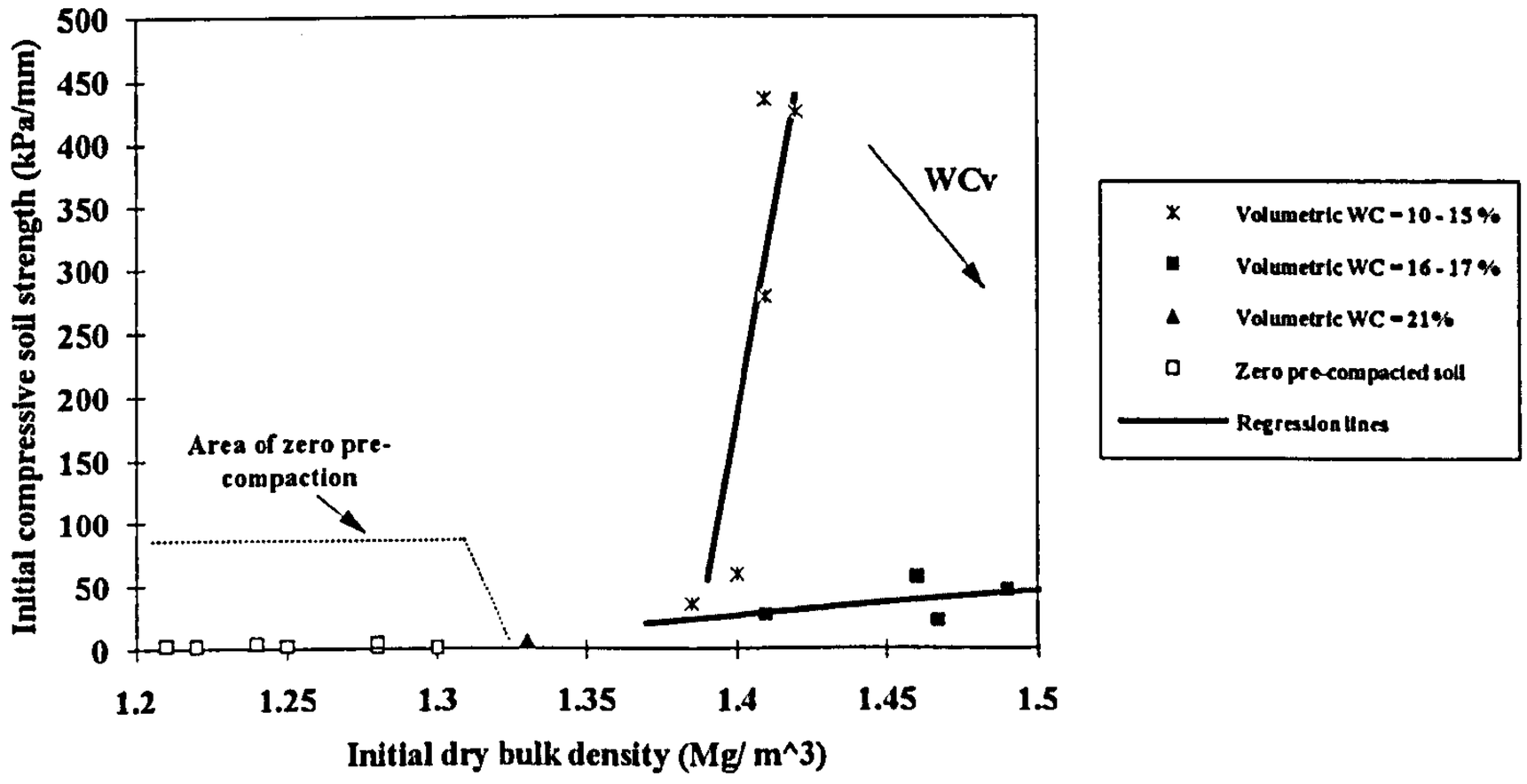

Figure 4.6. The relationship between initial compressive soil strength, volumetric water content and initial dry bulk density (field sandy loam soil).

The field sandy loam topsoil was very weak, due to its low bulk density. Initial compressive soil strength can be predicted using initial dry bulk density (for soils with D_B less than 1.30 Mg/m^3 initial compressive soil strength is very low). The family of curves for the subsoil can not be used reliably to predict strength since due to practical constrains, the limited number of data points has not allowed the derivation of a statistically significant relationship. The general trend of the data conforms to that found for the soil bin sandy loam i.e. a soil strength tends to increase as dry bulk density increases for constant volumetric moisture content, and soil strength tends towards lower values as volumetric water content increases for constant initial dry bulk density.

4.3.1.2 Clay soil

Data obtained from the clay field site are presented in *Figure 4.7*. The relationship between soil strength, volumetric water content and initial dry bulk density is confused. This may be indicative of the low dependence of soil strength on frictional resistance for this soil. To examine this further, the data were re-analysed as presented in *Figure 4.8*.

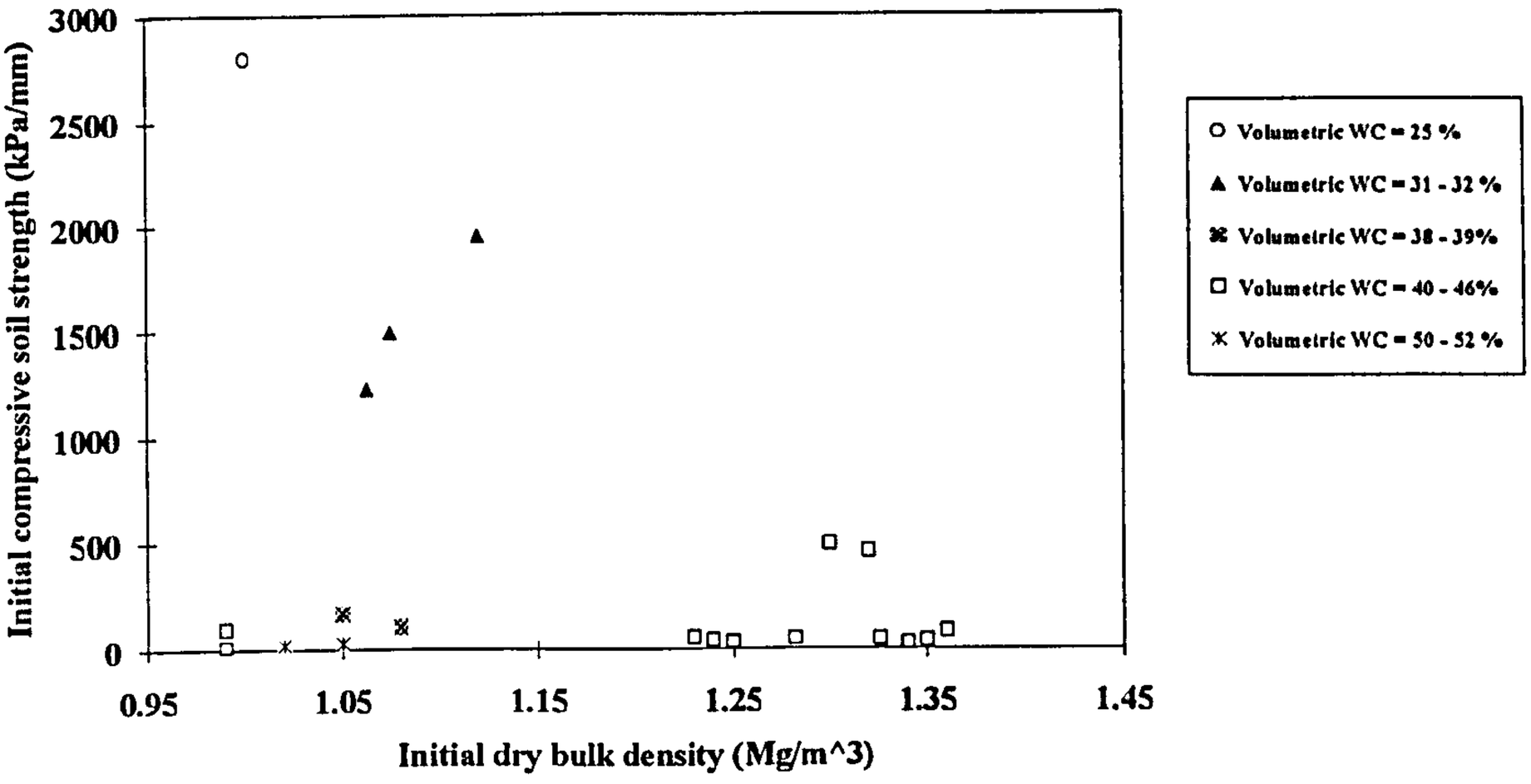

Figure 4.7. The relationship between initial compressive soil strength, volumetric water content and initial dry bulk density (clay soil).

The relationship for all the data, independent of initial dry bulk density becomes:-

$$m_p = 4654.21 - 102.13 \cdot WC_v \qquad (4.3)$$

with coefficient of determination $R^2 = 0.73$ ***.

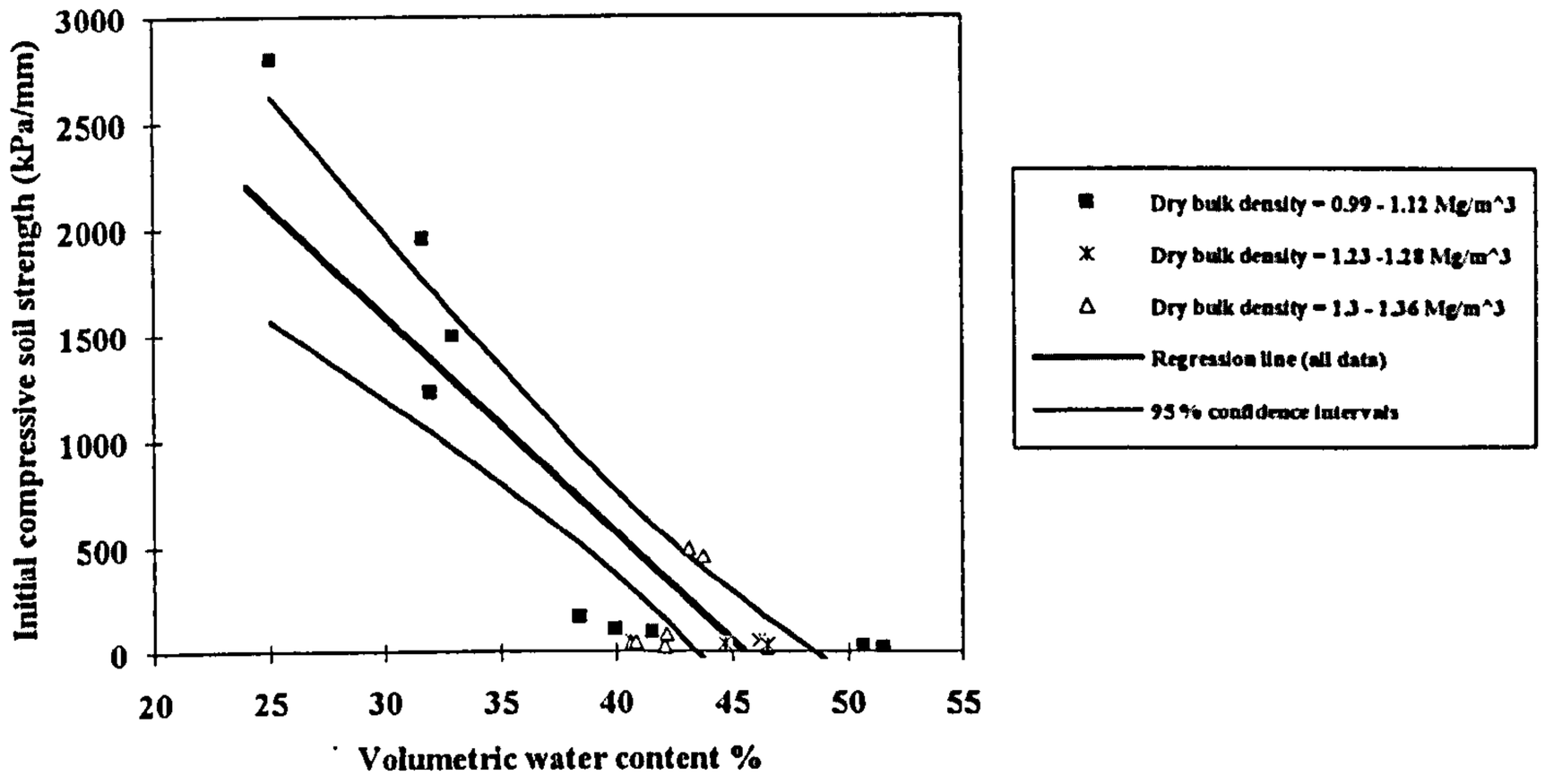

Figure 4.8. The relationship between initial compressive soil strength, initial dry bulk density and volumetric water content (field clay soil).

Initial compressive soil strength for clay soil can be predicted from readily available data with some accuracy, if volumetric water content of a clay soil is known.

The difference in the behaviour of the clay soil compared to that of the sand can be attributed to the cohesive forces developed. Strength is imparted by bonds limiting clay crystals into clay packets and packets into aggregates (Marshall and Holmes 1988). The bond strength is reduced as more water is absorbed and this is reflected in *Figure 4.8*.

4.3.2 Initial compressive soil strength, void ratio and degree of saturation

4.3.2.1 Sandy loam soil

Data for the soil bin sandy loam are presented in *Figure 4.9*. It is expected that soil strength should increase as void ratio decreases for constant volumetric water content, since soil grains will be packed more closely together and this is reflected in *Figure 4.9*. Linear equations were used to approximate the results (*Table 4.5*). The confidence intervals for these relationship are presented in *Figure 4.9 b* and *c*.

Table 4.5

Derived relationships for soil bin soil

Volumetric water content %	Derived equation	R^2	Significance
9-12	$m_p = 148.76 - 143.17 * e$	0.89	***
13-16	$m_p = 107.18 - 105.97 * e$	0.74	***
19-22	No statistically significant relationship		

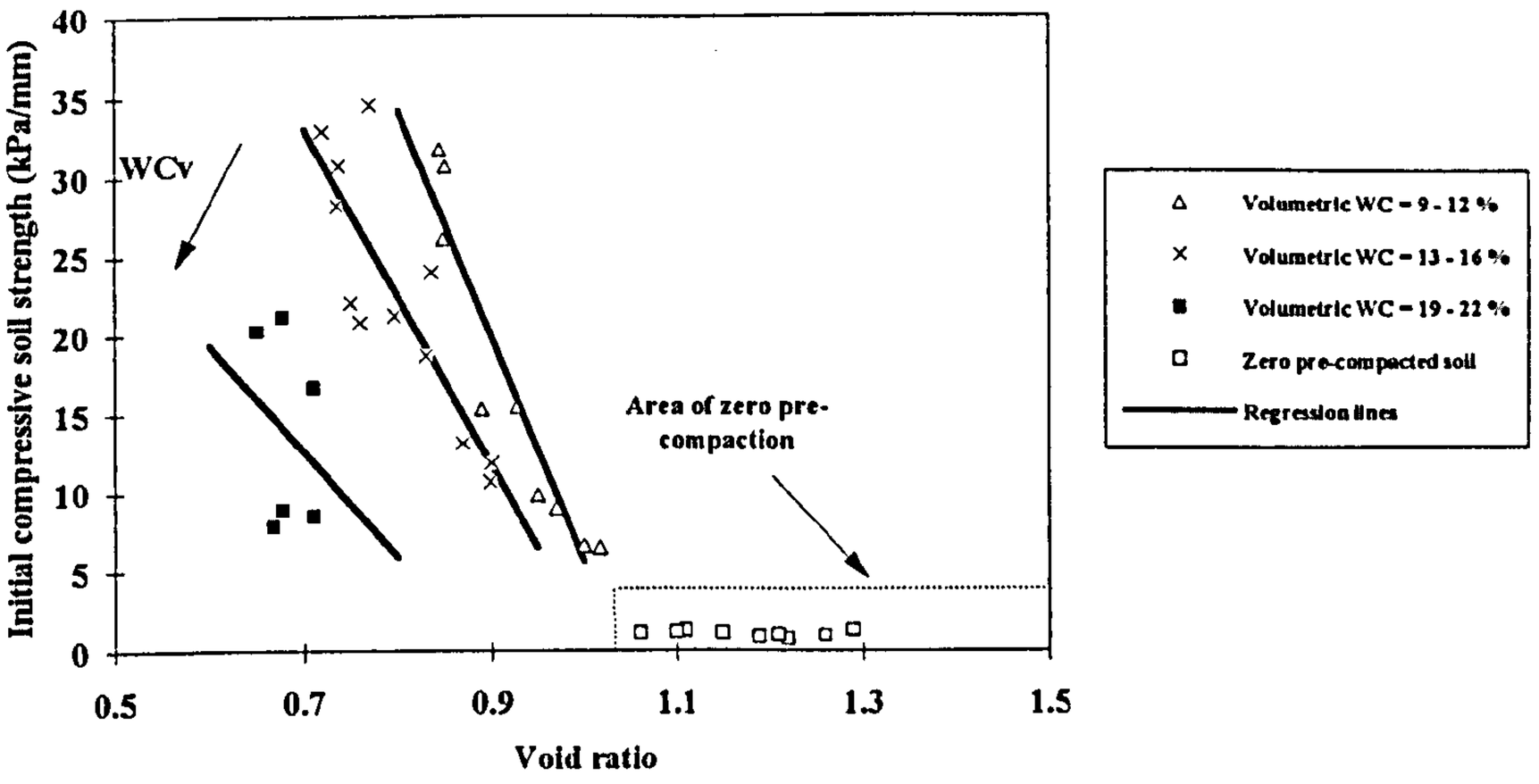

a)

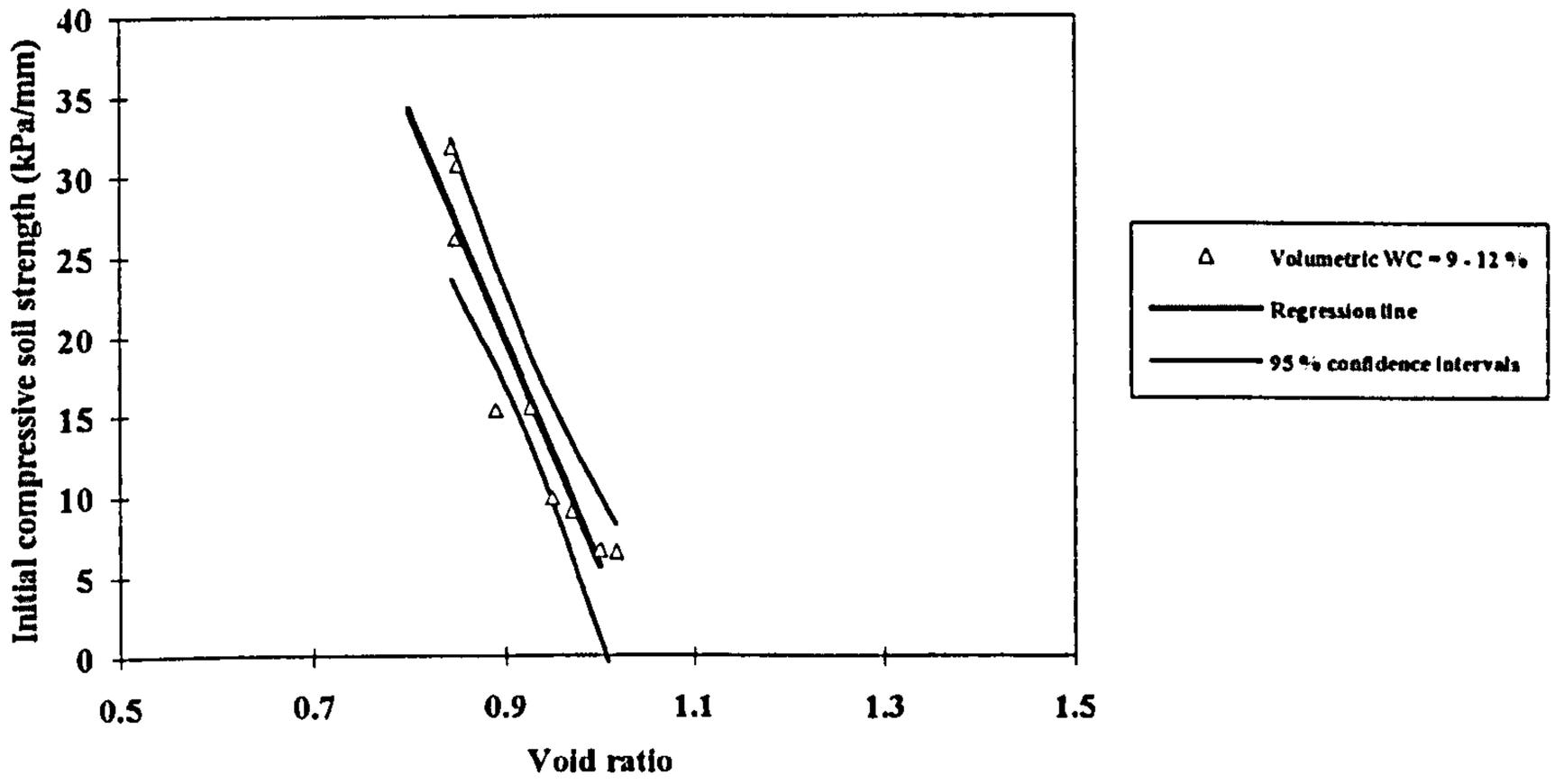

b)

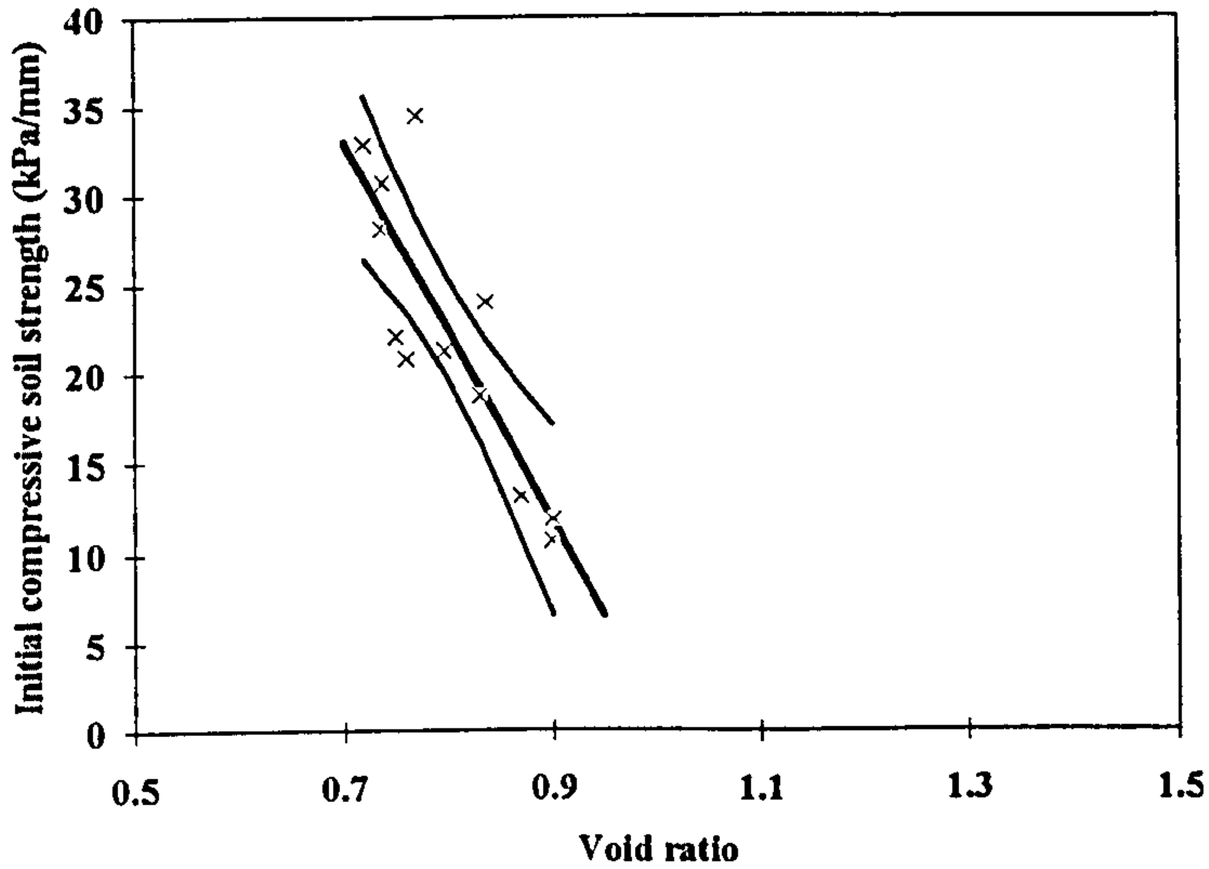

c)

Figure 4.9. The relationship between initial compressive soil strength, volumetric water content and void ratio (bin sandy loam soil). a) all water contents; b) 9-12 % water content range and c) 13-16 % water content range.

The family of curves in *Figure 4.9* can be used for prediction purposes, however, further data are required for the water content range 19-22 % for this soil. As expected soil strength tends to decrease with void ratio for a given volumetric water content. For constant void ratio, as volumetric water content increases the initial compressive soil strength decreases.

For the field sandy loam soil the initial compressive soil strength also increases as void ratio decreases at a volumetric water content (*Figure 4.10* and *Table 4.6*).

Table 4.6

Derived relationships for field sandy loam soil

Volumetric water content %	Derived equation	R^2	Significance
10-15	$m_p = 6835.17 - 7448.23 \cdot e$	0.98	**
16-17	No statistically significant relationship		

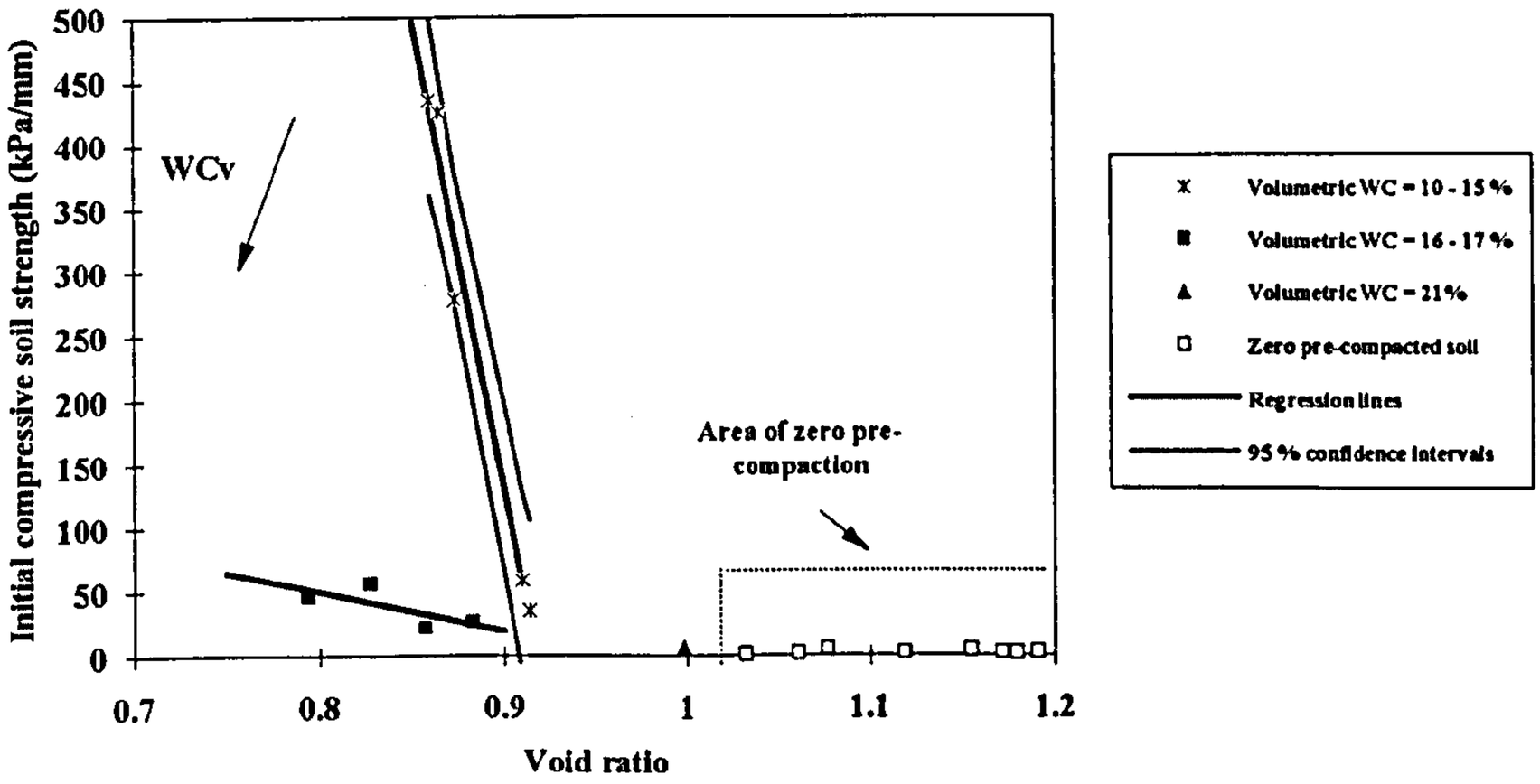

Figure 4.10. The relationship between initial compressive soil strength, volumetric water content and void ratio (field sandy loam soil).

The limited amount of data for the subsoil make the use of this graph for prediction purposes questionable. If void ratio is less than 1.02 then initial compressive strength is very low (less than 5 kPa/mm) and can be considered negligible.

4.3.2.2 Clay soil

Due to the sensitivity of clay soil to water, as explained in section 4.3.1.2, the relationship between initial compressive soil strength, initial dry bulk density and degree of saturation was used.

For all data independent of dry bulk density the relationship becomes:-

$$m_p = 3719.88 - 43.71 \cdot S_r \qquad (4.4)$$

with coefficient of determination $R^2 = 0.68$ ***.

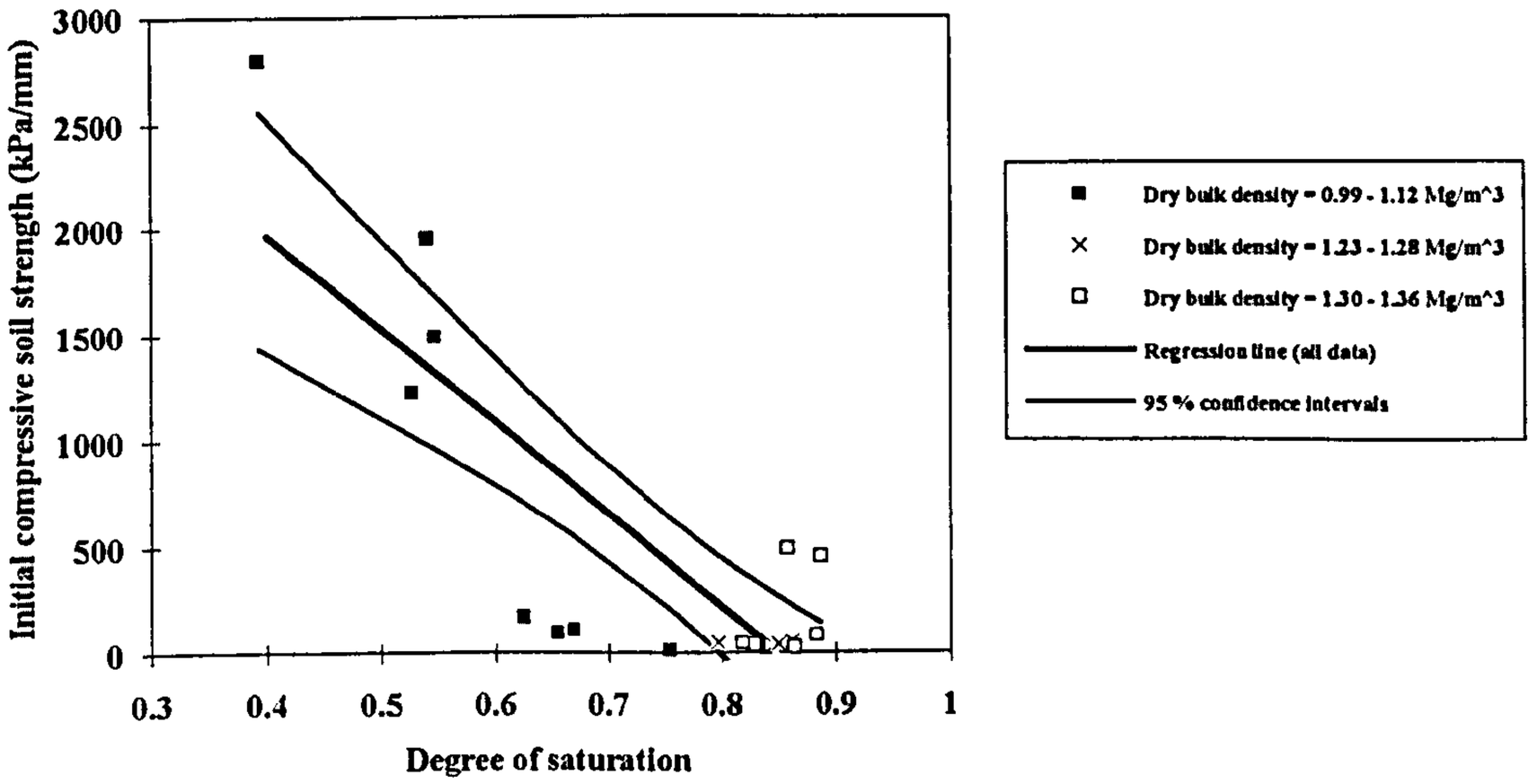

Figure 4.11. The relationship between initial compressive soil strength, initial dry bulk density and degree of saturation (clay soil).

For the clay soil, initial compressive soil strength can be predicted if degree of saturation is known.

4.4. Conclusions

The concept of initial compressive soil strength has been introduced in this chapter and its use for soil compactibility assessment was examined on two different soil types. A method has been proposed for its evaluation using plate sinkage test results.

Experiments were carried out in soil bin as well as in field soils. Initial compressive soil strength in the case of soil bin soil can be predicted with some accuracy, if initial dry bulk density or void ratio and volumetric water content of the soil in question are known. In the case of field sandy loam soil subsoil, the lack of data did not allow the derivation of any significant relationship. For loose sandy loam soil (initial dry bulk density less than 1.30 Mg/m^3 or void ratio less than 1.02) initial compressive soil strength is low and can be considered negligible. Initial compressive soil strength in the case of clay soil can be predicted with good accuracy if degree of saturation or volumetric water content of the soil are known.

CHAPTER 5

MECHANISMS OF FAILURE BELOW A PLATE

5.1 Introduction

In the introductory chapter the mode and extent of deformation for a given loading situation was suggested as a variable in soil compactibility description. It can be obtained from a plate sinkage test. One major drawback with the sinkage test is that whilst it gives information on load vs sinkage, it gives no indication of the extent of deformation below the plate. The failure mechanisms below a plate sinking on a sandy loam soil, are reported in this chapter. The point at which the deformation process changes from one of pure compaction to lateral soil displacement is identified, and a model is proposed which predicts the extent of soil disturbance below a circular plate sinking on a sandy loam soil.

Soil movement below a plate can be approximated using a theory developed by Prandlt (1921 and 1920), Terzaghi (1943) and Meyerhof (1951 and 1961). They proposed that the failure pattern in close proximity to foundations can be approximated by a logarithmic spiral. The need for the development of this theory was prompted by civil engineering problems, and consequently the rate of application of the load as well as the way that the load has been applied (incrementally), differ from the corresponding used in this work. Vesic (1963) carried out load bearing tests on sandy soil in laboratory conditions and identified the types of failure under cylindrical and prismatic foundations. He found that, depending on the relative density of sand, Terzaghi's shear failure theory reliably describes the phenomenon when the load is applied incrementally every minute. Chancellor et al (1962) applied a surface deformation using a piston at a rate of 12.7 mm/min and measured the changes in soil bulk density under the piston. They concluded that the soil failure below the piston was circular in pattern. Earl (1993) proposed a theoretical model which predicts the extent of soil disturbance below a circular plate based on the theories of Prandlt (1920 and 1921), Terzaghi (1943) and Meyerhof (1951 and 1961). He identified the 'compaction point', the point at which the deformation process changes from one of vertical soil compaction to vertical and lateral soil compaction. The point of change, which Earl named compaction point (CP), can be identified if results from a confined compression test are

superimposed onto those from a plate sinkage test (*Figure 5.1*). Although this technique looks promising, further work is necessary to observe soil movement below the plate with particular reference to changes in the mode of deformation, extent of disturbance and development of a model.

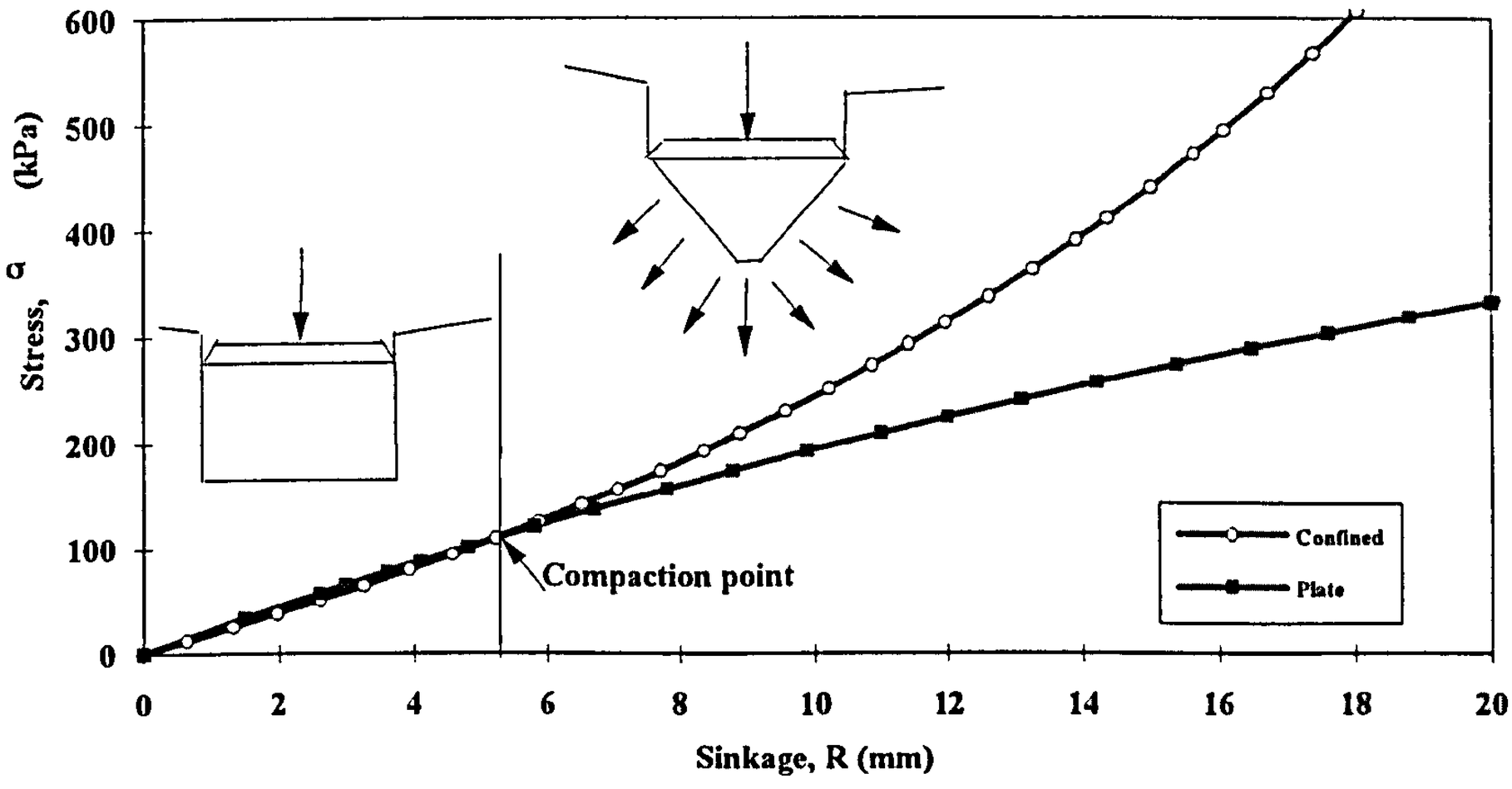

Figure 5.1. Compaction point.

To this end, a technique was developed in the soil bin whereby soil failure patterns would be observed behind a sheet of glass. The first step in such analysis is to envision the pattern of deformation that would accompany such a failure. These patterns can been studied by simulation of the actual situation. This was the approach which has been adopted during this work.

5.2 Experimental procedure

Tests were conducted on a sandy loam soil, under controlled conditions, in the soil bin. The results of the mechanical analysis of the soil are presented in Table 2.1.

The soil was prepared uniformly throughout its depth to given bulk density and water content specifications using tools and a roller mounted on the carrier following the procedure explained in 2.1.1. For these tests, soil was prepared to initial dry bulk densities of 1.37 Mg/m^3 (dense soil) and 1.08 Mg/m^3 (loose soil) with gravimetric water content, in both cases, of approximately 10%.

The following procedure was carried out:-

1. A plate sinkage test was performed in the soil bin.
2. A soil core was sampled from the soil bin for use in a confined compression test.
3. A confined compression test was performed using an Avery universal testing machine.
4. Initial water content and bulk density were determined from the soil core after compression.
5. A soil profile pit was excavated across the full width of the bin to allow a glass sheet to be placed against the soil face (*Figure 5.2*).
6. A plate sinkage test was performed immediately behind the glass using a semi-circular plate.

Figure 5.2. Soil profile and the glass sheet.

Visual recording of the experiments was carried out, using still cameras set on long exposure and camcorders. Two basic operational modes were employed to visualise the experiments (Hettiaratchi and Reece, 1975) as explained in chapter 1. For mode 'A', a camcorder and still camera were fixed to a specially manufactured camera carrier which moved with the sinkage plate. For mode 'B' a camcorder, together with a still camera, were placed on tripods in a cleared area at the bottom of the soil

bin. As Hettiaratchi and Reece (1975) explain, mode 'A' is particularly suitable for picking out, in sharp focus, the boundary zones in an overall blurred field. On the other hand, mode 'B' brings out the line of velocity discontinuity between the rupture zone in the blurred field against the parent soil, which is in sharp focus. Due to technical problems with the still cameras, long exposure photographs of the video were used during the analysis of this work. The following assumptions were made:-

1. Soil failure takes place in a two-dimensional field.
2. The soil is an isotropic material which has been prepared uniformly along its width and depth.
3. Soil behaves as a Mohr-Coulomb material.
4. Small fluctuations in the penetration velocity do not influence the failure pattern below the plate.
5. Friction between glass and soil is negligible.
6. Pore water pressure does not influence the failure patterns.

5.3 Failure under a plate in sandy loam soil

A sequence of photographs taken from the video at a long exposure (2 seconds) is presented in *Figure 5.3*. The scales shown in the photographs are 0 to 150 mm (diameter of the sinkage plate) in 50 mm intervals. During the initial stages of a plate sinkage test in loose soil, sinkage will be predominately due to vertical soil compaction under the plate (*Figure 5.3b*). As the axial stress increases and the plate continues to sink, a point will be reached when the deformation process will change and further sinkage will be predominately due to lateral compaction (*Figure 5.3e*). A third phase should be introduced to take into account the transition between the two phases and include the mechanism of change of mode of deformation from pure compaction to lateral soil displacement but can not be identified from the pictures taken during this work. Schematic diagram of these phases are presented in *Figure 5.4*. The phases observed during this work generally concur with those distinguished by Earl (1993).

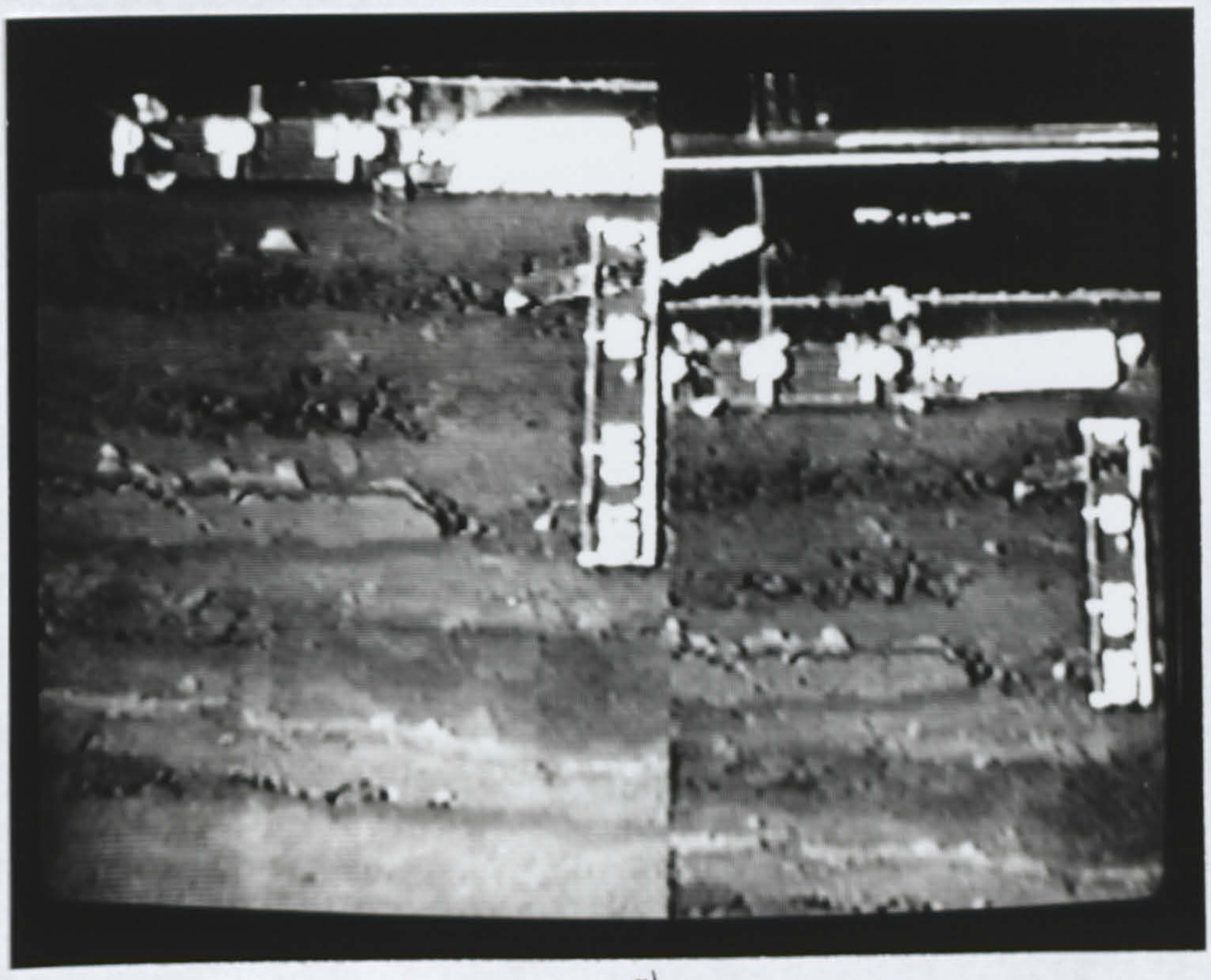

a)

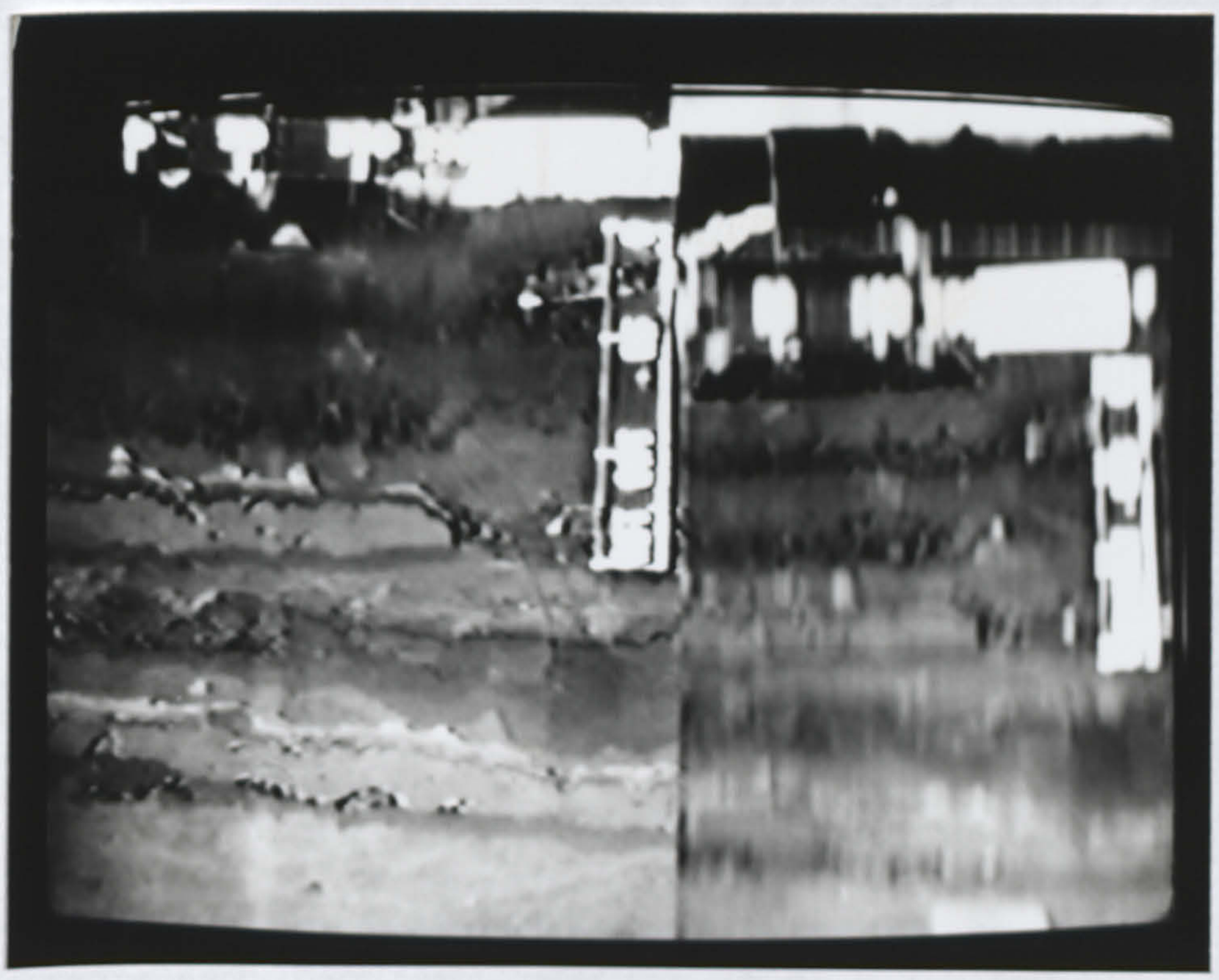

b)

c)

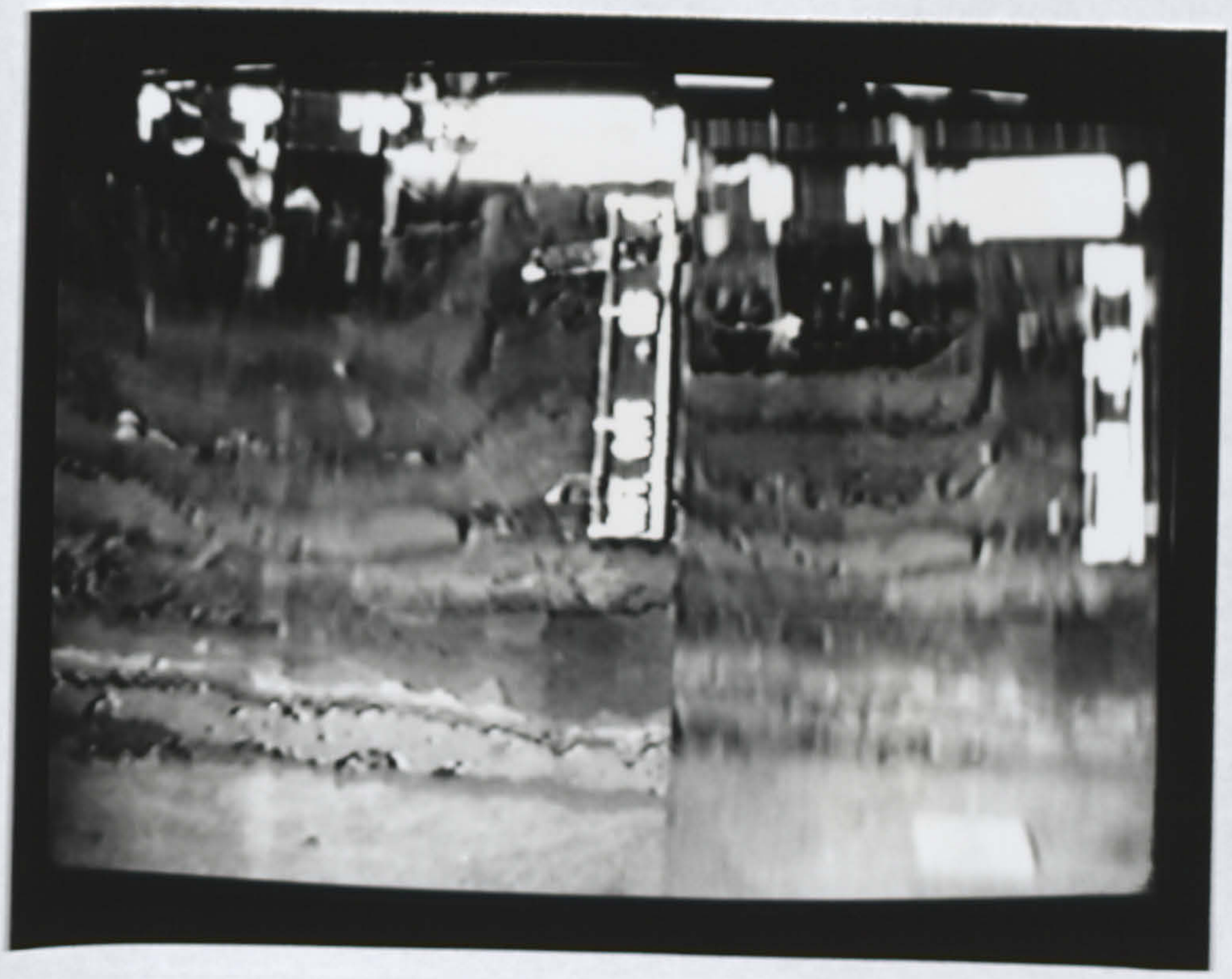

d)

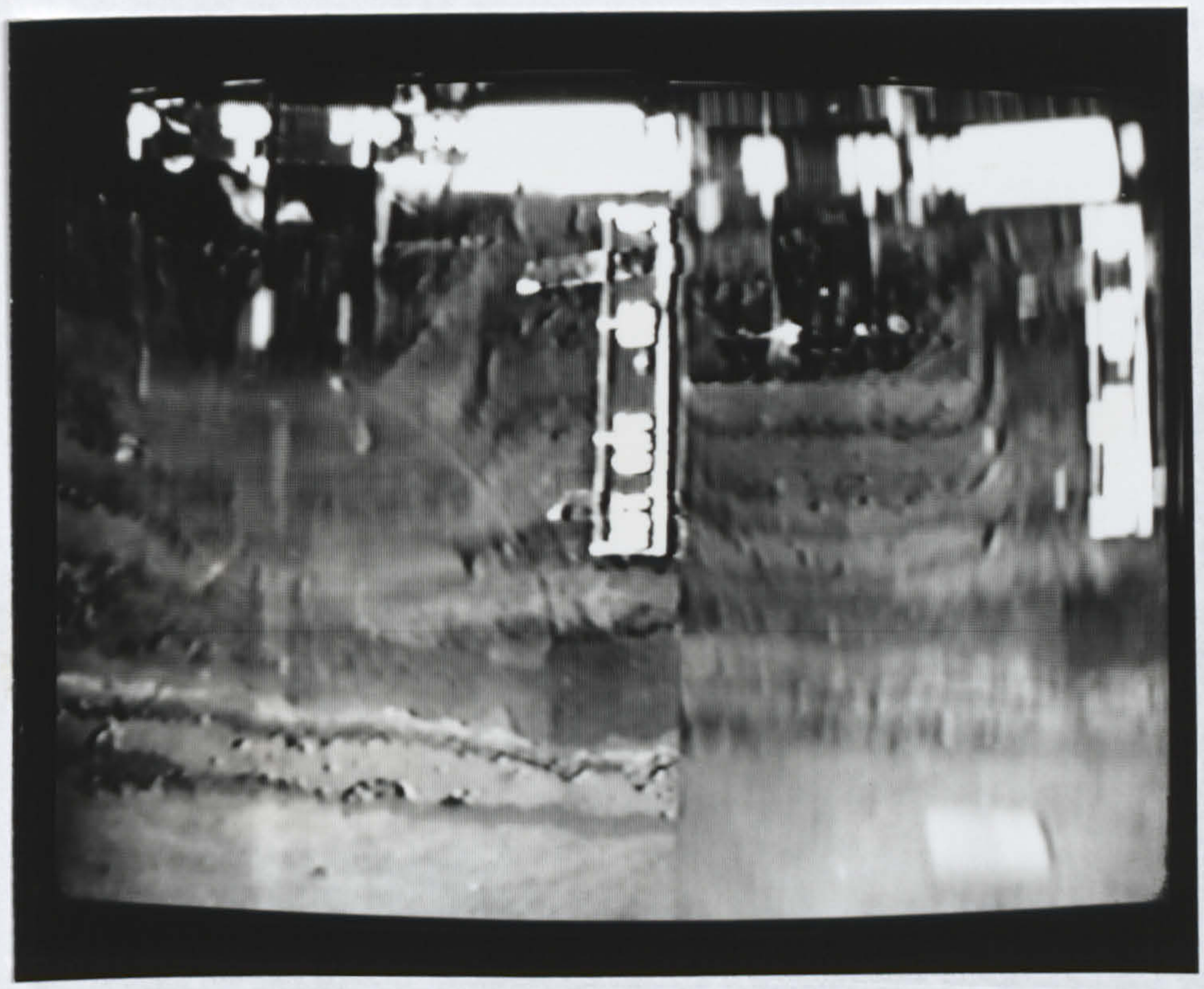

e)

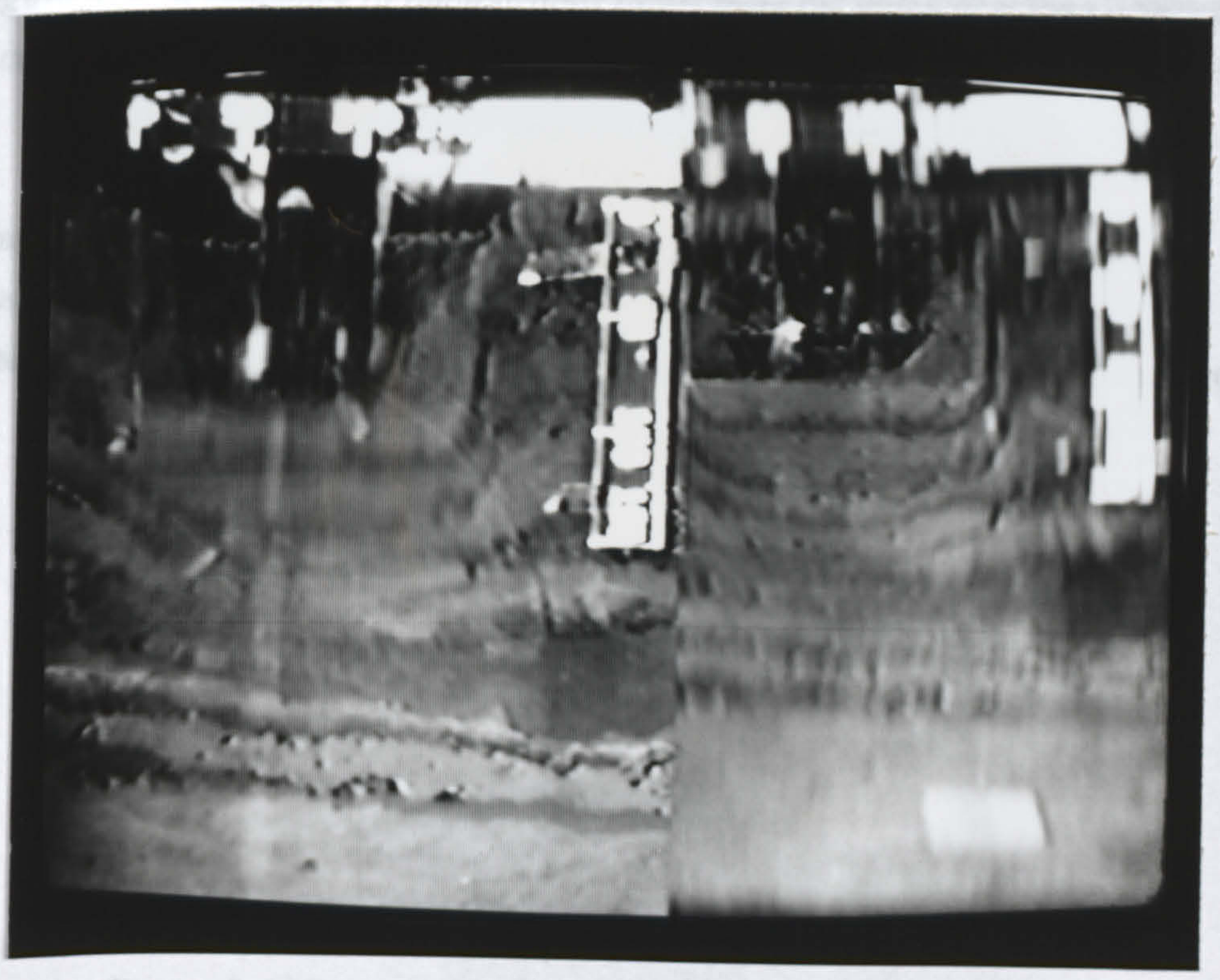

f)

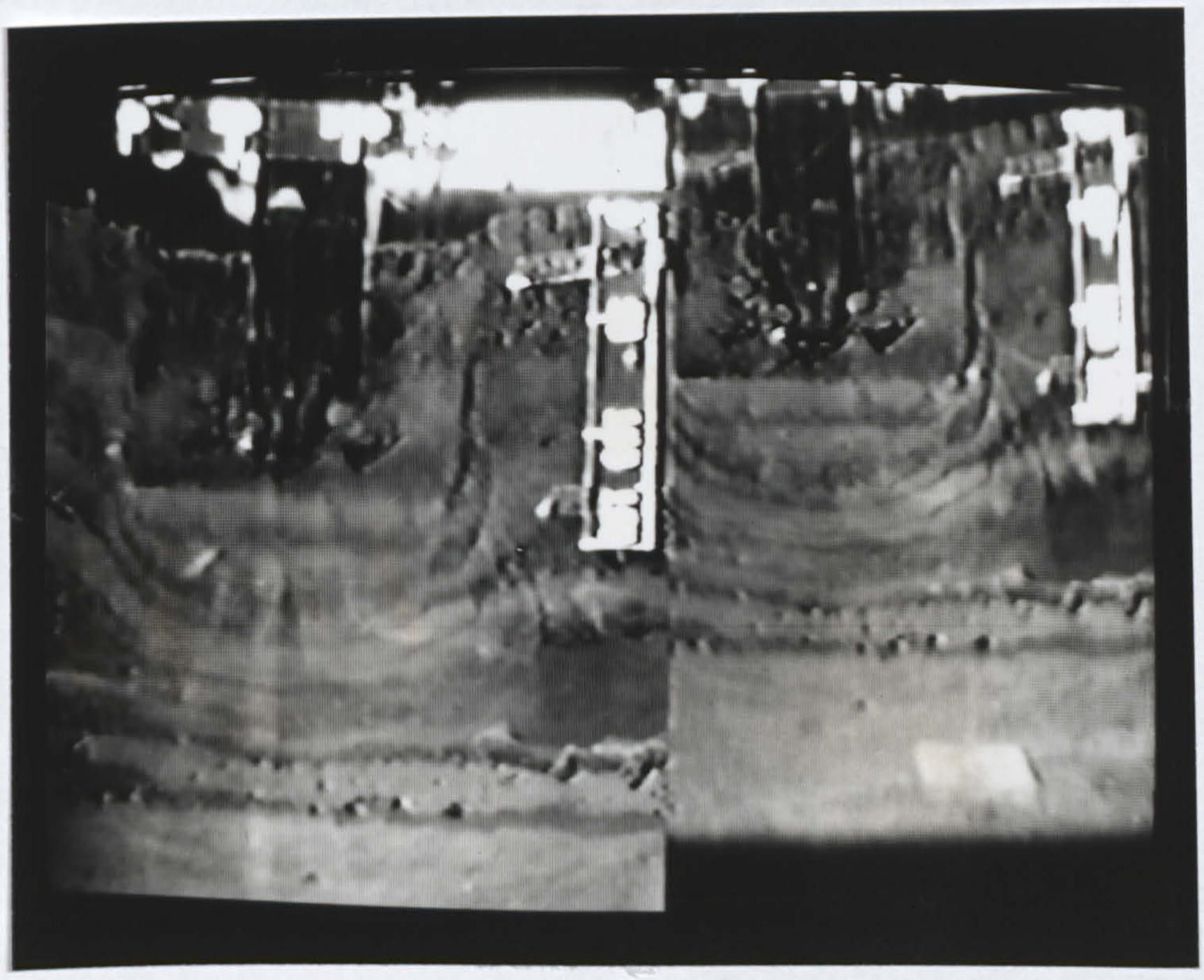

g)

Figure 5.3. A sequence of photographs taken from the video at a long exposure (2 seconds) for a plate sinkage test on loose sandy loam soil. The right and left hand sides of the screen correspond to modes 'A' and 'B' respectively.

Phase I where radial stress is constant (pure compaction) (*Figure 5.3b*)

Phase II radial stress is increasing (pure compaction)

Phase III compaction point is reached and soil displaces and compacts laterally (*Figure 5.3d*)

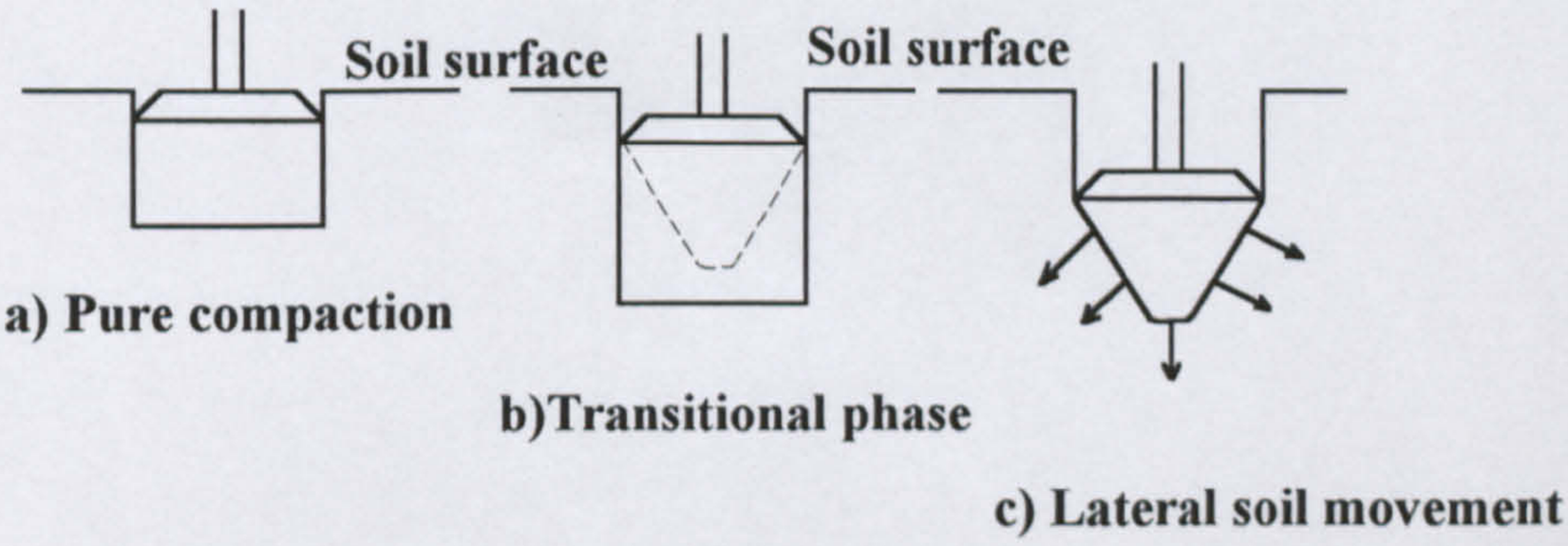

Figure 5.4. Proposed failure phases during a plate sinkage test.

5.3.1 Radial stress

Earl (1993) suggested the use of radial stress in order to distinguish between the three phases. His suggestion is based on the hypothesis that soil below a plate behaves in a similar manner to that in confined compression for stresses less than those at the compaction point. There is no reason to suggest that this is not the case. During the phase of pure compaction little lateral stress is expected. Once the compaction point is approached an increase in the radial stress is expected. A typical relationship between radial stress and axial stress, derived from a confined compression test, is presented in *Figure 5.5*.

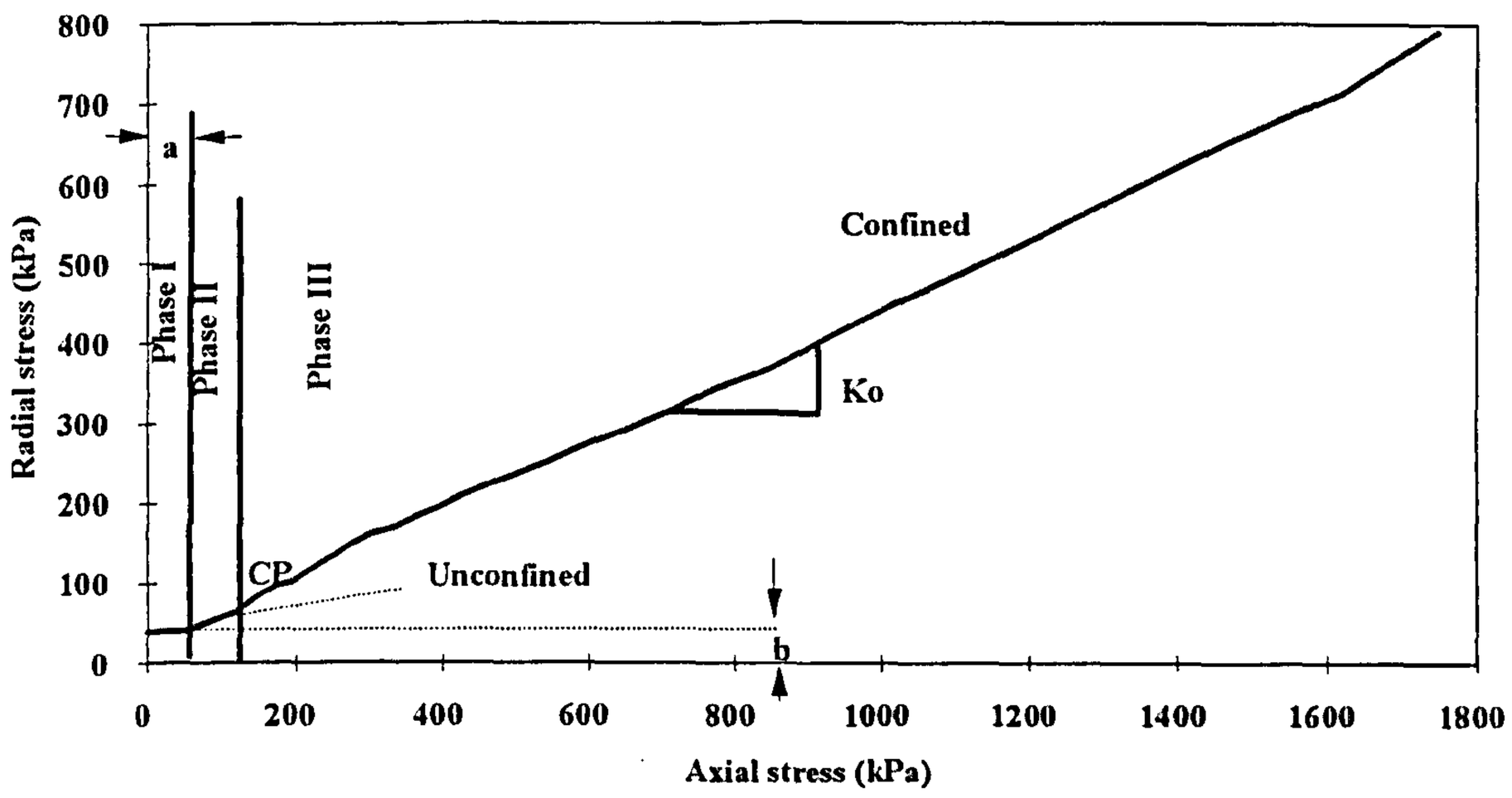

Figure 5.5. Typical relationship between radial stress and axial stress for sandy loam soil under compression.

From Figure 5.5 the compression process in terms of radial stress (σ_R) can be described by (Earl 1993):-

Phase I: $\sigma_R = b$ (constant)

Phases II $\sigma_R = K_o(\sigma_A - a) + b$

Phase III: $\sigma_R = K_o(\sigma_A - a) + b$

Where:-

a = value of axial stress for which radial stress is constant (kPa)

K_o = coefficient of earth pressure at rest
σ_R = radial stress (kPa)
σ_A = axial stress (kPa)
b = confining stress of the soil (kPa)

Although during phases II and III radial stress is expressed by the same equation, the mode of deformation below the plate differs. In the following paragraphs these phases will be analysed in more details. For phases I and II the analysis developed by Earl (1993) has been entirely adopted. During phase III the model proposed by Earl (1993) in the absence of visual data, does not adequately describe the experimental results encountered during this work and, therefore, a new model is proposed.

5.3.2 Phase I

During phase I, the disturbed zone below the plate is cylindrical (*Figure 5.3b*). The forces applied are as illustrated in *Figure 5.6*.

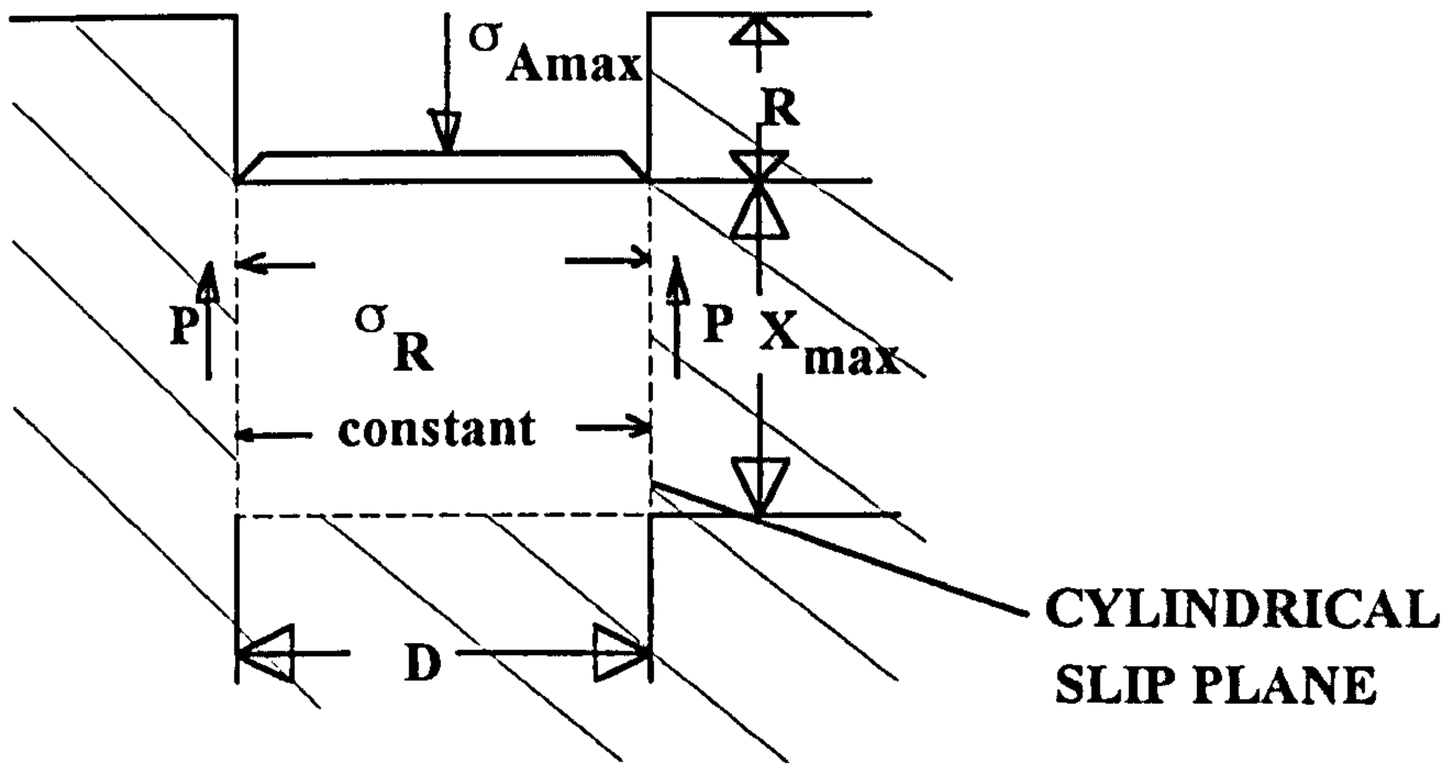

Figure 5.6. Schematic diagram illustrating failure below a plate in sandy loam soil during phase I.

From Coulomb law:-

$$\tau = c + \sigma_R \tan\varphi \qquad (5.1)$$

Where:-

τ = shear stress (kPa)
φ = angle of shearing resistance (internal friction)
σ_R = radial stress (kPa)
c = cohesion (kPa)

but radial stress during this phase remains constant.

For the cylindrical slip plane the total shear resistance is equal to *cylindrical area· shear stress*:-

$$P = \pi D X_{max}(c + \sigma_R \tan\phi) \qquad (5.2)$$

Where:-

P = total shear resistance (kN)
D = diameter of the plate (m)
X_{max} = depth of disturbance below the plate from the soil surface (m)

But the total shear resistance is equal to the applied force:-

$$P = [\sigma_{Amax} + \gamma(R + X_{max})]\frac{\pi D^2}{4} \qquad (5.3)$$

Where:-

γ = bulk unit weight (water, soil, air) (kN)

Substituting (5.3) in (5.2) and rearranging:-

$$X_{max} = \frac{D(\sigma_{Amax} + \gamma R)}{4(c + \sigma_R \tan\phi) - \gamma D} \qquad (5.4)$$

Depth of disturbance from the soil surface:-

$$= R + X_{max} \tag{5.5}$$

The maximum dry bulk density below the plate can be predicted from:-

$$\text{Initial } D_B = \frac{\text{mass of dry solids}}{\text{plate area} \cdot (R + X_{max})} \tag{5.6}$$

$$\text{Average final } D_B = \frac{\text{mass of dry solids}}{\text{plate area} \cdot X_{max}} \tag{5.7}$$

Substituting (5.6) in (5.7):-

$$\text{Average final } D_B = \frac{\text{Initial } D_B \cdot (R + X_{max})}{X_{max}} \tag{5.8}$$

If dry bulk density is assumed to decrease linearly with X from a maximum at $X=0$ to the initial state $X=X_{max}$ then:-

$$\text{Average final } D_B = \frac{\text{Initial } D_B + D_{Bmax}}{2} \tag{5.9}$$

Substituting (5.8) in (5.9) and rearranging:-

$$D_{Bmax} = \frac{\text{Initial } D_B \cdot (2R + X_{max})}{X_{max}} \tag{5.10}$$

5.3.3 Phase II

During phase II, stress-strain curve for confined compression and plate sinkage tests still coincide and so data obtained during confined compression test can be still used for analysis purposes. Although radial stress increases during this phase (*Figure 5.5*), there is no lateral soil movement (*Figures 5.3 b, c*), leading to the assumption that this increase is "consumed" by the internal mechanisms which lead to the formation of the soil cone. These mechanisms can not be described since there is no

experimental evidence of them obtained during this work. *Figure 5.7* illustrates the forces developed below a plate during phase II. Axial stress due to plate can be assumed to be at a maximum immediately below the plate but tending towards zero at some point down the soil profile (*Figure 5.7*). On the other hand axial stress due to soil weight is greater at maximum soil disturbance and tends towards zero immediately below the plate. Radial stress will diminish with depth till it reaches the constant minimum value *b* at a depth when no longer exceeds the maximum axial stress for phase I (*Figure 5.7*).

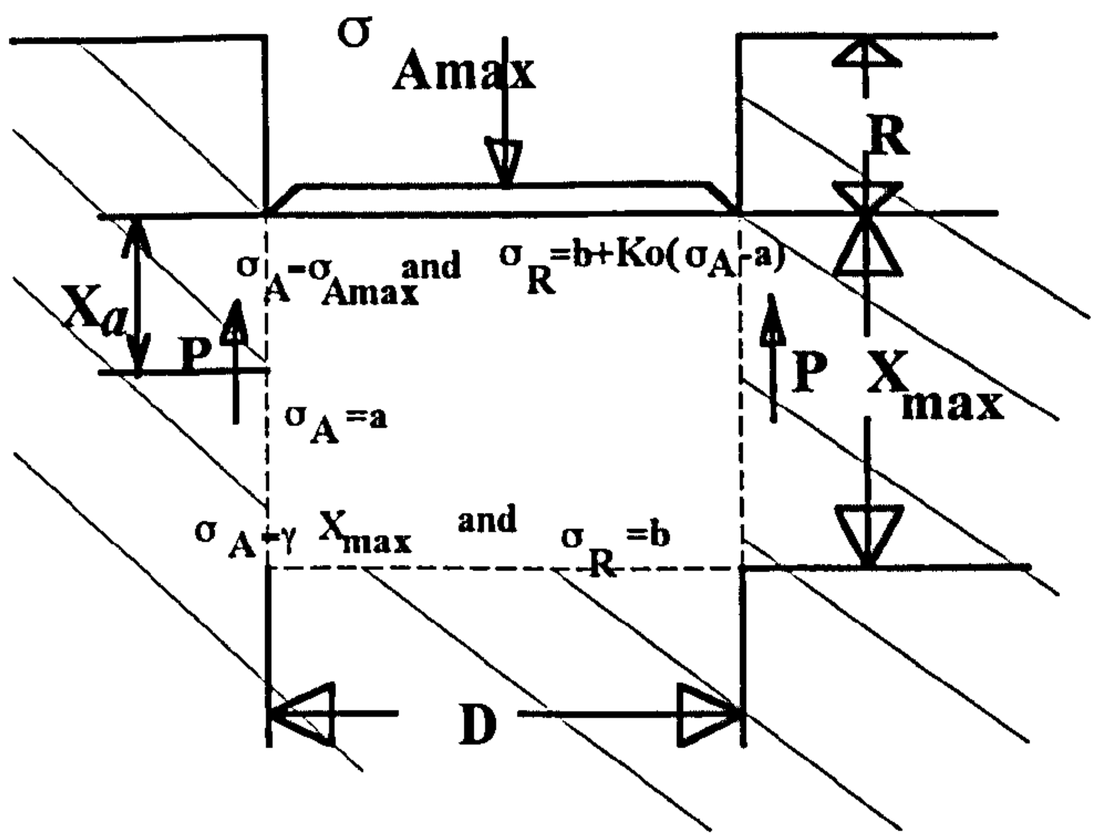

Figure 5.7. Schematic diagram of forces during phase II in terms of axial and radial stress.

During phase II shear resistance will be:-

$$P = cA + \sigma_R A \tan\varphi \qquad (5.11)$$

Where:-

A = cylindrical area (m^2)

Integrating between *0* to $X=X_a$ and $X=X_a$ to $X=X_{max}$:-

$$P = \pi D \int_{X_0}^{X_a} \{c + \tan\varphi [b + K_o(\sigma_A - a)]\} dx \quad \text{phase II}$$

$$+\pi D \int_{Xa}^{X_{max}} \{c + b \tan \varphi\} dx \qquad \text{phase I} \qquad (5.12)$$

Where:-

K_o = coefficient of earth pressure at rest

To solve equation (5.12), an equation describing the decrease in σ_A with X is required. During phase II, axial stress generated in the soil as a result of plate pressure, is assumed to be at a maximum immediately below the plate but tends towards zero at a point down the soil profile where soil remains undisturbed by the sinkage test. If axial stress is assumed to diminish linearly with X then this can be represented by the diagram in *Figure 5.8*.

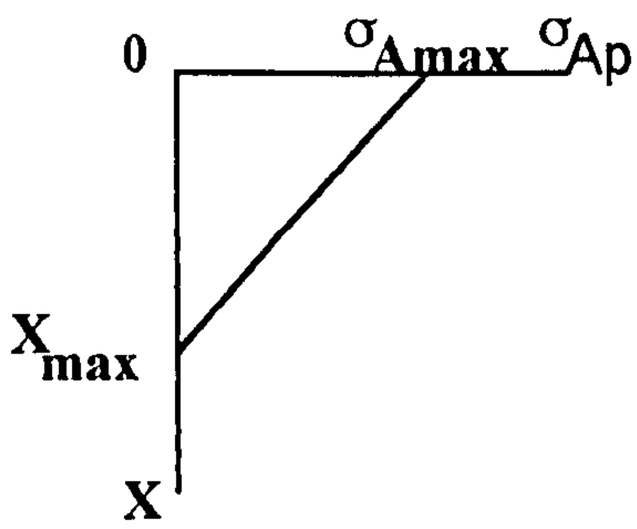

Figure 5.8. The assumed relationship between axial stress and distance below sinkage plate.

With reference to *Figure 5.8*, for a straight line:-

$$\sigma_{Ap} = \sigma_{Amax}(1 - \frac{X}{X_{max}}) \qquad (5.13)$$

If the axial stress due to soil weight σ_{Aw} is assumed to be at a minimum immediately below the plate but tend linearly towards maximum at a point down the soil profile the relationship illustrated in *Figure 5.9* is obtained.

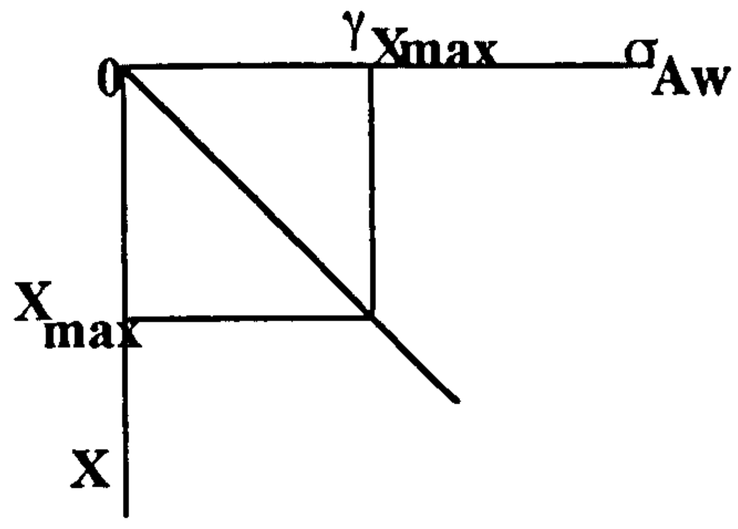

Figure 5.9. The assumed relationship between axial stress due to soil weight and distance below a sinkage plate.

With reference to *Figure 5.9* the stress due to the soil weight (σ_{Aw}) will become:-

$$\sigma_{Aw} = \gamma X \tag{5.14}$$

Total axial stress below the sinkage plate:-

$$\sigma_A = \sigma_{Ap} + \sigma_{Aw} \tag{5.15}$$

Substituting (5.13) and (5.14) into (5.15):-

$$\sigma_A = \sigma_{Amax}(1 - \frac{X}{X_{max}}) + \gamma X \tag{5.16}$$

Substituting (5.16) in (5.12) and integrating with respect to X:-

$$\frac{P}{\pi D} = \frac{a - \sigma_{A\max}}{\gamma - \dfrac{\sigma_{A\max}}{X_{\max}}}\{c + (b - a + K_o\sigma_{A\max})\tan\phi + \frac{K_o}{2}(\frac{\gamma - \sigma_{A\max}}{X_{\max}})(\frac{a - \sigma_{A\max}}{\gamma - \dfrac{\sigma_{A\max}}{X_{\max}}})\tan\phi\} + (c + b\tan\phi)(X_{\max} - (\frac{a - \sigma_{A\max}}{\gamma - \dfrac{\sigma_{A\max}}{X_{\max}}})) \tag{5.17}$$

To solve equation (5.17), a value for the disturbed bulk unit weight is required. Average disturbed bulk unit weight can be assumed to be:-

$$\gamma_{Dist} = \frac{\gamma(R + X_{max})}{X_{max}} \qquad (5.18)$$

Substituting (5.18) in (5.17) and rearranging:-

$$\sigma_{Amax} = \frac{4X_{max}(a - \sigma_{Amax})}{D(\gamma(R + X_{max}) - \sigma_{Amax})}\{c + (b - a + K_o\sigma_{Amax})\tan\phi +$$

$$\frac{K_o}{2}(\gamma(R + X_{max}) - \sigma_{Amax})\frac{a - \sigma_{Amax}}{\gamma(R + X_{max}) - \sigma_{Amax}}\tan\phi\} + \qquad (5.19)$$

$$\frac{4X_{max}}{D}(c + b\tan\phi)(1 - \frac{a - \sigma_{Amax}}{\gamma(R + X_{max}) - \sigma_{Amax}})$$

Depth of disturbance from the soil surface:-

$$= R + X_{max} \qquad (5.21)$$

Equation (5.19) can be solved iteratively to predict X_{max} and hence depth of disturbance from the soil surface (Earl 1993).

5.3.4 Phase III

During phase III, a stable cone of soil forms under the plate causing lateral displacement and compaction. It is normally expected that the failure pattern of soil pushed by the cone can be approximated by a logarithmic spiral (Prandlt 1920 and 1921, Terzaghi 1943, Meyerhof 1951 and 1961 and Earl 1993). This, however, was not observed during the soil bin experiments (*Figure 5.2e*), where it can be seen that soil failure is better approximated by a segment of a sphere. The reason for that might be attributed to the shape of the cone. It is widely assumed that the soil cone

is triangular in section. For the conditions encountered during this work the apical angle was difficult to distinguish as it appeared to push soil ahead of the tip rather than to each side (*Figure 5.10*).

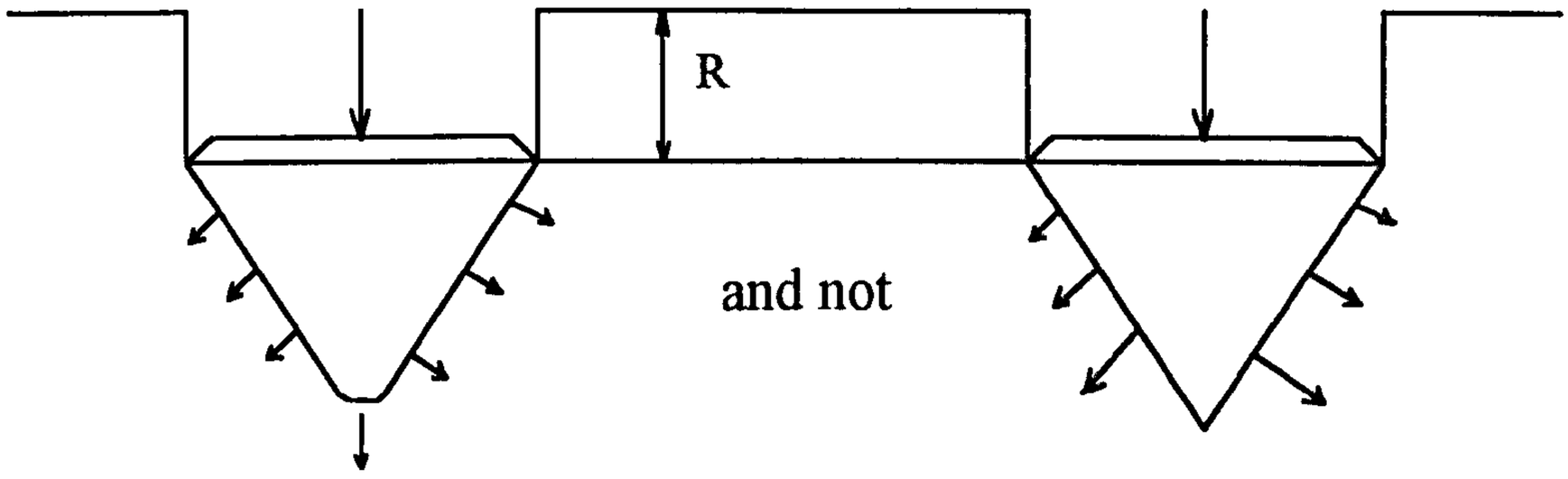

Figure 5.10. Schematic diagram of the soil cone during phase III.

This difference in the failure patterns between the classical approach of the logarithmic spiral and the segment of a sphere encountered during this work may be a result of the difference in the rate of load application between the situations to which they refer. As noted in paragraph 5.1, logarithmic spiral approach was developed to model soil behaviour below a footing, where the rate of load application is low (authors like Das, 1993 refer to it as static). In contrast, during this experimentation the penetration velocity of the plate was approximately 10 mm/s. Das (1993) points out that at high loading rates, soil particles in the failure zone do not always follow the path of least resistance.

5.3.4.1 Determination of the extent of soil disturbance

Figure 5.11 illustrates the extent of the soil disturbance under the plate during phase III. The failure pattern in close proximity to plate can be approximated by a segment of a sphere (*Figures 5.2d and g*).

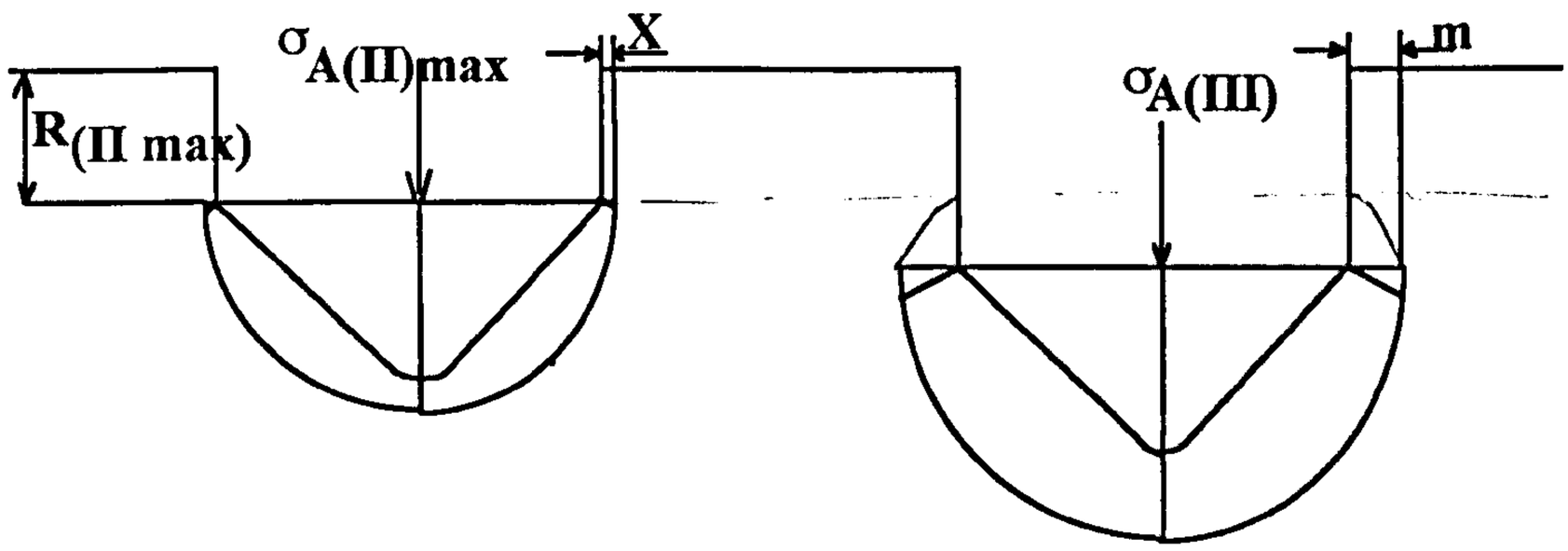

Figure 5.11. Diagram illustrating the extent of soil disturbance below a plate.

As soil passes from phase II to phase III the lateral soil disturbance can be assumed to be *X* (*Figure 5.11a*). As load increases and the plate sinks, further lateral soil disturbance is increased further to *m* (*Figure 5.12b*).

A mathematical expression can be developed for phase III by balancing the moment of forces about the point O (*Figure 5.12*). Forces included on this expression are:-

Passive force due to applied load	(F_f)
Soil weight on the lower slip-plane	(W_1)
Soil weight of the disturbed area	(W_2)
Soil weight on the upper slip-plane	(W_3)
Resultant of normal and frictional forces along upper slip plane	(F_2)
Soil force due to the confined stress of the soil	(F_s)

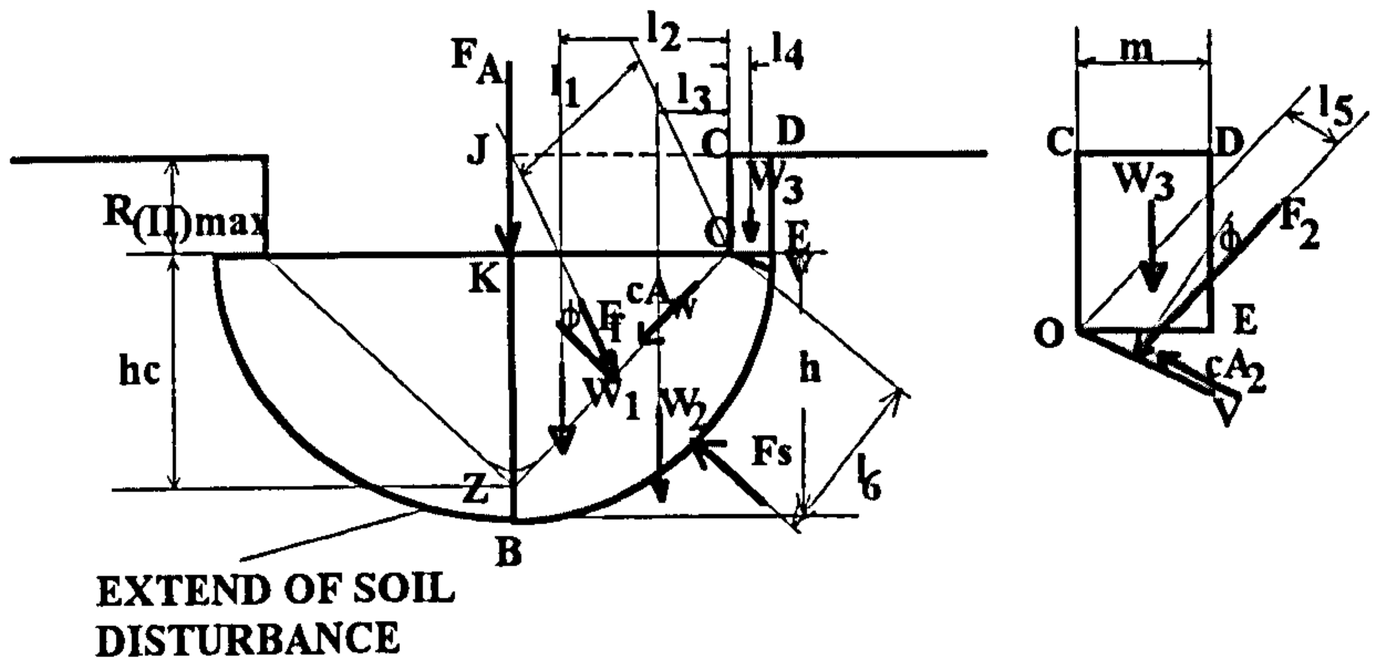

Figure 5.12. Force diagram (RHS only) for the failure zone under a plate at maximum phase II sinkage.

Determination of passive force (F_f)

With reference to *Figure 5.13* the disturbed soil surrounding the soil cone is subject to passive earth pressure F_p. The proportion and direction of the axial stress resulting in passive force is governed by the cohesion *c* and the resultant Fp of the normal and frictional stresses along the slip surface.

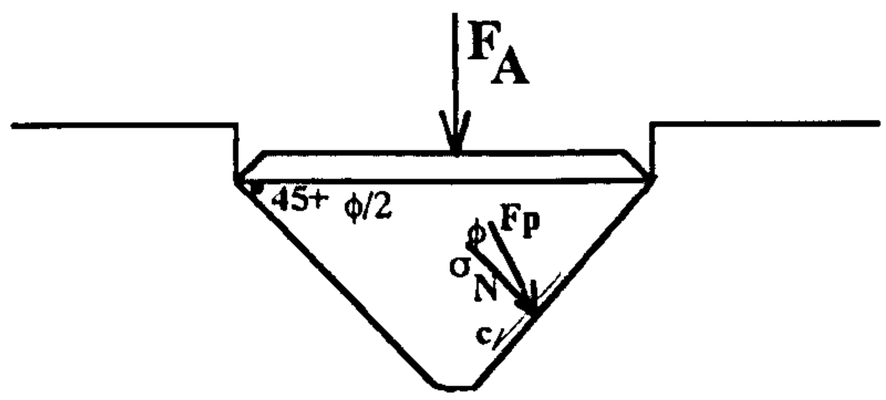

Figure 5.13. Diagram of forces (RHS only) acting on soil surrounding a sinkage plate

With reference to *Figure 5.13*:-

$$F_p = \sigma_N \sec\varphi \qquad (5.22)$$

F_p can be expressed in terms of total passive force F_f by multiplying F_p by the cone area, A:-

$$F_f = F_p A = \sigma_N \sec\varphi A \tag{5.23}$$

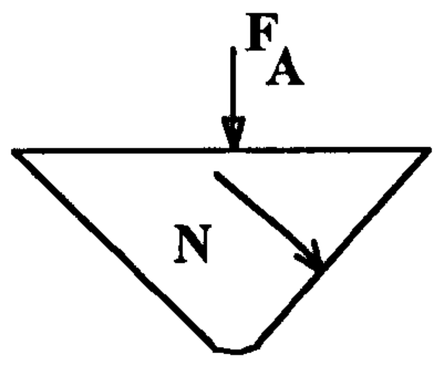

(a)

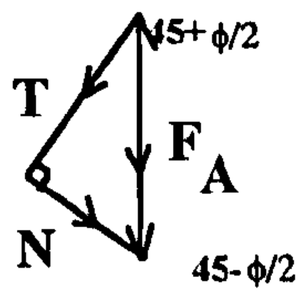

(b)

Figure 5.14. Vector diagram of forces at failure for the cone area.

From the vector of forces in (*Figure 5.14*):-

$$N = F_A \cos(45 + \frac{\varphi}{2}) \tag{5.24}$$

and

$$\sigma_N = \frac{N}{A} = \frac{F_A \cos(45 + \frac{\varphi}{2})}{A} \tag{5.25}$$

Substituting (5.25) in (5.23):-

$$F_f = F_A \cos(45 + \frac{\varphi}{2}) \sec\varphi \tag{5.27}$$

Location of slip-planes

Assume that *Figure 5.15* represents the force diagram for the failure zone at phase III. The forces acting on the failure zone (right hand side) are:-

Passive force due to applied load	(F_f)
Soil weight on the lower slip-plane	(W_1)
Soil weight of the disturbed area (exclusive of W_1)	(W_2)
Soil weight on the upper slip-plane	(W_3)
Resultant of normal and frictional forces along upper slip plane	(F_2)
Resultant of the cohesive force along VO	(cA_2)
The cohesion along ZO	(cA_w)
Soil force due to the confined stress of the soil	(F_s)

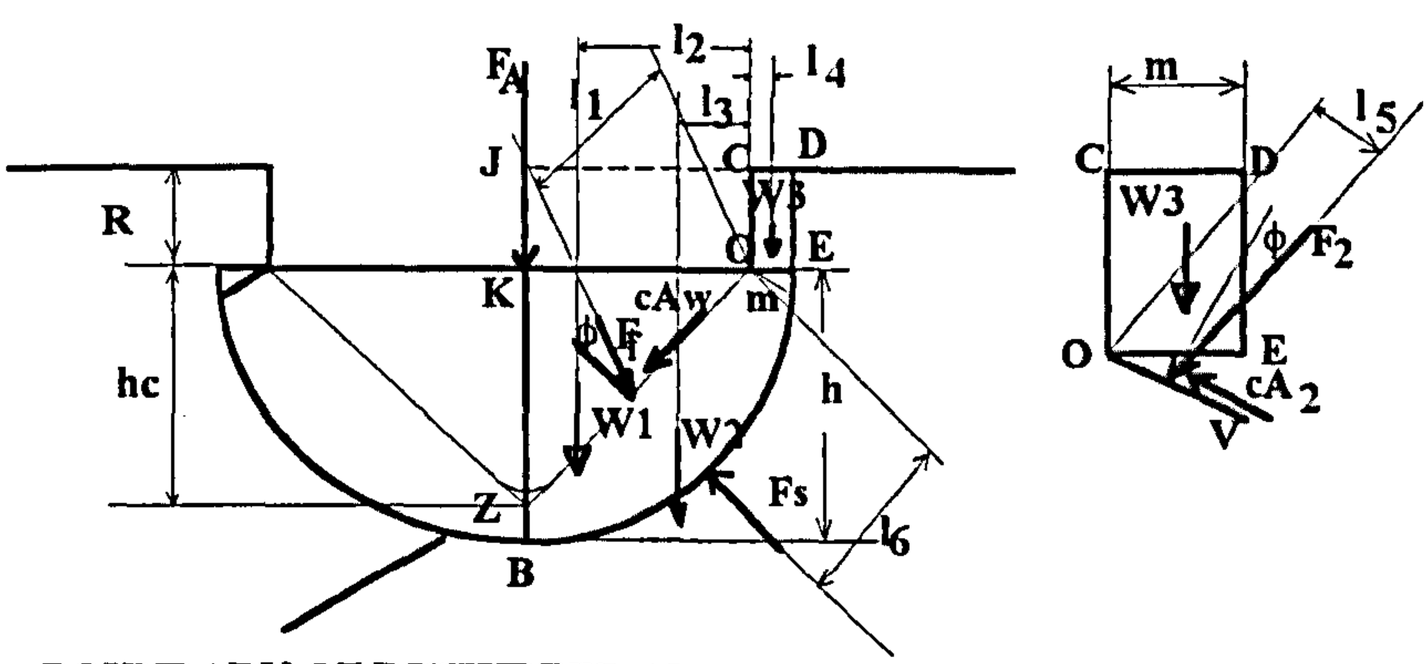

Figure 5.15. Force diagram (RHS only) for the failure zone under a plate during phase III.

The direction of cA_w along ZO and cA_2 along OV pass through O and therefore have no moment about O. Taking moments about O:-

$$F_f l_1 = -W_1 l_2 - W_2 l_3 + W_3 l_4 + F_2 l_5 + F_s l_6 \qquad (5.27)$$

For the calculations following, it has been assumed that the soil cone below the plate is normal.

Distance l_1

Earl (1993) noted for the determination of l_1 that it is complex and therefore assumptions concerning its position are required to simplify the analysis. Terzaghi (1943) developed a technique for solving passive earth pressure of cohesive soils on walls. This involved the resolving of the pressure into two parts, namely that due to soil weight alone and that due to cohesion. The former acts at a point 2/3 down the wall while the latter acts halfway down the wall. Terzaghi points out that the above mentioned theory is strictly correct only when the back of the wall is vertical and perfectly smooth. For all other conditions the procedure is approximate. If the point of application is assumed to lie in the range 1/2 to 2/3 down the wedge face, l_1 can be determined by following an iterative procedure. This technique has been proposed by Earl (1993) and adopted during this work. With reference to *Figure 5.16*, a range within which l_1 lies can be determined.

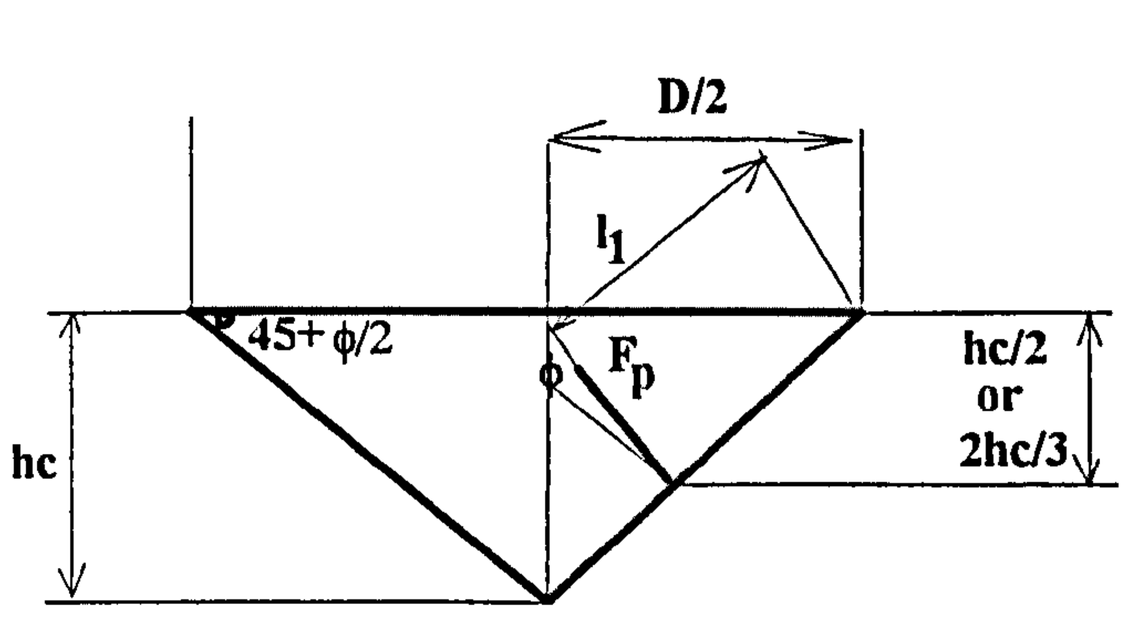

Figure 5.16. Diagram illustrating the determination of the point of application of passive pressure l_1.

$$l_1 = \frac{\frac{h_c}{2} or \frac{2h_c}{3}}{\sin(45 + \frac{\varphi}{2})} \cos\phi \qquad (5.28)$$

but

$$h_c = \frac{D}{2} tan(45 + \frac{\varphi}{2}) \qquad (5.29)$$

and therefore:-

$$l_1 = \frac{D}{4\,cos(45 + \frac{\varphi}{2})} cos\,\phi \qquad (5.30)$$

to

$$l_1 = \frac{D}{3\,cos(45 + \frac{\varphi}{2})} cos\,\phi \qquad (5.31)$$

Weight of the soil W_1

If we assume that R is the maximum sinkage occurred during phase II, then the weight of soil W_1 can be assumed to comprise of soil in the disturbed area KZO and the soil which moved downwards during phase II.

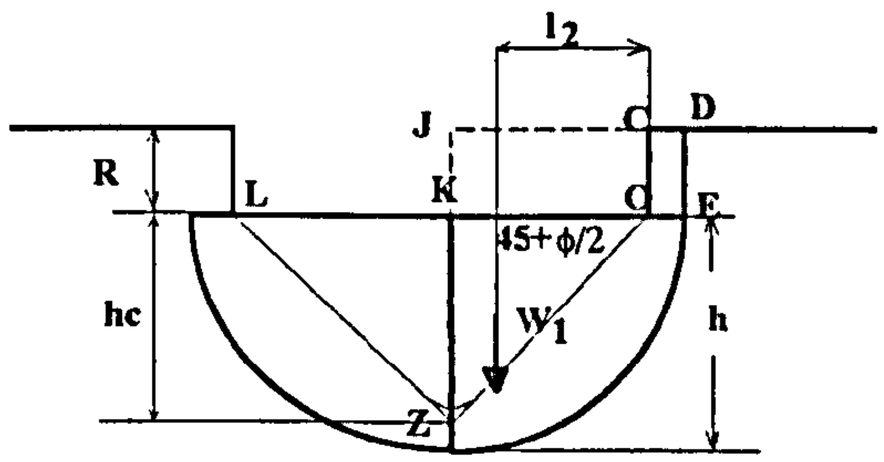

Figure 5.17. Diagram to illustrate computation of W_1.

Dry bulk density:-

$$D_B = \frac{W}{V} \qquad (5.32)$$

Where:-

W = mass of dry solids (kg)
V = volume of the soil sample (m^3)

The volume of the cone is:-

$$V_{LOZ} = \frac{\pi}{3}\frac{D^2}{4}h_c \qquad (5.33)$$

The weight of the soil into the half conical area becomes:-

$$W_1 = D_B(\frac{1}{2}V_{LZO} + V_{KJCO})$$

Where:-

D_B = initial dry bulk density (kg/m^3)

$$W_1 = D_B(\frac{1}{2}\frac{\pi}{3}\frac{D^2}{4}h_c + \frac{\pi}{2\cdot 4}D^2 R_{I\,Imax}) \qquad (5.34)$$

Where:-

R_{IImax} = the maximum sinkage during phase II (m)

Substituting (5.29) in (5.34):-

$$W_1 = \frac{\pi D^2 D_B}{8}[\frac{D}{6}tan(45^o + \frac{\varphi}{2}) + R_{I\,Imax})] \qquad (5.35)$$

Determination of distance l_2

The point of application of W_1 can be assumed to be the centre of gravity of the half cone KOZ (*Figure 5.17*).

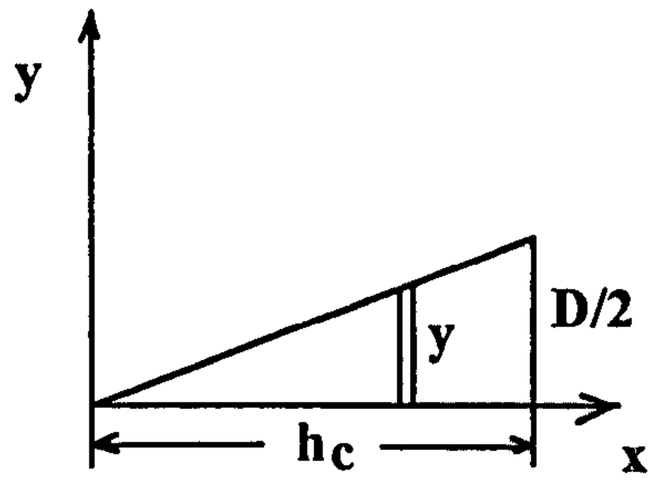

Figure 5.18. Diagram to illustrate computation of centre of gravity of half cone.

From *Figure 5.18*:-

$$y = \frac{D/2}{h_c}x$$

$$\therefore dy = (\frac{D/2}{h_c})dx$$

$$\therefore dx = (\frac{h_c}{D/2})dy$$

Integrating the volume of half cone between *0* to $X=h_c$:-

$$\frac{\pi}{6}\frac{D^2}{4}h_c \cdot \bar{y} = \int_0^{h_c} \frac{1}{2}\pi y^2 (\frac{4y}{3\pi})dx$$

$$= \frac{2}{3}\int_0^{h_c} y^3 dx = \frac{2}{3}\int_0^{D/2} y^3 (\frac{h_c}{D/2})dy$$

$$= \frac{D^3}{48}h_c$$

$$\therefore \bar{y} = \frac{D/2}{\pi} = 0.16D \qquad (5.36)$$

and the distance l_2 from point O will be:-

$$l_2 = 0.34D \qquad (5.37)$$

Determination of W_2

The weight of the area OEBZ (*Figure 5.19*) can be determined as follows:

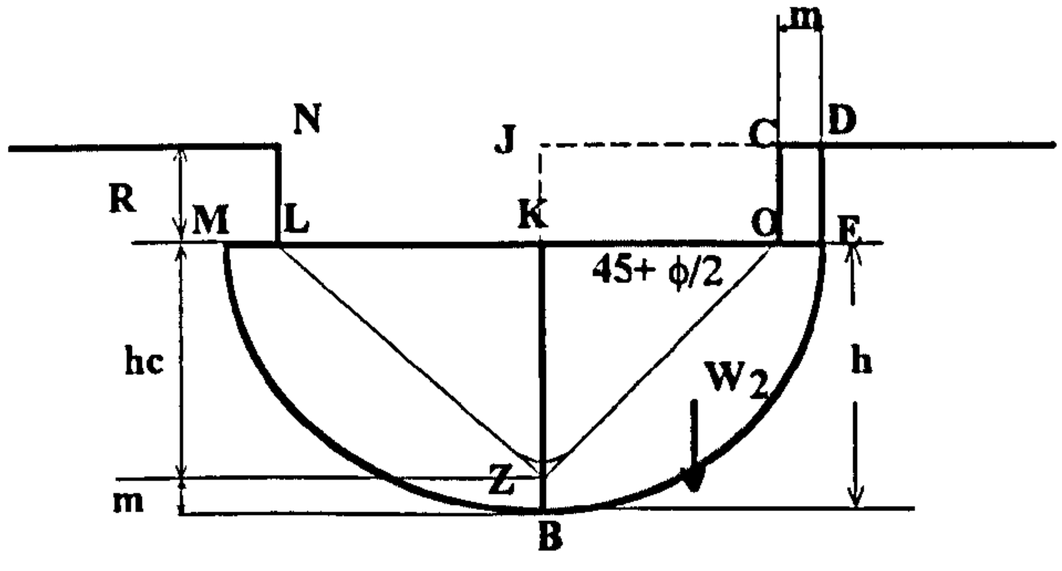

Figure 5.19. Diagram to illustrate computation of W_2.

Assuming that during phase III maximum vertical soil disturbance is given by:-

$$h = h_c + m \qquad (5.38)$$

If the area MEB is considered to be a segment of a sphere then the volume of KEB is given by:-

$$V_{KEB} = \frac{1}{2}\,\frac{\pi}{6}\,h\left[\frac{3}{4}\,(D+2m)^2 + h^2\right] \qquad (5.39)$$

Substituting (5.38) in (5.39):-

$$V_{KEB} = \frac{\pi}{2\cdot 6}(h_c + m)\cdot$$

$$\left\{\frac{3}{4}(D+2m)^2 + (h_c+m)^2\right\} \qquad (5.40)$$

but this area contains the half cone which has already been disturbed. OEBZ can be obtained by subtracting the volume of the half cone from the volume KEB.

$$V_{OEBZ} = V_{KEB} - V_{KOZ} \therefore$$

$$V_{OEBZ} = \{\frac{\pi}{12}(h_c + m) \cdot [\frac{3}{4}(D + 2m)^2 + (h_c + m)^2]\} -$$

$$\frac{1}{2}\frac{\pi}{3}\frac{D^2}{4}h_c \qquad (5.41)$$

Assuming that the bulk density between the edge of the cone and the limit of the disturbed area varies with the distance *m* as shown in *Figure 5.20* then the average bulk density is:-

$$D_{BA} = \frac{D_{B\,max} - D_B}{2} \qquad (5.42)$$

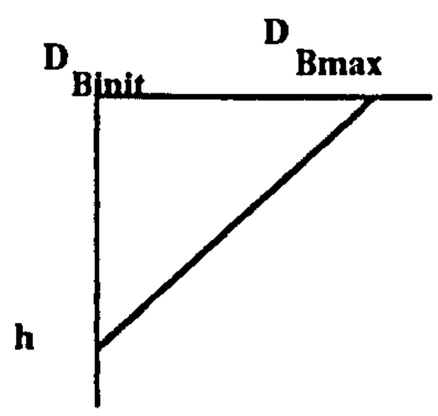

Figure 5.20. The assumed relationship between bulk density and distance below plate.

D_{Bmax} can be calculated from equation (5.32) if the weight W_1 and the half cone volume are substituted:-

$$D_{Bmax} = \frac{W_1}{V_{KOZ}} = \frac{W_1}{\frac{1\pi D^2}{2 \cdot 3 \cdot 4}h_c} \qquad (5.43)$$

The weight of the soil in this area is:-

$$W_2 = D_{BA} \cdot V_{OEBZ} =$$

$$(\frac{D_{B\,max} - D_B}{2})\{\frac{\pi}{12}(h_c + m)[\frac{3}{4}(D + 2m)^2 + (h_c + m)^2] -$$

$$\frac{1}{2}\frac{\pi}{3}\frac{D^2}{4}h_c\} \qquad (5.44)$$

Determination of l_3

For practical reasons it can be assumed that the point of application of W_2 will be on the centroid of the area OEBZ (*Figure 5.21*).

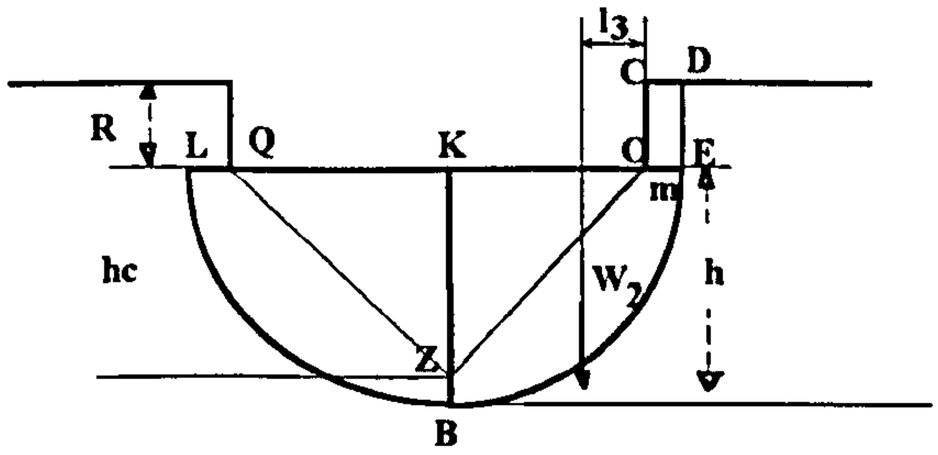

Figure 5.21. Schematic diagram to illustrate computation of l_3.

Assuming that ZB=OE=m, the distance from vertical plane yy' (*Figure 5.22*) is given by equation:-

$$\bar{y} = \frac{3\cdot[(\frac{D}{2}+m)^2+(h_c+m)^2]^4\cdot\sin^{-1}(\frac{2\cdot(\frac{D}{2}+m)\cdot(h_c+m)}{(\frac{D}{2}+m)^2+(h_c+m)^2}}{16\cdot\pi\cdot(h_c+m)^5\cdot[3(\frac{D}{2}+m)^2+(h_c+m)^2]}$$

$$\frac{-2\cdot(\frac{D}{2}+m)\cdot(h_c+m)\cdot[(\frac{D}{2}+m)^2-(h_c+m)^2]\cdot[3(\frac{D}{2}+m)^4+}{+14\cdot(\frac{D}{2}+m)^2\cdot(h_c+m)^2+3\cdot(h_c+m)^4]} \qquad (5.45)$$

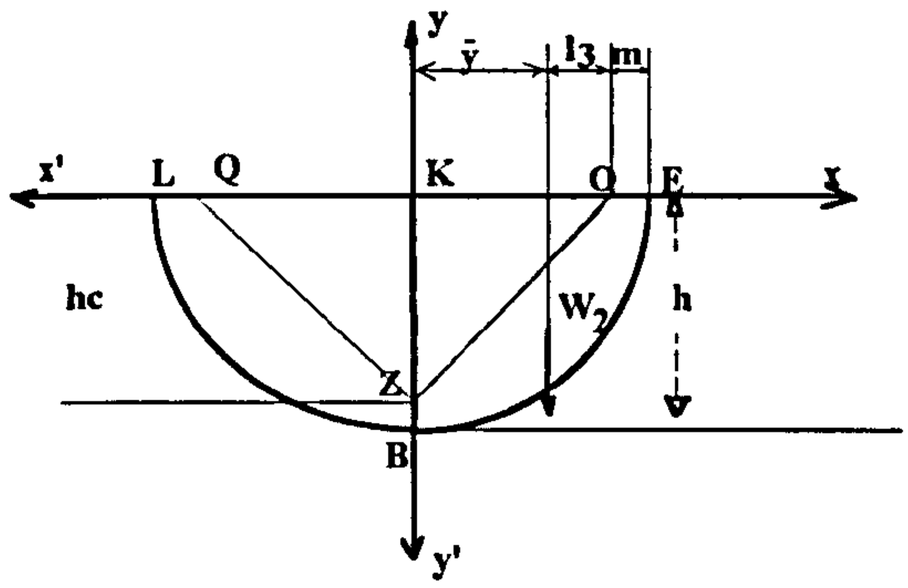

Figure 5.22. Diagram to illustrate computation of l_3.

The distance l_3 is:-

$$l_3 = \frac{D}{2} - \bar{y}$$

$$= \frac{D}{2} - \frac{3\cdot[(\frac{D}{2}+m)^2 + (h_c+m)^2]^4 \cdot \sin^{-1}(\frac{2\cdot(\frac{D}{2}+m)\cdot(h_c+m)}{(\frac{D}{2}+m)^2+(h_c+m)^2}}{16\cdot\pi\cdot(h_c+m)^5\cdot[3(\frac{D}{2}+m)^2+(h_c+m)^2]}$$

$$\frac{-2\cdot(\frac{D}{2}+m)\cdot(h_c+m)\cdot[(\frac{D}{2}+m)^2-(h_c+m)^2]\cdot[3(\frac{D}{2}+m)^4}{}$$

$$\frac{+14\cdot(\frac{D}{2}+m)^2\cdot(h_c+m)^2+3\cdot(h_c+m)^4]}{} \qquad (5.46)$$

Determination of W_3

Figure 5.23 illustrates the forces acting on the upper slip plane. It should be noted that no visual proof was obtained for this slip plane and it was assumed that it exists. It was also assumed that angle ZOV is equal to 90 degrees. Consequently, angle VOE becomes:-

$$\text{Angle VOE} = 45 - \frac{\varphi}{2} \qquad (5.47)$$

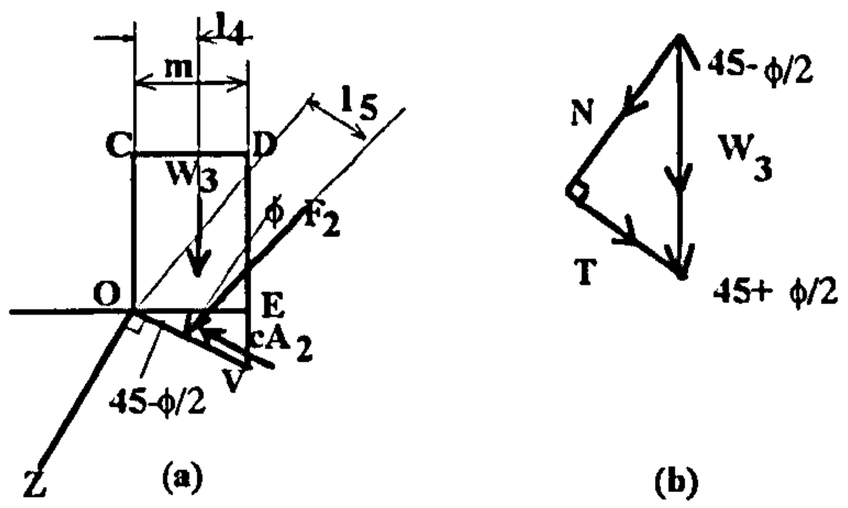

Figure 5.23. Force diagram on the OEDC.

The weight W_3 acts on the centroid of CDVO, and assuming that the soil in this area is undisturbed its magnitude can be determined from (5.32). The volume V_{CDVO} in this case is given by:-

$$V_{CDVO} = V_{CDEO} + V_{OVE}$$

$$\therefore V_{CDVO} = \frac{1}{2}\frac{\pi}{4} R[(D+2m)^2 - D^2] + \frac{1}{4}\frac{\pi}{4}[(m \cdot \tan(45-\frac{\varphi}{2})][(D+2m)^2 - D^2] \qquad (5.48)$$

substituting into (5.48) into (5.32):-

$$W_3 = D_B\{\frac{\pi}{8} R[(D+2m)^2 - D^2] + \frac{\pi}{16}[(m \cdot \tan(45-\frac{\varphi}{2})][(D+2m)^2 - D^2]\} \qquad (5.49)$$

Determination of l_4

W_3 has its point of application on the centre of gravity of the annulus CDVO. For practical reasons it has been assumed that its point of application could be on the centre of gravity of the annulus CDEO (*Figure 5.23*). From *Figure 5.24* first moment can be calculated as follows:-

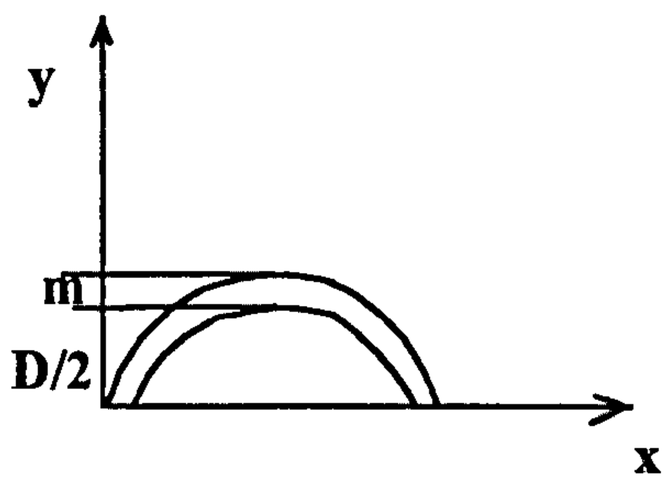

Figure 5.24. Diagram to illustrate computation of first moment about x-axis.

First moment about x-axis:-

$$\frac{(\frac{D}{2}+m)^3}{3}-\frac{(\frac{D}{2})^3}{3}=$$

$$\frac{1}{2}\pi[(\frac{D}{2}+m)^2-(\frac{D}{2})^2]\cdot\bar{y}$$

$$\therefore \bar{y}=\frac{\frac{(\frac{D}{2}+m)^3}{3}-\frac{(\frac{D}{2})^3}{3}}{\frac{1}{2}\pi[(\frac{D}{2}+m)^2-(\frac{D}{2})^2]}$$

$$=\frac{4}{3\pi}\frac{[(\frac{D}{2}+m)^2+(\frac{D}{2}+m)(\frac{D}{2})+(\frac{D}{2})^2]}{[(\frac{D}{2}+m)+(\frac{D}{2})]} \qquad (5.50)$$

and distance l_4 is given by:-

$$l_4=\frac{D}{2}-\frac{4}{3\pi}\frac{[(\frac{D}{2}+m)^2+(\frac{D}{2}+m)(\frac{D}{2})+(\frac{D}{2})^2]}{[(\frac{D}{2}+m)+(\frac{D}{2})]} \qquad (5.51)$$

Determination of F_2

With reference Figure 5.23:-

$$F_2 = N \sec \varphi \tag{5.52}$$

From the vector of forces (*Figure 5.22b*):-

$$N = W_3 \cos(45 + \frac{\phi}{2}) \tag{5.53}$$

Substituting 5.53 into 5.52:-

$$F_2 = W_3 \cos(45 + \frac{\varphi}{2}) \sec \varphi \tag{5.54}$$

Determination of l_5

With reference to *Figure 5.23*, l_5 lies in the range 1/2 to 2/3 down the wedge face.

$$l_5 = \frac{\dfrac{m}{2 \cdot \tan(45 - \frac{\varphi}{2})} \text{ or } \dfrac{2m}{3 \cdot \tan(45 - \frac{\varphi}{2})}}{\sin(45 - \frac{\varphi}{2})} \cos \phi \tag{5.55}$$

Soil resistance due to soil movement

Due to soil movement a soil resistance will be developed on the boundary of the disturbed area due to the confining stress of the soil (b). In can be expressed by:-

Soil resistance = confining stress · area

and for the half spherical segment it becomes:-

$$F_s = b \cdot \frac{1}{2} \frac{\pi}{4} [(D + m)^2 + 4(h_c + m)^2] \tag{5.56}$$

The value of b can be obtained from the confined compression test.

Determination of l_6

Soil resistance F_s acts in the middle of segment BE (*Figure 5.25*).

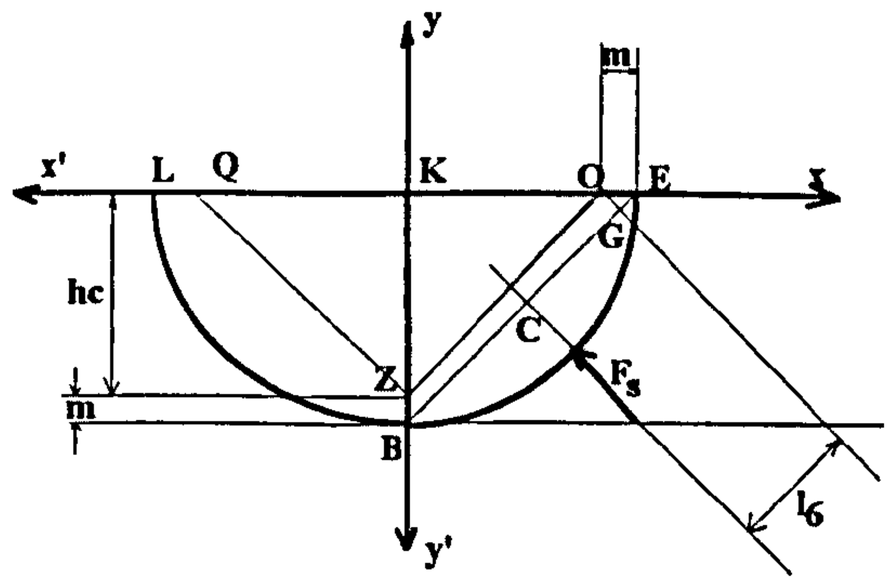

Figure 5.25. Diagram to illustrate computation of l_6.

l_6 can be calculated as follows.

From triangle KBE:-

$$BE = \sqrt{(h_c + m)^2 + (\frac{D}{2} + m)^2} \qquad (5.57)$$

and therefore

$$\frac{BE}{2} = \frac{1}{2}\sqrt{(h_c + m)^2 + (\frac{D}{2} + m)^2} \qquad (5.58)$$

Angle BEK:-

$$tan(BEK) = \frac{h_c + m}{\frac{D}{2} + m} \qquad (5.59)$$

and therefore

$$cos(BEK) = \frac{EG}{m} \therefore EG = m \cdot cos(BEK) \quad (5.60)$$

and consequently:-

$$CG = \frac{BE}{2} - GE$$

$$\therefore l_6 = \frac{1}{2}\sqrt{(h_c + m)^2 + (\frac{D}{2} + m)^2} - m \cdot cos[tan^{-1}(\frac{h_c + m}{\frac{D}{2} + m})] \quad (5.61)$$

Derivation of general equation:-

With reference to *Figure 5.15* the final expression obtained is:-

$$F_f l_1 = -W_1 l_2 - W_2 l_3 + W_3 l_4 + F_2 l_5 + F_s l_6 \quad (5.27)$$

$$\therefore F_A cos(45 + \frac{\varphi}{2}) sec\,\varphi \frac{D}{4cos(45 + \frac{\varphi}{2}) \text{ or } 3cos(45 + \frac{\varphi}{2})} cos\,\varphi$$

$$-\frac{\pi D^2 D_B}{8}[\frac{D}{6} tan(45^o + \frac{\varphi}{2}) + R_{I\,Imax})]0.34D$$

$$-\{(\frac{D_{Bmax} - D_B}{2})\{\frac{\pi}{12}(h_c + m)[\frac{3}{4}(D + 2m)^2 + (h_c + m)^2] -$$

$$\frac{1}{2}\frac{\pi}{3}\frac{D^2}{4}h_c\}\}.$$

$$\{\frac{D}{2}-\frac{3\cdot[(\frac{D}{2}+m)^2+(h_c+m)^2]^4\cdot\sin^{-1}(\frac{2\cdot(\frac{D}{2}+m)\cdot(h_c+m)}{(\frac{D}{2}+m)^2+(h_c+m)^2}}{16\cdot\pi\cdot(h_c+m)^5\cdot[3(\frac{D}{2}+m)^2+(h_c+m)^2]}$$

$$\frac{-2\cdot(\frac{D}{2}+m)\cdot(h_c+m)\cdot[(\frac{D}{2}+m)^2-(h_c+m)^2]\cdot[3(\frac{D}{2}+m)^4}{+14\cdot(\frac{D}{2}+m)^2\cdot(h_c+m)^2+3\cdot(h_c+m)^4]}\}$$

$$+D_B\{\frac{\pi}{8}R[(D+2m)^2-D^2]+\frac{\pi}{16}(m\cdot\tan\phi)[(D+2m)^2-D^2]\}\cdot$$

$$\{\frac{D}{2}-\frac{4}{3\pi}\frac{[(\frac{D}{2}+m)^2+(\frac{D}{2}+m)(\frac{D}{2})+(\frac{D}{2})^2]}{[(\frac{D}{2}+m)+(\frac{D}{2})]}\}$$

$$+W_3\cos(45+\frac{\varphi}{2})\sec\varphi\cdot\frac{\frac{m}{2\cdot\tan(45-\frac{\varphi}{2})}\ or\ \frac{2m}{3\cdot\tan(45-\frac{\varphi}{2})}}{\sin(45-\frac{\varphi}{2})}\cos\phi$$

$$+b\cdot\frac{1}{2}\frac{\pi}{4}[(D+m)^2+4(h_c+m)^2]\cdot$$

$$\frac{1}{2}\sqrt{(h_c+m)^2+(\frac{D}{2}+m)^2}-m\cdot\cos[\tan^{-1}(\frac{h_c+m}{\frac{D}{2}+m})] \qquad (5.62)$$

From equation (5.62) the maximum extent of lateral and vertical disturbance, for phase III, can be identified. The basic variables in this equation are:-

1) angle of shearing resistance (ϕ)
2) cohesion (c)
3) diameter of plate (D)
4) initial dry bulk density (D_B)
5) confined stress of the soil (b)
6) applied stress (σ_A)

The theory will be tested in the following section using data obtained during plate sinkage tests behind the glass.

5.4 Example of failure patterns below a sinking plate

5.4.1 Medium sandy loam soil

In order to test the above mentioned theory, the values of the angle of internal friction and cohesion are necessary. They were measured using triaxial test. The results for the medium sandy loam soil used during this work are presented in *Table 5.1*.

Table 5.1

Results obtained from triaxial test, for medium soil bin sandy loam soil

Cohesion, c, (kPa)	Angle of internal friction ϕ (degrees)	Moisture content (volumetric), %	Dry bulk density (Mg/m^3)
11.5	28	13.25	1.38

Values *a* of axial stress and *b* of radial stress were obtained from *Figures 5.26* and *5.27*.

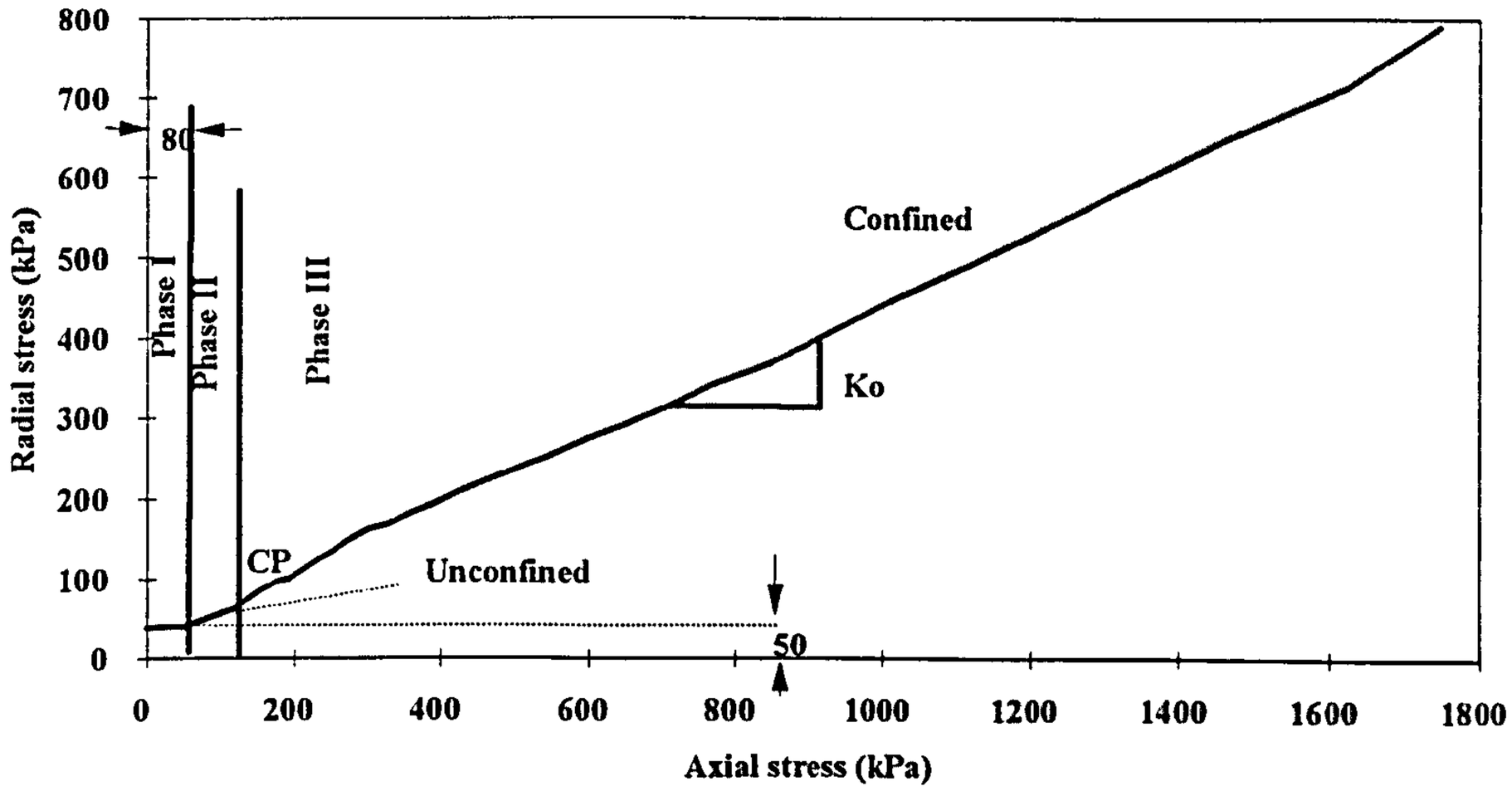

Figure 5.26. The relationship between radial stress and axial stress for medium sandy loam soil bin soil.

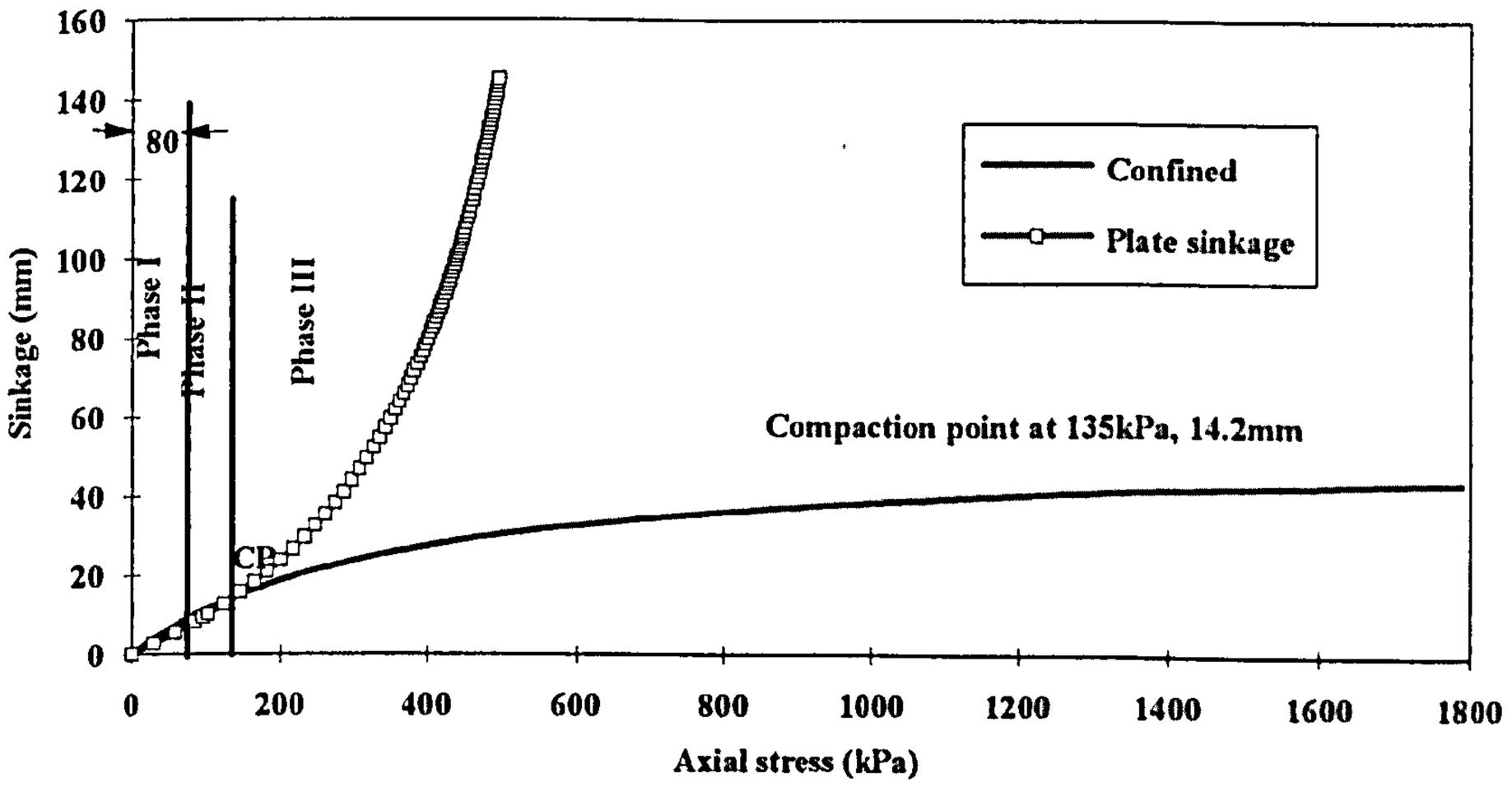

Figure 5.27. The relationship between compaction point and the three phases for medium sandy loam soil bin soil.

By substituting the experimental values of c, ϕ, a and b in equation (5.4), the maximum depth of soil disturbance below the plate during phase I can be obtained. During phase II, and for axial stress equal to the stress at compaction point, the maximum soil disturbance can be found from equation (5.19). At phase III, the maximum soil disturbance can be found if the data are substituted into equation

(5.62). The results are shown in Table 5.2. The approximate values were taken from pictures presented in *Figure 5.28*.

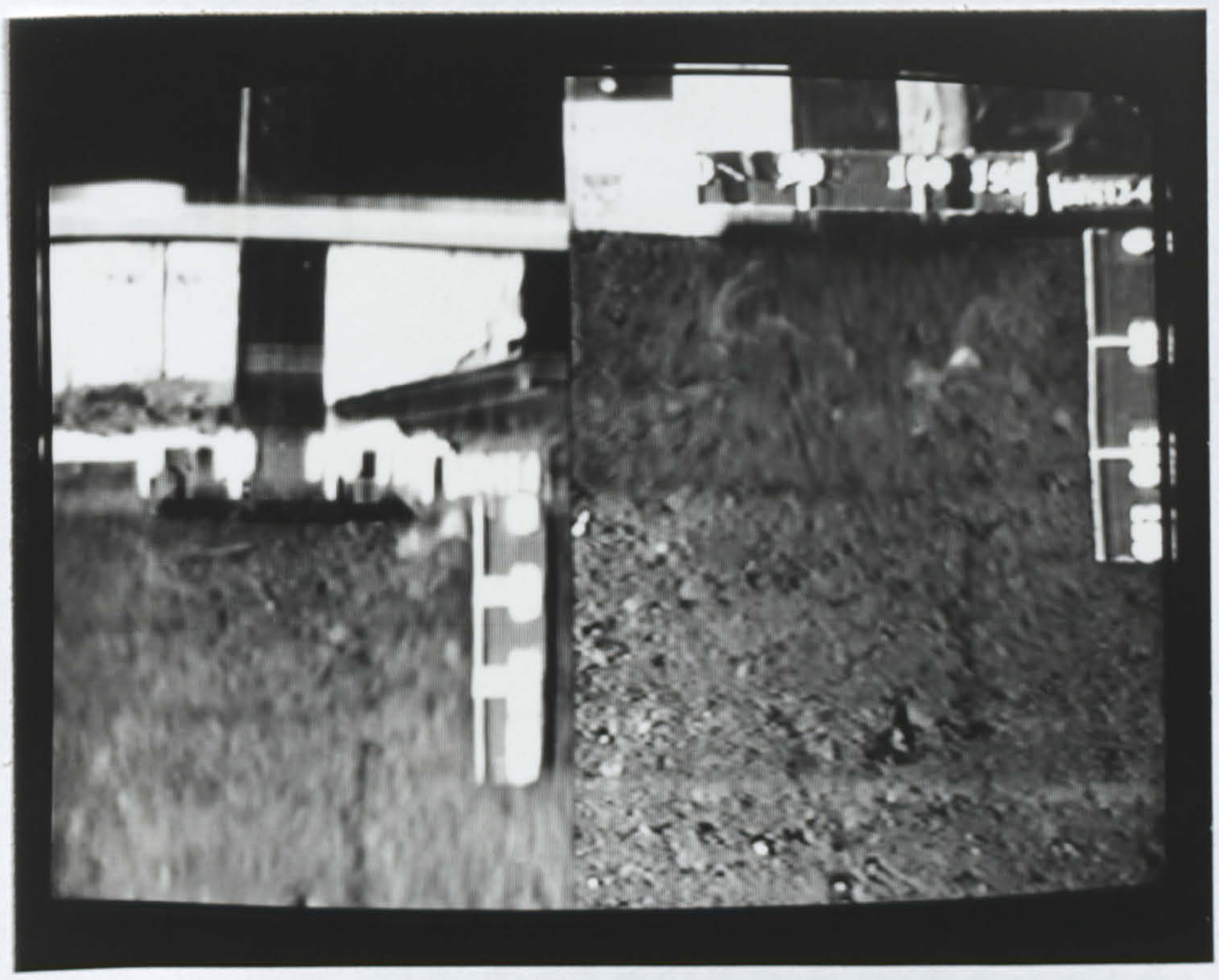

a)

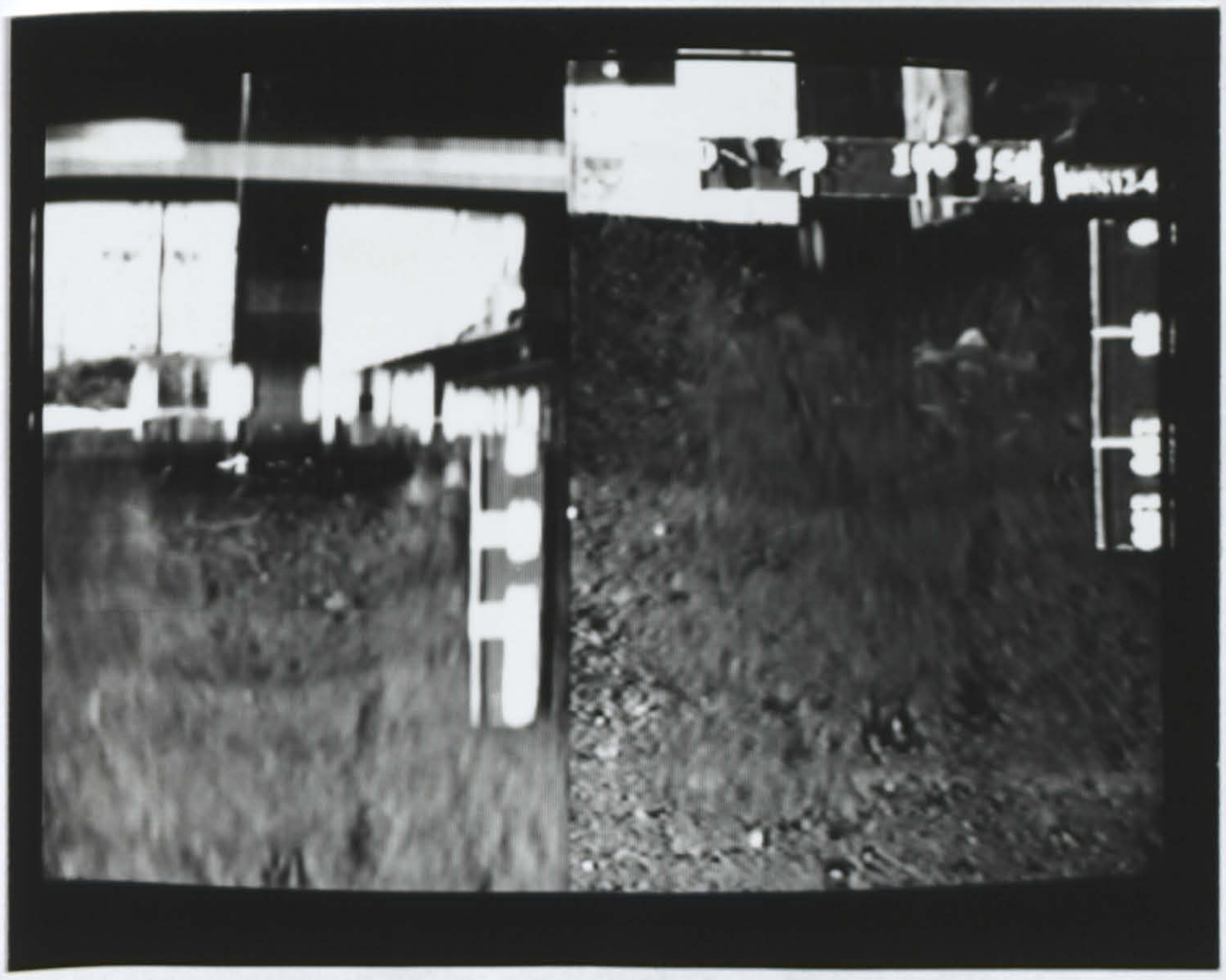

b)

c)

Figure 5.28. A sequence of photographs taken from the video at a long exposure (2 seconds) for a plate sinkage test on medium sandy loam soil.

Table 5.2. Extent of soil disturbance below plate during the three phases (medium soil).

	Applied axial stress (kPa)	Sinkage of the plate (m)	Maximum dry bulk density (Mg/m^3)	Maximum depth of disturbance X_{max} (m)	Disturbed volume of soil below the plate (m^3)	Maximum extent of disturbed area below the plate (m)	X_{max} shown in picture (approximate values in m)
Phase I	80	0.008	1.66	0.078	0.0014	0.150	0.070
Phase II	135	0.014	1.68	0.143	0.0025	0.150	
Phase III *l_1 from (5.30)*	356	0.080	n.a.	0.165	0.0058	0.230	0.180
Phase III *l_1 from (5.31)*	356	0.080	n.a.	0.185	0.0086	0.270	0.180

An indication of the effectiveness of above mentioned theory can be obtained if values of maximum soil disturbance derived from the model are compared with video evidence obtained during experiments behind the glass (*Figure 5.27).* The

accuracy of the model depends on the accuracy of the determination of the angle of shearing resistance and cohesion. For the soil used during this work, the method proved capable of identifying the extent of soil disturbance below the plate. The results of this comparison are summarised in *Table 5.2*. There it can be seen that the predicted values are close to values obtained from the video pictures.

5.4.2 Loose sandy loam soil

Measuring angle of shearing resistance and cohesion is problematical for loose soil. Triaxial, as well as translational, tests were used unsuccessfully due to the loose packing state of the soil. From the evidence presented during this work the failure patterns below the plate follow a similar pattern.

5.5 Summary

Three soil failure phases were distinguished during plate sinkage tests on a sandy loam soil. During phases I and II the disturbed area below the plate can be approximated by a cylinder. The disturbed area of the third phase can be approximated with a spherical segment. This does not agree with theories proposed by Prandlt (1920 and 1921), Terzaghi (1943) and Meyerhof (1951 and 1961), who approximated the failure pattern below a footing with a logarithmic spiral. The difference between the two approaches can be attributed to differences in penetration velocities under which the failure patterns took place. From an almost static test in the case of logarithmic spiral approach to the 1 cm/s for the segment of a sphere approach. Das (1993) states:-

> 'It is well known that stress-strain properties of a soil and its behaviour depend upon several factors and can be different in many ways under dynamic loading conditions as compared to the case of static loading.'

The accuracy of the method depends on the accuracy to which the values of friction angle and cohesion are predicted.

Ideally, the applied stress on soil should not exceed the maximum allowed stress during phase II so that the disturbed area remains relatively limited. This point can be identified if results from a plate sinkage test are superimposed onto those from a confined compression test. This point was named compaction point (Earl 1993). If the applied stress exceeds the stress at compaction point the disturbed area will be increased disproportionately with the increase of the applied stress (*Table 5.2*). Since the maximum allowed soil stress during phase II depends on friction angle, it is strongly dependent on the moisture content and the packing state of the soil. As a result of this, the maximum allowed stress during phase II can differ significantly during the year.

This method also allows the prediction of the dry bulk density below the plate and consequently of other soil properties such as void ratio.

5.6. Conclusions

Three phases of failure patterns have been distinguished below a sinking plate. Maximum soil disturbance as well as dry bulk density can be predicted for each phase. The accuracy of the prediction have been tested using visual evidence obtained during plate sinkage tests in the soil bin behind glass. Results from the model, for medium density sandy loam, were compared with visual observations from the soil bin, and were broadly in agreement. It was not possible to obtain visual observations of dense soil because the glass could not withstand the pressures generated behind it, however, there is no reason to reject the theory for this. Visual evidence was obtained for loose soil, however, model could not be tested since the value of angle of shearing resistance could not be obtained due to the loose state of the soil.

CHAPTER 6

STRESS AT THE COMPACTION POINT

A technique is presented which can be used to identify the stress at which the mode of soil deformation below a sinkage plate changes from pure compaction below the plate to lateral compaction and displacement (the compaction point). The relationship of the stress at this point to various soil properties is also investigated.

6.1 Introduction

In chapter 5, soil failure below a plate was investigated and a mathematical model proposed which predicts the extent of the disturbed area below a sinkage plate. The point at which the mode of deformation changes from one of vertical displacement to one of vertical plus lateral displacement has been named compaction point (Earl 1993). *Figure 6.1* illustrates results of plate sinkage test superimposed onto those from a confined compression test. Initially, both curves follow a similar pattern, i.e. during the initial stages of a plate sinkage test, the sinkage will be predominately due to compaction under the plate with negligible lateral compaction as demonstrated in chapter 5. The same mode of deformation occurs during the initial stages of a confined compression test, but during confined compression, the mode of deformation remains unchanged. In the case of the plate sinkage test, a point will be reached where the deformation process will change to lateral soil compaction (*Figure 6.1*). The compaction point can be identified as the point at which the two curves diverge. The two curves, between the origin and the CP, do not coincide exactly. This can be explained by the reduced friction between soil particles and the inner wall of the cylinder (covered with lubricant) in the case of confined compression test, when compared with particle-particle friction on the slip plane in the case of the plate sinkage test.

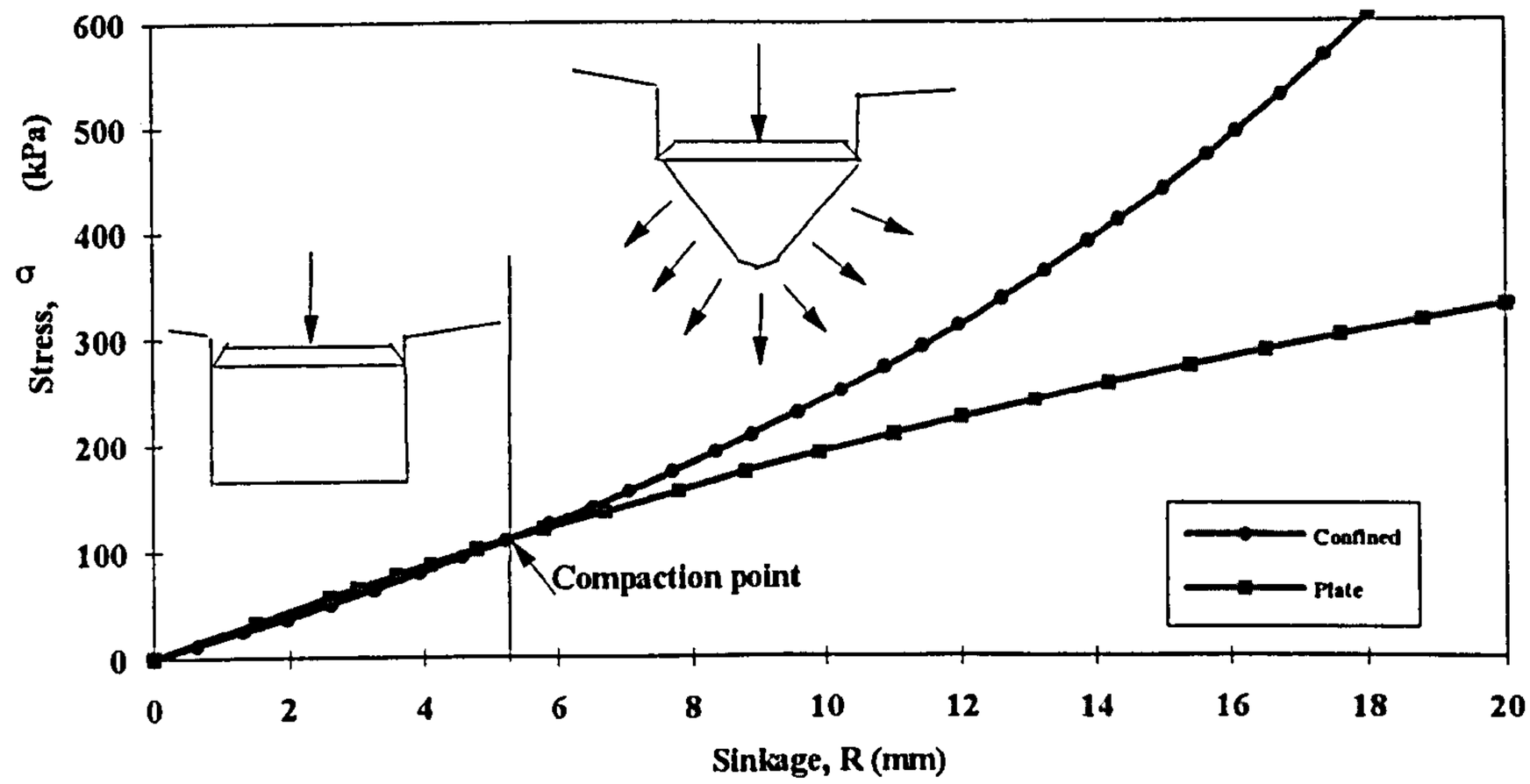

Figure 6.1. Compaction point.

The compaction point can be quantified using stress and corresponding sinkage at this point. Stress is related to the applied mechanical load and is a variable which could be 'controlled' so that the 'damage' will be limited. The 'damage' below the plate can be directly related to the sinkage depth as demonstrated in chapter 5.

6.2 Confined compression test

Earl (1993) approximated the stress-strain relationship obtained from confined compression test using a hyperbola of the form:-

$$\sigma = \frac{m_c R}{1 - \frac{R}{R_{ULT}}} \qquad (6.1)$$

Where:-

σ = axial stress (kPa)
R_{ULT} = asymptotic maximum value of R (mm)
R = sinkage (mm)
m_c = initial modulus (kPa/mm)

Typical stress-sinkage results from a confined compression test is presented in *Figure 6.2* along with a regression curves generated using equation 6.1.

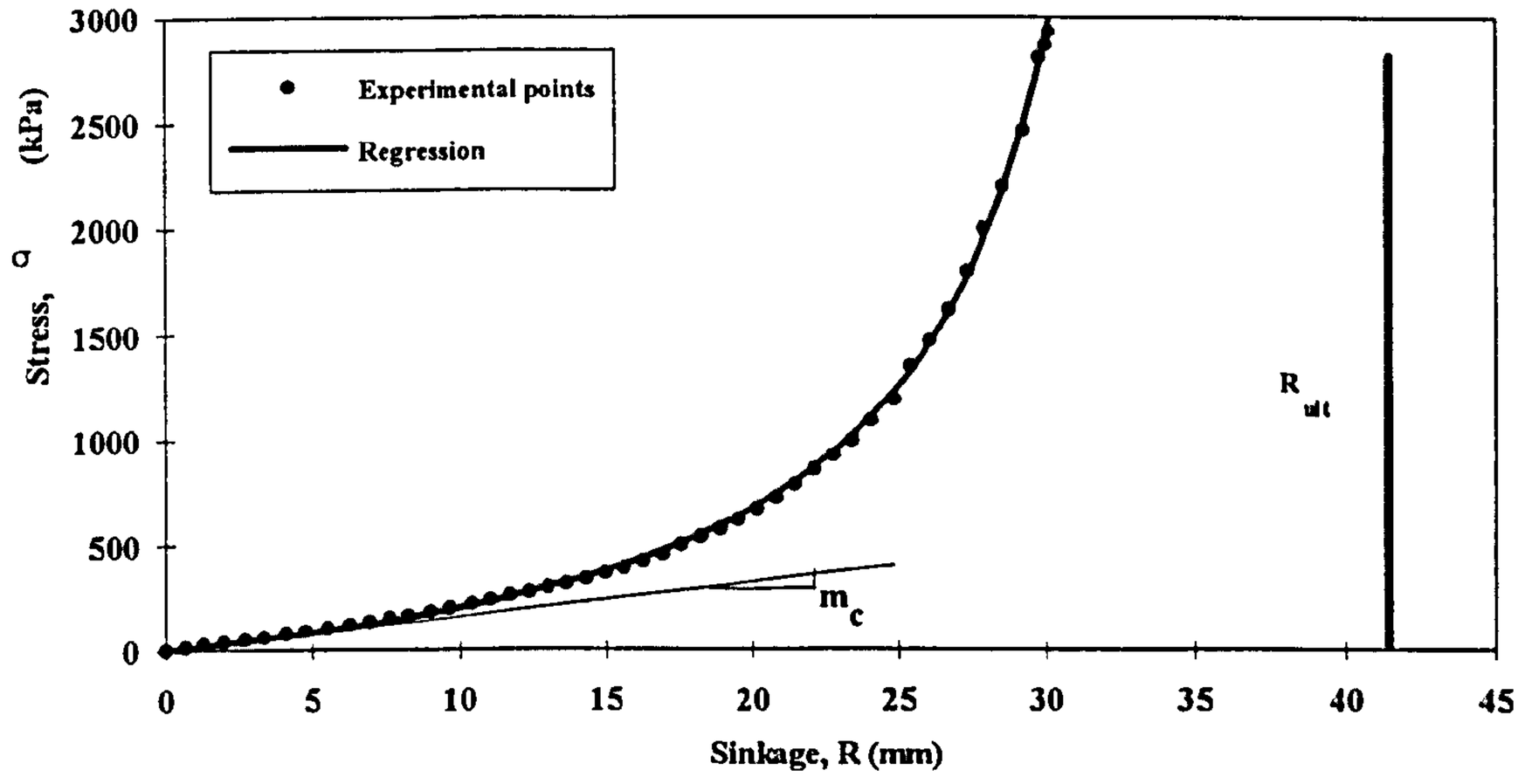

Figure 6.2. Typical stress-sinkage curve obtained from a confined compression test.

The software 'Table Curve (version 3.01)' was used to non-linearly fit the data to the curve (Bevington, P. R 1969 and Press, W. H. et al 1988) as in the case of plate sinkage test results.

A summary of statistical analyses carried out on results from confined compression tests conducted in the soil bin and at the sandy and clay sites are presented in *Tables 6.1, 6.2 and 6.3* respectively.

Table 6.1
Statistical values obtained from confined compression tests on sandy loam soil (soil bin)

Volumetric water content %	Dry bulk density (Mg/m^3)	m_c	R_{nlt}	R^2
12.78	1.40	20.00	41.70	0.99
12.42	1.41	18.90	37.80	0.99
12.80	1.40	19.90	43.50	0.99
12.92	1.41	9.49	47.70	0.99
13.00	1.41	9.39	47.00	0.99
12.11	1.35	12.50	48.20	0.99
11.14	1.29	6.35	72.20	0.99
11.18	1.30	6.30	72.00	0.99
10.61	1.31	8.68	50.80	0.99
14.55	1.50	16.28	44.80	0.99
14.75	1.49	17.10	55.37	0.99
14.21	1.45	11.74	44.00	0.99
13.95	1.51	20.00	42.16	0.99
11.73	1.33	7.06	72.60	0.99
13.48	1.42	10.10	49.10	0.99
13.43	1.37	6.95	52.70	0.99
13.39	1.38	6.85	53.00	0.99
20.38	1.42	3.60	43.10	0.99
20.45	1.43	4.60	41.25	0.99
21.89	1.43	4.20	36.50	0.99
19.22	1.55	14.40	35.20	0.99
20.65	1.50	8.90	33.68	0.99
19.14	1.55	14.20	35.00	0.99
15.17	1.43	18.10	38.90	0.99
15.98	1.47	17.40	40.70	0.99
15.38	1.45	18.40	40.40	0.99
14.89	1.47	14.85	44.30	0.99
9.79	1.13	2.17	53.46	0.99
10.08	1.20	11.17	51.36	0.99
10.11	1.15	4.88	61.91	0.99
12.79	1.17	5.02	51.61	0.99
15.23	1.18	3.03	53.75	0.99
14.00	1.17	3.02	58.80	0.99
18.04	1.23	2.25	52.29	0.99
18.31	1.26	2.24	52.89	0.99
17.86	1.23	2.17	53.46	0.99

Table 6.2
Statistical values obtained from confined compression test (field sandy loam soil)

Volumetric water content %	Dry bulk density Mg/m^3	m_c	R_{ult}	R^2
16.96	1.49	14.42	21.04	0.99
14.42	1.40	3.21	39.91	0.99
16.49	1.46	10.42	34.15	0.99
21.15	1.33	4.14	51.40	0.99
19.84	1.28	3.90	43.83	0.99
17.98	1.24	3.13	56.05	0.99
14.96	1.38	19.60	31.20	0.99
16.92	1.41	17.54	29.79	0.99
16.43	1.47	14.50	46.90	0.98
18.63	1.21	27.49	71.73	0.97
10.22	1.41	29.58	15.52	0.98
10.42	1.42	28.18	16.55	0.99
10.15	1.41	36.33	9.79	0.99
13.86	1.22	5.52	46.56	0.99
15.08	1.30	7.43	46.09	0.99
13.47	1.22	5.42	49.73	0.99
17.62	1.25	3.73	50.48	0.99
17.92	1.28	4.00	52.30	0.98

Table 6.3
Statistical values obtained from confined compression test (clay soil)

Volumetric water content %	Dry bulk density Mg/m^3	m_c	R_{ult}	R^2
46.16	1.23	17.31	21.0	0.99
46.50	1.25	14.44	22.1	0.99
44.70	1.24	14.44	22.0	0.99
51.55	1.02	7.17	14.2	0.99
46.53	0.99	6.35	19.6	0.98
50.66	1.05	12.59	12.8	0.99
40.64	1.28	9.23	20.4	0.99
41.56	1.35	44.99	9.1	0.99
38.43	0.99	7.02	46.7	0.99
39.96	1.05	11.02	81.5	0.99
43.78	1.08	14.26	55.7	0.99
43.16	1.32	13.86	19.0	0.99
42.16	1.30	19.72	17.3	0.99
42.08	1.36	3.66	11.2	0.99
32.95	1.34	12.53	14.6	0.99
31.97	1.07	22.75	5286.3	0.99
25.06	1.06	12.46	92.2	0.99
31.66	1.00	23.27	4722.4	0.99
40.63	1.12	18.72	1404.3	0.99
40.87	1.33	24.55	14.4	0.99

The high values of R_{ult} obtained for some clay samples can be attributed to the heterogeneity of the clay soil. For some samples the relationship obtained from the

confined compression test was linear (*Figure 6.3*). For the range concerned during this work, the hyperbola and data follow a similar trend (*Figure 6.3*), however, the regression equation tends towards a high asymptote as sinkage increases well beyond that experienced during normal agronomic practices.

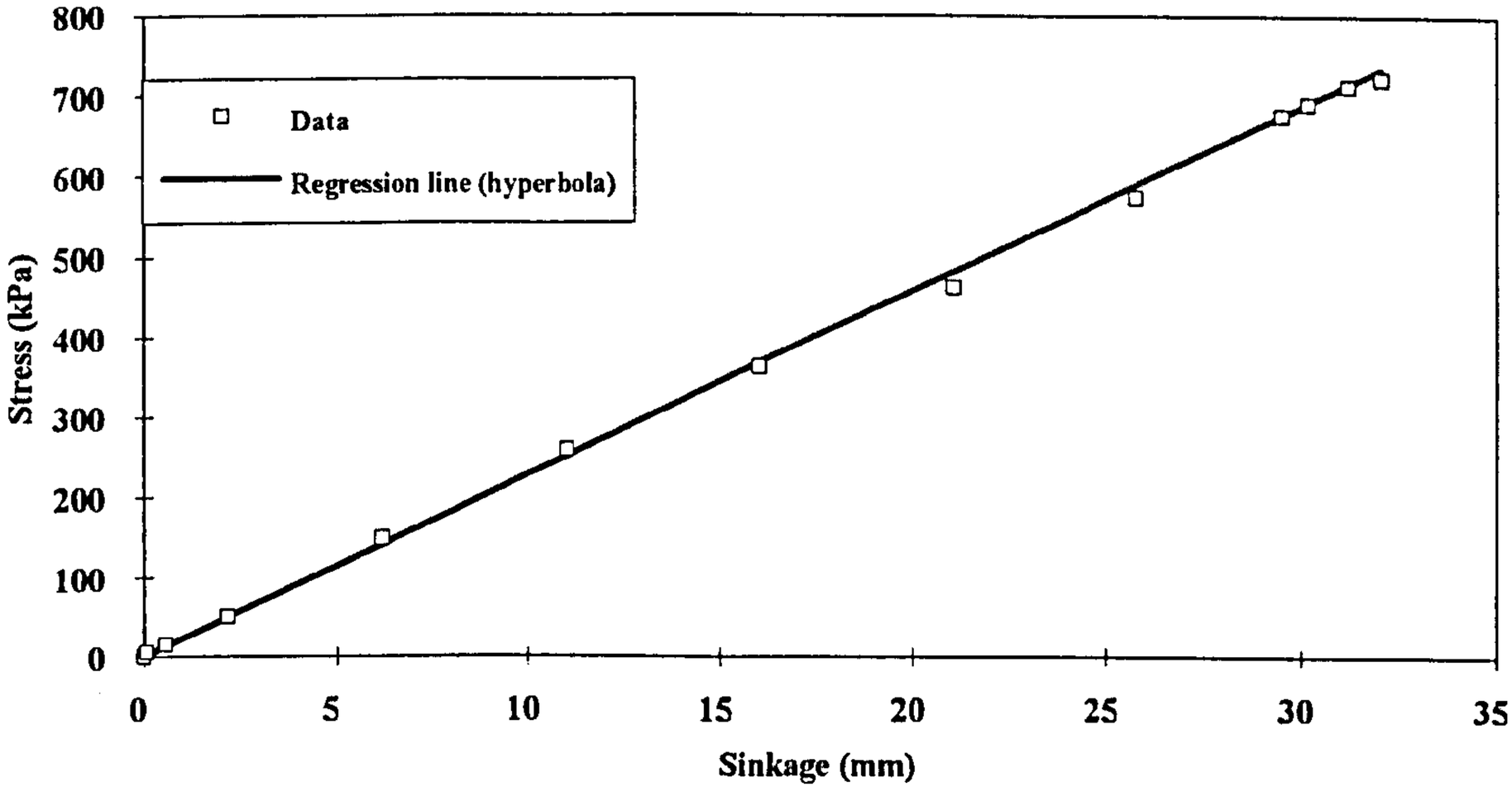

Figure 6.3. The data and the regression hyperbola for clay soil when, R_{ult} has a high value.

The compaction point can be determined from a plate sinkage and a confined compression test as follows:-

(1) Perform statistical analysis on data obtained from both plate sinkage and confined compression tests to evaluate the hyperbolic regression parameters (*Tables 4.1, 4.2., 4.3* and *6.1, 6.2, 6.3*).

(2) Calculate the co-ordinates of the compaction point by combining equations (4.2) and (6.1) as shown below:-

$$\frac{R}{\frac{1}{m_p}+\frac{R}{\sigma_{ULT}}} = \frac{m_c R}{1-\frac{R}{R_{ULT}}} \qquad (6.2)$$

A summary of results obtained for all tests conducted is presented in *Tables 6.4, 6.5,* and *6.6.*

Table 6.4
Experimental results for the soil bin sandy loam soil

Volumetric water content %	Dry bulk density (Mg/m^3)	Stress at CP (kPa)	Sinkage at CP (mm)	Void ratio	Degree of saturation
15.38	1.45	86.20	4.20	0.75	0.37
13.00	1.41	103.30	8.90	0.87	0.27
15.17	1.43	133.40	6.20	0.84	0.32
13.48	1.42	228.60	15.50	0.83	0.30
14.21	1.45	219.63	13.13	0.80	0.32
14.55	1.50	327.70	13.90	0.74	0.34
14.75	1.49	277.50	12.55	0.73	0.35
13.95	1.51	257.00	9.85	0.72	0.33
15.98	1.47	83.30	4.28	0.76	0.37
14.89	1.47	399.00	16.70	0.77	0.34
13.43	1.37	135.70	14.25	0.90	0.28
13.39	1.38	120.30	13.20	0.90	0.28
19.22	1.55	128.00	7.10	0.68	0.47
20.65	1.50	150.00	11.20	0.71	0.50
19.14	1.55	109.40	6.30	0.65	0.46
20.38	1.42	119.20	18.73	0.67	0.46
20.45	1.43	112.75	15.37	0.68	0.47
21.89	1.43	109.40	15.20	0.71	0.50
12.11	1.35	76.30	5.42	0.93	0.25
11.14	1.29	4.80	0.70	1.02	0.22
11.18	1.30	12.30	1.90	1.00	0.22
10.61	1.31	9.00	1.01	0.97	0.22
11.73	1.33	92.50	11.10	0.95	0.24
12.78	1.40	152.50	6.45	0.85	0.27
12.42	1.41	267.40	10.30	0.84	0.28
12.80	1.40	157.00	6.70	0.85	0.28
12.92	1.41	146.50	11.70	0.89	0.27
15.23	1.18	0	0	1.19	0.28
14.00	1.17	0	0	1.22	0.25
9.79	1.13	0	0	1.29	0.17
10.08	1.20	0	0	1.15	0.19
10.11	1.15	0	0	1.26	0.18
12.79	1.17	0	0	1.21	0.23
18.04	1.23	0	0	1.11	0.34
18.31	1.26	0	0	1.06	0.35
17.86	1.23	0	0	1.10	0.34

Table 6.5
Experimental results for the field sandy loam soil

Volumetric water content %	Dry bulk density (Mg/m^3)	Stress at CP (kPa)	Sinkage at CP (mm)	Void ratio	Degree of saturation
16.96	1.49	403.87	16.76	0.79	0.38
14.42	1.40	553.64	32.41	0.91	0.30
16.49	1.46	440.50	18.90	0.83	0.36
14.96	1.38	197.60	7.60	0.91	0.31
16.92	1.41	128.45	5.88	0.88	0.36
16.43	1.47	165.95	9.20	0.86	0.37
13.86	1.22	0	0	1.18	0.26
15.08	1.30	0	0	1.03	0.30
13.47	1.22	0	0	1.17	0.25
21.15	1.33	0	0	0.99	0.42
19.84	1.28	0	0	1.08	0.38
17.98	1.24	0	0	1.15	0.33
18.63	1.21	0	0	1.19	0.34
17.62	1.25	0	0	1.12	0.34
17.92	1.28	0	0	1.06	0.35
10.22	1.41	574.63	8.63	0.86	0.22
10.42	1.42	572.18	9.12	0.86	0.23
10.15	1.41	612.91	6.19	0.87	0.22

Table 6.6
Experimental results for the field clay soil

Volumetric water content %	Dry bulk density (Mg/m^3)	Stress at CP (kPa)	Sinkage at CP (mm)	Void ratio	Degree of saturation
46.16	1.23	247.63	8.52	1.15	0.86
46.50	1.25	185.85	8.13	1.13	0.84
44.70	1.24	213.08	8.84	1.14	0.85
51.55	1.02	92.45	6.76	1.60	0.84
46.53	0.99	67.38	6.88	1.65	0.75
50.66	1.05	99.28	4.87	1.51	0.85
40.64	1.28	347.01	13.24	1.07	0.80
40.63	1.35	303.97	12.53	0.96	0.83
41.56	0.99	392.27	25.42	1.68	0.65
38.43	1.05	654.99	34.36	1.53	0.62
39.96	1.08	472.64	20.77	1.45	0.67
43.78	1.32	366.15	11.04	1.00	0.89
43.16	1.30	429.15	9.65	1.04	0.86
42.16	1.36	295.16	9.87	0.94	0.88
42.08	1.34	201.25	7.66	0.98	0.86
32.95	1.07	688.50	30.10	1.47	0.55
31.97	1.06	730.94	35.86	1.49	0.53
25.06	1.00	901.48	38.42	1.67	0.39
31.66	1.12	789.15	40.93	1.37	0.54
40.70	1.33	177.77	4.82	0.99	0.82

It was not possible to identify the compaction point for very loose sandy loam soil. This contradicts observations made in chapter 5 where even for loose soil, the mode of deformation below a sinkage plate followed a similar pattern to more densely packed. An explanation for this anomaly may lie with the dimensions of the confining cylinder. Phase III for a loose sandy loam soil can start at a plate sinkage of 30 mm or more (*Figure 5.3d*) and so a corresponding confined compression test may need to be conducted with a longer sampler. Future work should be carried out to investigate the influence of confining cylinder length on determination of the compaction point of soil with particular reference to loose soil.

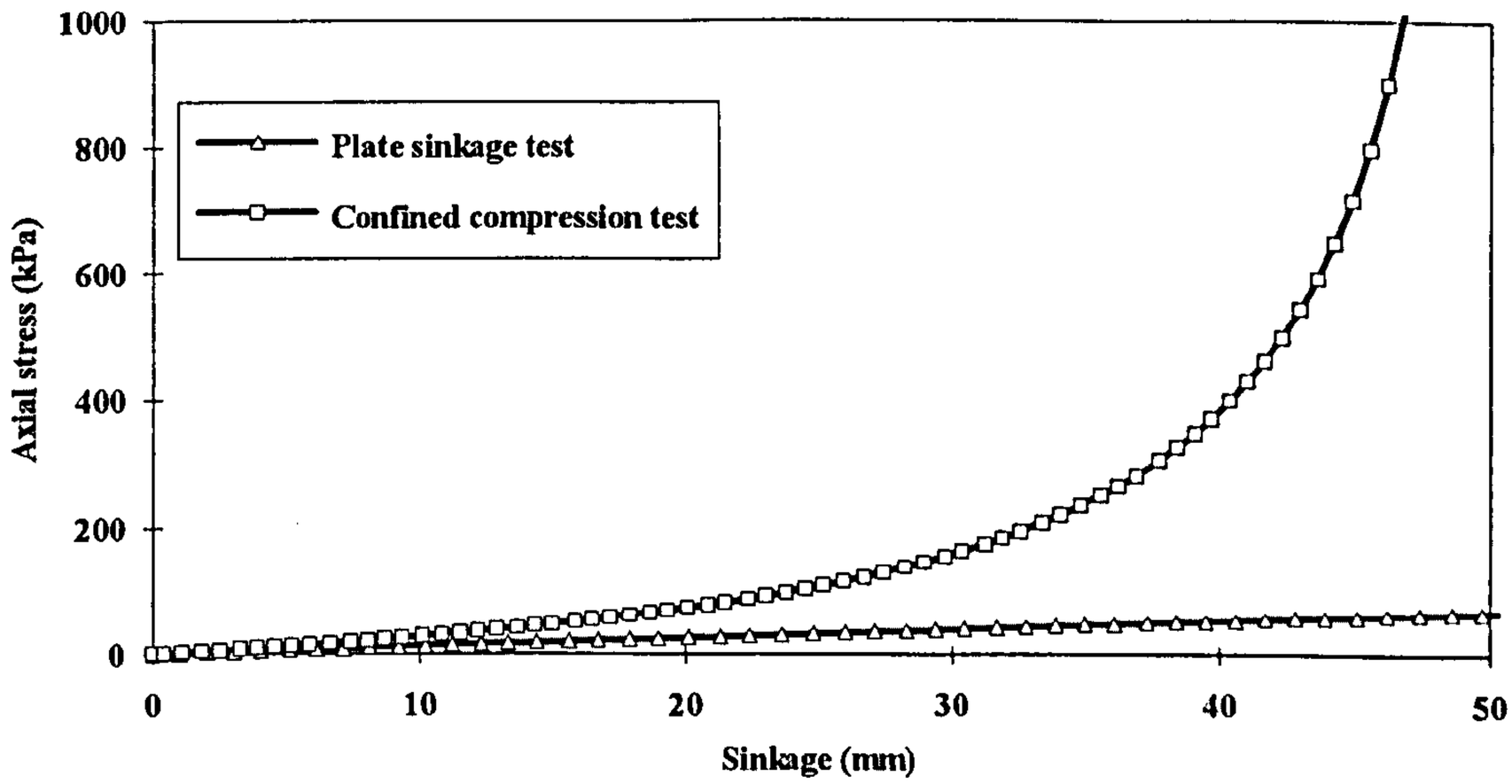

Figure 6.4. Typical stress-sinkage curves obtained from confined compression and plate sinkage tests on loose sandy loam soil.

6.3 The relationship between stress at compaction point and a range of soil properties

Stress at compaction point has been considered a function of angle of shearing resistance (equation 5.62). As such, it is expected to increase with initial dry bulk density and decrease with volumetric water content for a sandy loam soil. As in the cases of pre-compaction stress and initial compressive soil strength, the prediction of stress at compaction point from easily determined soil properties would enable the cumbersome and time consuming procedure of its determination to be avoided. For this purpose the same soil properties used in the other two cases will be used here.

6.3.1 Stress at the compaction point, volumetric water content and initial dry bulk density.

6.3.1.1 Sandy loam soil

The relationship between stress at the compaction point and initial dry bulk density at three different volumetric water contents for the bin's sandy loam soil is presented in *Figure 6.5*. The same categories for water content used in the analysis of pre-compaction stress, were also used in this case. For the soil bin soil the derived equations are presented in *Table 6.7* and the confidence intervals in *Figure 6.5*.

Table 6.7

Derived relationships for soil bin soil

Volumetric water content %	Derived equation	R^2	Significance
9-12	$\sigma_{cp} = -2070.83 + 1602.94 * D_B$	0.83	***
13-16	$\sigma_{cp} = -1698.57 + 1311.50 * D_B$	0.33	*
19-22	No statistically significant relationship		

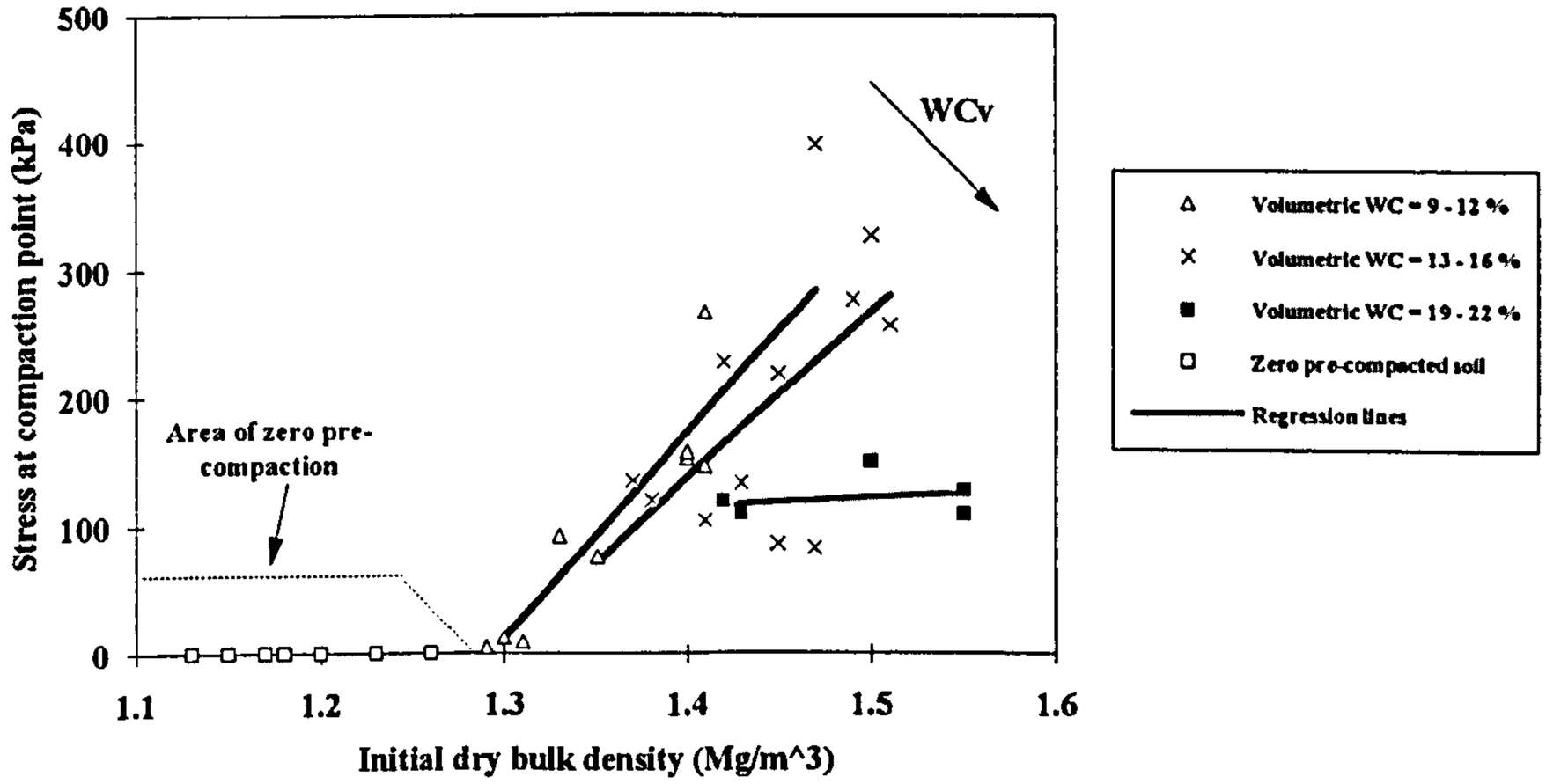
Stress at compaction point (kPa)
500
400
300
200
100
0
1.1
1.2
1.3
1.4
1.5
1.6
Initial dry bulk density (Mg/m^3)
WCv
Area of zero pre-compaction
Volumetric WC = 9 - 12 %
Volumetric WC = 13 - 16 %
Volumetric WC = 19 - 22 %
Zero pre-compacted soil
Regression lines

a)

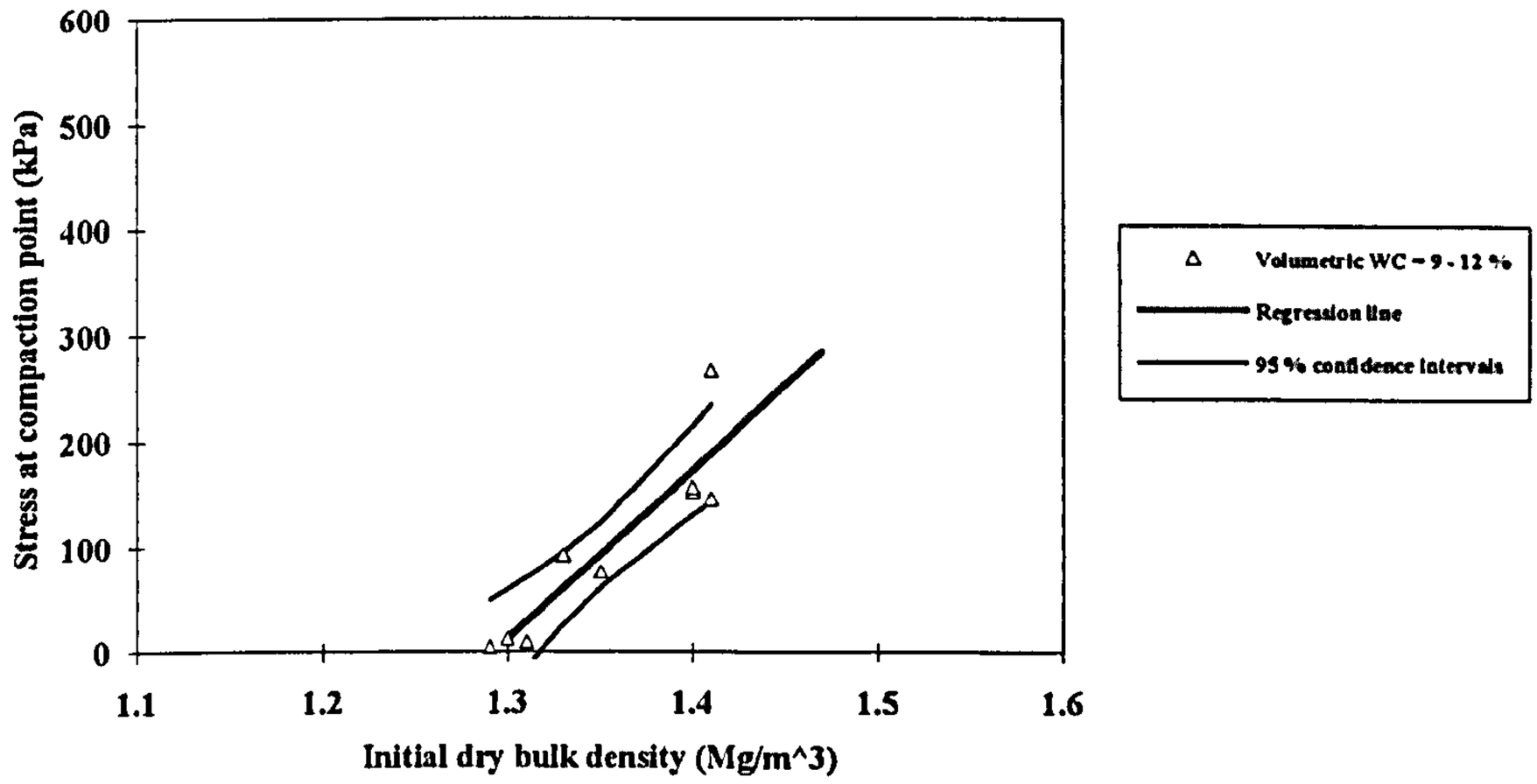
Stress at compaction point (kPa)
600
500
400
300
200
100
0
1.1
1.2
1.3
1.4
1.5
1.6
Initial dry bulk density (Mg/m^3)
Volumetric WC = 9 - 12 %
Regression line
95 % confidence intervals

b)

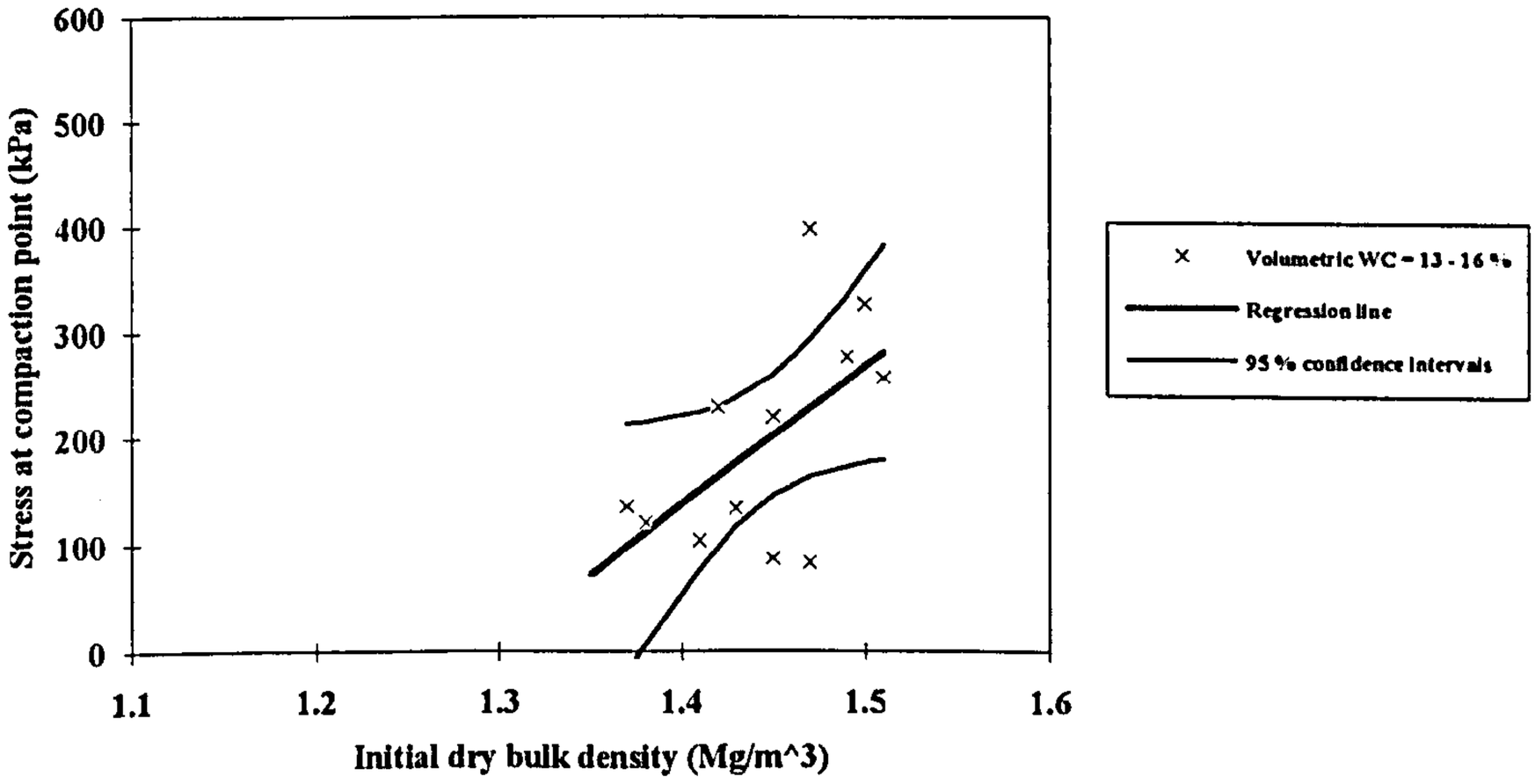

c)

Figure 6.5. The relationship between stress at compaction point, volumetric water content and initial dry bulk density (soil bin sandy loam). a) all water contents; b) 9-12 % water content range and c) 13-16 % water content range.

The relationship is highly significant only for the soil with volumetric water contents in the range 9-12%. Much more data, in discrete water content categories, would be required to generate a reliable prediction tool for a range of soil conditions.

A similar relationship for the field sandy loam soil is presented in *Figure 6.6*. The soil has been divided into two categories. The relationships were also approximated by straight lines for data points outside the very loose soil area (*Table 6.8*).

Table 6.8

Derived relationships for field sandy loam soil

Volumetric water content %	Derived equation	R^2	Significance
10-15	$\sigma_{cp} = -15153.94 + 11143.14 * D_B$	0.74	*
16-17	No statistically significant relationship		

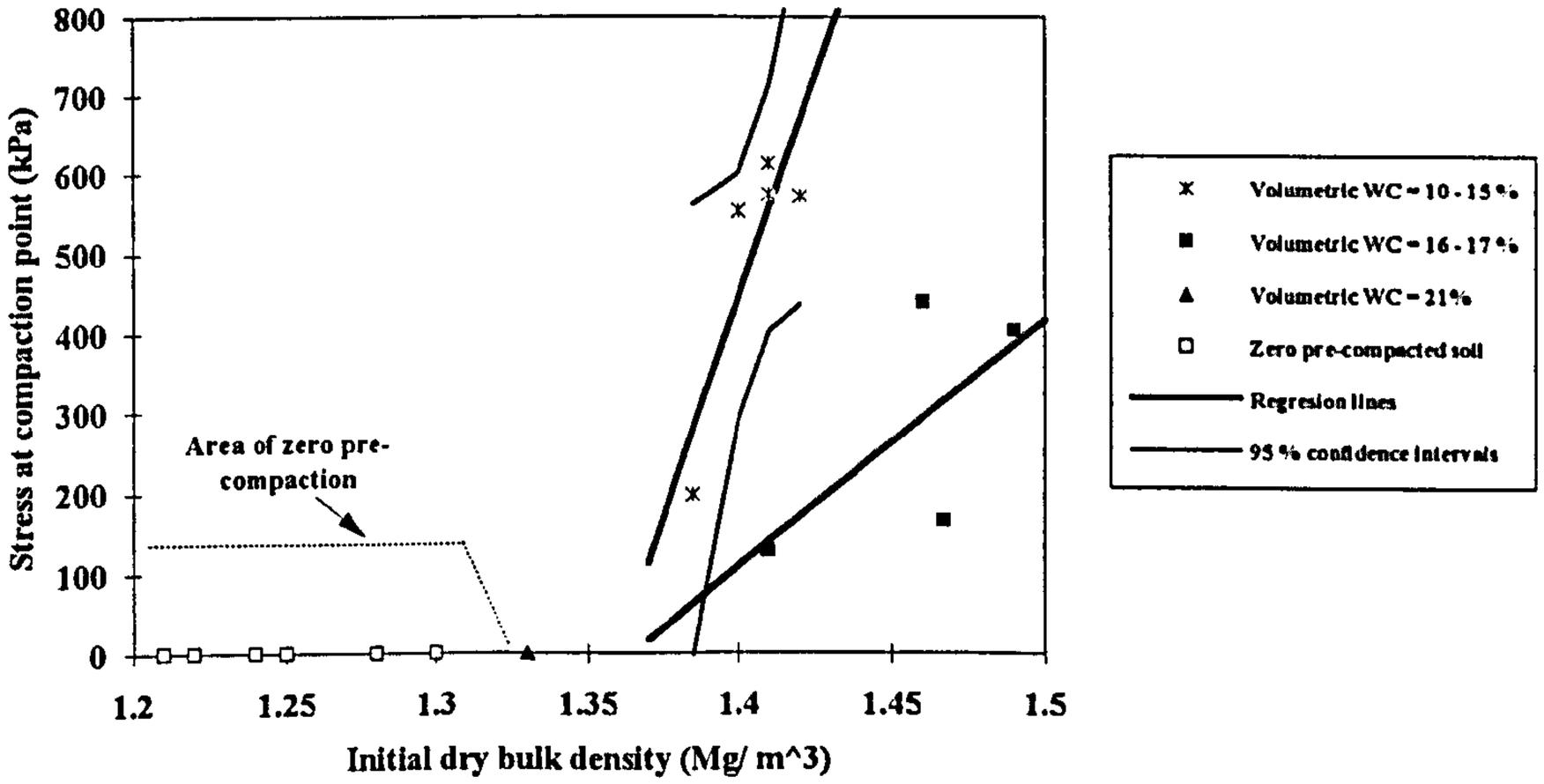

Figure 6.6. The relationship between stress at compaction point, volumetric water content and initial dry bulk density (field sandy loam soil).

Stress at the compaction point, for soil bin sandy loam, can be predicted from readily available soil properties, with some accuracy for the soil at 9-12% volumetric water content. The spread of the data at other water contents questions the appropriateness of this prediction procedure until further data becomes available.

For field soils the relationship is significant for the 10-15% volumetric water content range however, further data are required for other ranges. This situation is complicated further by the need for further investigations into the length of samples required in determining the compaction point of loose soils.

6.3.1.2 Clay soil

In 4.3.1.2. it was shown that the behaviour of clay soil is more dependent on volumetric water content rather than packing state of a soil and therefore, a similar relationship used in that section will be used here. The relationship between stress at compaction point, volumetric water content at a initial dry bulk density is presented in *Figure 6.7.*

The relationship can be approximated by:-

$$\sigma_{pr} = 1819.81 - 35.00 \cdot WC_v \qquad (6.3)$$

with coefficient of determination, $R^2 = 0.85$ ***.

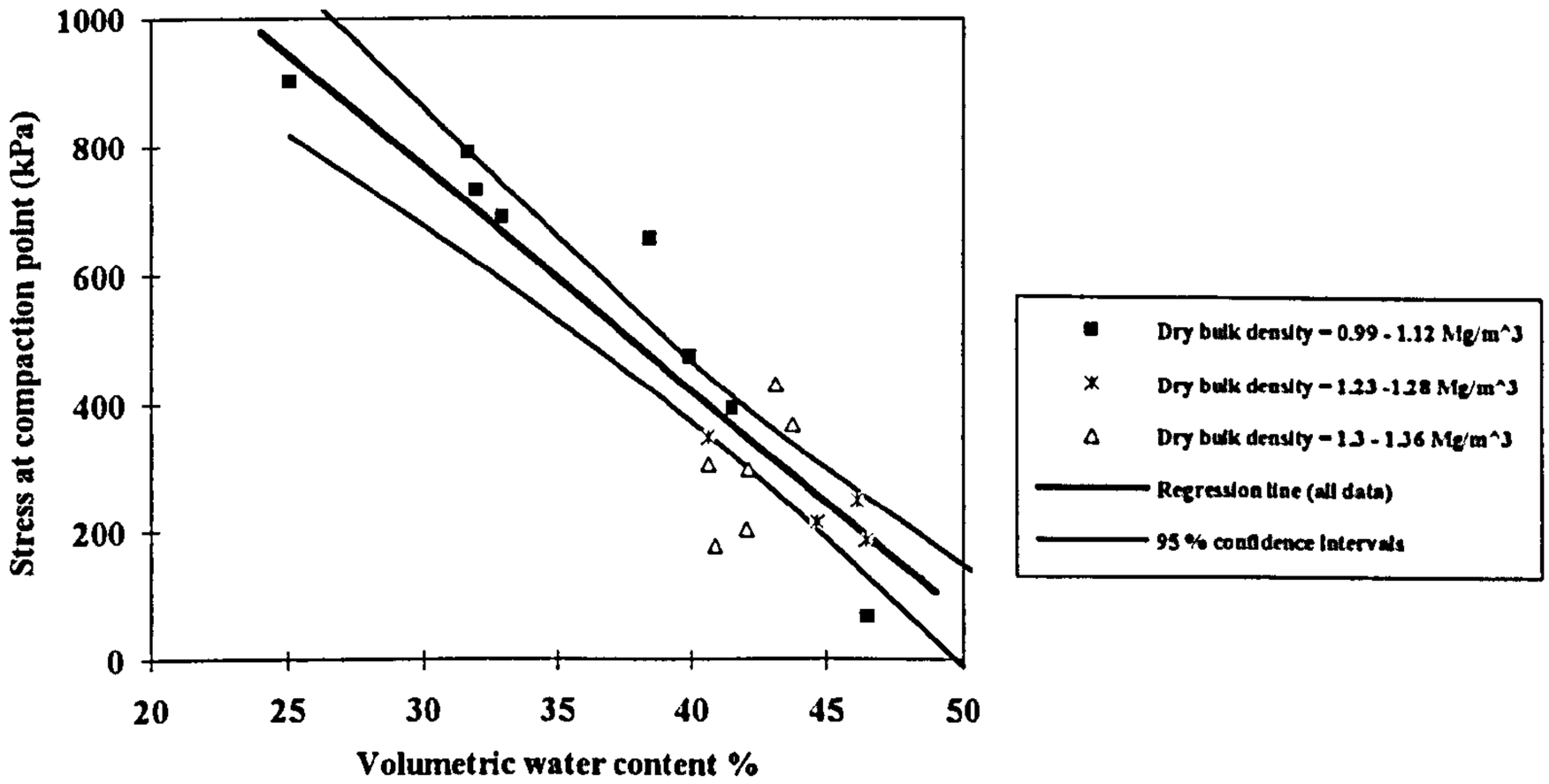

Figure 6.7. The relationship between stress at compaction point, volumetric water content and initial dry bulk density (clay soil).

It can be seen that for the clay soil stress at compaction point increases as volumetric water content decreases as expected. The relationship can be predicted with good accuracy.

6.3.2 Stress at the compaction point, void ratio and degree of saturation

6.3.2.2 Sandy loam soil

Figure 6.8 shows the relationship between stress at compaction point and void ratio for the soil bin sandy loam. Stress at compaction point tends to decrease as void ratio increases which is expected since soil becomes looser as void ratio increases. For data outside the loose soil region, the derived equations are presented in *Table 6.9*.

Table 6.9

Derived relationships for soil bin soil

Volumetric water content %	Derived equation	R^2	Significance
9-12	$\sigma_{cp} = 1206.44 - 1198.13 * e$	0.84	***
13-16	No statistically significant relationship		
19-22	No statistically significant relationship		

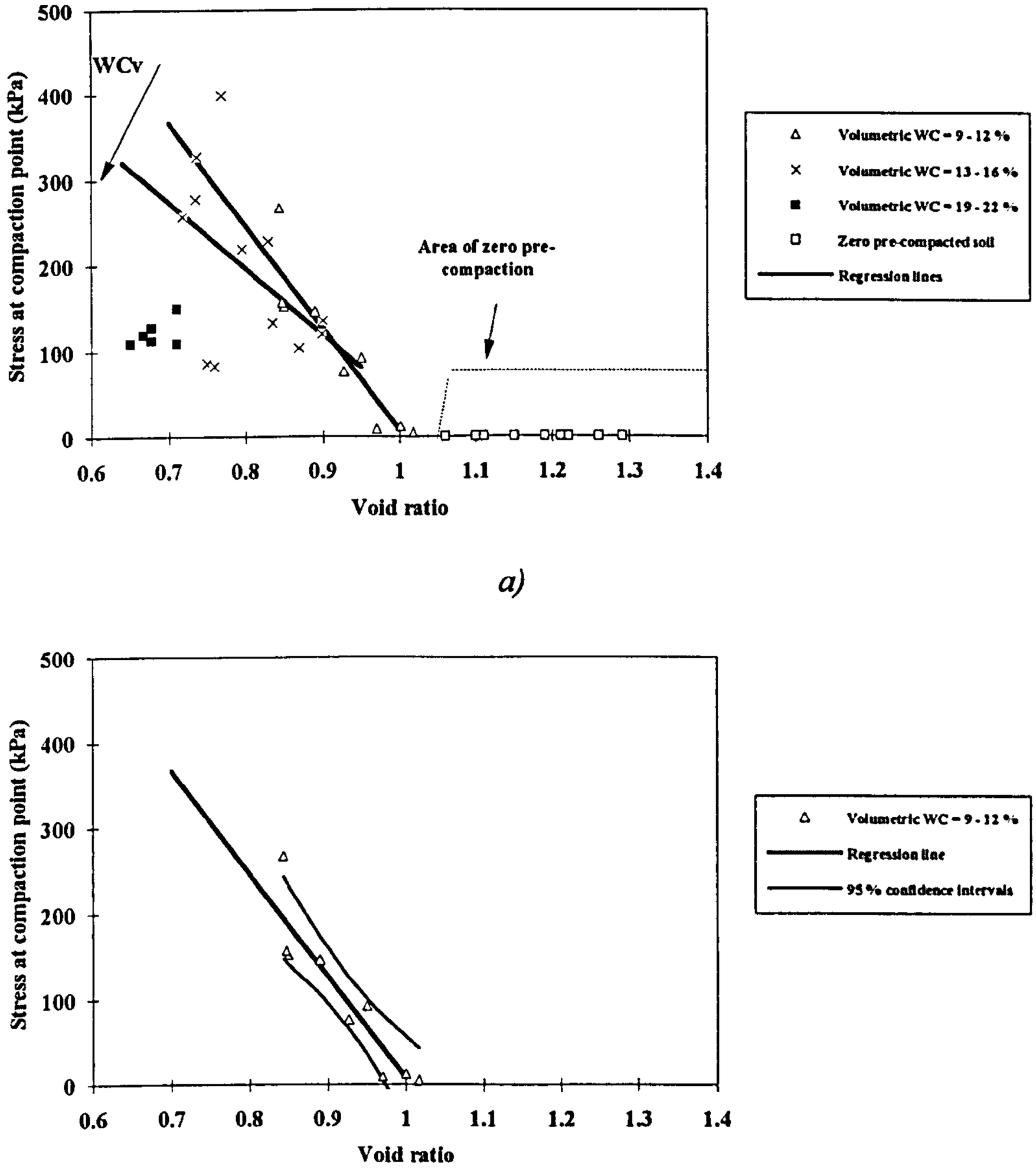

Figure 6.8. The relationship between stress at compaction point, volumetric water content and void ratio (soil bin sandy loam) a) all water contents; b) 9-12 % water content range.

The same relationship for the field sandy loam soil is presented in *Figure 6.9*. The relationships are not statistically significant due to insufficient data.

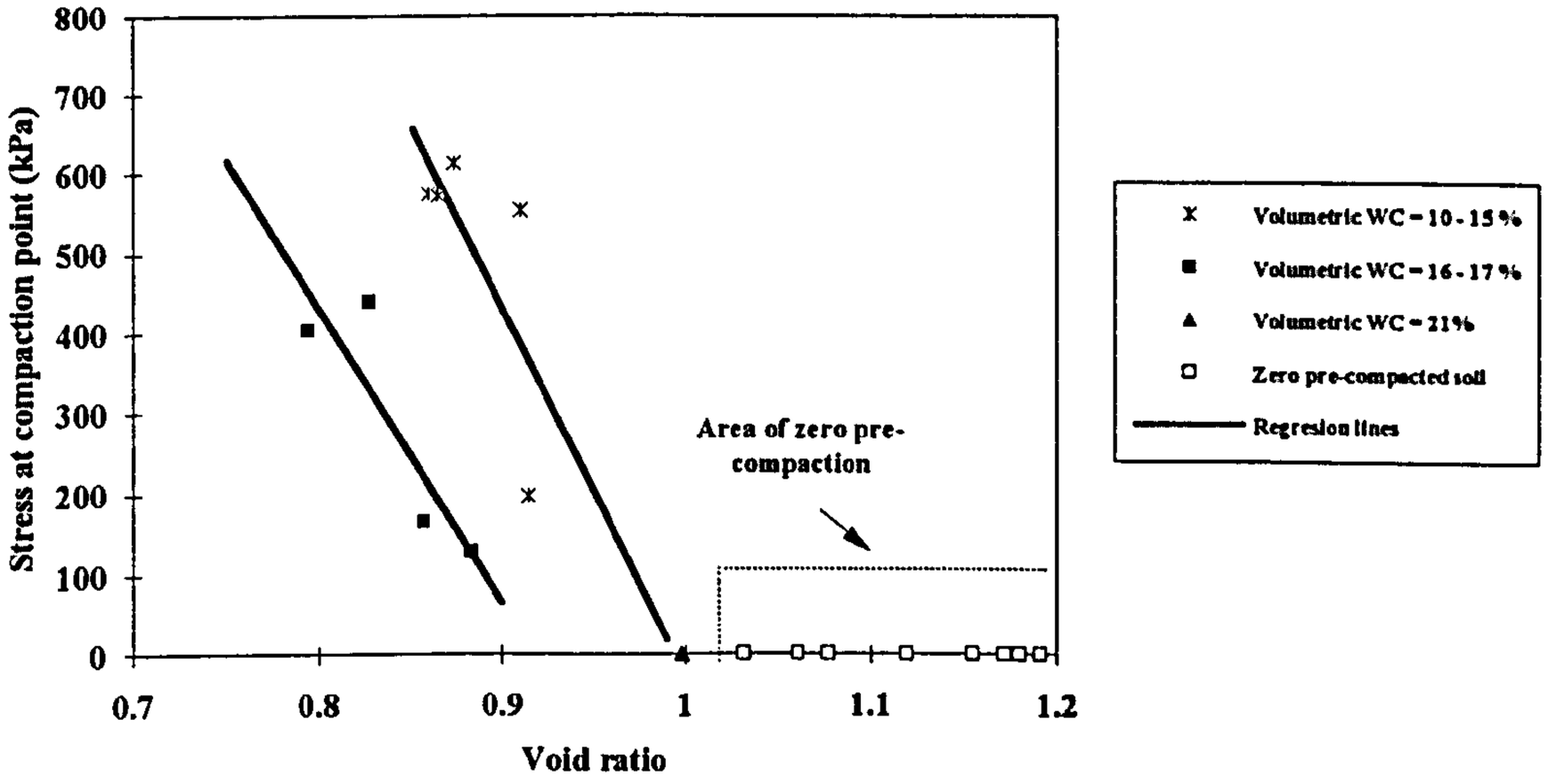

Figure 6.9. The relationship between stress at compaction point, volumetric water content and void ratio (field sandy loam soil).

For the soil bin sandy loam, the relationship is significant at volumetric water content 9-12% . For all other ranges the relationships are not statistically significant due to lack of data.

6.3.2.2 Clay soil

The relationship between stress at compaction point and degree of saturation for discrete ranges of initial dry bulk density are presented in *Figure 6.10*. For the clay soil, the relationship can be approximated by the following equation:-

$$\sigma_{pr} = 1473.80 - 1465.74 \cdot S_r \quad (6.4)$$

with coefficient of determination $R^2 = 0.76$ ***.

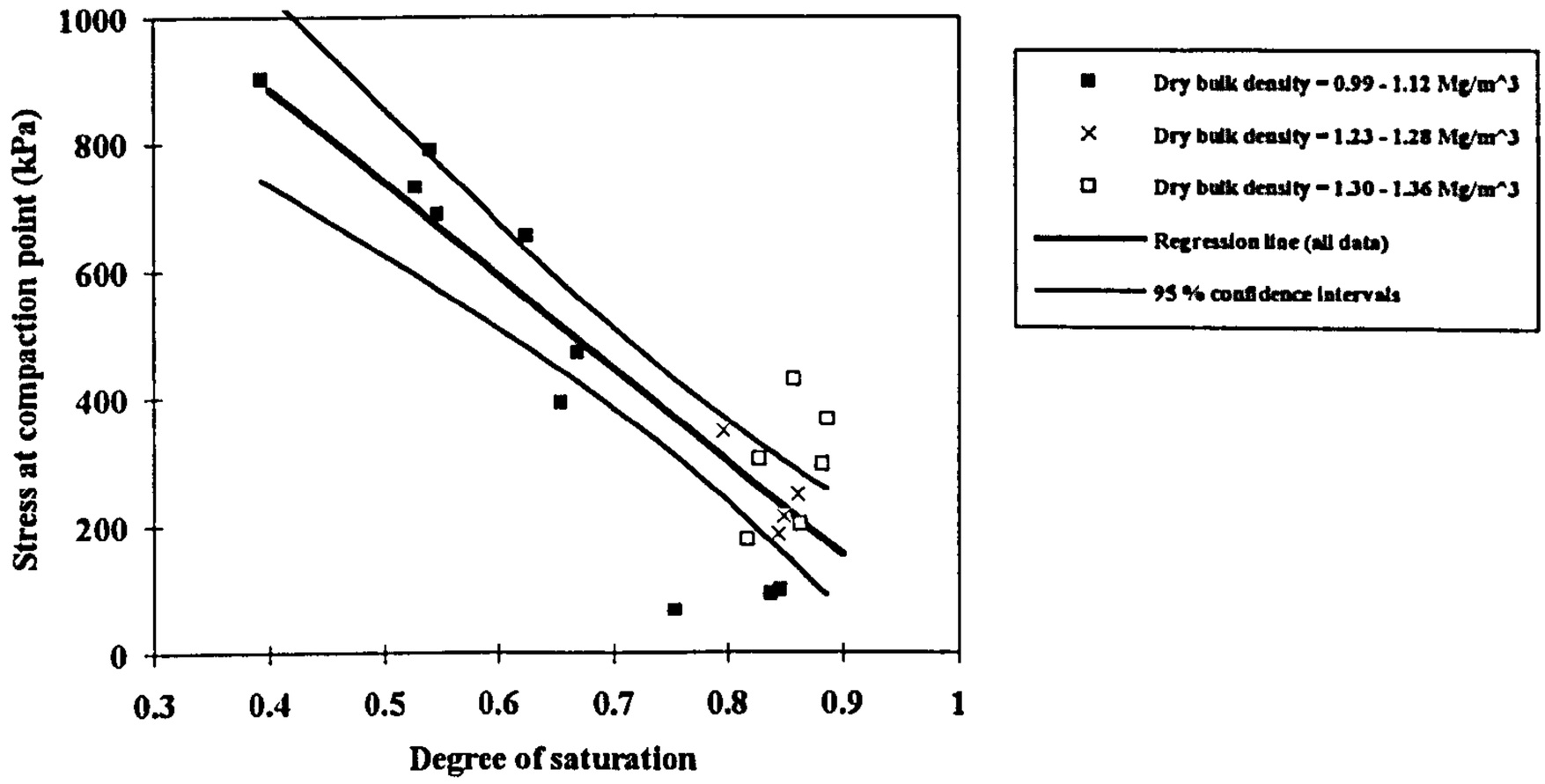

Figure 6.10. The relationship between stress at compaction point, initial dry bulk density and degree of saturation (clay soil).

For the clay soil stress at compaction stress can be predicted if the volumetric water content of the soil is known.

6.4 Conclusions

Stress at compaction point has been determined and related to various soil properties. The technique has been put in question since it is not able to accommodate loose sandy loam soil. More research is required to evaluate the influence of the confining cylinder length on compaction point theory. For a given volumetric water content, stress at compaction point increases as initial dry bulk density increases or void ratio decreases in the case of sandy loam soil. For the bin soil, stress at the compaction point can be predicted with good accuracy for soil with volumetric water content in the range 9-12%. In the case of clay soil, a strong relationship exists between stress at compaction point and with volumetric water content or degree of saturation and it can be reliably predicted from either.

CHAPTER 7

THE RELATIONSHIPS BETWEEN PRE-COMPACTION STRESS, INITIAL COMPRESSIVE SOIL STRENGTH AND STRESS AT THE COMPACTION POINT

In chapters 3, 4 and 6 pre-compaction stress, initial compressive soil strength and stress at the compaction point have been investigated. In this chapter, the inter-relationships between these three properties is investigated and the feasibility of predicting anyone of them from the other two is examined.

7.1 Introduction

In chapters 3, 4 and 6 pre-compaction stress, initial compressive soil strength and stress at compaction point were investigated (*Figure 7.1*). Each of these variables has been related to soil behaviour. In the following paragraphs, the inter-relationships between these three predictors of soil behaviour will be investigated.

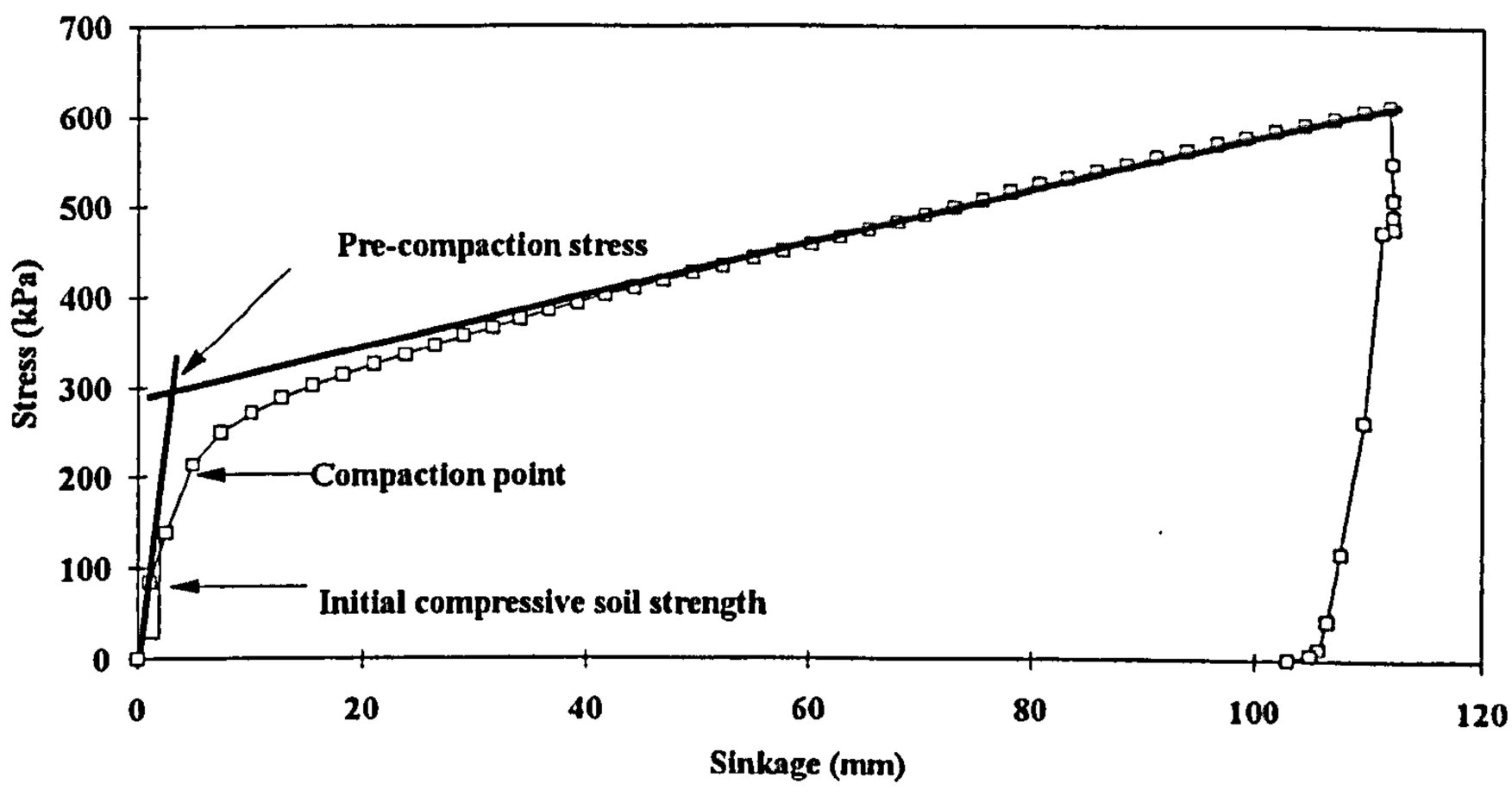

Figure 7.1. Typical stress-sinkage relationship of soil obtained from a plate sinkage test.

7.2 The relationship between pre-compaction stress and initial compressive soil strength

The relationship between pre-compaction stress and initial compressive soil strength can be approximated by a hyperbola of the general form:-

$$\sigma_{pr} = \frac{m_p}{\frac{1}{g_i} + \frac{m_p}{\sigma_{prult}}} \qquad (7.1)$$

Where:-

σ_{pr} = pre-compaction stress (kPa)
σ_{prult} = asymptotic value of σ_{pr} (kPa)
m_p = initial compressive soil strength (kPa/mm)
g_i = initial gradient (mm^{-1})

Non-linear regression analysis was performed on the data obtained during this work using 'Table curve 3.1' and the results are presented in *Figures 7.2, 7.3, 7.4* and *Table 7.1.*

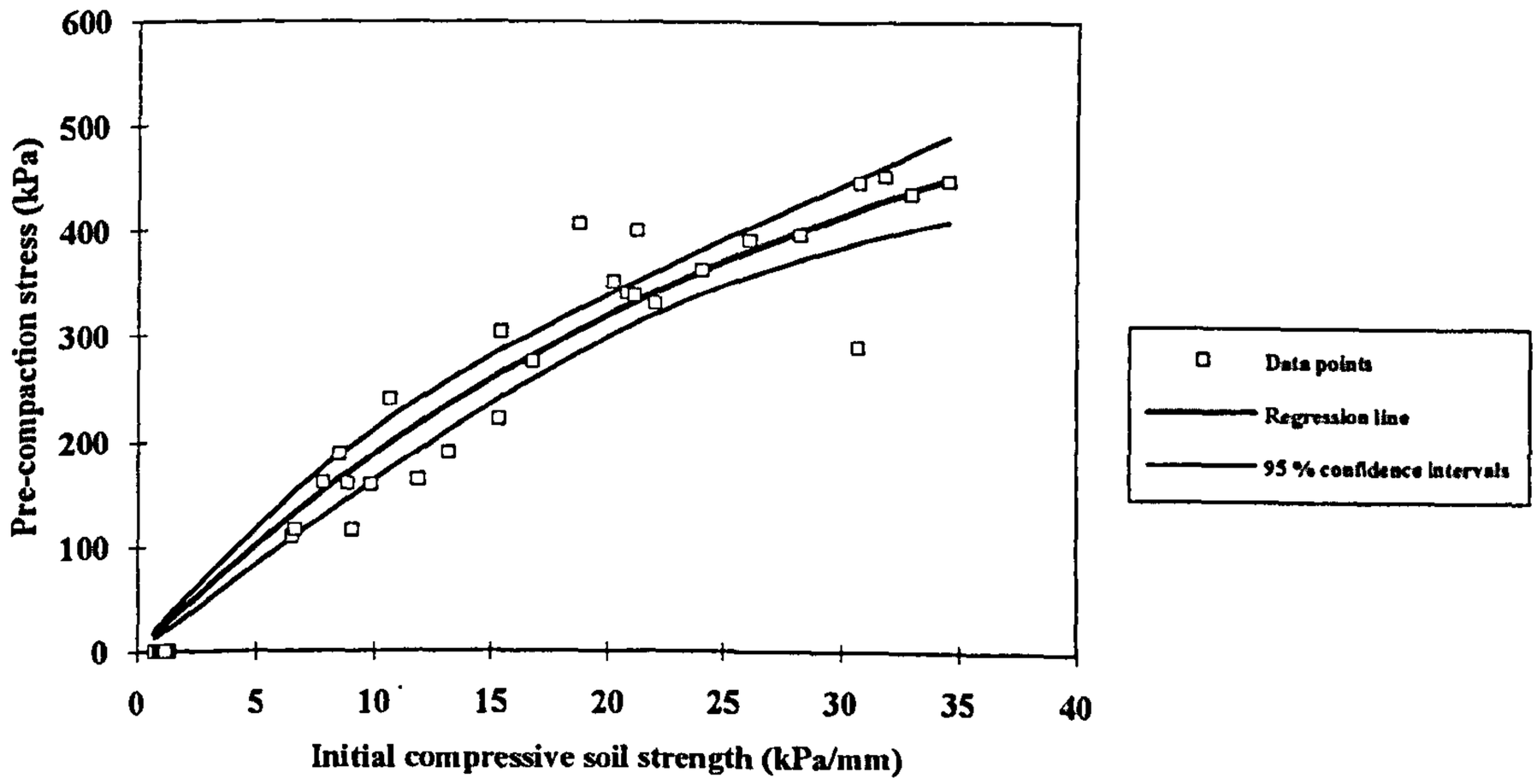

Figure 7.2. The relationship between initial compressive soil strength and pre-compaction stress for the soil bin sandy loam.

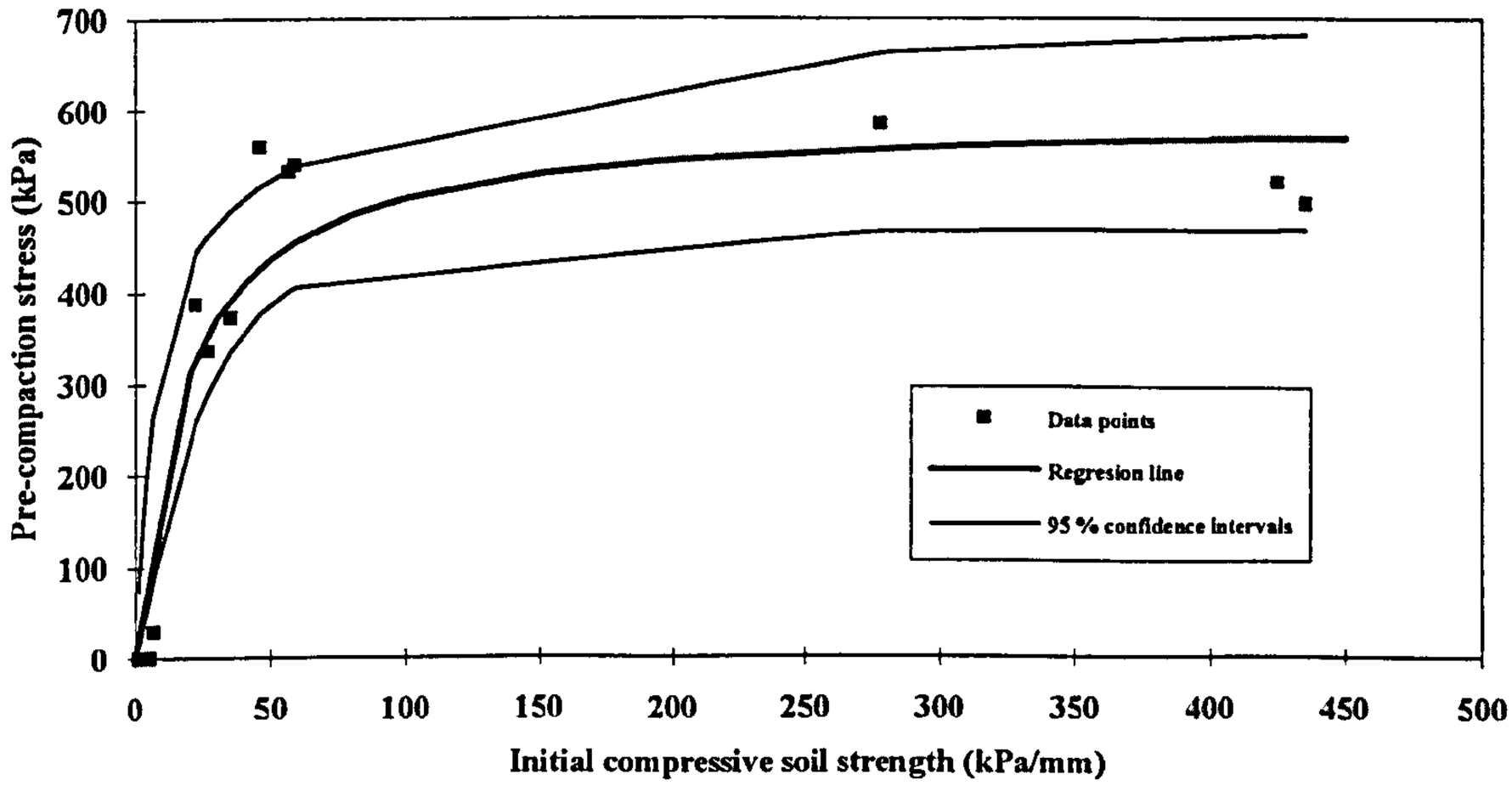

Figure 7.3. The relationship between initial compressive soil strength and pre-compaction stress for field sandy loam soil.

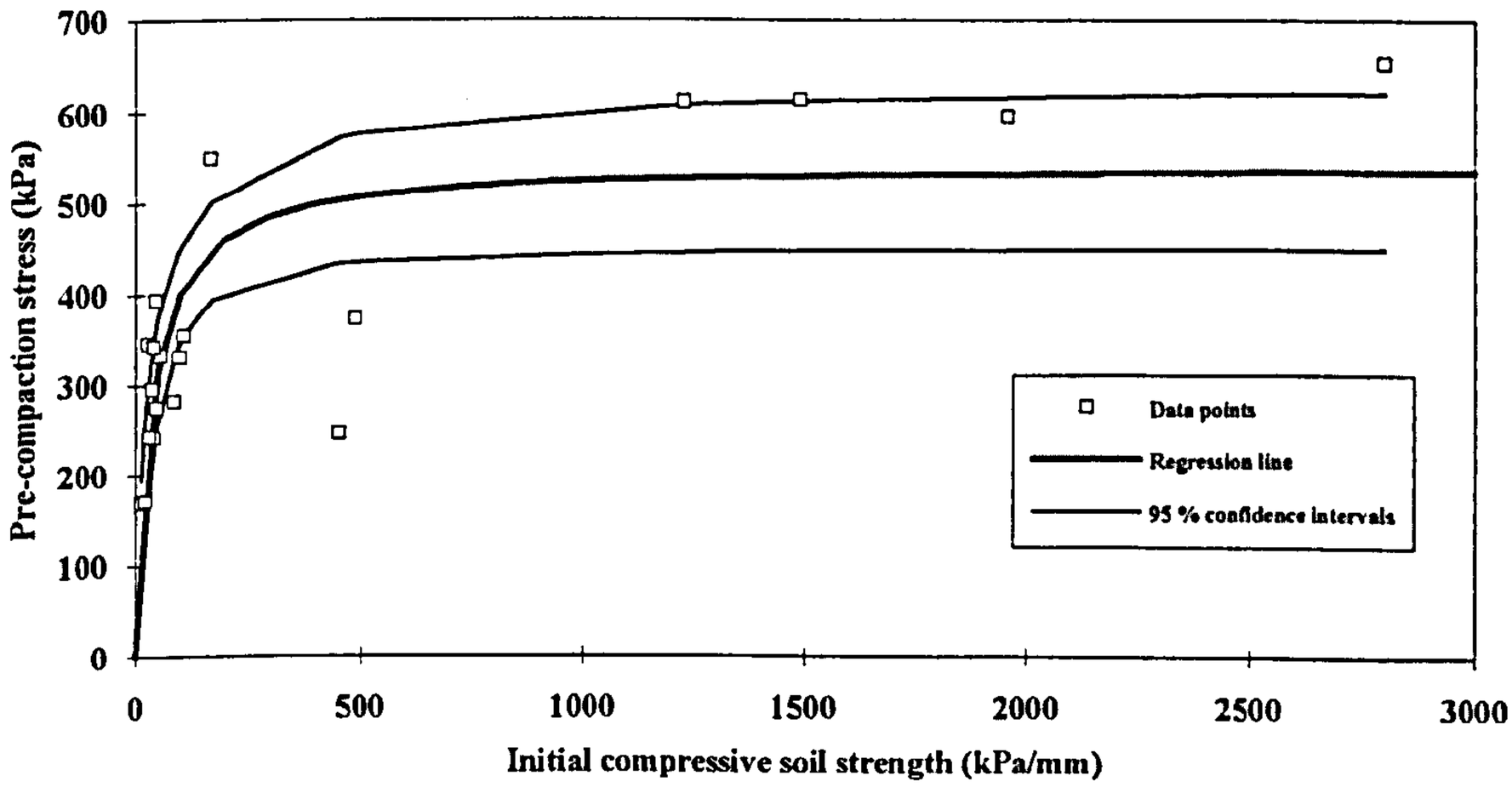

Figure 7.4. The relationship between initial compressive soil strength and pre-compaction stress for field clay soil.

Table 7.1

Statistical analysis results for pre-compaction stress vs initial compressive soil strength

Soil type	Derived equation	R^2	Significance
Sandy soil (bin)	$\sigma_{pr} = \frac{m_p}{\frac{1}{22.98} + \frac{m_p}{1049.76}}$	0.86	***
Sandy soil (field)	$\sigma_{pr} = \frac{m_p}{\frac{1}{38.31} + \frac{m_p}{598.80}}$	0.77	***
Clay soil (field)	$\sigma_{pr} = \frac{m_p}{\frac{1}{15.24} + \frac{m_p}{542.59}}$	0.61	***

The relationship between pre-compaction stress and initial compressive soil strength for both clay and sandy soils was found to be adequately approximated by a hyperbolic curve which tends towards an asymptote (σ_{prult}). In other words, the pre-compaction stress of a soil tends towards a maximum value which depends on the initial compressive soil strength of the soil in question. Soil will be able to withstand higher loads with limited soil compaction when initial compressive soil strength is high. This may be desirable for civil engineering purposes but for agronomic reasons high soil strength can be undesirable. For the conditions encountered during this investigation this value was found to be close to 600 kPa independent of field soil type (*Figure 7.5*). For the soil bin sandy loam, the limited range of the obtained during tests data, resulted in an asymptote which is a meaningless number.

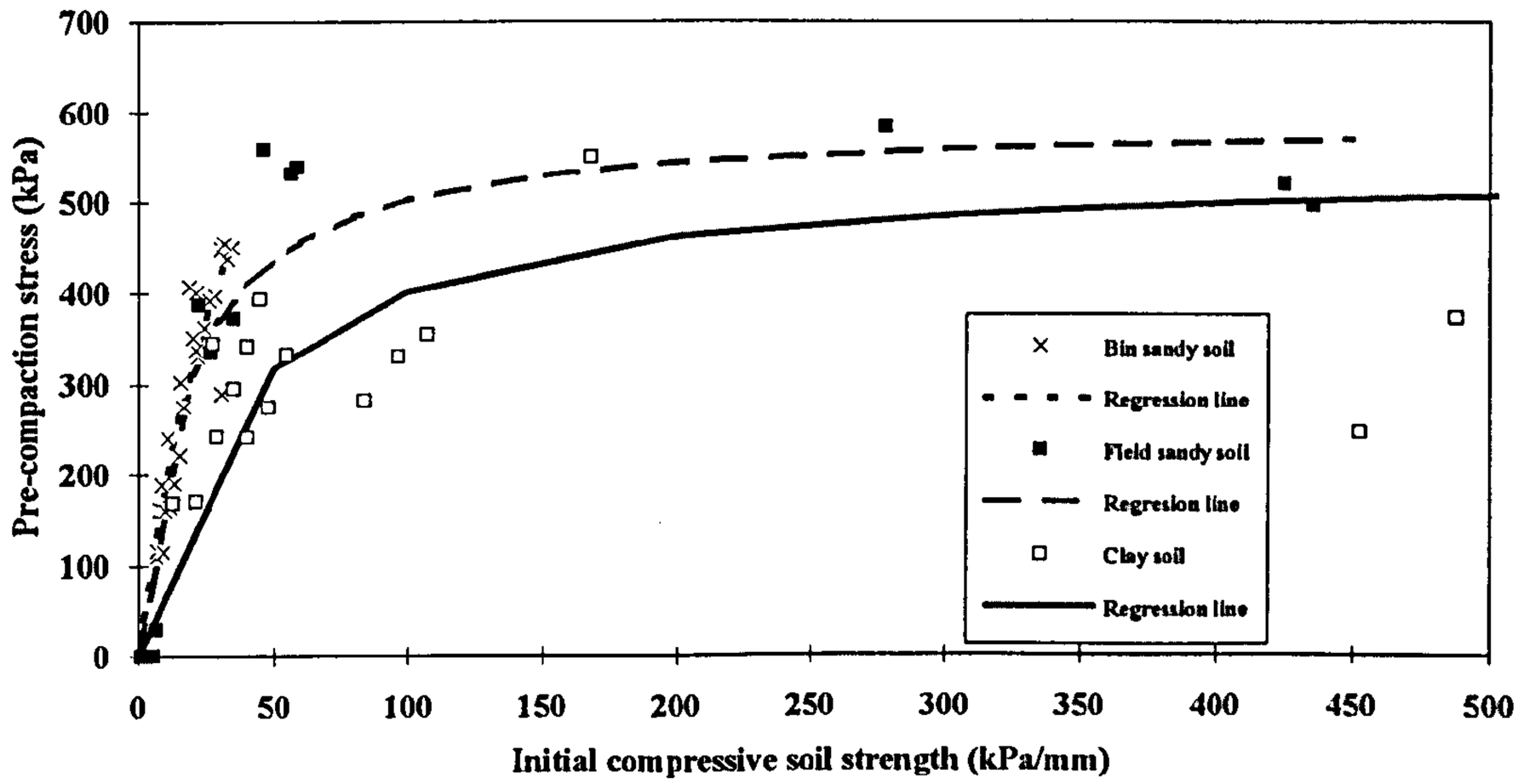

Figure 7.5. The relationship between initial compressive soil strength and pre-compaction stress for the soil bin sandy loam and both field soils.

7.3 The relationship between stress at compaction point and pre-compaction stress

The relationships between stress at compaction point and pre-compaction stress for the soils encountered during this work are presented in *Figures 7.6, 7.7, 7.8* and can be approximated by an equation of the following form:-

$$\sigma_{cp} = a + b\sigma_{pr} \qquad (7.2)$$

Where:-

σ_{cp} = stress at compaction point (kPa)
a = is the theoretical value of stress at compaction point at zero pre-compaction stress.
b = the initial slope of the line.

It should be noted that the relationship between stress at the compaction point and pre-compaction stress for sandy loam soil, can also be approximated with a hyperbola of the general form of equation (7.1). During this work the linear approach was adopted because the regression analysis results were better.

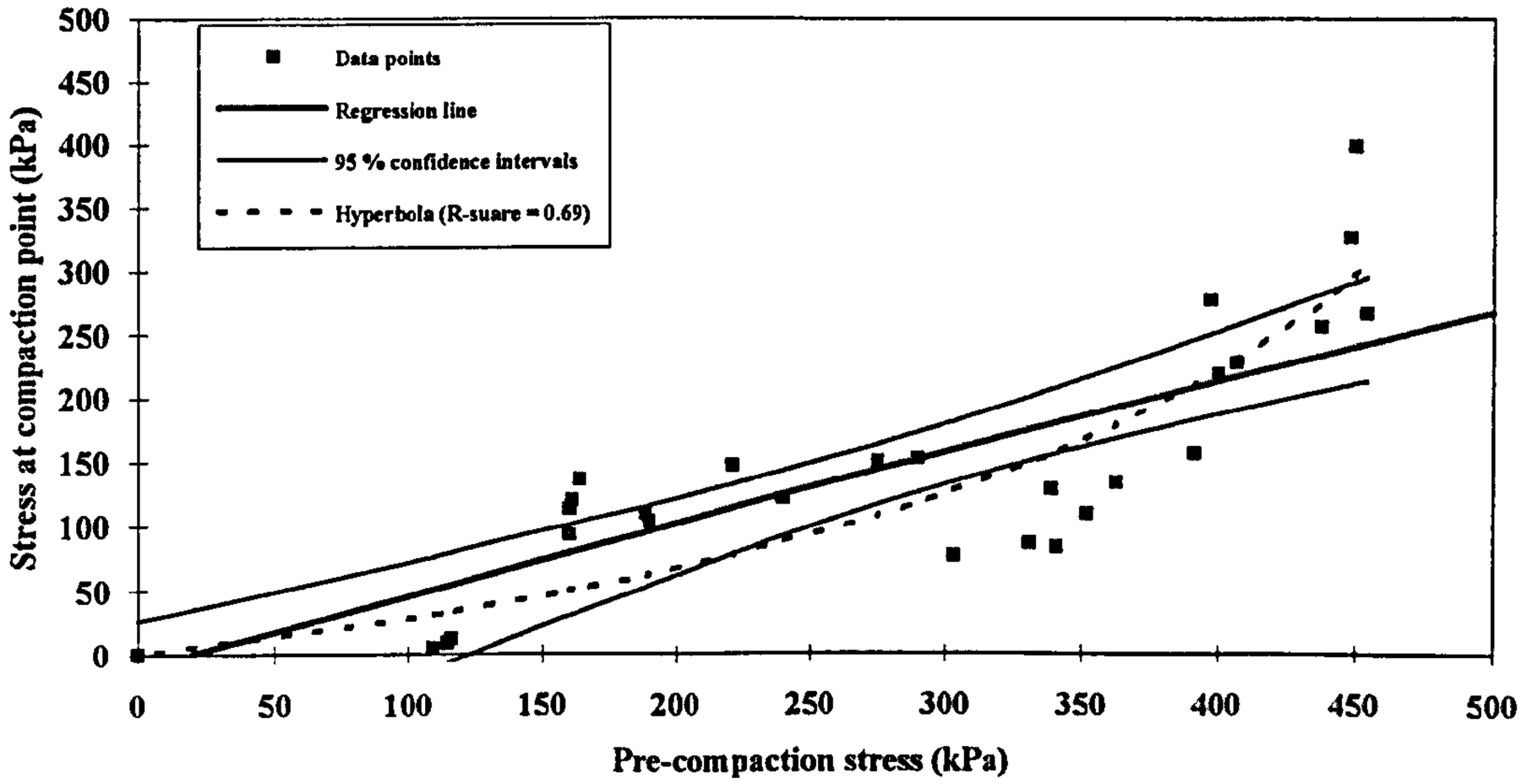

Figure 7.6. The relationship between stress at compaction point and pre-compaction stress (bin sandy loam soil).

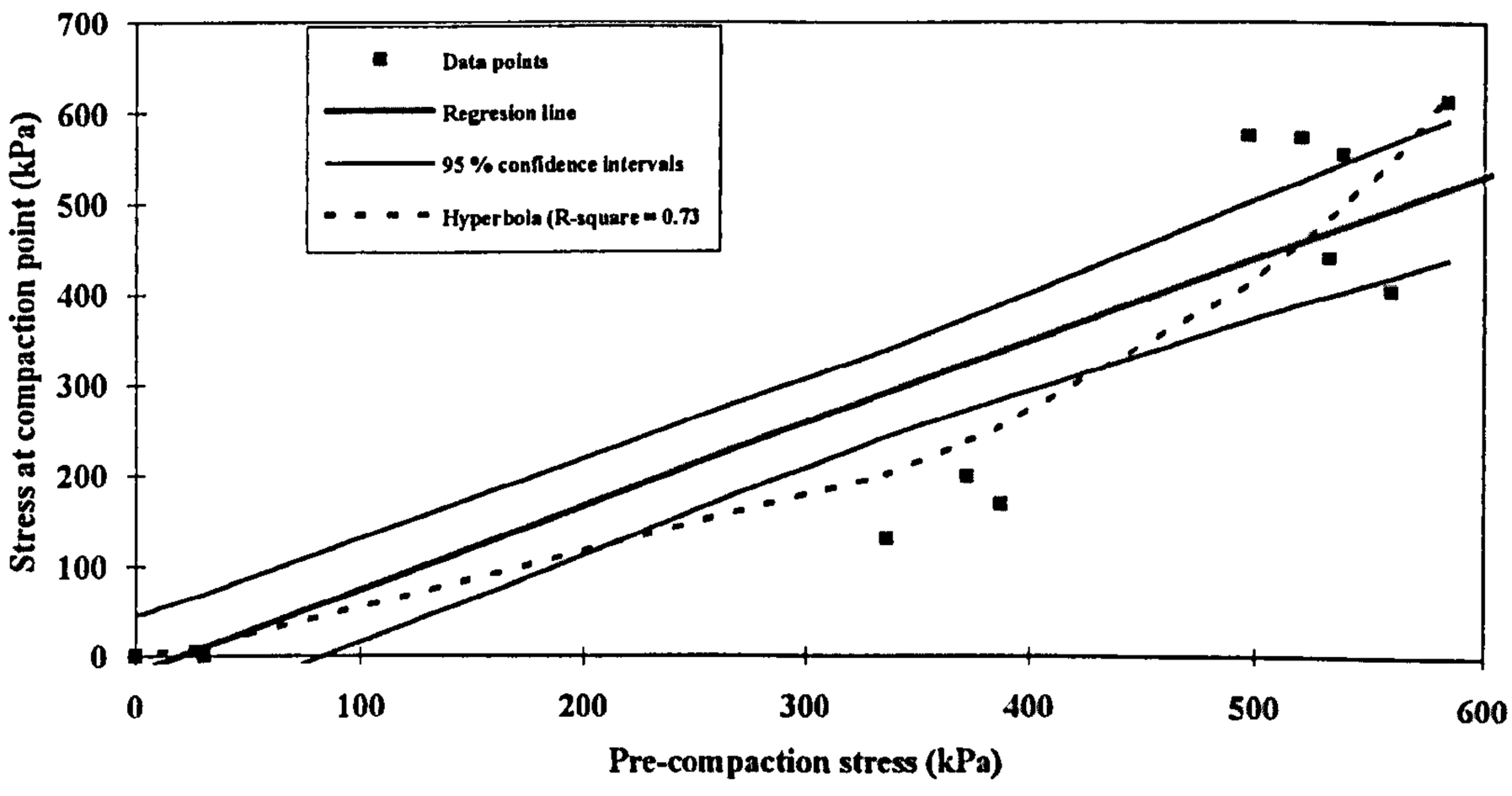

Figure 7.7. The relationship between stress at compaction point and pre-compaction stress (field sandy loam soil).

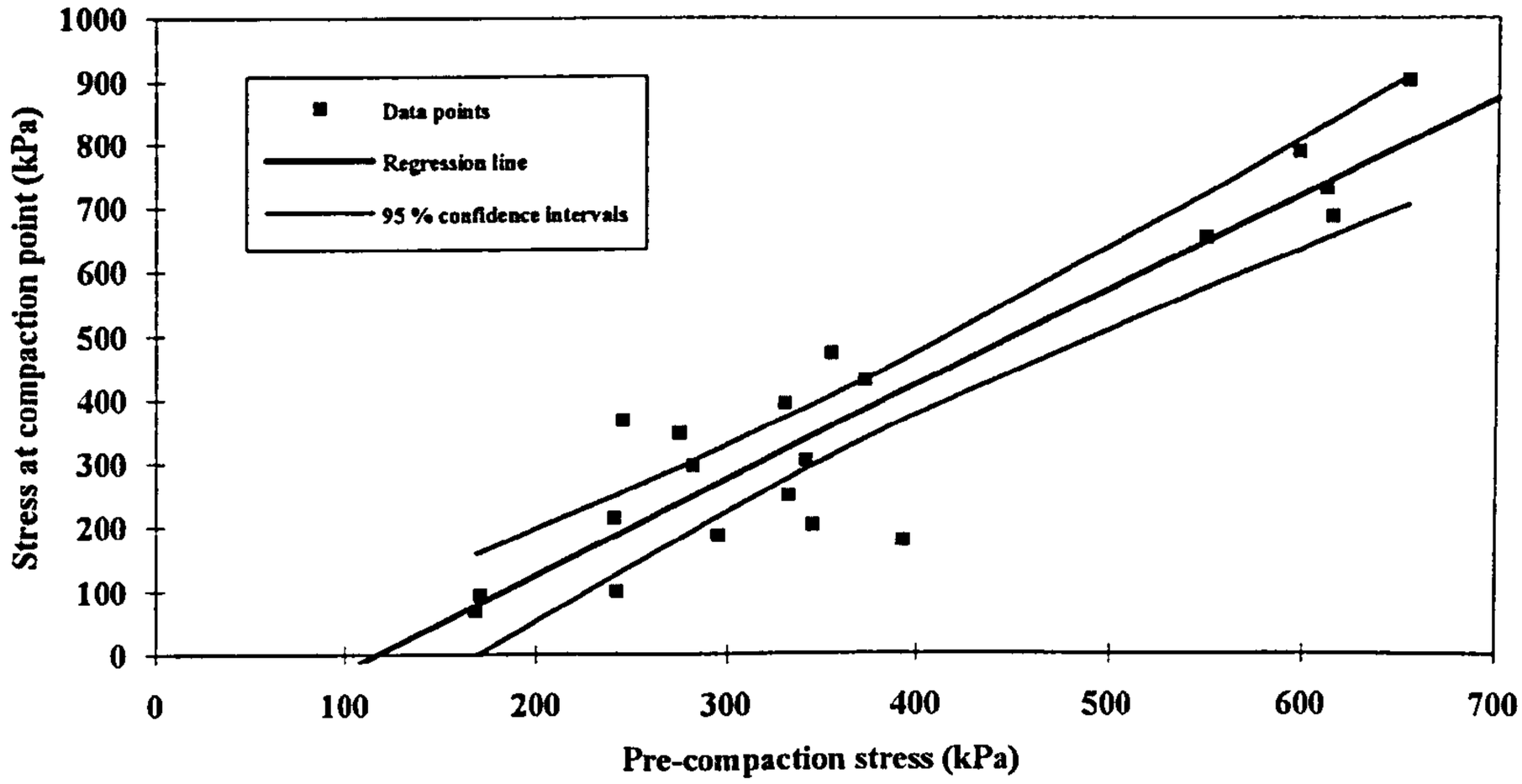

Figure 7.8. The relationship between stress at compaction point and pre-compaction stress (clay soil).

A summary of results from a statistical analysis of the data is presented in *Table 7.2*.

Table 7.2

Statistical analysis results for stress at compaction point vs pre-compaction stress

Soil type	Derived equation	R^2	Significance
Sandy soil (bin)	$\sigma_{cp} = -10.80 + 0.56\sigma_{pr}$	0.76	***
Sandy soil (field)	$\sigma_{cp} = -18.16 + 0.91\sigma_{pr}$	0.87	***
Clay soil (field)	$\sigma_{cp} = -175.47 + 1.50\sigma_{pr}$	0.85	***

For all the soils examined in this work stress at compaction point increases with pre-compaction stress (*Figure 7.9*). It should be noted that the stress at compaction point of a soil has a value which sometimes exceeds its pre-compaction stress.

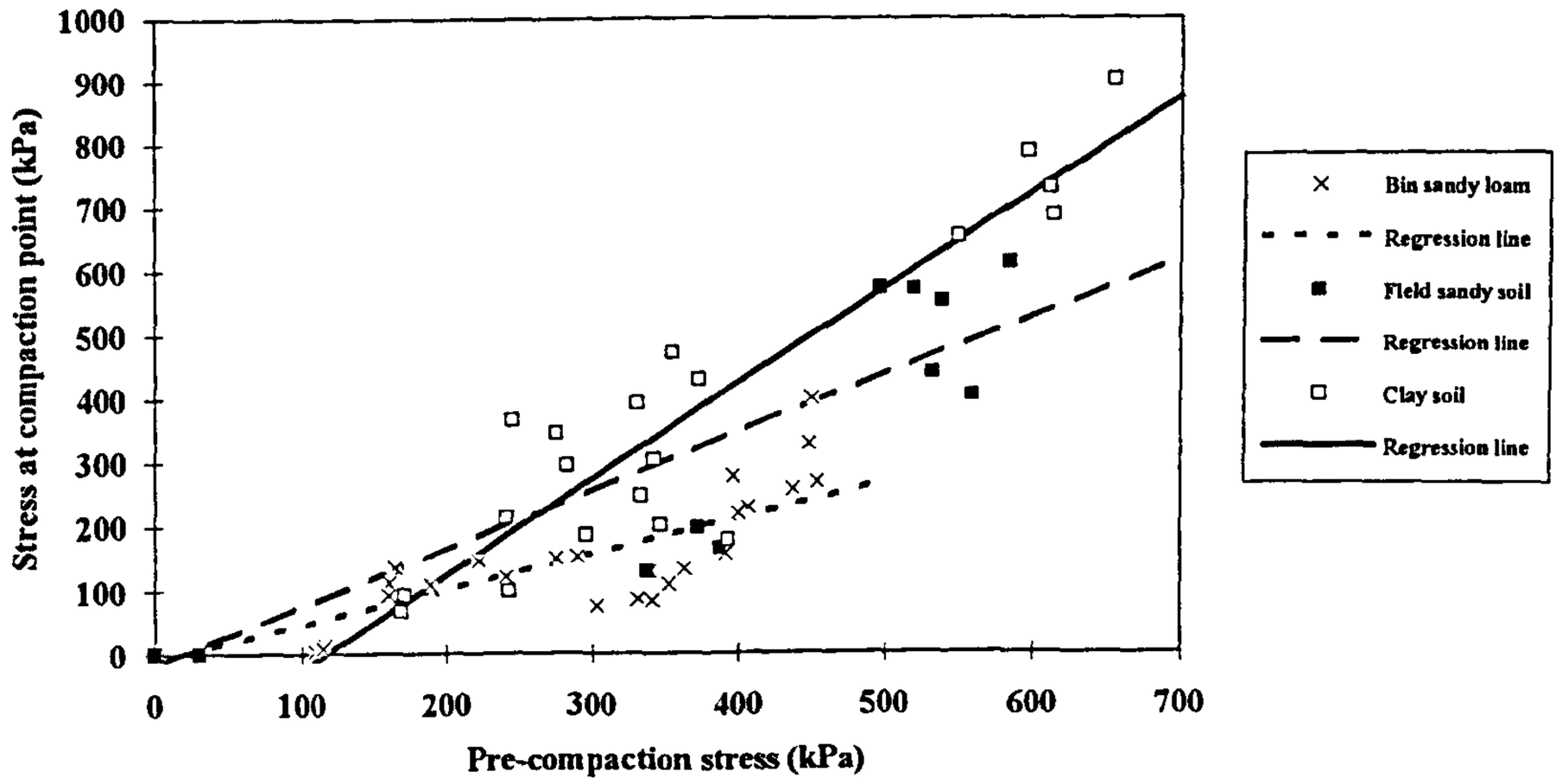

Figure 7.9. The relationship between stress at compaction point and pre-compaction stress for the soil bin sandy loam soil and both field soils.

7.4 The relationship between stress at compaction point and initial compressive soil strength

The relationships between stress at compaction point and initial compressive soil strength for the soils encountered during this work, can be approximated by an equation of the general form:-

$$\sigma_{cp} = \frac{m_p}{\frac{1}{g_i} + \frac{m_p}{\sigma_{cpult}}} \qquad (7.3)$$

Where:-

σ_{cp} = stress at compaction point (kPa)
σ_{cpult} = asymptotic value of σ_{ult} (kPa)
g_i = initial modulus (mm^{-1})
m_p = initial compressive soil strength (kPa/mm)

Non-linear regression analysis was also performed on the data and the relationships and the results of the statistical analysis are presented in *Figures 7.10, 7.11, 7.12* and *Table 7.3* respectively.

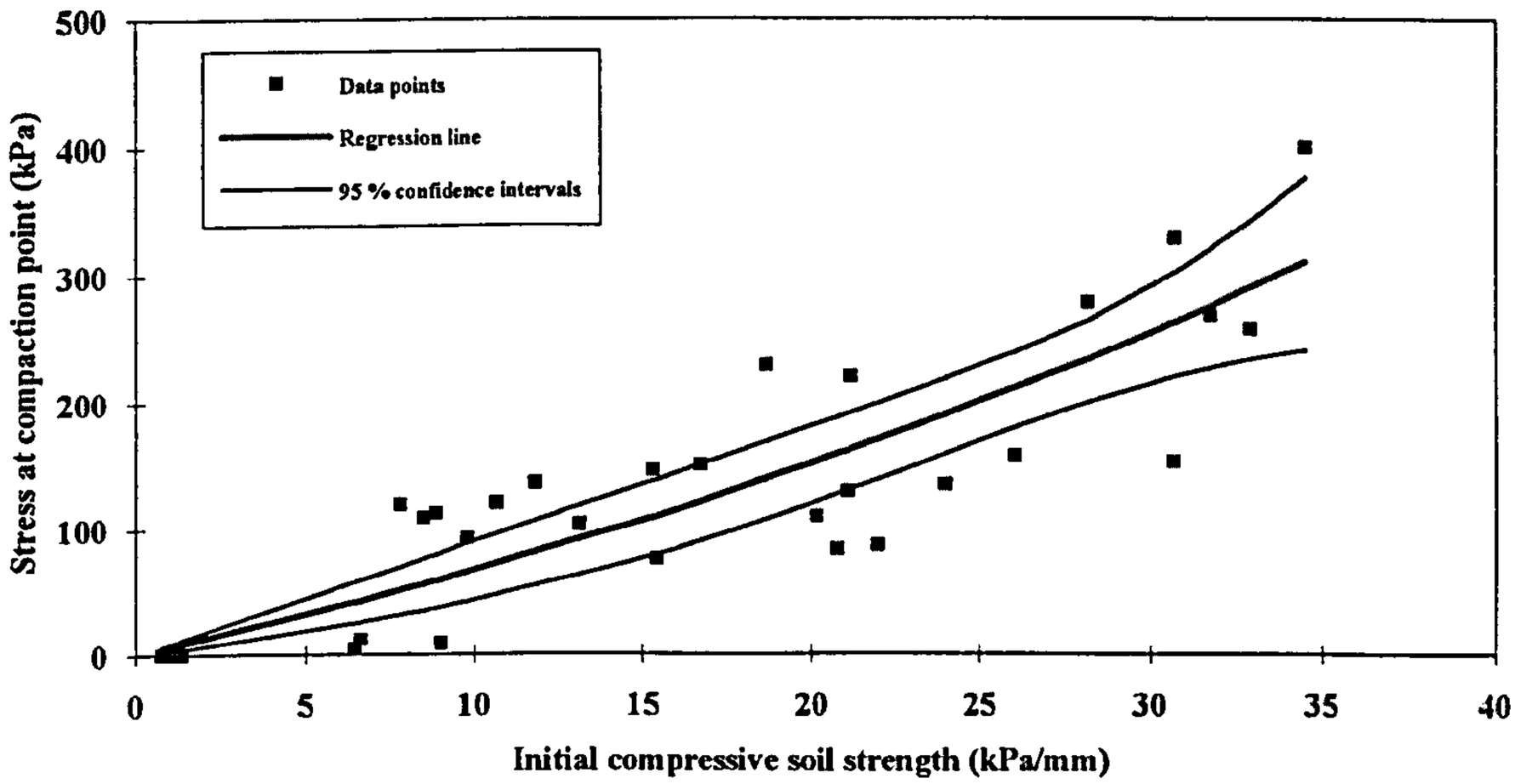

Figure 7.10. The relationship between stress at compaction point and initial compressive soil strength (bin sandy loam soil).

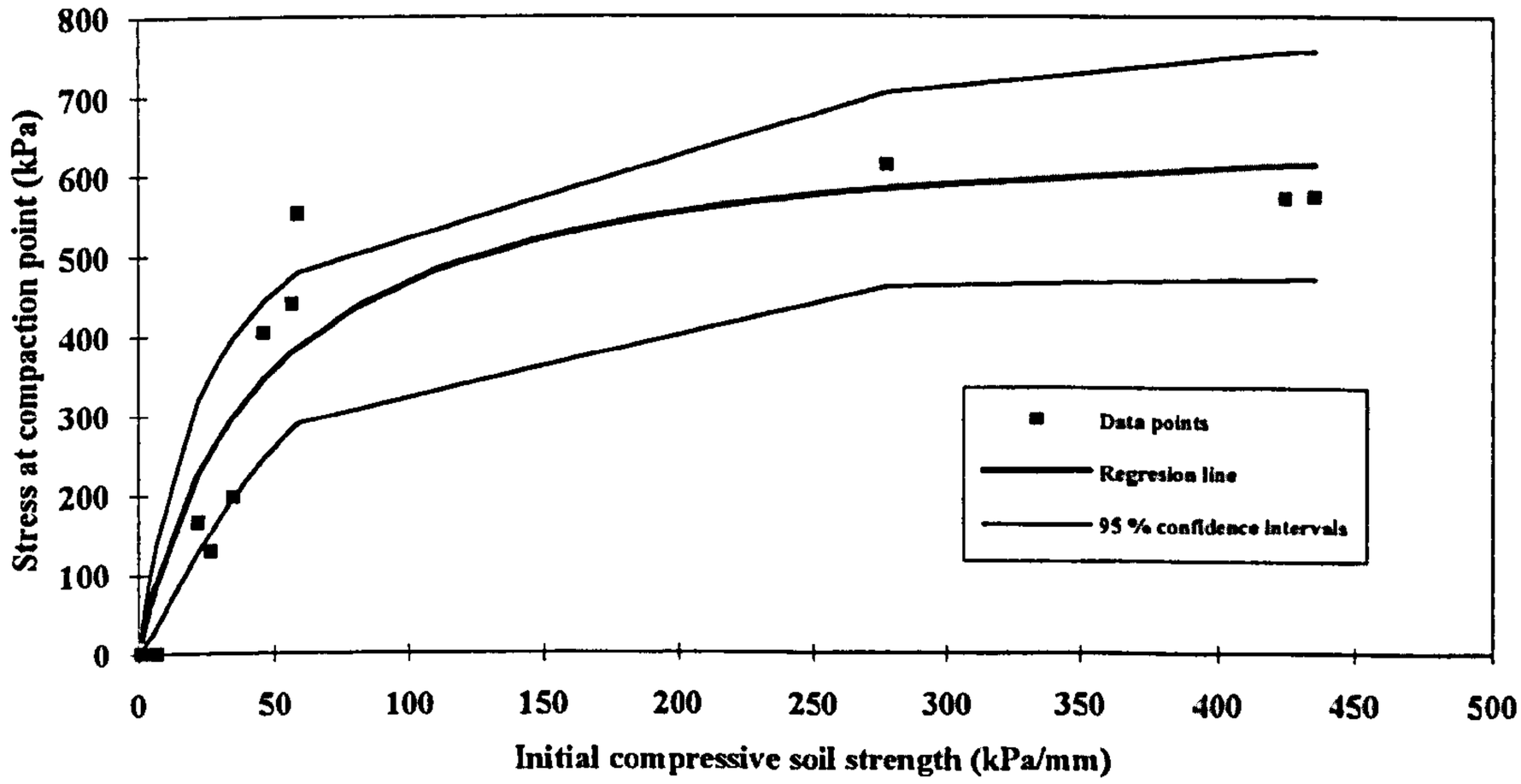

Figure 7.11. The relationship between stress at compaction point and initial compressive soil strength (field sandy loam soil).

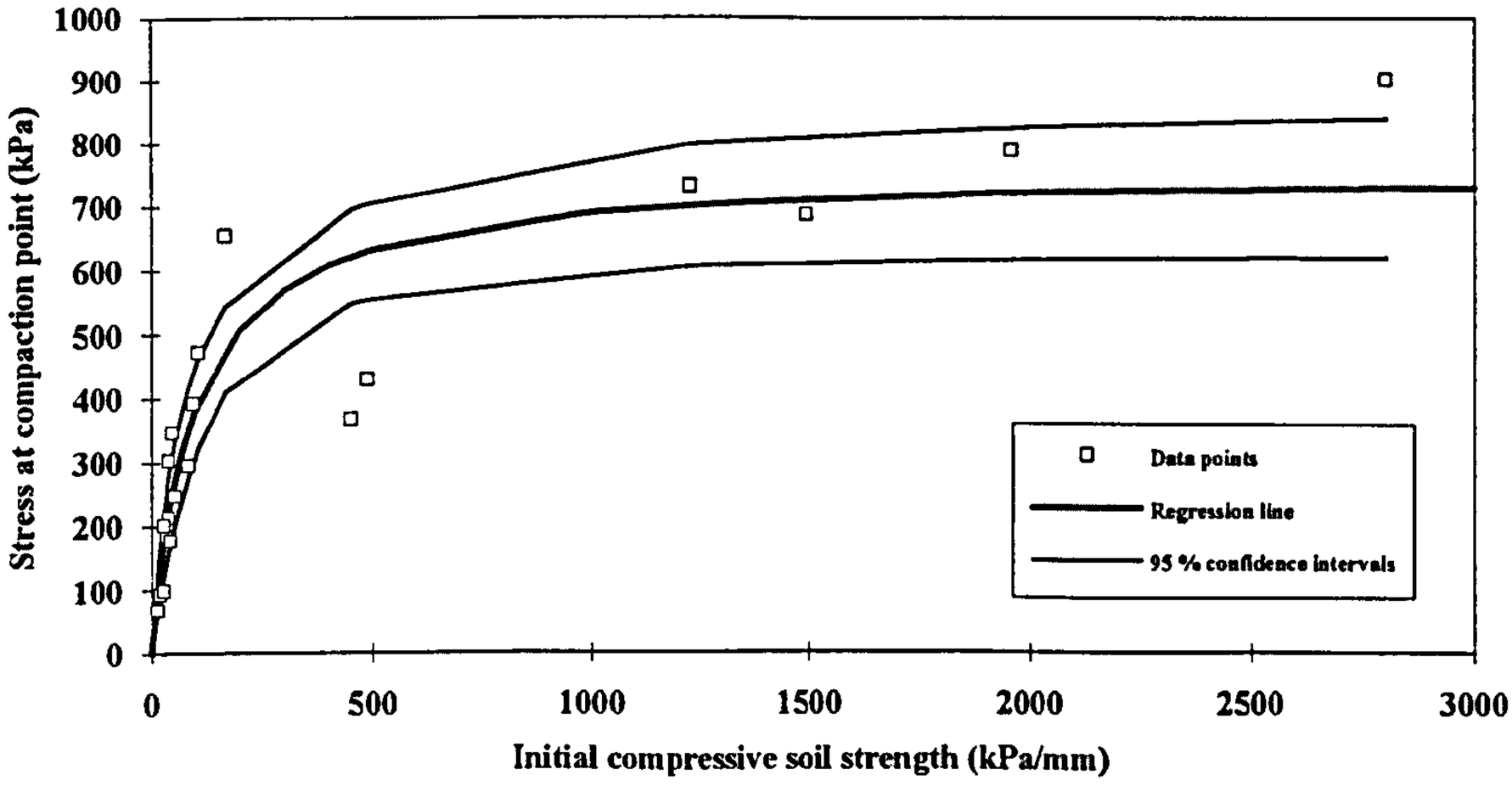

Figure 7.12. The relationship between stress at compaction point and initial compressive soil strength (field clay soil).

Table 7.3

Statistical analysis results for stress at compaction point and initial compressive soil strength

Soil type	Derived equation	R^2	Significance
Sandy soil (bin)	$\sigma_{cp} = \dfrac{m_p}{\dfrac{1}{6.13} + \dfrac{m_p}{-667.67}}$	0.64	***
Sandy soil (field)	$\sigma_{cp} = \dfrac{m_p}{\dfrac{1}{15.18} + \dfrac{m_p}{678.00}}$	0.77	***
Clay soil (field)	$\sigma_{cp} = \dfrac{m_p}{\dfrac{1}{7.66} + \dfrac{m_p}{757.58}}$	0.82	***

The negative values of the of σ_{cpult} obtained for bin sandy soil can be attributed to the limited range of data. For the range concerned during this work, the hyperbola and data follows similar trends (*Figure 7.10*), however, regression equation tends towards a negative asymptote as sinkage increases well beyond that experienced during normal

agronomic practices. Stress at compaction point for both field soils tends towards an asymptote as initial compressive soil strength increases (*Figure 7.13*).

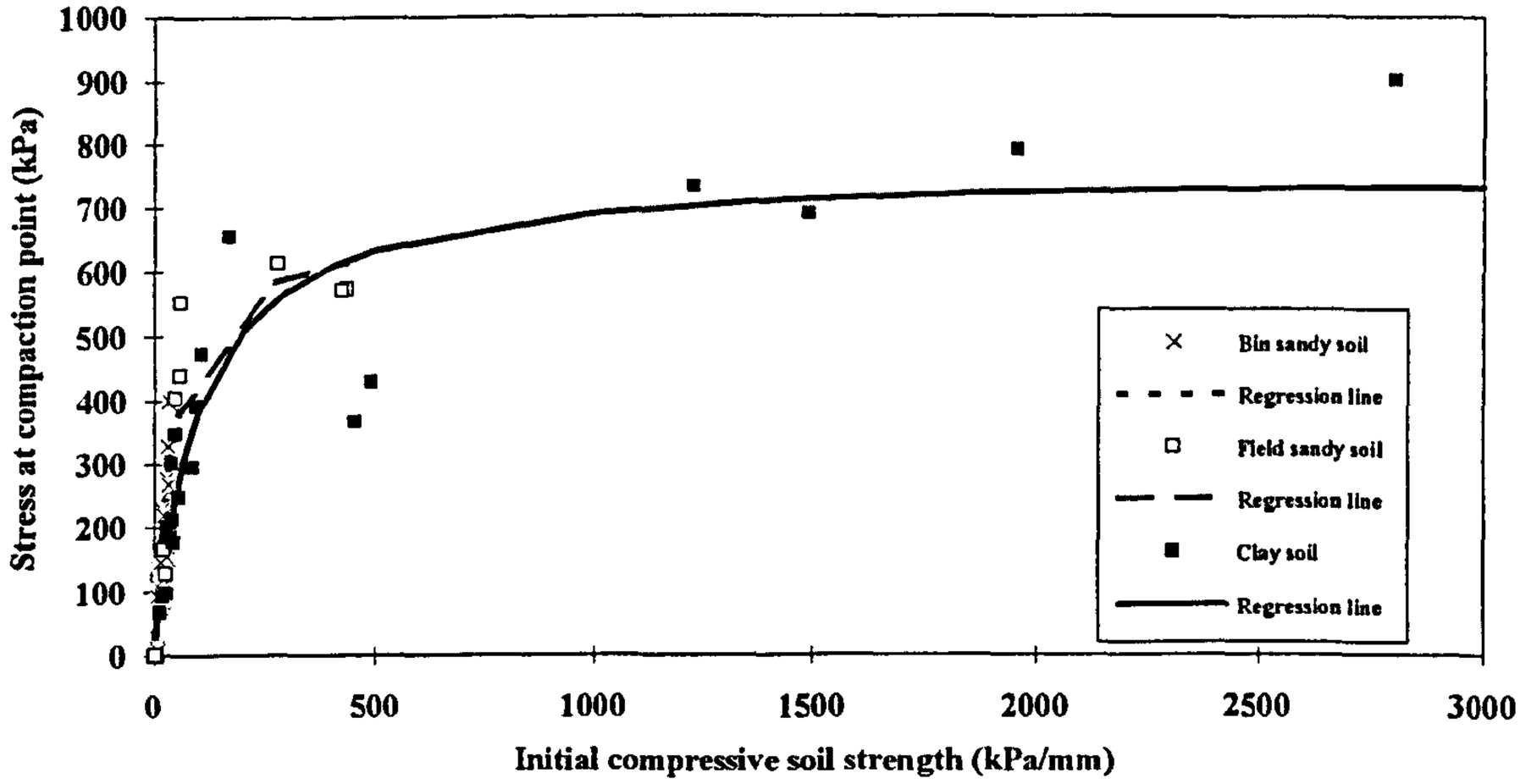

Figure 7.13. The relationship between stress at compaction point and initial compressive soil strength for both field soils.

7.5 Summary

The relationships between pre-compaction stress, stress at compaction point and initial compressive soil strength were investigated in this chapter. For both the bin and the two field soils the following have been shown to apply:-

1) A hyperbolic relationship exists between pre-compaction stress and initial compressive soil strength. All cases were highly significant.

2) The relationship between stress at the compaction point and initial compressive soil strength was also a hyperbola for all soils examined in this study. This is highly significant in all cases.

3) Initial compressive soil strength is the major factor that influences the mode of deformation below a plate and its pre-compaction stress.

4) Stress at the compaction point increases linearly with pre-compaction stress. The relationship is highly significant.

CHAPTER 8

GENERAL DISCUSSION, CONCLUSIONS AND RECOMMENDATIONS FOR FUTURE WORK

In the preceding chapters, pre-compaction stress, initial compressive soil strength, stress at compaction point and extent of deformation below a circular plate have been investigated. These variables can be derived from the stress-strain relationship of soil and describe soil compactibility in terms of sinkage caused to soil due to stress application, soil strength, mode of soil failure and extent of deformation within the soil profile. In chapter 7 these properties have been interrelated allowing their prediction from each other. In this chapter, these properties are combined in the form of a compactibility assessment diagram which can be used to predict the mechanical behaviour of soil under a sinkage plate.

8.1 Introduction

'Scientific understanding proceeds by way of constructing and analysing models of the segments or aspects of reality under study. The purpose of these models is not to give a mirror image of reality, not to include the all its elements in their exact sizes and proportions, but rather to single out and make available for intensive investigation those elements which are decisive. We abstract from non-essentials, we blot out the unimportant to get an unobstructed view of the important, we magnify in order to improve the range and accuracy of our observation. A model is, and must be, unrealistic in the sense in which the word is most commonly used. Nevertheless, and in a sense, paradoxically, if it is a good model it provides the key to understanding reality (Baran and Sweezy, 1968)'.

This is particularly true for soil. It is difficult, for example, to accurately predict the behaviour of soil in field conditions since a multitude of factors come together to contribute towards soil variability. It is feasible, however, to determine essential soil properties which influence soil behaviour and create a model using these properties in order to analyse and predict, although not completely, the likely outcome of a given set of circumstances on soil status.

During this work, the analysis of soil behaviour, in terms of compactibility, has been approached from a stress-strain point of view using plate sinkage tests. Three points on the stress-strain curve have been identified as important indicators of

compactibility, namely pre-compaction stress, stress at compaction point and initial compressive soil strength (*Figure 8.1*). Each of these variables has been related to soil characteristics, and can be used to assess the likely behaviour of the material. Pre-compaction stress, initial compressive soil strength and stress at compaction point provide information on pre-existing stress state, strength and mode of failure respectively and therefore, all three can be used for soil compactibility assessment purposes. In addition, extent of disturbance due to stress application can be determined using the model developed in chapter 5 and, therefore, can also be used for soil compactibility assessment purposes.

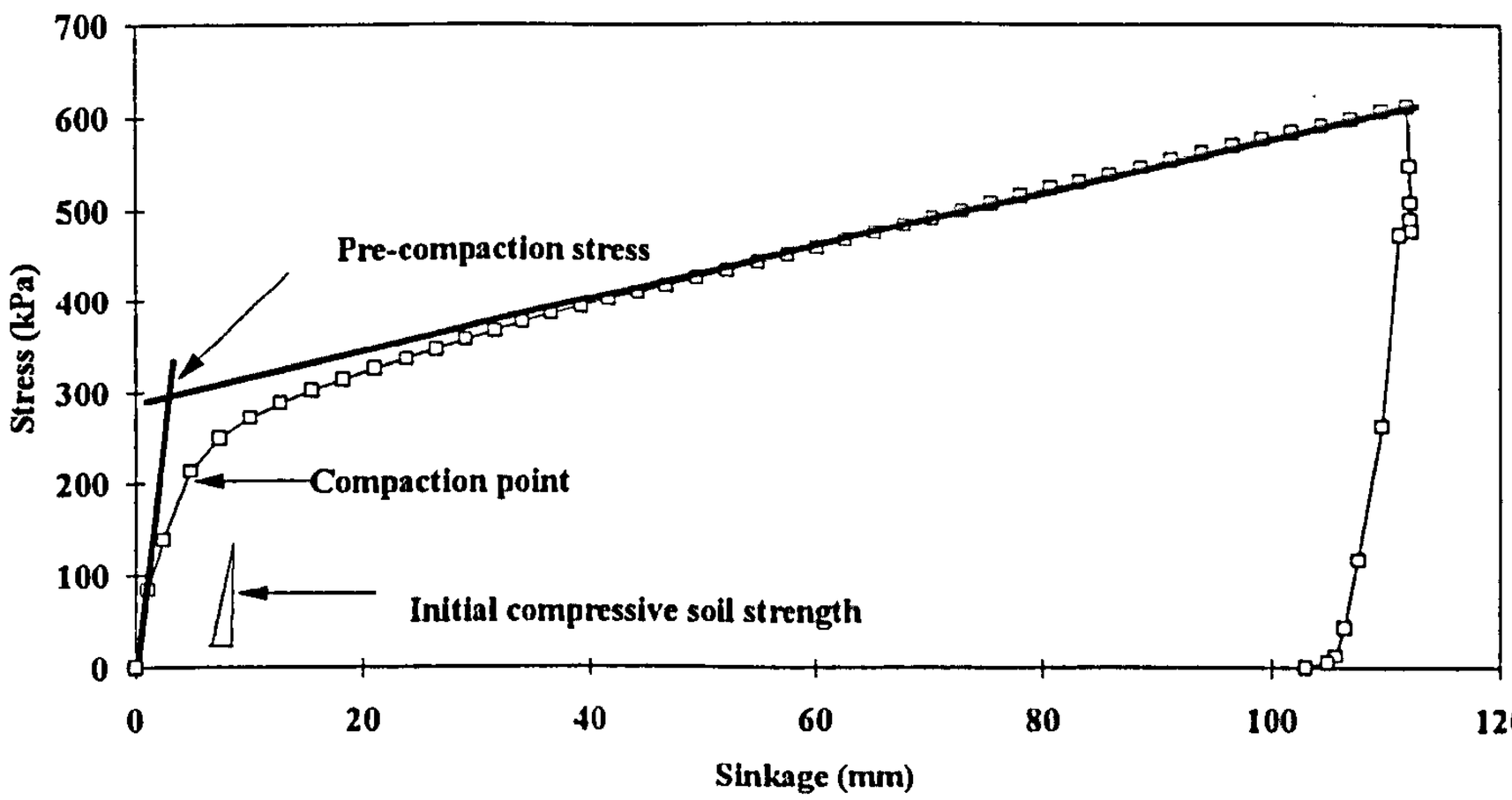

Figure 8.1. Typical stress-sinkage relationship of soil obtained from a plate sinkage test.

8.2 Assessing soil compactibility

In the introductory chapter, measurement of the following components was proposed for soil compactibility assessment:-

(1) the stress-strain (load-sinkage) characteristics of a soil,

(2) soil strength prior to loading, and

(3) the mode and extent of soil deformation within the soil profile for a given loading situation.

Stress-strain characteristics:-

The stress-strain characteristics of a soil can be used to determine pre-compaction stress. As noted in chapter 3, pre-compacted soil will largely resist further mechanical loading until that loading exceeds the pre-existing load of the soil. Koolen (1982) also noted that it is desirable to limit soil loading to below the pre-compaction stress of a soil in order to minimise further soil compaction. This therefore provides an indirect measure of pre-existing soil compaction. As such, pre-compaction stress is an important factor for soil compactibility assessment since it assigns a number to the existing level of compaction. It is a function of soil strength (it has been also used to quantify soil strength (Horn and Lebert 1994)), and consequently, its value varies with physical properties of soil such as water content and bulk density. During this work, it was found to range from zero, for none pre-compacted soil, to approximately 600 kPa for very compacted soil.

Soil strength:-

Soil strength is an expression of the resistance of that soil to loading and is directly related to soil compaction since soil compaction is the result of an applied load. Resistance to deformation is related to cohesion and friction and is, therefore, strongly dependent on the water content and packing state of the soil. During this work, initial compressive soil strength was found to be a reliable variable for evaluating soil strength prior to loading in situ.

Mode and extent of deformation:-

Mode and extent of deformation below a sinkage plate offers an insight into soil behaviour below an applied load. The mode can be identified by superimposing results from a confined compression test onto those from a plate sinkage test (section 6.2). The point at which the mode of deformation of soil under load changes from pure compaction to a combination of lateral and vertical compaction is named the compaction point (CP) (Earl 1993). It is a function of cohesion and angle of shearing resistance and as such is a unique property for soil in a given situation. The mode of deformation directly affects the direction and extent of deformation within the soil profile. This information, in conjunction with soil bin experiments behind glass, has been used to develop a mathematical model for predicting extent of deformation. To date, this model has been tested on sandy

loam soil with encouraging results, however, further work is required to validate the model for other soil types.

It is proposed that the bulk of the information required for an assessment of soil compactibility can be contained within one powerful diagram referred to as "compactibility assessment diagram" (*Figure 8.2*).

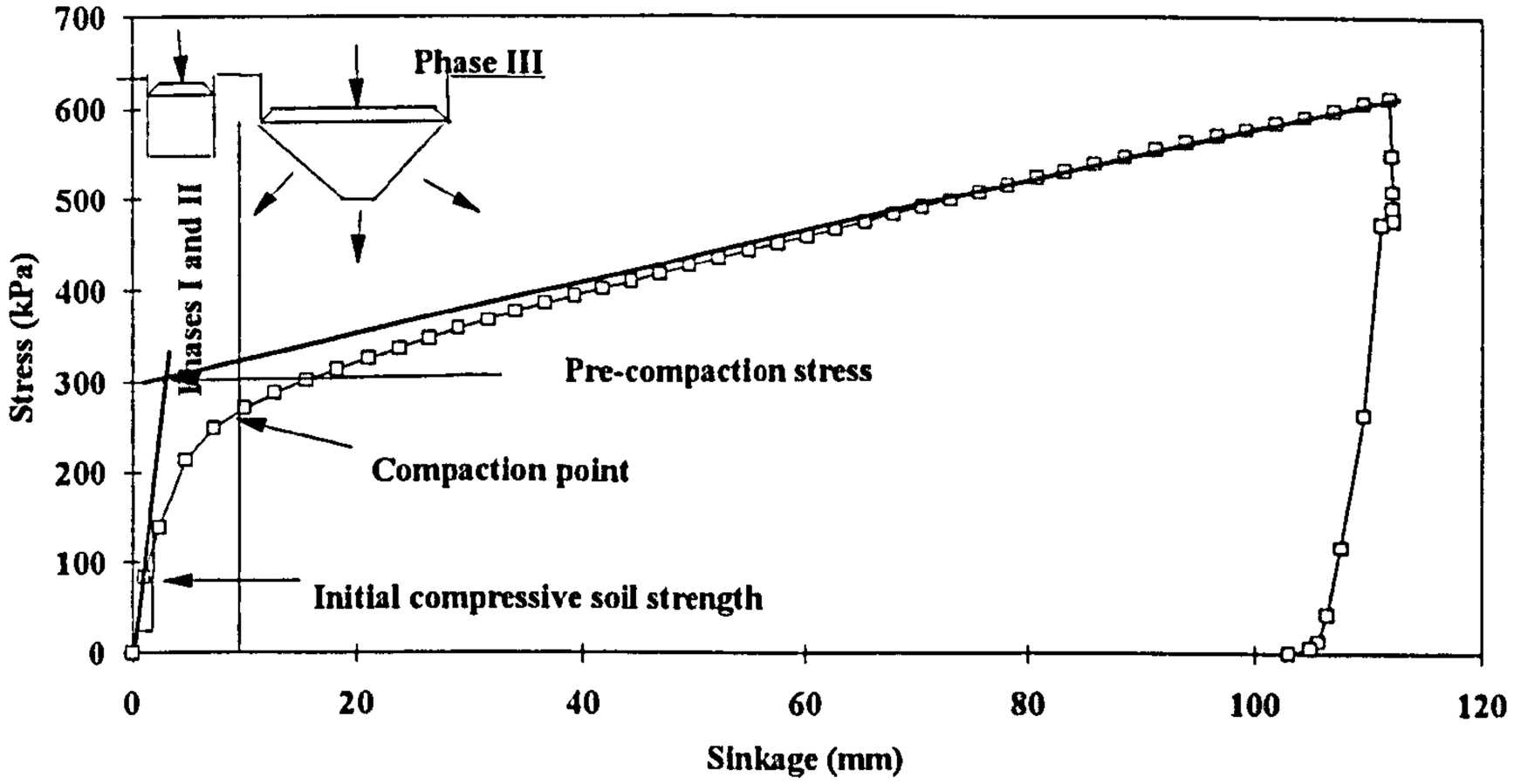

Figure 8.2. Compactibility assessment diagram.

8.2.1 Examples illustrating use of compactibility assessment diagram

Two examples are presented to illustrate use of compactibility assessment diagrams for a sandy, and a clay, soil. Three different loading situations have been selected to provide a range of scenarios:-

a) 45 kPa (equivalent to a low ground pressure wheel)

b) 70 kPa (equivalent to a conventional 70 kW tractor)

c) 95 kPa (equivalent to a four-wheel drive tractor)

Sandy loam soil:-

Results from the compactibility assessment diagram and the mathematical model are presented in *Figure 8.3* and *Table 8.2*. Calculations using the model are presented in Appendix I.

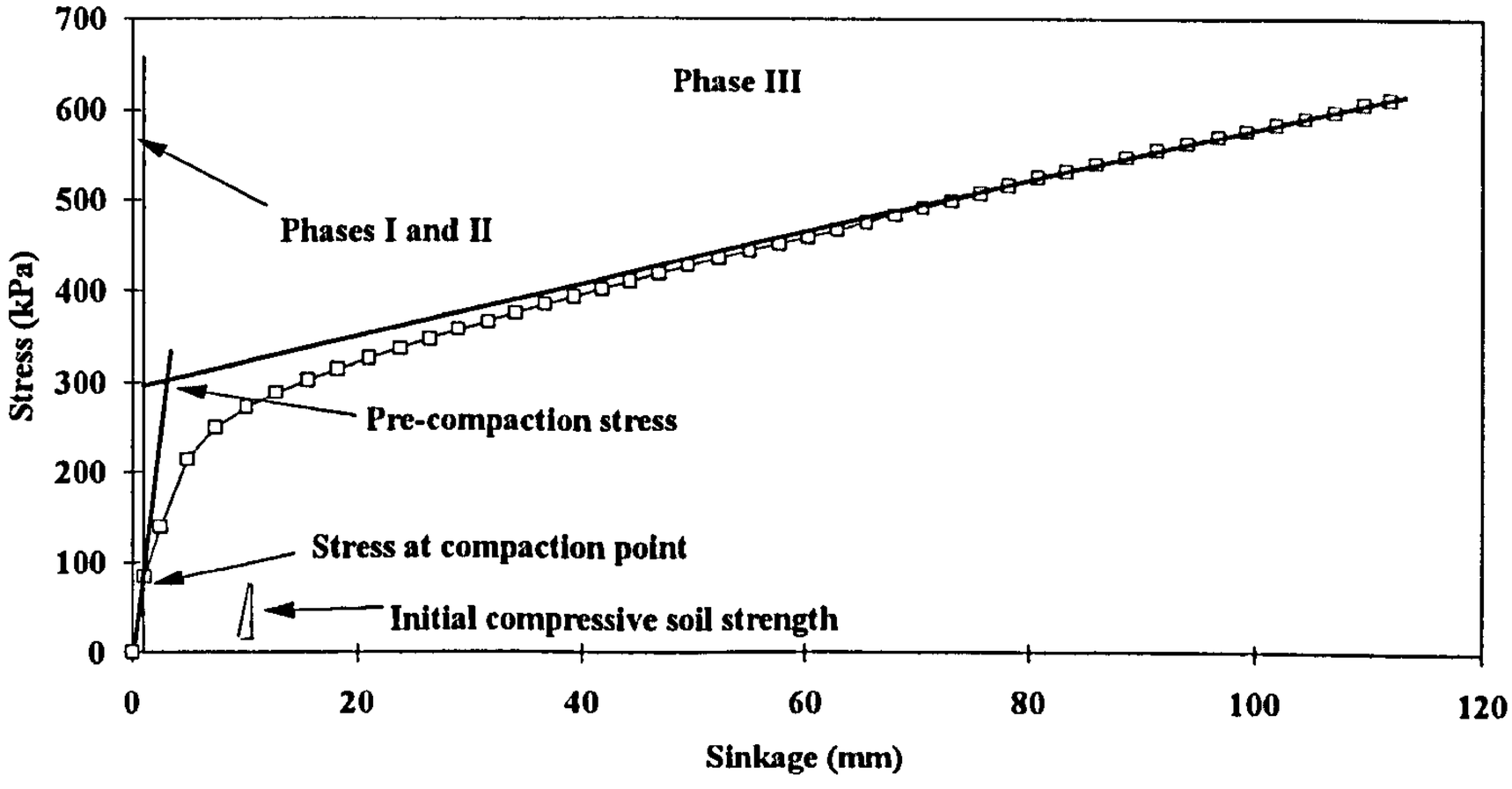

Figure 8.3. Compactibility assessment diagram for a sandy loam soil.

Table 8.1

Determination of soil characteristics (real data)

Soil type	Volumetric water content %	Initial dry bulk density (kg/m^3)	Pre-compaction stress (kPa)	Initial compressive soil strength (kPa/mm)	Stress at compaction point (kPa)
Sandy loam	12.1	1.35	303	15.4	76.3

For a ground pressure of 45 kPa, sinkage is virtually negligible (1.5 mm) because the applied stress is well below its pre-compaction stress). The mode of soil deformation is phase I, and therefore, soil will be displaced vertically to a depth of 67.5 mm below the soil surface. The initial compressive soil strength value can be considered medium.

If the ground pressure is increased to 70 kPa, sinkage increases to 1.8 mm, however, this is still limited since the applied stress is still below the pre-compaction stress. The mode and extent of soil disturbance below the plate is governed by phase II because the load is approaching the stress at the compaction point. The

depth of soil disturbance from the soil surface is 95.8 mm, higher than in the previous case.

For an applied pressure of 95 kPa, sinkage will be greater than in the previous cases (3.2 mm), but still below the pre-compaction stress. The mode of deformation corresponds to phase III. The depth of the disturbed area below the soil surface lies between 134.2 and 150.2 mm and the disturbed area can be approximated by the segment of a sphere with a chord of 152 or 184 mm. This depends on the point of application of passive force (see section 5.3.4). The results are presented in *Table 8.2*.

Table 8.2
Mode and extent of deformation (sandy soil)

Soil type	Applied stress (kPa)	Sinkage (mm)	Extent of deformation (mm)	Mode of deformation
Sandy loam	45	1.5	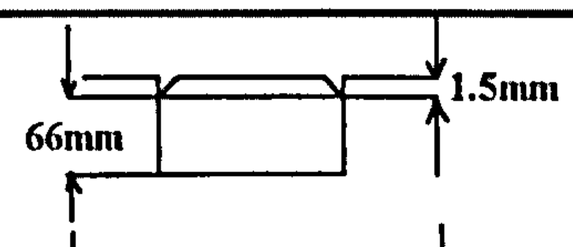	Phase I
	70	1.8	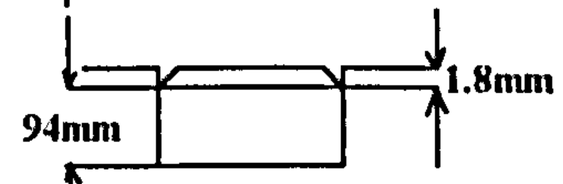	Phase II
	95	3.2	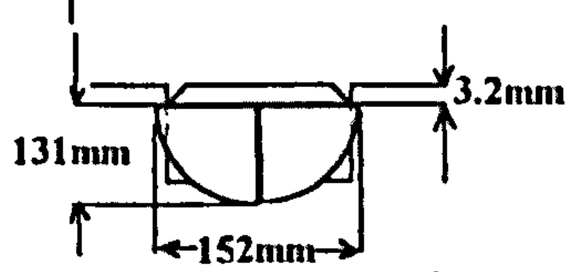	Phase III *l_1 from (5.30)*
or	95	3.2	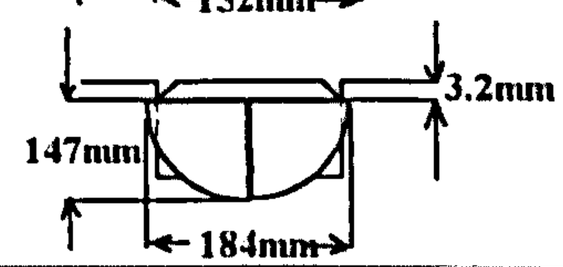	Phase III *l_1 from (5.31)*

Clay soil:-

Results from the compactibility assessment diagram and the mathematical model for the clay soil are presented in *Figure 8.4* and *Table 8.4*. Calculations using the model are presented in Appendix I.

Table 8.3

Determination of soil characteristics (real data)

Soil type	Volumetric water content %	Initial dry bulk density (kg/m^3)	Pre-compaction stress (kPa)	Initial compressive soil strength (kPa/mm)	Stress at compaction point (kPa)
Clay soil	53	1.02	171	21	92.5

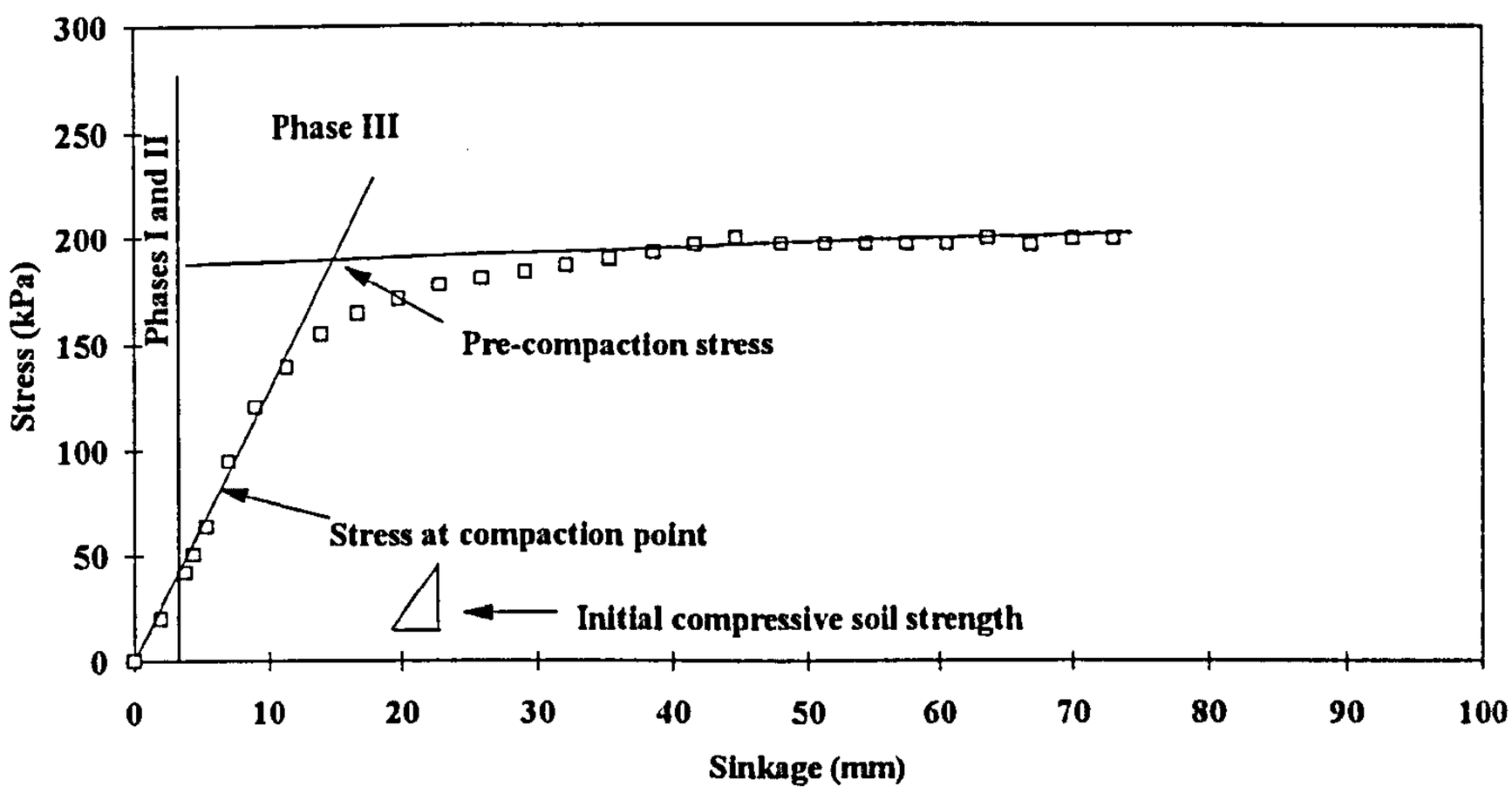

Figure 8.4. Compactibility assessment diagram for a clay soil.

In the case of the clay soil, for a ground pressure of 45 kPa, sinkage will be limited to 3.2 mm because the applied stress is well below its pre-compaction stress. The mode of deformation corresponds to phase I and the depth of soil disturbance from the soil surface is 28.3 mm. The initial compressive soil strength of this soil can be considered low 21 kPa/mm.

If the applied stress is increased to 70 kPa, sinkage increases to 5.5 mm, still below its pre-compaction stress. The mode of deformation corresponds to phase II and the depth of soil disturbance from the soil surface increases to 43.5 mm.

For a applied pressure of 95 kPa, sinkage will increase to 7 mm. The mode of deformation is on the boundary between phases II and III and it has been assumed that it is still in phase II. The depth of soil disturbance increases to 57 mm. The results are presented in *Table 8.4.*

Table 8.4
Mode and extent of deformation (clay soil)

Soil type	Applied stress (kPa)	Sinkage (mm)	Extent of deformation (mm)	Mode of deformation
Clay soil	45	3.8	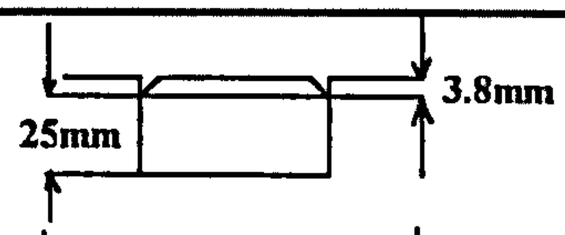	Phase I
	70	5.5	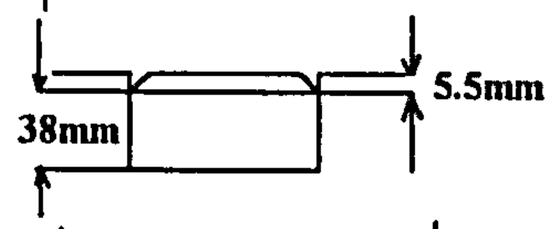	Phase II
	95	7	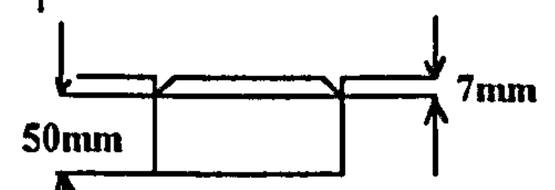	Phase II

8.2.2 Predicting soil compactibility characteristics from easily determined soil properties

In chapters 3, 4, and 6 pre-compaction stress, initial compressive soil strength and stress at the compaction point were determined and their relationship with easily determined soil properties investigated. Examples of these relationships, for prediction purposes will be presented in this section.

Compactibility assessment data, measured during this study, are presented in *Table 8.5*. The same data have been predicted from more easily determined soil properties and are presented in *Table 8.6* for comparative purposes. For the sandy loam soil, pre-compaction stress, initial compressive soil strength and stress at the compaction point were predicted using *Figures 3.9, 4.4* and *6.5*, respectively. For the clay soil, the same variables were predicted using *Figures 3.13, 4.8* and *6.7*, respectively. Lack of data, limited range of data and errors introduced through categorisation of data, did not allow the derivation of statistically significant relationships in all cases, however, prediction of these soil characteristics from more readily available data looks promising and warrants further investigation.

Table 8.5

Soil characteristics (real data)

Soil type	Volumetric water content %	Initial dry bulk density (kg/m^3)	Pre-compaction stress (kPa)	Initial compressive soil strength (kPa/mm)	Stress at compaction point (kPa)
Bin sandy loam	13	1.41	190	13	103
Clay	33	1.08	614	1492	688

Table 8.5

Prediction of soil characteristics from easily determined data

Soil type	Volumetric water content %	Initial dry bulk density (kg/m^3)	Pre-compaction stress (kPa)	Initial compressive soil strength (kPa/mm)	Stress at compaction point (kPa)
Bin sandy loam	13	1.41	282.5	17	151
Clay	33	1.08	540.5	1284	665

It should be noted that pre-compaction stress can be also determined using critical state theory. Figure 8.5 presents the projection of the normal consolidation line on the q=0 plane (q is the deviatoric stress). Pre-compaction stress on this plane using a similar procedure to that developed in chapter 3.

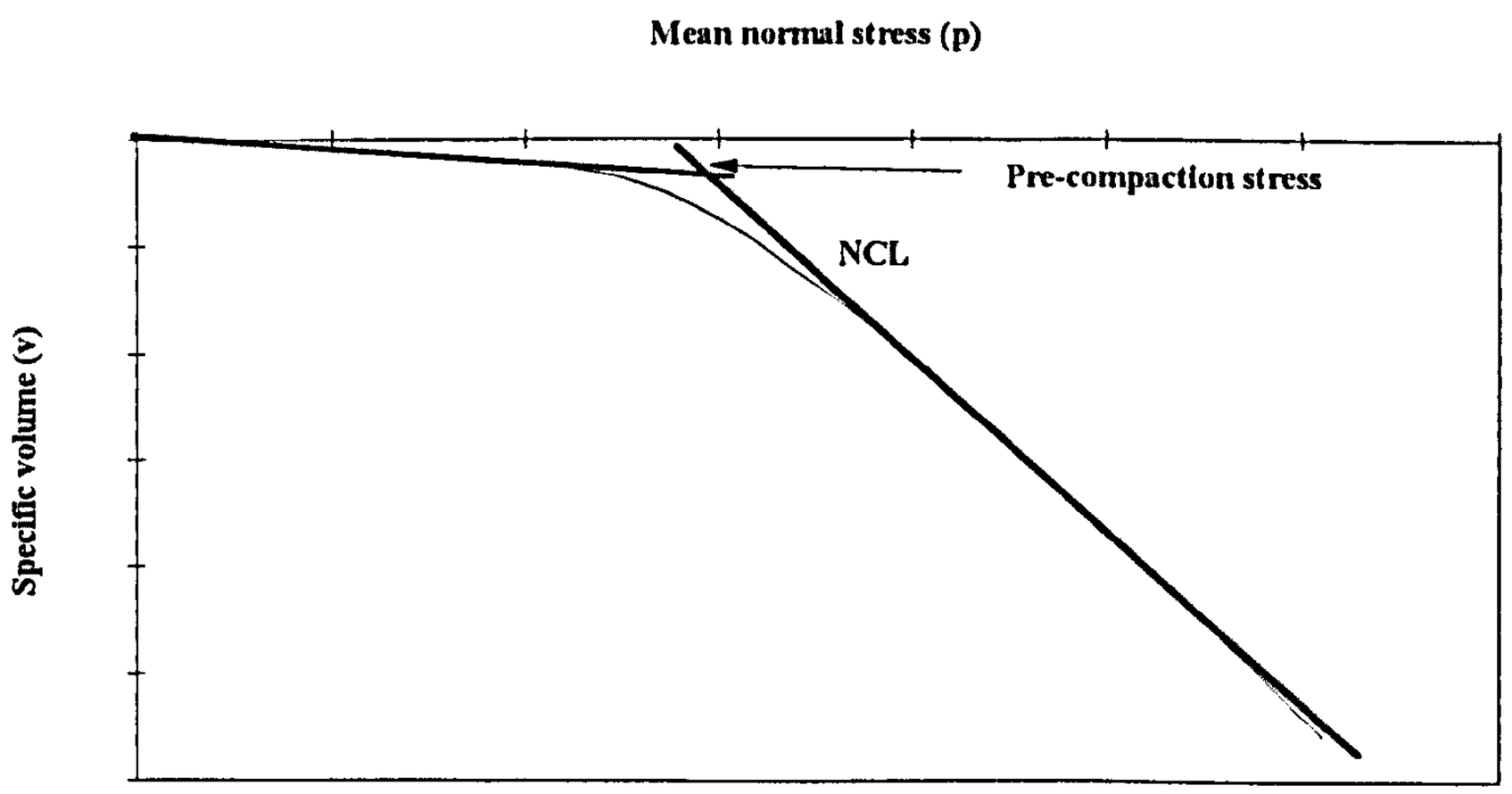

Figure 8.5. Determination of pre-compaction stress using critical state theory.

8.3 Summary, conclusions and recommendations

8.3.1 Summary

The findings of this work are summarised below:-

1) Pre-compaction stress of soil can be determined, with good accuracy, in situ using a plate sinkage test. It can also be predicted from volumetric water content, initial dry bulk density, void ratio and degree of saturation.

2) The plate sinkage test can also be used for soil strength assessment. Initial compressive soil strength has been introduced as a direct measure of soil strength. This can also be predicted, for field soils, from volumetric water content, initial dry bulk density, void ratio and degree of saturation.

3) The compaction point theory has been visually verified. Soil deformation below a plate was found to be governed by three phases:-
   a) Compaction at uniform radial stress.
   b) Compaction with increasing radial stress.
   c) Compaction with increasing radial stress and lateral soil movement.

4) Stress at the compaction point can be predicted from volumetric water content, initial dry bulk density, void ratio and degree of saturation.

5) Stress at the compaction point could not be determined for very loose soil using techniques developed during this study. This contradicts visual evidence and questions the validity of the theory for this special case.

6) Soil compactibility can be assessed by a combination pre-compaction stress, initial compressive soil strength and stress at compaction point of a soil, and a model to predict extent of deformation within the soil profile.

8.3.2 Detailed conclusion

Data from a 'compactibility assessment diagram', in conjunction with the results from a mathematical model, can be used to assess the behaviour of field soils in terms of compactibility.

8.3.3 Overall conclusion

The techniques developed during this study provide a new approach to assessing the behaviour of field soils under load.

8.3.4 Recommendations for future work

Further work is required in the following areas:-

1) To establish the influence of penetration velocity on the failure patterns below a sinkage plate.

2) To validate the proposed model for predicting extent of deformation for other soil types.

3) To establish the influence of the confining cylinder length on the determination of the compaction point with particular reference to very loose soils.

4) To examine the relationship between soil failure patterns below sinkage plate and other causes of soil failure.

5) To validate the proposed techniques for other soil types.

6) To investigate the relationship between initial compressive soil strength and resistance to root penetration.

APPENDIX I

CALCULATION OF EXTENT OF SOIL DISTURBANCE BELOW A PLATE

In chapter 5, a model was developed for calculating the extent of soil disturbance below a plate. In this appendix, the calculation of extent of deformation below a plate, at three different pressures, is presented for two soils, a sandy and a clay. Equations presented in chapter 5 are used to calculate the extent of soil disturbance. Variables used in the calculation of the extent of soil disturbance were obtained from confined, plate sinkage and triaxial tests. Input data for the sandy loam are presented in *Table 1a, Figure 1a* and *Figure 2a.*

Table 1a

Results obtained from triaxial test, for sandy loam soil

Cohesion, c, (kPa)	Angle of internal friction ϕ (degrees)	Moisture content (volumetric), %	Dry bulk density (Mg/m^3)
11	30	12.1	1.35

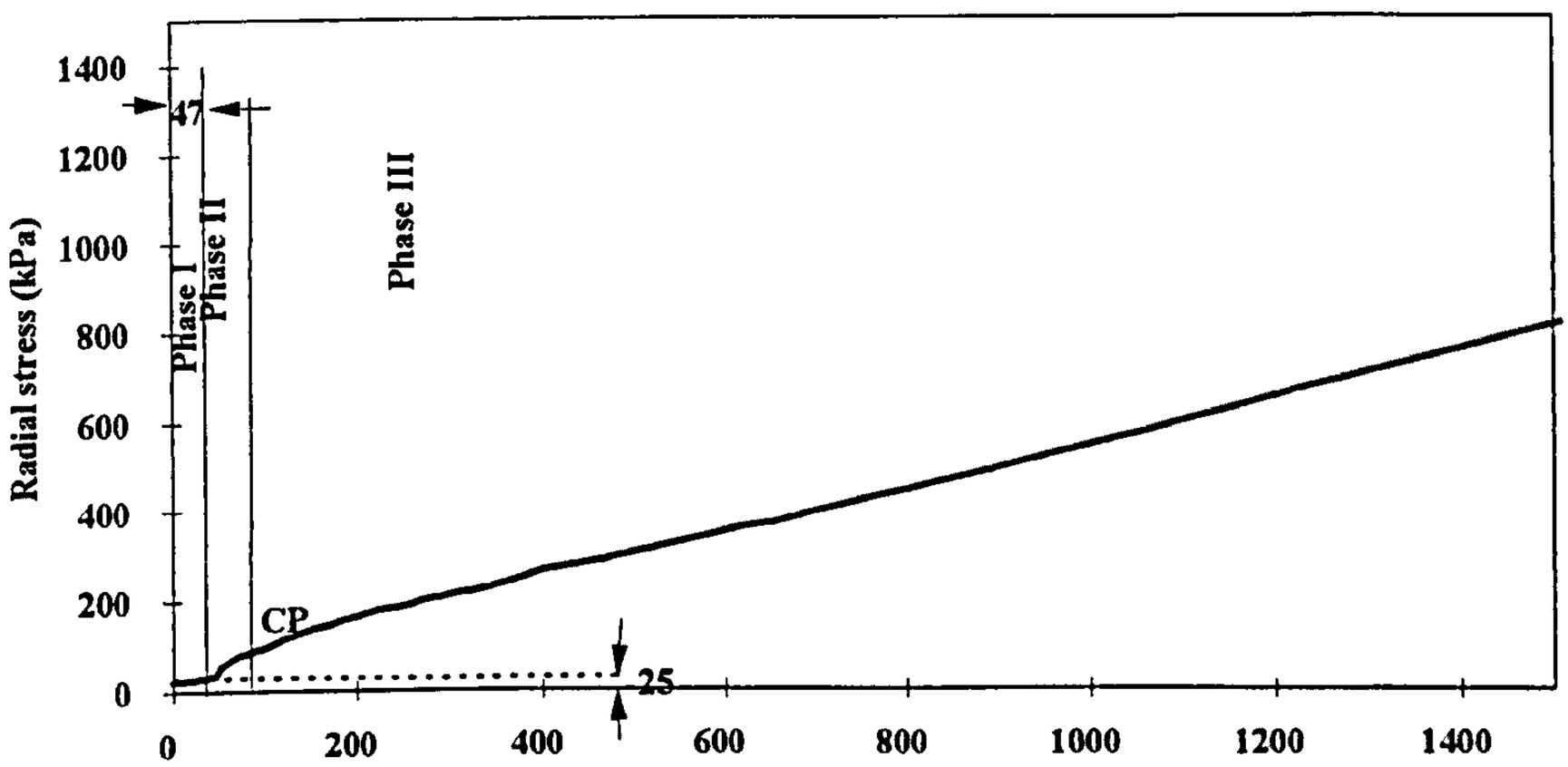

Figure 1a. The relationship between radial stress and axial stress for sandy loam soil.

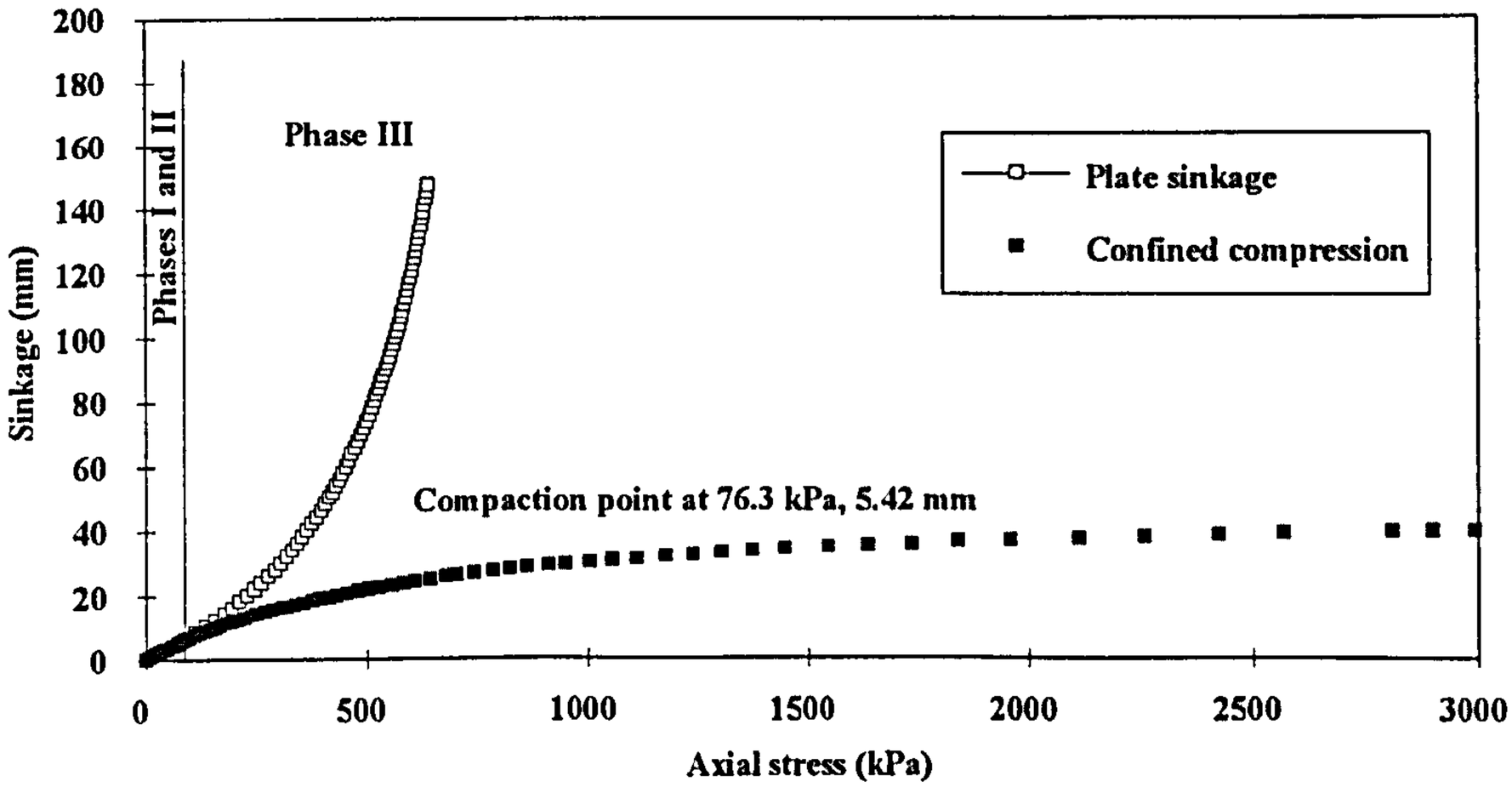

Figure 2a. The compaction point for sandy loam soil.

Three different loading situations have been selected to provide a range of scenarios:-

a) 45 kPa (equivalent to a low ground pressure wheel)

b) 70 kPa (equivalent to a conventional 70 kW tractor)

c) 95 kPa (equivalent to a four-wheel drive tractor)

An applied load of 45 kPa corresponds to a phase I loading situation (*Figure 1a*). For phase I, the maximum depth of disturbance is given by equation (5.4):-

$$X_{max} = \frac{D(\sigma_{Amax} + \gamma R)}{4(c + \sigma_R \tan\phi) - \gamma D} \qquad (5.4)$$

Substituting values from *Table 1a* and *Figure 1a* in equation (5.4):-

$$X_{max} = \frac{0.15 \cdot (45 + 1.47 \cdot 0.0015 \cdot \frac{1}{9.81}) \; m(\frac{kN}{m^2})}{4 \cdot (11 + 25 \cdot \tan 30) - 1.47 \cdot 0.15 \cdot \frac{1}{9.81} \; \frac{kN}{m^2}}$$

$$\therefore X_{max} = 0.066m$$

At an applied load of 70 kPa, the loading situation corresponds to phase II and is expressed by equation (5.19):-

$$\sigma_{Amax} = \frac{4X_{max}(a-\sigma_{Amax})}{D(\gamma(R+X_{max})-\sigma_{Amax})}\{c+(b-a+K_o\sigma_{Amax})\tan\phi+$$
$$\frac{K_o}{2}(\gamma(R+X_{max})-\sigma_{Amax})\frac{a-\sigma_{Amax}}{\gamma(R+X_{max})-\sigma_{Amax}}\tan\phi\}+ \qquad (5.19)$$
$$\frac{4X_{max}}{D}(c+b\tan\phi)(1-\frac{a-\sigma_{Amax}}{\gamma(R+X_{max})-\sigma_{Amax}})$$

Substituting values from *Table 1a* and *Figure 1a* into equation (5.19):-

$$70(\frac{kN}{m^2}) = \frac{4\cdot X_{max}\cdot(47-70)}{0.15\cdot(1.47\cdot\frac{1}{9.81}(0.0018+X_{max})-70)}$$
$$\{11+(25-47+1.05\cdot 70)\cdot\tan 30+\frac{1.05}{2}\cdot(1.47\cdot\frac{1}{9.81}$$
$$\cdot(0.0018+X_{max})-70)\cdot\frac{47-70}{1.47\cdot\frac{1}{9.81}\cdot(0.0018+X_{max})-70}\tan 30\}(\frac{kN}{m^2})$$
$$+\frac{4X_{max}}{0.15}\cdot(11+25\cdot\tan 30)\cdot(1-\frac{47-70}{1.47\cdot\frac{1}{9.81}\cdot(0.0018+X_{max})-70})(\frac{kN}{m^2})$$

Solving this equation iteratively X_{max} the depth of disturbance, is 0.094 m.

At 95 kPa the loading situation corresponds to phase III (section 5.3.4). The following variables should be determined to calculate the maximum depth of disturbance:-

Passive force F_f

$$F_f = F_A \cos(45+\frac{\varphi}{2}) \sec\varphi \qquad (5.27)$$

$$\therefore F_f = 95 \cdot 0.0171 \cdot \cos(45+\frac{30}{2}) \cdot \sec 30 (kN) = 0.938 (kN)$$

Distance l_1

$$l_1 = \frac{D}{4\cos(45+\frac{\varphi}{2})} \cos\phi \qquad (5.30)$$

$$= \frac{0.15}{4 \cdot \cos(45+\frac{30}{2})} \cos 30 = 0.065m$$

to

$$l_1 = \frac{D}{3\cos(45+\frac{\varphi}{2})} \cos\phi \qquad (5.31)$$

$$= \frac{0.15}{3 \cdot \cos(45+\frac{30}{2})} \cos 30 = 0.087m$$

Weight W_1

$$W_1 = \frac{\pi D^2 D_B}{8} [\frac{D}{6} \tan(45^o+\frac{\varphi}{2}) + R_{I\,Imax})] \qquad (5.35)$$

$$\therefore W_1 = \frac{\pi 0.15^2 \cdot 1.35}{8 \cdot 9.81}[\frac{0.15}{6} tan(45+\frac{30}{2}) +0.0032)] = 0.000056kN$$

Distance l_2

$$l_2 = 0.34D = 0.051m \tag{5.37}$$

Weight W_2

$$W_2 = (\frac{D_{Bmax} - D_B}{2})\{\frac{\pi}{12}(h_c + m)[\frac{3}{4}(D+2m)^2 + (h_c + m)^2] -$$

$$\frac{1}{2}\frac{\pi}{3}\frac{D^2}{4}h_c\} \tag{5.44}$$

$$\therefore W_2 = (\frac{(1.45-1.35)}{2 \cdot 9.81})\{\frac{\pi}{12}(0.13+m)[\frac{3}{4}(0.15+2m)^2 + (0.13+m)^2] -$$

$$\frac{1}{2}\frac{\pi}{3}\frac{0.15^2}{4}0.13\}$$

Distance l_3

$$l_3 = \frac{D}{2} - \frac{3\cdot[(\frac{D}{2}+m)^2+(h_c+m)^2]^4\cdot\sin^{-1}(\frac{2\cdot(\frac{D}{2}+m)\cdot(h_c+m)}{(\frac{D}{2}+m)^2+(h_c+m)^2}}{16\cdot\pi\cdot(h_c+m)^5\cdot[3(\frac{D}{2}+m)^2+(h_c+m)^2]}$$

$$\frac{-2\cdot(\frac{D}{2}+m)\cdot(h_c+m)\cdot[(\frac{D}{2}+m)^2-(h_c+m)^2]\cdot[3(\frac{D}{2}+m)^4}{+14\cdot(\frac{D}{2}+m)^2\cdot(h_c+m)^2+3\cdot(h_c+m)^4]} \qquad (5.46)$$

$$\therefore l_3 = \frac{0.15}{2} - \frac{3\cdot[(\frac{0.15}{2}+m)^2+(h_c+m)^2]^4\cdot\sin^{-1}(\frac{2\cdot(\frac{0.15}{2}+m)\cdot(h_c+m)}{(\frac{0.15}{2}+m)^2+(h_c+m)^2}}{16\cdot\pi\cdot(h_c+m)^5\cdot[3(\frac{D}{2}+m)^2+(h_c+m)^2]}$$

$$\frac{-2\cdot(\frac{0.15}{2}+m)\cdot(h_c+m)\cdot[(\frac{0.15}{2}+m)^2-(h_c+m)^2]\cdot[3(\frac{0.15}{2}+m)^4}{+14\cdot(\frac{0.15}{2}+m)^2\cdot(h_c+m)^2+3\cdot(h_c+m)^4]}$$

Weight W_3

$$W_3 = D_B\{\frac{\pi}{8}R[(D+2m)^2 - D^2] + \frac{\pi}{16}[(m\cdot tan(45-\frac{\varphi}{2})][(D+2m)^2 - D^2]\} \quad (5.49)$$

$$\therefore W_3 = 1.35\cdot\frac{1}{9.81}\{\frac{\pi}{8}\cdot 0.0032\cdot[(0.15+2m)^2 - 0.15^2] + \frac{\pi}{16}[m\cdot tan(45-\frac{30}{2})][(0.15+2m)^2 - 0.15^2]\}$$

Distance l_4

$$l_4 = \frac{D}{2} - \frac{4}{3\pi}\frac{[(\frac{D}{2}+m)^2 + (\frac{D}{2}+m)(\frac{D}{2}) + (\frac{D}{2})^2]}{[(\frac{D}{2}+m) + (\frac{D}{2})]} \quad (5.51)$$

$$\therefore l_4 = \frac{0.15}{2} - \frac{4}{3\pi}\frac{[(\frac{0.15}{2}+m)^2 + (\frac{0.15}{2}+m)(\frac{0.15}{2}) + (\frac{0.15}{2})^2]}{[(\frac{0.15}{2}+m) + (\frac{0.15}{2})]}$$

Force F_2

$$F_2 = W_3 cos(45+\frac{\varphi}{2}) sec\,\varphi \quad (5.54)$$

$$\therefore F_2 = W_3 cos(45+\frac{30}{2}) sec30$$

Distance l_5

As in the case of l_1, l_5 lies in the range 1/2 to 2/3 down the wedge face.

$$l_5 = \frac{\frac{m}{2tan(45-\frac{\phi}{2})} \; or \; \frac{2m}{3tan(45-\frac{\phi}{2})}}{sin(45-\frac{\phi}{2})} cos\phi \qquad (5.55)$$

$$\therefore l_5 = \frac{\frac{m}{2tan(45-\frac{30}{2})} \; or \; \frac{2m}{3tan(45-\frac{30}{2})}}{sin(45-\frac{30}{2})} cos30$$

Soil resistance due to soil movement

$$F_s = b \cdot \frac{1}{2}\frac{\pi}{4}[(D+m)^2 + 4(h_c+m)^2] \qquad (5.56)$$

$$\therefore F_s = 25 \cdot \frac{1}{2}\frac{\pi}{4}[(0.15+m)^2 + 4(0.13+m)^2]$$

Distance l_6

$$l_6 = \frac{1}{2}\sqrt{(h_c+m)^2 + (\frac{D}{2}+m)^2} - m \cdot cos[tan^{-1}(\frac{h_c+m}{\frac{D}{2}+m})] \qquad (5.61)$$

$$\therefore l_6 = \frac{1}{2}\sqrt{(h_c+m)^2+(\frac{0.15}{2}+m)^2} - m\cdot cos[\tan^{-1}(\frac{h_c+m}{\frac{0.15}{2}+m})]$$

Derivation of general equation:-

With reference to *Figure 5.15* the final expression obtained is:-

$$F_f l_1 = -W_1 l_2 - W_2 l_3 + W_3 l_4 + F_2 l_5 + F_s l_6 \qquad (5.27)$$

$$0.938\cdot 0.065(or)0.087 = -0.000056\cdot 0.051 - (\frac{(1.45-1.35)}{2\cdot 9.81})\{\frac{\pi}{12}(0.13+m)[\frac{3}{4}(0.15+2m)^2 +$$

$$(0.13+m)^2] - \frac{1}{2}\frac{\pi}{3}\frac{0.15^2}{4}0.13\}\cdot\{\frac{0.15}{2} - \frac{3\cdot[(\frac{0.15}{2}+m)^2+(h_c+m)^2]^4\cdot sin^{-1}(\frac{2\cdot(\frac{0.15}{2}+m)\cdot(h_c+m)}{(\frac{0.15}{2}+m)^2+(h_c+m)^2}}{16\cdot\pi\cdot(h_c+m)^5\cdot[3(\frac{D}{2}+m)^2+(h_c+m)^2]}$$

$$\frac{-2\cdot(\frac{0.15}{2}+m)\cdot(h_c+m)\cdot[(\frac{0.15}{2}+m)^2-(h_c+m)^2]\cdot[3(\frac{0.15}{2}+m)^4}{+14\cdot(\frac{0.15}{2}+m)^2\cdot(h_c+m)^2+3\cdot(h_c+m)^4]}\}$$

$$1.35\cdot\frac{1}{9.81}\{\frac{\pi}{8}\cdot 0.0032\cdot[(0.15+2m)^2-0.15^2]+\frac{\pi}{16}[m\cdot tan(45-\frac{30}{2})]\cdot[(0.15+2m)^2-0.15^2]\}$$

$$\cdot\{\frac{0.15}{2}\frac{4}{3\pi}\frac{[(\frac{0.15}{2}+m)^2+(\frac{0.15}{2}+m)(\frac{0.15}{2})+(\frac{0.15}{2})^2]}{[(\frac{0.15}{2}+m)+(\frac{0.15}{2})]}\} + W_3 cos(45+\frac{30}{2})sec30$$

$$\cdot\frac{\frac{m}{2tan(45-\frac{30}{2})}or\frac{2m}{3tan(45-\frac{30}{2})}}{sin(45-\frac{30}{2})}cos30+25\cdot\frac{1}{2}\frac{\pi}{4}[(0.15+m)^2+4(0.13+m)^2]$$

$$\cdot\frac{1}{2}\sqrt{(h_c+m)^2+(\frac{0.15}{2}+m)^2} - m\cdot cos[\tan^{-1}(\frac{h_c+m}{\frac{0.15}{2}+m})]$$

This equation can be solved iteratively. Distance l_1 significantly influences the final result. In this case, m can be either 0.087 m or 0.065 m depending on the approach which has been adopted (equation 5.30 or 5.31). Distance l_5 does not significantly influences the final result.

The results of the analysis for the sandy soil are presented in *Table 2a*.

Table 2a

Extent of deformation below a plate at different applied stresses (sandy loam soil)

Soil type	Applied stress (kPa)	Sinkage (mm)	Extent of deformation (mm)	Mode of deformation
Sandy loam	45	1.5	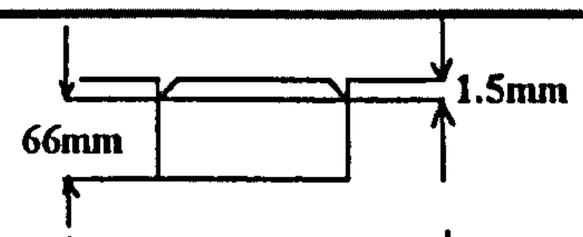	Phase I
	70	1.8	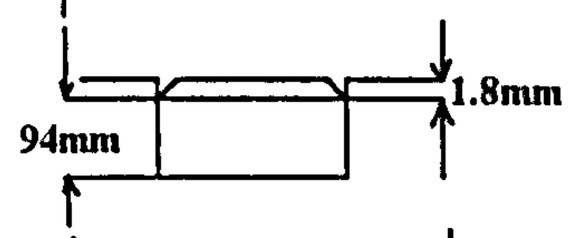	Phase II
	95	3.2	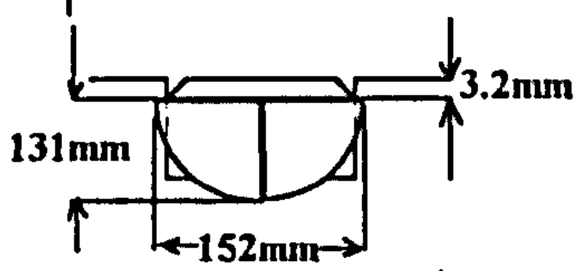	Phase III *l_1 from (5.30)*
or	95	3.2	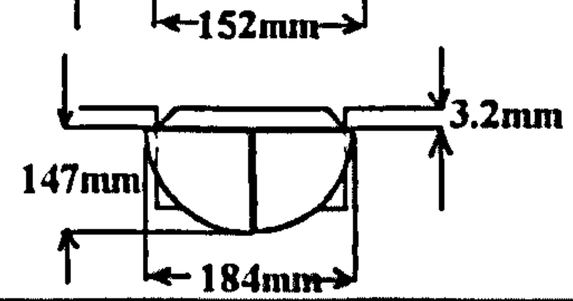	Phase III *l_1 from (5.31)*

For the clay soil the data obtained from confined compression and plate sinkage tests (*Figures 3a and 4a*) were also used in conjunction with data obtained from triaxial test for determination of cohesion and angle of shearing resistance at a similar soil (*Table 3a*).

Table 3a

Results obtained from triaxial test, for clay soil.

Cohesion, c, (kPa)	Angle of internal friction ϕ (degrees)	Moisture content (volumetric), %	Dry bulk density (Mg/m^3)
47	3.5	53	1.02

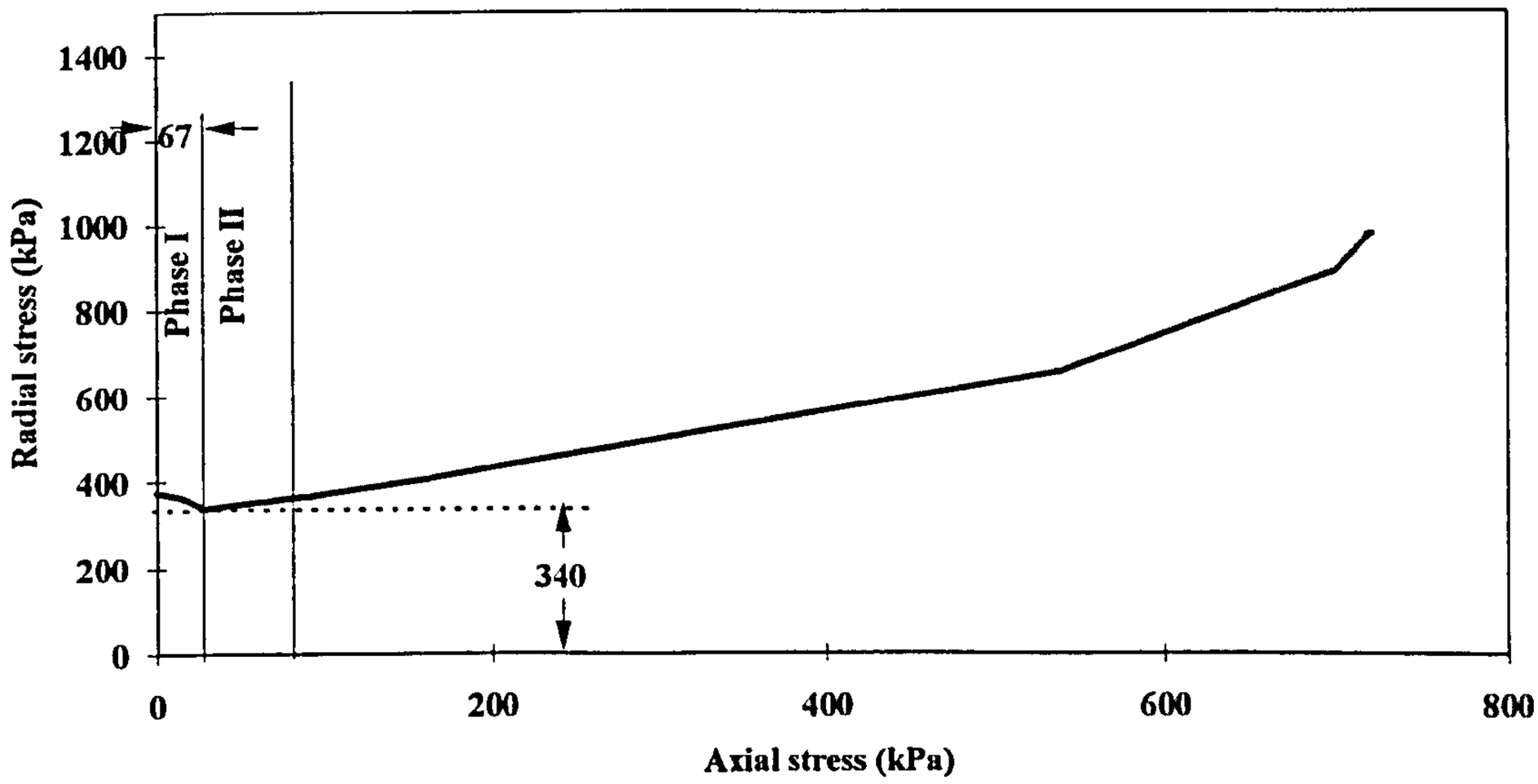

Figure 3a. The relationship between radial stress and axial stress for clay soil.

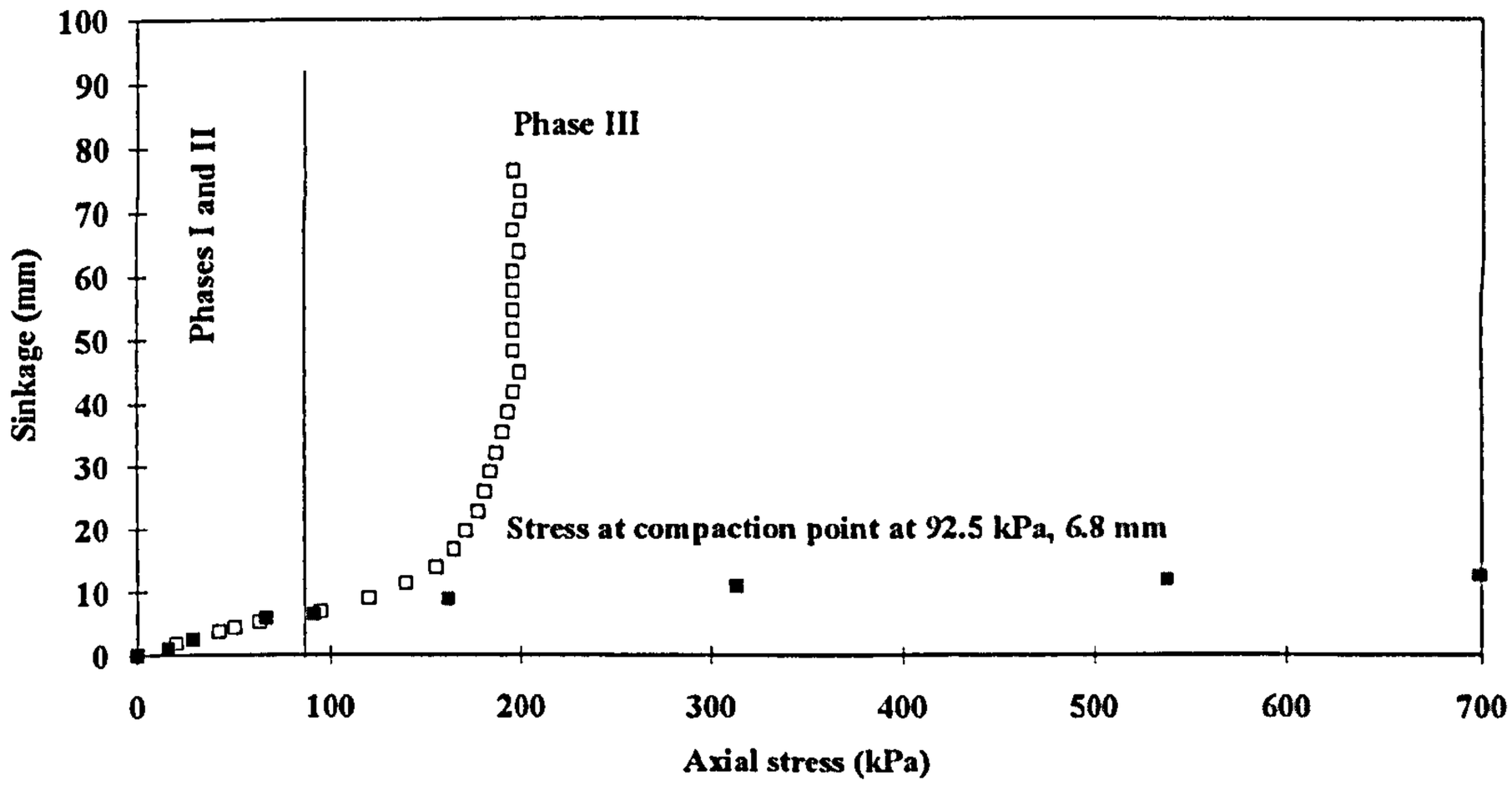

Figure 4a. The compaction point for clay soil.

An applied load of 45 kPa corresponds to a phase I loading situation (*Figure 3a*). For phase I, the maximum depth of disturbance is given by equation (5.4):-

$$X_{max} = \frac{D(\sigma_{Amax} + \gamma R)}{4(c + \sigma_R \tan\phi) - \gamma D} \qquad (5.4)$$

Substituting values from *Table 3a* and *Figure 3a* in equation (5.4):-

$$X_{max} = \frac{0.15 \cdot (45 + 1.47 \cdot 0.0038 \cdot \frac{1}{9.81})}{4 \cdot (47 + 340 \cdot tan3.5) - 1.47 \cdot 0.15 \cdot \frac{1}{9.81}} \frac{m(\frac{kN}{m^2})}{\frac{kN}{m^2}}$$

$$\therefore X_{max} = 0.025m$$

At an applied load of 70 kPa, the loading situation corresponds to phase II and is expressed by equation (5.19):-

$$\sigma_{Amax} = \frac{4X_{max}(a - \sigma_{Amax})}{D(\gamma(R + X_{max}) - \sigma_{Amax})} \{c + (b - a + K_o \sigma_{Amax}) tan\phi +$$

$$\frac{K_o}{2}(\gamma(R + X_{max}) - \sigma_{Amax}) \frac{a - \sigma_{Amax}}{\gamma(R + X_{max}) - \sigma_{Amax}} tan\phi\} + \qquad (5.19)$$

$$\frac{4X_{max}}{D}(c + b\,tan\phi)(1 - \frac{a - \sigma_{Amax}}{\gamma(R + X_{max}) - \sigma_{Amax}})$$

Substituting values from *Table 3a* and *Figure 3a* into equation (5.19):-

$$70(\frac{kN}{m^2}) = \frac{4 \cdot X_{max} \cdot (67 - 70)}{0.15 \cdot (1.47 \cdot \frac{1}{9.81}(0.0055 + X_{max}) - 70)}$$

$$\{67 + (340 - 67 + 3.90 \cdot 70) \cdot tan3.5 + \frac{3.90}{2} \cdot (1.47 \cdot \frac{1}{9.81}$$

$$\cdot (0.0055 + X_{max}) - 70) \cdot \frac{67 - 70}{1.47 \cdot \frac{1}{9.81} \cdot (0.0055 + X_{max}) - 70} tan3.5\}(\frac{kN}{m^2})$$

$$+ \frac{4X_{max}}{0.15} \cdot (67 + 340 \cdot tan3.5) \cdot (1 - \frac{67 - 70}{1.47 \cdot \frac{1}{9.81} \cdot (0.0055 + X_{max}) - 70})(\frac{kN}{m^2})$$

Solving this equation iteratively X_{max} the depth of disturbance, is 0.038 m.

At 95 kPa the loading situation corresponds to initial stages of phase III (section 5.3.4). Since during the initial stages lateral disturbance is zero, the assumption was made that the mode of deformation corresponds to phase II. Substituting values from *Table 3a* and *Figure 3a* into equation (5.19):-

$$95(\frac{kN}{m^2}) = \frac{4 \cdot X_{max} \cdot (67-95)}{0.15 \cdot (1.47 \cdot \frac{1}{9.81}(0.0070 + X_{max}) - 95)}$$

$$\{67 + (340 - 67 + 3.90 \cdot 95) \cdot \tan 3.5 + \frac{3.90}{2} \cdot (1.47 \cdot \frac{1}{9.81}$$

$$\cdot (0.0070 + X_{max}) - 95) \cdot \frac{67-95}{1.47 \cdot \frac{1}{9.81} \cdot (0.0070 + X_{max}) - 95} \tan 3.5\} (\frac{kN}{m^2})$$

$$+ \frac{4X_{max}}{0.15} \cdot (67 + 340 \cdot \tan 3.5) \cdot (1 - \frac{67-95}{1.47 \cdot \frac{1}{9.81} \cdot (0.0070 + X_{max}) - 95}) (\frac{kN}{m^2})$$

Solving this equation iteratively X_{max} the depth of disturbance, is 0.050 m.

The results of the analysis for the sandy soil are presented in *Table 4a*.

Table 4a
Extent of deformation below a plate at different applied stresses (clay soil)

Soil type	Applied stress (kPa)	Sinkage (mm)	Extent of deformation (mm)	Mode of deformation
Clay soil	45	3.8	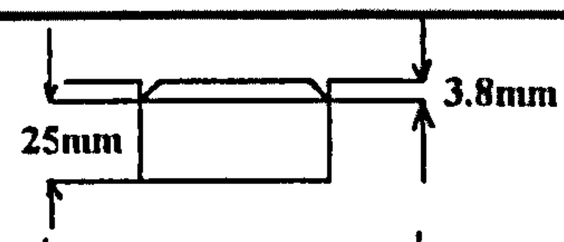	Phase I
	70	5.5	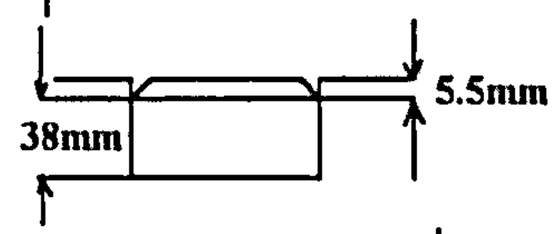	Phase II
	95	7	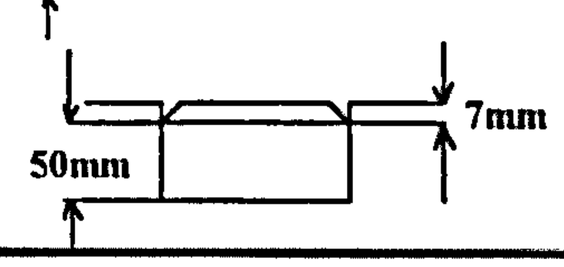	Phase II

REFERENCES

BARAN, P A and SWEEZY, P M (1968) Monopoly capital: An essay on the American economic and social order. Penguin Books, London.

BAILEY, A C, JOHNSON, C E and SCHAFER, R L (1984) Hydrostatic compaction of agricultural soils. Trans ASAE, 27, 952-955.

BAILEY, A C and JOHNSON, C E (1989) A soil compaction model for cylindrical stress states. Trans ASAE, 32(3), 822-825.

BAILEY, A C and VANDEN BERG, G E (1968) Yielding by compaction and shear in unsaturated soils. Trans ASAE, 12, 307-311, 317.

BERNSTEIN, R (1913) Probleme zur experimentellen Motorpflug-Mechanik. Der Motorwagen, 16.

BEVINGTON, P R (1969) Data reduction and error analysis for the physical sciences. New York: McGraw Hill.

BOONE, F R, VAN DER WERF, H M G, KROESBERGEN, B, HAG, B A, BOERS, A and TEN-HAG, B A. (1987) The effect of compaction of the arable layer in sandy soils on the growth of maize for silage. 2. Soil conditions and plant growth. Netherlands Journal of Agricultural Science, 35 (2), 113-128.

BRADFORD, G R and GUPTA, S C (1986) Soil Compressibility. In KLUTE, A (ed) Methods of soil analysis, part 1: Agronomy (2nd ed). American Society of Agronomy, Madison, WI, 479-492.

BURMISTER, D M (1951) Identification and classification of soils-an appraisal and statement of principles. Special technical publication No. 113, American Society for Testing of Materials, 1-24.

CARTER, L M and COLWICK, R F (1971) Evaluation of tillage systems for cotton. Trans ASAE 14 (6), 1116-21.

CASAGRANDE, A (1936) The determination of the pre-consolidation load and its practical significance. Proc 1st Int Conf Soil Mechanics, Cambridge, Mass, 3, 60-65.

CHANCELLOR, W J, SCHMIDT, R H and SOEHNE, W (1962) Laboratory measurement of soil compaction and plastic flow. Trans ASAE, 5, 235-239.

CORDIER, Y (1983) Etude de l' influence des travaux culturaux sur les propriétés mécaniques et physiques d'un sol limoneux (A study into the influence of cultivation operations on the mechanical and physical properties of a silty soil). PhD thesis, Faculté des Sciences Agronomiques de l' Etat a Gembloux, France.

DAS, K C (1972) Dynamics of corn root growth as affected by compact subsoil and its influence on crop response to irrigation. PhD thesis, University of California, Davis, U.S.A.

DAS, B M (1993) Principles of soil dynamics. PWS-KENT Publishing Company, Boston, USA.

DUNLAP, W H and WEBER, J A (1971) Compaction of an unsaturated soil under a general state of stress. Trans ASAE, 14, 601-607, 611.

EARL, R (1993) The development of techniques for assessing soil compaction. PhD Thesis, Silsoe College.

EMORI, R and SCHURING, D (1966) Static and dynamic penetration tests of soil. J Terranechanics, 3 (1), 23-30.

ERIKSSON, J (1982) Soil compaction and root enviroment. Swedish University of Agricultural Sciences, Report 126.

GILL, W R (1968) Influence of compaction hardening of soil on penetration resistance. Trans ASAE, 11, 741-745.

GILL, W R and VANDEN BERG, G E (1968). Soil dynamics in tillage and traction. Agricultural Handbook No 316, USDA.

GODWIN, R J (1975) An extended octagonal ring transducer for use in tillage studies. J Agric Engng Res, 20, 347-352.

GRAHN, M (1987) Investigation of the influence of penetration velocity on the pressure sinkage relationship. Proc 9th Int Conf ISTVS, Barcelona, Spain, 1, 37-44.

GREEN, W M, ROBERTS, R and PERFFLEY, E. (1988). Influence of soil compaction on soil water content and Norgold Russet potato yields. American Potato Journal, 65 (8), 480.

GUERIF, J (1984) The influence of water-content gradient and structure anisotropy on soil compressibility. J Agric Engng Res, 29, 367-374.

GUPTA, S C, HADAS, A, VOORHESS, W B, WOLF, D, LARSON, W E and SCHNELDER, E C (1985) Development of guides for estimating the ease of compaction of world soils. Research Report submitted to Binational Agricultural Research Development Fund, Bet Dagan, Israel.

HAKANSSON, I (1988) A method for characterising the state of compactness of an arable soil. in Impact of water and external forces on soil structure Drescher, J, Horn, R and M de Boodt (Eds.), Catena supplement 11,Hanover 1988.

HETTIARATCHI, D R P (1987) A critical state soil mechanics model for agricultural soils. Soil use Manag. 3, 94-105.

HETTIARATCHI, D R P and REECE, A R (1975) Boundary wedges in two-dimensional passive soil failure. Gèotechnique, 25 (2), 197-220.

HORN, R (1981) Eine methode zur Ermittlung der Druckbelastung von Boeden anhand von Drucksetzungsversuchen (A method for the determination of the pre-consolidation stress). Kultertechnik und Flurbereinigung, 22: 20-26.

HORN, R and LEBERT, M (1994) Soil compactability and compressibility in 'Soil compaction in crop production'. Soane, B D and Ouwerkerk (Eds.), Elsevier Science B. V., Amsterdam, 1994.

LARSON, W E, GUPTA, S C and USECHE, R A (1980) Compression of agricultural soils from eight soil orders. Soil Science. Soc. Am. J 44, 450-457.

LEBERT, M, BURGER, N and HORN, R (1987) Beuteilung und Vorhersage der mechanischen Belastbarkeit von Ackerboeden (Evaluation and prediction of the mechanical loading capacity of agricultural soils). Mitteilungen Deutschen Bodenkundlichen Gesellschaft, 53: 97-202.

LIPIEC, J and SIMOTA, C (1994) Role of soil and climate factors in influencing crop responses to soil compaction in central and eastern Europe, in 'Soil compaction in crop production'. Soane, B D and Ouwerkerk (Eds.), Elsevier Science B. V., Amsterdam, 1994.

KARAFIATH, L L and NOWATZKI, E A (1978) Soil mechanics for off-road vehicle engineering. Trans Tech Publications, Clausthal, Germany.

KACIGIN, V V and GUSTOV, V V (1968) The basis of tractor performance theory. J Terramechanics, 5 (3), 43-67.

KONDNER, R L and KRIZEK, R J (1962) Correlation of load bearing tests on soils. Highway Research Board Proceedings, 41, 557-590.

KONIJN, N J M (1978) Weerstand van grond tegen verdichting in een profiel (Resistance of soil to compaction in a profile). Thesis, Tillage laboratory, Agricultural University, Wageningen.

KOOLEN, A J (1974) A method for soil compactibility determination. J Agric Engng Res, 19, 271-278.

KOOLEN, A J (1982) Precompaction stress determination on precompacted soil. Proc 9th Conf Inter Soil Tillage Research Organisation, Osijek, Yugoslavia 1982, 225-230.

MARSHALL, T J and HOLMES, J W (1988) Soil physics. Second edition, Cambridge University Press, Cambridge, UK.

MEYERHOF, G G (1951) The ultimate bearing capacity of foundations. Gèotechnique, 2, 301-332.

MEYERHOF, G G (1961) The ultimate bearing capacity of wedge-shaped foundations. Proc 5th Int Conf on Soil Mechanics and Foundation Engineering, Paris.

NICHOLS, M L (1929) Methods of research in soil dynamics as applied to implement design. Bulletin 229, Alabama experimental station, Auburn, USA.

OSTENBERG, J O (1948) Discussion of symposium on load test bearing capacity of soils. American Society for Testing and Materials, Spec. Tech. Publ. No 79.

PERLOFF, W H and RAHIM, K S (1966) A study on the pressure-penetration relationship for model footing on cohesive soil. Highway Research Board Proceedings, 45.

PRANDTL, L (1920) Ueber die harte plastischer korper (on the hardness of plastic bodies). Nachr kgl Ges Wiss. Gottingen, Math-Phys, kl, 74-85.

PRANDTL, L (1921) Ueber die eindringungsfestigkeit plastishcer baustoffe und die festigkeit von schneiden. Zeitschrift fuer Angewandte Mathematic, 1 (1), 15-20.

PRESS, W H, FLANNERY, B P, TEUKOLSKY, S A and VETTERLING, W T (1988) Numerical recipes in C; The art of scientific computing. Cambridge university press.

PROCTOR, R R (1933) Fundamental principles of soil compaction. Engineering News Records 111 (9).

ROSCOE, K H, SCHONFIELD, A N, and WROTH, C P (1958). On the yielding of soils. Gèotechnique, 8, 22-53.

SCHAFER, R L, JOHNSON, C E, KOOLEN, A J, GUPTA, S C and HORN, R (1990). Future research needs in soil compaction. ASAE paper No 90-1078, ASAE, St. Joseph, MI, USA.

SCHMERTMANN, J H (1953) Estimating the true consolidation behaviour of clay from laboratory test results. Proc ASCE 79 separate 311, 1-26.

SCHMIDT, W (1980) Zur Ableitung der Verdichtungszahlen und der Vorbelastung von Torfen aus leicht bestimmbaren Bodenkenwerten (Derivation of compression index and the preloading of peats from easily determined soil properties). Wissenschattlich-Technische Information Meliorationswesen, Freienwalde, 61: 42-46.

SCHWANGHART, (1991) Measurement of contact area, contact pressure and compaction under tires in soft soil. J Terramechanics, 28, 309-318.

SOANE, B D (1985) Traction and transport systems as related to cropping systems. Proc 1st Inter Conf on Soil Dynamics, 5, 863-935.

SOEHNE, W H (1958) Fundamentals of pressure distribution and soil compaction under tractor tyres Agric Eng. 39, 276-281, 290.

TAYLOR, H M (1971) Effects of soil strength on seedling emergence, root growth and crop yield. Compaction of agricultural soils, ASAE monograph, St Joseph, Michigan USA, 1971.

TERZAGHI, K (1943) Theoretical soil mechanics. Wiley and sons, New York, USA.

TERZAGHI, K and PECK, B R (1967) Soil mechanics in engineering practice. Second edition, Wiley and sons New York, USA.

TU, J C and TAN, C S (1991) Effect of soil compaction on growth, yield and root rots of white beans in clay loam and sandy loam soil. Soil-Biology and Biochemistry, 23 (3), 233-238.

VANDEN BERG, G E (1966) Triaxial measurements of shear strain and compaction in unsaturated soil. Trans ASAE, 9, 460-463, 467.

VANDEN BERG, G E BUCHELE, W F and MALVERN, L E (1958) Application of continuum mechanics to soil compaction. Trans ASAE, 1(1), 24-28.

VESIC, A B (1963) Bearing capacity of deep foundations in sand. Highway Research Board Proceedings, 42, 112-153.

UNIVERSITY OF CALIFORNIA BULLETIN 1881 (1975) Compaction of soils by agricultural equipment. University of California, Davis, USA.

YOUSSEF, A F A AND ALI, G A (1982) Determination of soil parameters using plate test. J Terramechanics, 19 (2), 129-147.